Preparation of electrospun core-sheath nanofibers from poly(lactic acid)-collagen polymers and their biomedical applications

A Dissertation Submitted to the Department of Applied Chemistry and Chemical Engineering, University of Dhaka, Bangladesh for the Accomplishment of Degree of Doctor of Philosophy

By

Nasima Akter Mukta

Registration No. 155

Session: Ph.D. (2017-2018)

Professor Dr. Papia Haque

Supervisor

Department of Applied Chemistry and Chemical Engineering, University of Dhaka, Bangladesh

Professor Dr. AM Sarwaruddin Chowdhury

Co-Supervisor

Department of Applied Chemistry and Chemical Engineering, University of Dhaka, Bangladesh

Dr. Samina Ahmed

Co-Supervisor

Chief Scientific Officer

Institute of Glass and Ceramic Research and Testing

Bangladesh Council of Scientific and Industrial Research

Department of Applied Chemistry and Chemical Engineering

University of Dhaka, Bangladesh

September, 2023

Dedicated

To

My Beloved

Teachers,

Parents and Family Members

DECLRATION

I hereby declare that the scientific work submitted as a PhD thesis with the title “Preparation of electrospun core-sheath nanofibers from poly(lactic acid)-collagen polymers and their biomedical applications" under the supervision of Professor Dr. Papia Haque, Professor Dr. AM Sarwaruddin Chowdhury, and Dr. Samina Ahmed to the Department of Applied Chemistry and Chemical Engineering, University of Dhaka, Dhaka-1205, Bangladesh for the Degree of Doctor of Philosophy is the result of my investigation and has never been presented in any form for any other degree anywhere. I further certify that the entire dissertation work submitted for the degree of Doctor of Philosophy at Dhaka University is based on my original research except for the references used in the text of the dissertation.

Nasima Akter Mukta
Registration No. 155
Session: 2017-2018
Department of Applied Chemistry and Chemical Engineering
University of Dhaka
Dhaka-1205, Bangladesh

CERTIFICATE

This is to certify that the Ph.D thesis submitted by Nasima Akter Mukta, Registration No. 155, Session: 2017-2018, Department of Applied Chemistry and Chemical Engineering, University of Dhaka, Dhaka, Bangladesh entitled "Preparation of electrospun core-sheath nanofibers from poly(lactic acid)-collagen polymers and their biomedical applications" has been completed under my observation. This is an authentic and reliable record of the research conducted by the candidate. To my knowledge, this work has not received a degree or award elsewhere.

Professor Dr. Papia Haque
Supervisor
Department of Applied Chemistry and Chemical Engineering
University of Dhaka, Bangladesh

Professor Dr. AM Sarwaruddin Chowdhury
Co-Supervisor
Department of Applied Chemistry and Chemical Engineering
University of Dhaka, Bangladesh

Dr. Samina Ahmed
Co-Supervisor
Chief Scientific Officer
Institute of Glass and Ceramic Research and Testing
Bangladesh Council of Scientific and Industrial Research

ACKNOWLEDGEMENT

First of all, I thank the Creator of all for giving me the opportunity, devotion, perseverance and strength to conduct this research.

As the probable results of this work, I wish to express my deep gratitude, debt and infinite respect to my reverend supervisor, Professor Dr. Papia Haque, Department of Applied Chemistry and Chemical Engineering, University of Dhaka for her constant inspiration, right guidance and demeanor, constructive and criticism, constant encouragement, helpful discussions, sensible recommendations, and effective monitoring throughout my research.

My heartfelt thanks and gratitude go to my distinguished Professor Dr. AM Sarwaruddin Chowdhury, in the Department of Applied Chemistry and Chemical Engineering, University of Dhaka for his philanthropic thoughts.

My heartfelt thanks and gratitude go to my co-supervisor, Dr. Samina Ahmed, Chief Scientific Officer, Institute of Glass and Ceramic Research and Testing, Bangladesh Council of Scientific and Industrial Research for his philanthropic thoughts.

I also express my appreciation and gratitude to all other esteemed professors in the Department of Applied Chemistry and Chemical Engineering at Dhaka University for their patiently listening and giving important directives during my presentations in the seminars, which is quite essential for a successful research.

Again, I remember the “advisers” and thank them for helping and inspiring me in my research. I am very grateful to the "people who helped with the lab work" for actively lending their helping hands in the lab work.

I would particularly like to say thank the scientists at Centre for Advanced Research in Sciences (CARS), University of Dhaka, Bangladesh Council for Science and Industrial Research (BCSIR) Laboratories, Dhaka, and all officials and administrators at the Department of Applied Chemistry and Chemical Engineering, University of Dhaka for their generous help in administrative, experimental and laboratory work.

Last but not least, I will forever be indebted to my family for the unwavering empathy I received during the long hours of study. I couldn't finish this degree if not for their support.

Nasima Akter Mukta

February 2023

EXECUTIVE ABSTRACT

Biomaterials are applied to living organisms and used as biomedical appliances to accomplish, enhance, or substitute particular natural functions. Completely hydrophobic or hydrophilic biomaterials are not suitable to be applied to cell growth. Poly(lactic acid) (PLA) is a biodegradable and bioresorbable synthetic polymer that is already in use in many commercial biomedical devices. In this study, commercial PLA was modified by grafting vinyl acetate (VAc) onto it using lithium tetrahydridoaluminate ($LiAlH_4$) or benzoyl peroxide (BPO) to increase the hydrophilic moiety. Resultant materials were characterized by FT-IR, ^{1}H-NMR, and ^{13}C-NMR, and hereafter the mechanism of the grafting processes was proposed. The materials were subjected to thermal analysis and X-ray diffraction studies for further characterization. Biocompatible and biodegradable polymers gelatins, a derivative of collagen and collagen, are used in biomedical applications. Additionally, electrospun nanofibrous scaffolds possess biomimic structures and have promising applications in tissue regeneration, especially for wound healing purposes. Electrospun nanofibrous scaffolds from the hydrophobic PLA, and hydrophilic gelatin blend solutions using Tween 80 were prepared. Solution properties such as conductivity, and viscosity of blended solutions were investigated, and the scaffolds were analyzed using FESEM. Moreover, core-sheath bi-polymeric scaffolds have been substantiated as promising materials centered on the requirements of scaffolds of component materials in which one polymer is covered (core) with another polymer. This work was also employed to prepare core-sheath scaffolds by using gelatin or collagen as core material and PLA or vinyl acetate grafted on PLA as sheath material to get the utmost properties of the polymers. Acid soluble collagen (ASC) was extracted from waste Tilapia fish skin. Amino acid profile of ASC revealed its triple helix structure whereas SDS-PAGE confirmed the existence of α1 (130 kDa), α2 (120 kDa) cross linked with a β (280 kDa) chain. Morphology of the scaffolds was determined by the FESEM. All the scaffolds were characterized further by FT-IR, TGA, DSC, and XRD. Cytotoxicity of all scaffolds were measured as well prior to in vivo application and cytotoxicity was not observed on Vero cell line. Water contact angle measurement of the scaffolds revealed that bi-polymeric scaffolds were more wettable than the single polymeric scaffold of PLA or grafted PLA. Scaffolds were applied to the surgically produced wounding of skin in a rat model followed by histological assay to observe their improved properties towards wound healing processes. Relative wound size reduction as well as healing

were observed using bi-polymeric scaffolds rather than the use of a single polymeric scaffold of PLA or Grafted PLA. Histological assay also supported the bi-polymeric scaffolds as encouraging materials for tissue regeneration.

List of Abbreviations

%	-Percentage
^{o}C	-Degree Celsius
cm	-Centimeter
g	-Gram
cm^{-1}	-Per centimeter
min	-Minute
h	-Hour
J	-Joule
PLA	-Polylactic acid
VAc	-Vinyl acetate
ASC	-Acid soluble collagen
DCM	-Dichloromethane
DMF	-Dimethylformamide
MeOH	-Methanol
AcOH	-Acetic acid
FESEM	-Field Emission Scanning Electron Microscopy
FT-IR	-Fourier Transform Infrared
TGA	-Thermogravimetric Analysis
DTG	-Derivative Thermogravimetry
DSC	-Differential Scanning Calorimetry
DDSC	-Derivative Differential Scanning Calorimetry
XRD	-X-ray diffraction
NMR	Nuclear Magnetic Resonance Spectroscopy

Content

List of Tables

List of Figures

CHAPTER ONE

INTRODUCTION

Chapter One

Introduction

1.1 Literature Review

The expansion of biomaterials is not a novel space of discipline, having be existent for about half of a century. The field of study of biomaterials is named as biomaterial science which is a challenging area of science, having practiced stable and robust development over the past, with numerous establishments participating huge quantities of effort as well money into the expansion of innovative produces. This field includes components of several areas such as biology, chemistry, material sciences, medicines, and tissue engineering [1]. One of the targets is biomaterials for up keeping the tissue regeneration progressions. Nano sized biomaterials are a comparatively a developing biomaterials that should constitute biodegradable biopolymer materials as well as mimic the structure of ECM (extra cellular matrix) through bioactive and simply bioresorbable polymers. Such nano sized materials widely based on two types of polymers, natural and synthetic. Natural polymer based biomaterials usually fabricated for the reinforcement of natural polymer including cellulose, chitosan, alginate, collagen, gelatin, and silk fibroin have been studied concerning their current researches on the integration of natural polymers for tissue restoration [2]. Synthetic polymers that have been applied for biomaterials are PEG (polyethylene glycol), PCL (polycaprolactone), PLA (polylactic acid), poly (lactic-co-glycolic) acid (PLGA), and polyurethane (PU). Several nano sized fillers such as hydroxyapatite, zirconia, silica, silver, titanium dioxide, graphene oxide have been established widening applications in tissue regeneration [3]. Combination of a natural polymer with a synthetic polymer matrix influences positively to cell viability which has been established through both in vivo and in vitro investigations [4]. Amongst the current technologies for regenerative medicine or tissue engineering, scaffolds are now the strategically best materials for repairing, sustaining and successful tissue function. They perform a distinctive role in mending and more outstandingly restoration of tissues by giving a proper base, allowing necessary resources of numerous aspects related with continued existence, propagation and cells differentiations. Few techniques have been employed to make scaffolds, From these techniques, four main scaffolding methodologies comprise the application of ECM discharging cellular sheets, pre-prepared scaffolds of

biocompatible, and biodegradable, synthetic, and natural biomaterials, decellularized extra cellular matrix scaffolds and the form in which cells are trapped in hydrogels [4]. With the growing trend, and the capability to get the highly precise, and controlled scaffolding materials, simple sophisticated techniques taking into considerations of quality, and cost effectiveness is important. Nanofibrous scaffolds have a great surface-to-volume proportion, such scaffolds increases adhesion of cell as migration, propagation, and differentiations of cells are associated with cellular adhesion, and these might be the crucial achievement from nanofibrous structures. With the advancing of such materials, three distinctive approaches to the development of nanofibrous scaffolds have occurred, such as phase separation, electrospinning, and self-assembly [5]. Different fabrication techniques are also employed, and amongst them, EHD (electro-hydrodynamic) is now promising technique that comprises electrospinning, and electrospraying. Over the past two decades, electrospinning process has achieved global consideration from the end of biomedical research as a pioneering technology for the fabrication of micro or nano scale structures applied as scaffolds and drug delivery appliances [6]. Usually it applies electric field to produce polymer based non-woven fibrous structure or scaffolds. This technology is also talented in the arenas due to the widespread choice of constituents that can be engaged [6]. PLA as a polymer that can be obtained from renewable carbohydrate sources has come to be a material of choice in the biomedical applications due to its capability to comply multifaceted requirements such as cytocompatibility, biodegradability, good mechanical strength point, and finally processable properties. Even though the benefits of PLA in an extensive range of applications, its application is restricted for its hydrophobic nature, poor influence on toughness, and relaxed degradation level [7]. Extra cellular matrix proteins that are in general produced and released by fibroblasts cells along with other cells as for example epithelial cells, perform substantial roles in cell progress and growth in vivo. A number of types of collagen which is the greatest abundant extra cellular matrix protein offer robust tensile strength and integration of structures in skins, interconnected tissues, and tendons. Use of collagen as biomaterials offer the regulation of the cell propagation and differentiation capability along with the structural integration. Collagen proteins comprise crucial sites for the cellular interactions in cellular membranes. Thus these proteins are also accountable for the stimulation and initiation of fundamental signaling pathways of molecules. There are challenges to the use of such an ECM proteins for biomaterial research considering effort, cost and times required for extraction [8]. In this study, a simple approach and available

waste materials source are engaged for the production of targeted biomaterials. Furthermore, gelatin could be a substitute to extracellular protein for the biomaterial applications. On the other hand, gelatin polymer is a renowned biodegradable and cytocompatible material that contains about 85 to 92 % of proteins, minerals, and water. Gelatin which is a derivative (molecular) of collagen (type I) has a widespread choice of pharmaceutical, food, and cosmetic applications. Gelatin is generally obtained through hydrolyzation (irreversible) from type I collagen in which the triple helix arrangement of collagen is usually destroyed through enzymatic denaturation, and temperature dependent denaturation that is producing random twisted sites in the structure of gelatin. Though gelatin has poor molecular organization but it could be a good substitute of collagen in case of biomaterial functions alike collagen for cellular interactions. It can be readily obtainable and can be taken out from a number of sources including fish, cattle bones, pig skins, and also from certain insects. Numerous cytocompatibility studies of the gelatin exhibits that the gelatin usually does not encourage cytotoxicity, antigenicity, and additional adversative impacts in cells, but shows some cytotoxicity based on toxic reagent application [9]. Blending PLA with other polymers offers a convenient option to enhance its properties or generate novel properties for target applications without the need to develop new materials. Blends of PLA with a no. of synthetic, and natural polymeric materials have been advanced by solvent blending techniques as well melt blending methods which is further deal for the applications of biomaterials. A diversity of PLA blends has been revealed for several biomedical applications as for example, implants, drug transport, sutures, and other regenerative medicines as well as tissue engineering [10]. This is one of the ways to prepare sustainable bi-polymeric electrospun scaffolds to obtain the utmost properties of polymer constituents specially combination of hydrophilic polymer with the hydrophobic polymer towards for several biomaterials applications. The coaxial electrospinning is an advanced amendment in traditional electrospinning process that enables the fabrication of core-sheath nanofibers in which one polymer solution is treated as core solution, and another polymer solution is treated as sheath solution to get the bi polymeric scaffolds. PLA based core-sheath electrospun scaffolds with a several synthetic and natural polymers have also been reported for a no. of tissue engineering purposes where PLA was used as the core or the sheath materials based on final use of the materials. A general coaxial settings contains of two concentrically fitted needles, by which core and sheath solutions are delivered and subsequently come through the tip producing tailor cone at the tip of the needle to be stretched as fiber under suitable electric voltage.

Such advancement not only facilitates the electrospinning of poor spinnable materials with the support of a greatly spinnable material but also enhances the physicochemical properties of constituent single polymers. With a greater performance in the transport of drug, the coaxial scaffolds with well-regulated discharge are encouraged as having their improved performances than the single polymeric fibers towards regenerative medicines [11].

Skin wound is still challenging towards clinical treatment. Several transplant devices are not sufficient to come across the necessary weights for the management of injury. Electrospun nanofibrous bi-polymeric scaffolds as an ideal material for skin tissue regeneration own ideal properties for skin wound repairing. As usual it provides cell permeability, neither hydrophilic nor hydrophobic base, regulated biodegradability and preferable cytocompatibility. For these benefits, the scaffolds enable the removal of exudates from the injured domain, prevent water loss and encourage diffusion of oxygen passing through the wound tissue. In recent times, many research works are reported using electrospinning either blend or coaxial for the searching of suitable scaffolds particularly by natural polymers (such as collagen, silk fibrin, chitosan, and gelatin) and synthetic polymers which are biodegradable (alike PGA, PCL, PLGA, and PLA) [11]. This endeavor was taken for the preparation of bi-polymeric biomaterials (electrospun scaffolds) by using PLA or amended PLA as synthetic polymer and gelatin or collagen as natural polymer with blend electrospinning and also with coaxial electrospinning to observe their potentials in tissue regenerations as wound dressings.

1.2 Biomaterials

Biomaterials are said for the essential materials that are employed and amended for medical uses. As the general definition, biomaterials should have cellular functions as well own bioactive components, and applied for more communicating biomedical purposes. Biomedical appliances such as dental applications, drug transportations, surgery sutures, tissue engineering transplant materials as well all regenerative biomedicines comply biomaterials. Structured definition of biomaterials is somewhat difficult to state. More acceptable definition is that the materials synthetic or natural that is employed for the interactions with living structures to perform several medical functions are well-known as biomaterials [1]. Biomaterials are applied as several joint substitutes, bone plates, and cements, synthetic tendons, and ligaments, dental sutures, and transplants, artificial blood vessels, heart valves, skin restoration devices, and cochlear substitutes, and contact lenses etc. The only utmost key feature that differentiates a biomaterial from other

materials is its capability to be existent in interaction with tissues of the human's organization without affecting an undesirable amount of damage to that organization. The way in which the equally sustainable co-existence, and development of such tissues as well biomaterials recognized as biocompatibility or cytocompatibility [12]. Main material characteristics such as material composition, whether it is micro-sized, or nano sized structure, morphology of the materials, crystallinity percentage and other crystallographic parameters, elastic coefficients, water percentage, hydrophilic to hydrophobic balance, porosity whether it is macro, micro, or nano, external composition (chemical), chemical potentials, several surface properties, various decomposition parameters, several bioactive molecules release profile, toxicity from metallic elements, degradation pattern for polymeric materials, along with dissolution/degradation ratio, and toxicity from degradation products are prime concerns for biomaterials [13].

1.3 Tissue Engineering

In the past few decades, a basic change in the architecture and applications of biomedical materials has been observed from the period when the concept of regenerative medicine initiated which is an interdisciplinary arena that pools the values of engineering and life science disciplines to the aim of regeneration of tissues impaired by disease, trauma, age or any other causes. Regenerative medicines comprises several approaches followed by implanting or the combination of cells bioactive components to support tissue restoration, and the second approach is recognized as tissue engineering [14]. Tissue engineering may comply with in vitro or in vivo procedures but it constantly count on the usage of a biomaterial. The scaffolds function through cellular adhesion, proliferation, differentiation followed by the deposition of new extracellular matrix which gradually mimic the structure, directing to the restoration of the tissue (new). Thus the biomaterial is gradually resorbed [15].

1.4 Scaffold Requirements

Simple remark of living tissues displays that they are exceptionally complex organizations and these structural architectures depend on their roles. The first stage to scaffold construction is to ascertain a biomaterial that might be mimic to complement precise tissue functions agreeing the formation of an environs appropriate for cell progress, propagation, differentiation and extracellular matrix deposition for a positive restoration. Conditions for the select of a appropriate biomaterial take account of the probability i) to be decomposed without any general adversative

effects to the host; ii) to accept appropriate mechanical characteristics to reflect that of the host; iii) to adopt a proper inner structural design; and iv) to prompt neighboring tissues response (biological) [14].

1.5 Synthetic Polymers for Scaffolds

Synthetic polymers characterize the major group of biodegradable polymer materials. They are extensively applied in biomedical purposes as their characteristics such as biodegradability, mechanical features, and porosity could be custom-made for the particular usage throughout their production and a lot of are also appropriate for printing purpose [16]. Amongst them, aliphatic polyesters are the greatest group potentials as their ester group is certainly available by enzymes (human). Their degradation degree can be regulated by observing their synthesis and conditions of polymerization or introduction of particular functional groups. In addition, their degradation by products are accepted by the living cells and also can be eliminated by the usual metabolism [13]. The utmost common polyesters are polyglycolic acid (PGA) and polylactic acids (PLA) that can be easily modified to form their copolymers. Both PLA and PGA have been revealed to own excessive capability to sustenance the adhesion and propagation of cells. Moreover, the by-products of the degradation of those polymers are lactic acid, and glycolic acid which does not own any cytotoxicity, and easily eliminated from the body by usual physiological metabolism [3]. PCL (poly-ε-caprolactone) is a sustainable substitute to the usage of PLA or PGA polymers. Amongst the synthetic polymers, PCL possesses poor mechanical characteristics but recently it has been considered due to its greater viscoelasticity and to its flexible rheological characteristics that permit its use for the preparation of widespread scaffolds [17].

1.6 Natural Polymers for Scaffolds

Natural polymers which comprise polysaccharides or proteins could be chosen to synthetic polymers as their repeating entities (monosaccharaides, and amino acids) are supplementary alike to those generally metabolized by the living organisms (human body) and also as they own proper requisite structural organizations for cells within their molecules [18]. Collagen is the utmost plentiful structural protein of the humans, is possibly the supreme used biopolymer in regenerative medicines. It is generally obtained from porcine, bovine, and equine of animals. It has potential in cartilage, and bone tissue engineering [19]. Collagen retains degradability characteristics and its biodegradation possibly will be completed by collagenase, and lysosomal enzymes. Crosslinking

would be possible important modification of collagen which can be controlled [20]. Gelatin is another protein polymer which is a renowned biodegradable and cytocompatible material, and is a derivative (molecular) of collagen (type I). Though gelatin has poor molecular organization but due to the presence of almost similar molecular composition like collagen it could be a good substitute of collagen in case of biomaterial functions [9]. Moreover, another protein has currently exposed excessive usage in regenerative medicine is silk (fibroin), that is extracted from the silkworm cocoon (Bombyx mori) which can be degraded by hydrolases (human) [21]. Polysaccharides are also attaining attention among because of their capability to activate particular cell signaling. Hyaluronan is also extra cellular matrix's component and thus it offers excellent cytocompatibility with tissues, and cells. Moreover, hyaluronan own outstanding solubility in water that contributes to a very short existence period next to its imbedding and prompt resorption [22]. Alginate is a polysaccharide based polymer which can be isolated from brown algae, and it comprises as an inflammatory bioactive components. Though purification of the polymer limits its application in tissue engineering, tissue forming alginate is a suitable material for scaffolds, and it does not prompt host response up to one year [23]. On the other hand, chitosan that is the derived of chitin, and can be obtained through the N-deacetylation of chitin polysaccharide which is the main constituents of exoskeleton of crustacean, is frequently applied for scaffold manufacturing. Recently chitosan has revealed to activate hemostasis and platelet triggering. Numerous chitosan based scaffolds have been by now accepted for commercial wound dressings, the scaffolds are unable to overawe the matter of injury chronicization. Recently a chitosan with silk (fibroin) patch seeded with ADSC (adipose-derived stem cells) for scaffolds in particularly diabetic wound curing, and exposed a great capability of the material to improve wound remedial rate [24].

1.7 Properties of Scaffolds and Various Forms

As the choices for scaffolds comprise a widespread range of polymer materials. Polymers having the huge mechanical characteristics may contribute to their applicability in different usages. Since polysaccharides own poor strength and firmness, they can be used in soft tissue restoration purposes, whereas fibrous proteins usually provide mechanical strength to living structures, and can be employed for hard tissues. In addition, overall mechanical strength of the scaffolds mostly governed by the manufacturing process, that frequently modifies the functions of the macro molecular materials. Taking into account this feature, scaffolds of the same material may be designed as hydrogel, porous, and fibrous scaffolds.

Porous scaffolds constitutes sponges, and foams, and their porous network can be regulated during process. They own comparatively low mechanical properties which limits their application ranges. Hydrogels are capable to swell in water due to their crosslinked networks, and they have the similarity with GAG (glycosaminoglycan) biochemically that is a constituent of extracellular matrix. Hydrogels can be formed either by chemical gelation or on physical gelation. In case of chemical gelation, biocompatible properties could be retained through controlled process by avoiding the formation of toxic components. However, some advances in nano sized hydrogel formation with highly controlled organizations were reported [25]. Mechanical strength of hydrogels by integrating numerous materials, also as nanoparticles such as calcium phosphates, silica nanoparticles were revealed as modified [26]. In addition, soft mechanical characteristics of hydrogel form of polymers have been used cellular encapsulation and transportation particularly in cardiac tissue engineering [27].

Scaffolds of structural organizations that mimic tissue structure at a micro level can be achieved by the formation of fibrous scaffolds. Nano sized fibrous scaffolds has all potentials to be used in tissue regenerations as it exhibits high surface to volume ratio in combination of micro porous structure that enhances cellular responses [11].

1.8 Methods of Designing Fibrous Scaffolds and Electrospinning

Methods employed to synthesized nanofibrous scaffolds comprise i) electrospinning, ii) self-assembly and iii) phase separation. EHD (Electro-hydrodynamic) methods that contain electrospinning, and electrospraying had robust effect to the development of biomaterials and drug transport research arenas throughout the last 20 to 30 years. The processes that utilize electrostatic forces to make fibers with different structural and morphological properties are said as electro-hydrodynamic (EHD) methods. Such fabrication methods can be employed by amending the methods, polymer solution properties and other parameters. EHD methods can be applied specifically to drug transportations as well as encapsulation and regulation of drugs in the drug delivery system. Electrospraying and electrospinning are two possible approaches can be applied either individually or at the same time to get the desired structures.

Electrospraying is an encouraging method for the fabrication of particles in the micro level. Electrospraying is possibly a one-step method that requires strong electric field, and usually leads to greater loading proficiency, and thinner particle distributions. Electrospraying method is alike to electrospinning and both methods can be applied with the similar equipmental setup.

Electrospinning is a cost effective, simple and tailor-made approach to produce scaffolds of 3D shape with particularly nano sized fibers. A common setup of electrospinning machine contains of three basic components such as a high electric voltage power supply, a grounded metal collector, and a solution tank linked with an electro-spinneret [28]. Solution properties, the operational (processing) parameters are crucial for the physical, morphological, and biomechanical characteristics of scaffolds.

The polymer solution is ejected in the direction of a metal collector (grounded) in electrospinning. At first, a drop of the liquid (polymeric) is shaped at the tip of the electro-spinneret. While a pump is associated to the reservoir (polymer liquid) that forces the liquid to out. After the electrical field is employed, electric charge drives the liquid to the grounded collector. With the increase of electric voltage, electrical field raises, and thus repulsive forces in the liquid and attraction between the oppositely charged collector and liquid arise. This results the elongation of the drop initially shaped at the tip. With the increasing electric field, a critical point has established in where the liquid surface tension will be well-adjusted by the forces (electrostatic) and thus the Taylor cone formation will result. The polymer liquid at that point, ejected from the edge of the cone resulting in thinner fibers with the adjustable diameters. During travelling under the electrical field, the polymer flow experiences an instability (bending) that rises the path and the time it requisites to arrive the collector, causes jet withdrawing and vaporization of the solvent followed by the formation of fibrous scaffolds [29].

The fundamental electrospinning set-up as well as the process itself is simple in compare to the several parameters for most outcome from the process. Parameters that affect the spinning method can be categorized as three major categories: solution parameters, process parameters, and ambient parameters.

The solution parameters could be adjustable, comprising with polymer, concentration, and molecular weight as well as surface tension, viscosity, and electrical conductivity of the electrospinning liquid. This is governed mostly by the choice of solvent as well as choice of polymer. Fiber morphology such as diameter, and pore size are also determined by the solution concentration, and lower concentration of polymer liquid leads to beads formation rather than continuous fiber [30].

Process parameters include distance from needle tip to collector, flow rate, applied voltage, design, and geometry of collectors. Higher flow rate must require in case of volatile solvents along with

higher voltage to discharge the liquid to the collector. Higher flow rate may cause thicker fibers from the thicker liquid jet which may also cause of beaded fibers or chances to remaining solvent on the collector. The optimal voltage will be influenced by conductivity, viscosity, and surface tension. Sometimes greater voltages lead to narrower fibers for the wide-ranging stretching of the electrospinning liquid, and also responsible for beaded fibers. The distance from needle tip to collector with an applied voltage and with the solution flow rate may also be the prime concerns. There should be the minimum distance for the liquid jet getting enough time to dry until it arrives the surface of the collector as under high electric voltage, evaporation of solvent is secured during the electrospinning [31].

Surrounding temperature also affects the vaporization rate of the solvent and as well the viscosity of the solution. Viscosity will be higher at lower temperature, and thus lead to thick fibers. Relative humidity which depends on the nature of liquid (polymer solution) also effects the fiber morphology, and at low relative humidity thicker fiber will be resulted from hydrophilic polymers when it will be dissolved in aqueous solution as faster solvent evaporation will lead to solution solidification before it will exit the spinneret [32].

1.9 Bi-Polymeric Blend and Core-sheath Electrospun Scaffolds

The traditional electrospinning method is the blend or single flow electrospinning, where all the component polymers are mixed together using a single solvent system. Blend electrospinning allows the encapsulation of both hydrophilic and lipophilic biomolecules. Polymer blending is a suitable physical modification method to blend the characteristics of diverse polymers or to produce new properties. Blending removes the condition to development new polymeric materials or copolymers and thus can modify a material with the preferred properties through a thermally focused mixing of two or more polymers. Many polymers from natural and synthetic sources have been considered for PLA blends for usage in a diversity of uses such as biomedical, textiles, consumer products, and packaging materials. In compare to blend electrospinning, core-sheath electrospinning is an innovative modification of the electrospinning technique that holds the use of two nozzles having the same center, and connected to a high voltage. By using two separate pumps with individual control of the of liquid flow rate, the polymer liquids are directed from respective polymer reservoirs into the coaxial spinneret. This set-up avoid any mixing of the liquids, and only become in interaction at the tip of the electro-spinneret where the ends of the nozzles terminate. This core-sheath setting resulted in fibrous scaffolds having a structure that can

be used as carriers of drugs and other bioactive biological molecules. Core-sheath electrospinning is widely employed to protect bioactive component by the use of two distinct solutions that could minimize the interaction between them, and thus shielding the inner solution from the environs. Electrospinning parameters in coaxial electrospinning are as usual the polymer concentrations and the ratio amongst the flow rate of the inner and the outer solution. Inner solutions with lower flow rate have been ascribed as more favorable towards a steady process [33]. As the electrospun fibers can be applied as a scaffold for tissue engineering due to a comparable morphology to extracellular matrix. The intrinsically great surface to volume proportion of electrospun scaffolds can improve loading of drug, transfer of mass, attachment of cell, cell proliferation, and cell differentiation. With this better role in drug transport as said above, the core-sheath fibers with controlled discharge are established to have improved performance than single polymeric fibers on tissue regeneration [33]. The core-sheath fibrous scaffold own mechanical properties near to the structural site where the scaffolding is to be embedded. Natural polymers such as gelatin, chitosan, and collagen generally have weak physical characteristics. The mechanical characteristics of core-sheath PLA and chitosan nanofibrous scaffolds with changed compositions showed better mechanical strength than that of the single polymeric scaffolds [34]. Core-sheath TCP (tricalcium phosphate) and PLA fibrous scaffolds were investigated for the drug release pattern, and tissue engineering (bone) areas. Constant release was revealed for coaxial scaffolds and the rate of discharge continued equally for about 36 days [31]. Core-sheath PCL-gelatin electrospun nanofibrous into gelatin matrix (hydrogel showed the required mechanical strength to enhance the cell proliferation of stem cells (bone marrow mesenchymal) [35].

1.10 Electrospinning and Wound Healing

Wound dressings were initially invented from natural polymers to only shield the injuries. This has changed to the current day whereby synthetic materials can be invented by numerous progressive technologies to produce multifunctional wound bandages. Two necessary requirements of proper present wound coverings comprise fast hemostasis characteristics and worthy antibacterial characteristics. The goal of a wound covering is to attain fast hemostasis function and it might also own upright antibacterial characteristics to avoid contagions from nearby bacteria. Electrospinning has concerned more attention for its changeability to produce nanofibrous scaffolds for wound bandage that can produce a moist environs to the wound region to encourage curing. Several scaffolds stated for the skin tissue regeneration but greatly porous

nanofibrous structure have received more attraction because of their fibrous structural similarity to extracellular matrix, proficiency for assistance of nutrients interchange and elimination of metabolic left-over; and capability to contain the permeation of microbes because of small size of pore. There are sufficiently of natural macro molecules being used for nanofiber scaffolds production with uses as skin replacements and wound coverings. Chitosan based nanofibrous mats have been perceived to function improved manner than sponges of chitosan considering cell adhesion, cellular growth and as well differentiation of endothelial, keratinocytes, and fibroblasts cells. Currently, the use of ultrathin bioceramic fibers has been stated for their usage in skin restoration. It has been reported that natural polymer based electrospun scaffolds can encourage cell adhesion and propagation whereas the synthetic polymer based scaffolds offers the stability of scaffolds. The electrospun PLGA nanofibrous structures were applied to make a mat and revealed that skin keratinocytes (human) can propagated on the scaffold and enter into the scaffold. However, a no. of core-sheath and blend bi-polymeric (natural, and synthetic) scaffolds were also investigated towards wound covering for prompt curing [4].

1.11 Study Background

PLA (Polylactic acid) is one of the supreme encouraging biopolymers that can be obtained from non-hazardous renewable feedstock. PLA has appeared as a vital polymer material for biomedical purposes considering of its cytocompatibility, biodegradability, good mechanical properties and processable properties. In addition, lactic acid can be found by sugar fermentation, and resulted from renewable sources such as sugarcane, corn etc. PLA is therefore an environment-friendly polymer with no cytotoxic features which allow the use of PLA in the living cells. Though PLA has a widespread of usages, there are definite restrictions for its poor degradation rate, hydrophobic properties, and poor control of toughness related its usage. Blending of PLA with other polymers especially natural polymers provides appropriate choices to mend allied features or to produce new PLA polymers or blends for targeted purposes. A no. of PLA blends have been recommended for numerous biomedical purposes such as drug transport, transplants, sutures and tissue regeneration. PLA with their copolymers are gradually attractive to use in tissue regeneration for its function of repairing of damaged tissues for their exceptional cytocompatibility and mechanical strength [36]. On the other hand, hydrophobic bioactive components that are easily soluble in organic solvent systems can be directly miscible into the solution of PLA for electrospun fibers, and hydrophilic bioactive components which are soluble in water can be easily incorporated into PLA through

water-oil emulsifying agents. This agreeing for an economical, and simple method for electrospinning of bioactive component loaded nanofiber scaffolds which resulted higher loading of such components as well higher encapsulation efficiency of other bioactive component transportation technologies [11]. Natural polymers alike gelatin, collagen, chitosan, and silk fibrin polymers, and synthetic polymers which are biodegradable alike PLA, PGA, PCL, and PLGA are now encouraged in scaffold preparations. Electrospun scaffolds prepared by collagen promote cell progression and the permeation of cells into the fibrous matrix, and it is the utmost biomimetic replacements of the skin [6]. It has been revealed that natural polymers like gelatin, and collagen are capable to encourage cell adhesion and propagation whereas the synthetic polymer like PLA offers the stability of scaffold [2]. Tissue regeneration applications with the advanced technology such as coaxial electrospinning could be a choice in the combination of hydrophobic PLA with hydrophilic gelatin, or collagen. Co-axial electrospinning has developed as a technique to spin fibers with a core-sheath morphology, where one bioactive component is used as the core, and the other bioactive component is used as sheath material, and the choice of materials as core or sheath widely governed by the end uses of the scaffolds [11]. Considering the continuous demand of suitable wound dressings, this study was targeted to combine PLA or copolymer of PLA with gelatin or collagen through electrospinning to obtain the electrospun blend, and core-sheath scaffolds for further wound healing applications.

1.12 Aim of the Study

The definitive goal of the study was to prepare electrospun nanofibrous scaffolds by using hydrophobic synthetic polymer, PLA or its copolymer with natural hydrophilic polymers such as gelatin or collagen applying blend, and coaxial electrospinning technology for wound dressing purposes. PLA was aimed to modify by grafting vinyl acetate (VAc) onto it using lithium tetrahydridoaluminate ($LiAlH_4$) or benzoyl peroxide (BPO). Acid-soluble collagen (ASC) was expected to be extracted from waste Tilapia fish skin. Electrospun nanofibrous scaffolds from PLA and gelatin blend solutions with Tween 80, and core-sheath nanofibrous scaffolds using gelatin or collagen as core material, PLA or VAc grafted on PLA as sheath material were aimed to prepare to get the utmost properties of the polymers. With subsequent characterizations, all scaffolds were targeted to analyze for the observation of their efficiency in cellular environments through in vivo and in vitro analysis.

1.13 Objectives of the Study

The conclusive objectives of the present research work are:

Modification of polylactic acid to prepare vinyl acetate grafted polylactic acid.

Extraction of acid soluble collagen from waste Tilapia fish skin.

Characterization of PLA, gelatin, and acid soluble collagen.

Preparation of electrospun PLA-gelatin blend scaffolds.

Preparation of electrospun core-sheath scaffolds by considering gelatin or acid soluble collagen as core, and PLA or vinyl acetate grafted on PLA as sheath.

Characterization of the prepared electrospun scaffolds.

Observation of the properties of scaffolds by applying in vitro and in vivo tests.

References

[1] A. Tathe, M. Ghodke, and A. P. Nikalje, “A brief review: Biomaterials and their apllication,” *Int. J. Pharm. Pharm. Sci.*, vol. 2, no. SUPPL. 4, pp. 19–23, 2010.

[2] A. Bharadwaz and A. C. Jayasuriya, “Recent trends in the application of widely used natural and synthetic polymer nanocomposites in bone tissue regeneration,” *Mater. Sci. Eng. C*, vol. 110, no. January, p. 110698, 2020, doi: 10.1016/j.msec.2020.110698.

[3] M. Mir *et al.*, “Synthetic polymeric biomaterials for wound healing: a review,” *Prog. Biomater.*, vol. 7, no. 1, pp. 1–21, 2018, doi: 10.1007/s40204-018-0083-4.

[4] A. A. Chaudhari *et al.*, “Future prospects for scaffolding methods and biomaterials in skin tissue engineering: A review,” *Int. J. Mol. Sci.*, vol. 17, no. 12, 2016, doi: 10.3390/ijms17121974.

[5] L. A. Smith and P. X. Ma, “Nano-fibrous scaffolds for tissue engineering,” *Colloids Surfaces B Biointerfaces*, vol. 39, no. 3, pp. 125–131, 2004, doi: 10.1016/j.colsurfb.2003.12.004.

[6] A. Repanas, S. Andriopoulou, and B. Glasmacher, “The significance of electrospinning as a method to create fibrous scaffolds for biomedical engineering and drug delivery applications,” *J. Drug Deliv. Sci. Technol.*, vol. 31, pp. 137–146, 2016, doi: 10.1016/j.jddst.2015.12.007.

[7] F. Ebrahimi and H. Ramezani Dana, “Poly lactic acid (PLA) polymers: from properties to biomedical applications,” *Int. J. Polym. Mater. Polym. Biomater.*, vol. 71, no. 15, pp. 1117–1130, 2022, doi: 10.1080/00914037.2021.1944140.

[8] R. Parenteau-Bareil, R. Gauvin, and F. Berthod, “Collagen-based biomaterials for tissue engineering applications,” *Materials (Basel).*, vol. 3, no. 3, pp. 1863–1887, 2010, doi: 10.3390/ma3031863.

[9] J. B. Rose *et al.*, “Gelatin-based materials in ocular tissue engineering,” *Materials (Basel).*, vol. 7, no. 4, pp. 3106–3135, 2014, doi: 10.3390/ma7043106.

[10] P. Saini, M. Arora, and M. N. V. R. Kumar, “Poly(lactic acid) blends in biomedical applications,” *Adv. Drug Deliv. Rev.*, vol. 107, pp. 47–59, 2016, doi: 10.1016/j.addr.2016.06.014.

[11] M. Santoro, S. R. Shah, J. L. Walker, and A. G. Mikos, “Poly(lactic acid) nanofibrous scaffolds for tissue engineering,” *Adv. Drug Deliv. Rev.*, vol. 107, pp. 206–212, 2016, doi:

10.1016/j.addr.2016.04.019.

[12] "Book Reviews," *Nature*, vol. 171, no. 4351, p. 503, 1953, doi: 10.1038/171503a0.

[13] L. Parisi, A. Toffoli, G. Ghiacci, and G. M. Macaluso, "Tailoring the interface of biomaterials to design effective scaffolds," *J. Funct. Biomater.*, vol. 9, no. 3, pp. 1–31, 2018, doi: 10.3390/jfb9030050.

[14] F. J. O'Brien, "Biomaterials & scaffolds for tissue engineering," *Mater. Today*, vol. 14, no. 3, pp. 88–95, 2011, doi: 10.1016/S1369-7021(11)70058-X.

[15] S. Chahal, A. Kumar, and F. S. J. Hussian, "Development of biomimetic electrospun polymeric biomaterials for bone tissue engineering. A review," *J. Biomater. Sci. Polym. Ed.*, vol. 30, no. 14, pp. 1308–1355, 2019, doi: 10.1080/09205063.2019.1630699.

[16] B. Dhandayuthapani, Y. Yoshida, T. Maekawa, and D. S. Kumar, "Polymeric scaffolds in tissue engineering application: A review," *Int. J. Polym. Sci.*, vol. 2011, no. ii, 2011, doi: 10.1155/2011/290602.

[17] N. Siddiqui, S. Asawa, B. Birru, R. Baadhe, and S. Rao, "PCL-Based Composite Scaffold Matrices for Tissue Engineering Applications," *Mol. Biotechnol.*, vol. 60, no. 7, pp. 506–532, 2018, doi: 10.1007/s12033-018-0084-5.

[18] D. F. Williams, "On the mechanisms of biocompatibility," *Biomaterials*, vol. 29, no. 20, pp. 2941–2953, 2008, doi: 10.1016/j.biomaterials.2008.04.023.

[19] M. E. Nimni *et al.*, "Biochemical differences between dystrophic calcification of cross-linked collagen implants and mineralization during bone induction," *Calcif. Tissue Int.*, vol. 42, no. 5, pp. 313–320, 1988, doi: 10.1007/BF02556366.

[20] L. Buttafoco *et al.*, "Electrospinning of collagen and elastin for tissue engineering applications," *Biomaterials*, vol. 27, no. 5, pp. 724–734, 2006, doi: 10.1016/j.biomaterials.2005.06.024.

[21] Y. Cao and B. Wang, "Biodegradation of silk biomaterials," *Int. J. Mol. Sci.*, vol. 10, no. 4, pp. 1514–1524, 2009, doi: 10.3390/ijms10041514.

[22] I. Velter, B. La Ferla, and F. Nicotra, *Carbohydrate-based molecular scaffolding*, vol. 25, no. 2–3. 2006. doi: 10.1080/07328300600733020.

[23] P. De Vos, B. J. De Haan, G. H. J. Wolters, J. H. Strubbe, and R. Van Schilfgaarde, "Improved biocompatibility but limited graft survival after purification of alginate for microencapsulation of pancreatic islets," *Diabetologia*, vol. 40, no. 3, pp. 262–270, 1997,

doi: 10.1007/s001250050673.

[24] Y. Y. Wu *et al.*, "Experimental study on effects of adipose-derived stem cell-seeded silk fibroin chitosan film on wound healing of a diabetic rat model," *Ann. Plast. Surg.*, vol. 80, no. 5, pp. 572–580, 2018, doi: 10.1097/SAP.0000000000001355.

[25] X. Guan *et al.*, "Development of hydrogels for regenerative engineering," *Biotechnol. J.*, vol. 12, no. 5, pp. 1–19, 2017, doi: 10.1002/biot.201600394.

[26] J. R. Xavier *et al.*, "Bioactive nanoengineered hydrogels for bone tissue engineering: A growth-factor-free approach," *ACS Nano*, vol. 9, no. 3, pp. 3109–3118, 2015, doi: 10.1021/nn507488s.

[27] S. Bhutani *et al.*, "Evaluation of Hydrogels Presenting Extracellular Matrix-Derived Adhesion Peptides and Encapsulating Cardiac Progenitor Cells for Cardiac Repair," *ACS Biomater. Sci. Eng.*, vol. 4, no. 1, pp. 200–210, 2018, doi: 10.1021/acsbiomaterials.7b00502.

[28] A. Szentivanyi, T. Chakradeo, H. Zernetsch, and B. Glasmacher, "Electrospun cellular microenvironments: Understanding controlled release and scaffold structure," *Adv. Drug Deliv. Rev.*, vol. 63, no. 4, pp. 209–220, 2011, doi: 10.1016/j.addr.2010.12.002.

[29] T. J. Sill and H. A. von Recum, "Electrospinning: Applications in drug delivery and tissue engineering," *Biomaterials*, vol. 29, no. 13, pp. 1989–2006, 2008, doi: 10.1016/j.biomaterials.2008.01.011.

[30] N. Okutan, P. Terzi, and F. Altay, "Affecting parameters on electrospinning process and characterization of electrospun gelatin nanofibers," *Food Hydrocoll.*, vol. 39, pp. 19–26, 2014, doi: 10.1016/j.foodhyd.2013.12.022.

[31] J. Zeng *et al.*, "Influence of the drug compatibility with polymer solution on the release kinetics of electrospun fiber formulation," *J. Control. Release*, vol. 105, no. 1–2, pp. 43–51, 2005, doi: 10.1016/j.jconrel.2005.02.024.

[32] J. Pelipenko, P. Kocbek, B. Govedarica, R. Rošic, S. Baumgartner, and J. Kristl, "The topography of electrospun nanofibers and its impact on the growth and mobility of keratinocytes," *Eur. J. Pharm. Biopharm.*, vol. 84, no. 2, pp. 401–411, 2013, doi: 10.1016/j.ejpb.2012.09.009.

[33] Y. Lu *et al.*, "Coaxial electrospun fibers: applications in drug delivery and tissue engineering," *Wiley Interdiscip. Rev. Nanomedicine Nanobiotechnology*, vol. 8, no. 5, pp.

654–677, 2016, doi: 10.1002/wnan.1391.

[34] T. T. T. Nguyen, C. Ghosh, S.-G. Hwang, N. Chanunpanich, and J. S. Park, “Porous Core/Sheath Composite Nanofibers Fabricated by Coaxial Electrospinning as a Potential Mat for Drug Release System,” *Int. J. Pharm.*, vol. 439, no. 1–2, p. 296, 2012.

[35] D. Kai, M. P. Prabhakaran, B. Stahl, M. Eblenkamp, E. Wintermantel, and S. Ramakrishna, “Mechanical properties and in vitro behavior of nanofiberhydrogel composites for tissue engineering applications,” *Nanotechnology*, vol. 23, no. 9, 2012, doi: 10.1088/0957-4484/23/9/095705.

[36] M. S. Singhvi, S. S. Zinjarde, and D. V. Gokhale, “Polylactic acid: synthesis and biomedical applications,” *J. Appl. Microbiol.*, vol. 127, no. 6, pp. 1612–1626, 2019, doi: 10.1111/jam.14290.

CHAPTER TWO

MATERIALS AND METHODS

Chapter Two

Materials and Methods

2.1 Materials

2.1.1 Polylactic acid

Polylactic acid (PLA), NatureWorksTM 3025 D, was obtained from NatureWorks LLC, USA.

2.1.2 Gelatin

Gelatin (bovine skin, Type B was purchased from Sigma Aldrich, USA.

2.1.3 Acid Soluble Collagen

Acid soluble collagen was extracted from waste Tilapia fish skin, local market, Dhaka.

2.1.4 Protein Marker

Protein marker was purchased from Sigma Aldrich, USA.

2.1.5 Vero Cell Line

Kidney epithelial cells extracted from an African green monkey which was preserved in DMEM (Dulbecco's Modified Eagles' medium).

2.1.6 Chemicals

The following chemicals were used for the entire experiment.

Sl No.	Name of Chemicals	Producers
1	Vinyl acetate (VAc)	Sigma Aldrich (USA)
2	Lithium tetrahydridoaluminate ($LiAlH_4$)	Sigma Aldrich (USA)
3	Benzoyl peroxide (BPO)	Sigma Aldrich (USA)
4	Tetrahydrofuran (THF)	Sigma Aldrich (USA)
5	Methanol (MeOH)	Merck (India)
6	Calcium oxide (CaO)	Merck (India)
7	N, N-dimethylformamide (DMF)	Merck (India)
8	Dichloromethane (DCM)	Merck (India)
9	TWEEN® 80 (T80, 1%, 400 - 620 mPa.s)	Sigma Aldrich (USA)
10	Sodium hydroxide (NaOH)	Merck (India)

11	Butan1-ol	Merck (India)
12	Acetic acid (AcOH)	Merck (India)
13	Sodium chloride (NaCl)	Merck (India)
14	Na-acetate buffer (pH- 2.9 to 3.1)	Sigma Aldrich (USA)
15	Ninhydrin reagent	Merck (India)
16	Tris–HCl buffer (0.5 M, pH 6.8)	Sigma Aldrich (USA)
17	Glycerol	Merck (India)
18	β-mercaptoethanol	Sigma Aldrich (USA)
19	Sodium dodecyl sulphate	Sigma Aldrich (USA)
20	Bromophenol blue	Sigma Aldrich (USA)
21	Coomassie Brilliant Blue	Sigma Aldrich (USA)

2.1.7 Apparatus and Instruments

The following instruments were used to characterize, and analysis of the prepared materials.

Sl No.	Apparatus/ Instruments
1	Water bath
2	Oven
3	Autoclave
4	Electro spinneret
5	Heating mantle
6	Hot plate with magnetic stirrer
7	Centrifuge machine
8	Shaking incubator
9	Incubator
10	Optical Microscope
11	Bio-safety cabinet
12	Amino acid analyzer
13	Contact angle analyzer
14	X-ray diffractometer
15	Thermal analyzer (STA)
16	FT-IR spectrometer
17	Field emission scanning electron microscope (FESEM)

Figure 2.1 Instruments used for the study (A) Electro spinneret, (B) FT-IR spectrometer, (C) X-ray diffractometer, (D) Thermal analyzer, (E) Amino acid analyzer, (F) Gel electrophoretic system

Figure 2.2 Instruments used for the study (G) Oven, (H) FESEM, and (I) Optical Microscope, (J) Contact angle analyzer

2.2 Preparation of Modified PLA

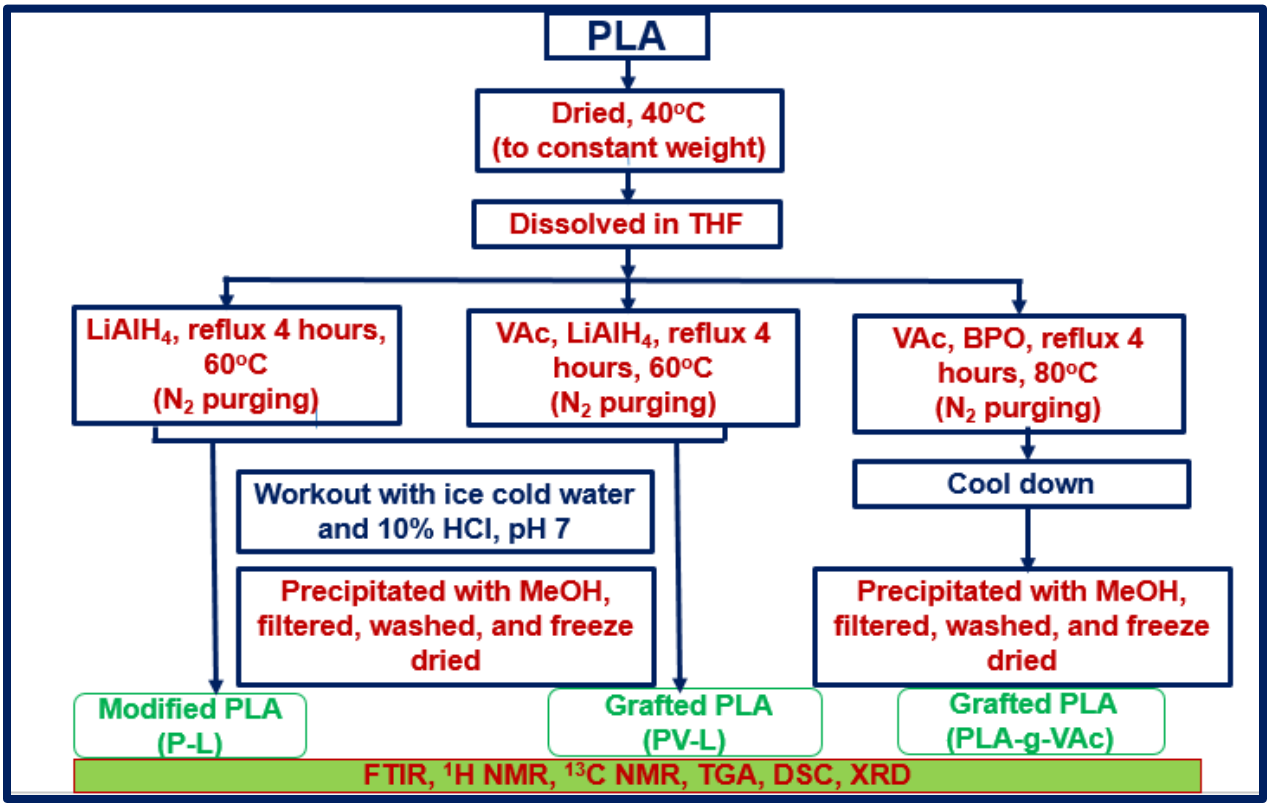

Figure 2.3 Process flow diagram PLA modifications (Preparation of P-L, PV-L, and PLA-g-VAc)

PLA was dried (at 40 ^{o}C for 72 hours) in an oven to a constant weight and then kept in a desiccator for further use. Solvents such as THF and methanol that used for the preparation and subsequent purification were distilled with calcium oxide. Dried PLA (1.35 g, 15 m mol) was taken in a three neck round bottom flask and was dissolved in THF (25 ml) with continuous stirring at room temperature. The number of moles of PLA was calculated taking as the molecular weight of the repeating unit of PLA. $LiAlH_4$ (1.14 g, 30 m mol) was then added to the solution and refluxed the resultant solution in an oil bath for 4 hours at 60 ^{o}C with moderate stirring and N_2 purging. It was then cooled and around 3 ml of ice cold water was added to destroy the excess reagent. The resultant solution showed the alkaline pH (9.5), it was then hydrolyzed by the addition of 10% ice cold HCl until the pH was 7. Sufficient methanol was added for the precipitation of the desired macromolecule. The precipitate was separated through filtration, washed several times with methanol and dried through freeze drying process and labeled as P-L. Grafted copolymer (PV-L) was prepared taking PLA (1.35 g, 15 m mol) and VAc(1.3 g, 15 m mol) together in a three neck

round bottom flask and was dissolved in THF (25 ml) with continuous stirring at room temperature and then $LiAlH_4$ (1.14g, 30 m mol) was added following the same procedure that mentioned for the preparation of P-L. Grafted copolymer (PLA-g-VAc) was prepared taking PLA (2.25 g, 25 m mol) and VAc (1.13 g, 13 m mol) together in a three neck round bottom flask and was dissolved in THF (50 ml) with continuous stirring at room temperature and then BPO (1.12 g, 0.5 m mol) was added to the solution. The resultant solution was refluxed in an oil bath for 4 hours at 80 ^oC with moderate stirring and N_2 purging. It was then cooled and sufficient methanol was added for the precipitation of the desired macromolecule. The precipitate was separated through filtration, washed several times with methanol and dried through freeze drying process and labeled as PLA-g-VAc.

2.3 Characterizations of PLA, and Modified PLA

2.3.1. Viscosity Measurement of PLA

The viscosity of the PLA was measured from solutions of different concentrations of PLA (0, 0.01, 0.015, 0.020 and 0.025 g/ml) in chloroform using Anton Paar Lovis falling ball type viscometer with Lovis current capillary (1.59 Steel) which was before calibrated with Millipore water. The relative viscosity, inherent viscosity, specific viscosity, and reduced viscosity were determined from these solutions and presented in Table 2.1. From the plot of the reduced viscosity against the concentration with a R^2 value of 0.927, the intrinsic viscosity was obtained by extrapolating the line to infinite dilution (zero concentration) of the studied polymer solutions. Intrinsic viscosity that is the intersection point with the y-axis was determined by using Huggins equation,

$$\eta_{sp}/c = [\eta] + k_H [\eta]^2 c \qquad (1)$$

where η_{sp} is the specific viscosity, c is the concentration (g/dl), and k_H is the Huggins constant. The intrinsic viscosity of the PLA solution by considering Huggins constant is thus obtained 35.15794 ml/g.

Table 2.1 Viscosity measurement of PLA in chloroform

PLA Concentrations (g/ml)	Relative Viscosity	Inherent Viscosity (ml/g)	Specific Viscosity	Reduced Viscosity* (ml/g)
0	-	-	-	-
0.010	1.474	38.7931	0.474	47.3928
0.015	1.761	37.7249	0.761	50.7324
0.020	2.109	37.3061	1.109	55. 4404
0.025	2.605	38.2916	1.605	64.1852

*standard error within 0.00002 to 0.00005 ml/g

2.3.2. Solubility Test

20 mg of each sample was tried to dissolve into different (common organic solvents) solvents of the same volume at room temperature and their solubility behavior in those solvents were tabulated.

2.3.3 Infrared Spectroscopy

IR spectra were recorded on an IR Prestige-21 spectrometer, Schimadzu, Japan, by casting KBr plate. Wave number of 4000 to 400 cm^{-1} was used to obtain the spectra with a resolution (spectral) of 8 cm^{-1} and the no. of scans as 64.

2.3.4 Nuclear Magnetic Resonance Spectroscopy

BRUKER Ascend ^{TM} Spectrometer, BRUKER BioSpin AG, Switzerland, operating at 400 MHz was used to record all the ^{1}H-NMR and ^{13}C-NMR spectra of the materials by using $CDCl_3$ as solvent.

2.3.5 Thermogravimetric Analysis

TGA-50H.tad, Shimadzu, Japan was used to record the thermal decomposition pattern of PLA, P-L, PV-L, and PLA-g-VAc taking 5 mg of each sample (priorly dried in an oven below 40 ^{o}C for 24 h) in an aluminum pan and within the temperature range from room temperature to 600 ^{o}C with heating rate as 10 ^{o}C min^{-1} in a nitrogen environment. Data obtained from the TGA were plotted with temperature and weight percentage by using Origin Pro 2018-64 bit software. DTG graphs were also plotted from the temperature and the corresponding derivative of weight percentage to recognize the peak decomposition temperature.

2.3.6. Differential Scanning Calorimetry

TA DSC with detector DSC-60, Shimadzu, North America was used to measure the thermal transitions of the materials. Around 2.5 mg of each of the dried powdered samples was sealed in a pan (aluminum) and heated up to 200 ^{o}C at a rate of 10 °C min^{-1} under nitrogen purging at a rate of 20 ml/min. A reference sealed pan (aluminum) was also used for the relative measurement. An isothermal condition was maintained for 1 min and then the sample was cooled at the same rate to 0 °C. It was then heated to 200 °C. Data were considered from the second heating examination to remove the thermal history of the polymer. Glass transition and melting temperature (Tg, and Tm), specific heat capacity (ΔC_p), heat of melting (ΔH_m), were calculated from the thermograms plotted by using Origin Pro 2018-64 bit software.

2.3.7. X-Ray Diffraction (XRD)

An X-ray diffractometer, PW3040/60 X'pert PRO, PANalytical, the Netherlands was used to study the X-ray refection pattern. Copper anode as radiation source of K_α, λ=1.54060 Å was used to attain the data within the angular region as 5 °-75 ° (2θ value) in consideration of 0.01 steps. The instrument was functioned at 40 kV and 30 mA conserving the cooling temperature at 19-20 °C. The achieved curves have been accurately expanded by using X'Pert High Score software. Crystallinity percentage was estimated with the area of the crystalline peaks and the area of all peaks region by using Origin Pro 2018-64 bit software, and crystallite size of the materials were estimated by Scherrer formula, $D = 0.89\lambda/\beta\cos\theta$. Here, D is the crystallite size, λ is the wavelength of X-ray (λ = 0.15406 nm), β is equal to the FWHM (full width at half maximum) in radiance and θ is the Bragg angle of diffraction line. Moreover, lattice parameters were also calculated from the profile of the diffraction allowing for orthorhombic pattern in the crystallite.

2.4 Preparation of the PLA-Gelatin Blend Scaffolds (Pg1-Pg5)

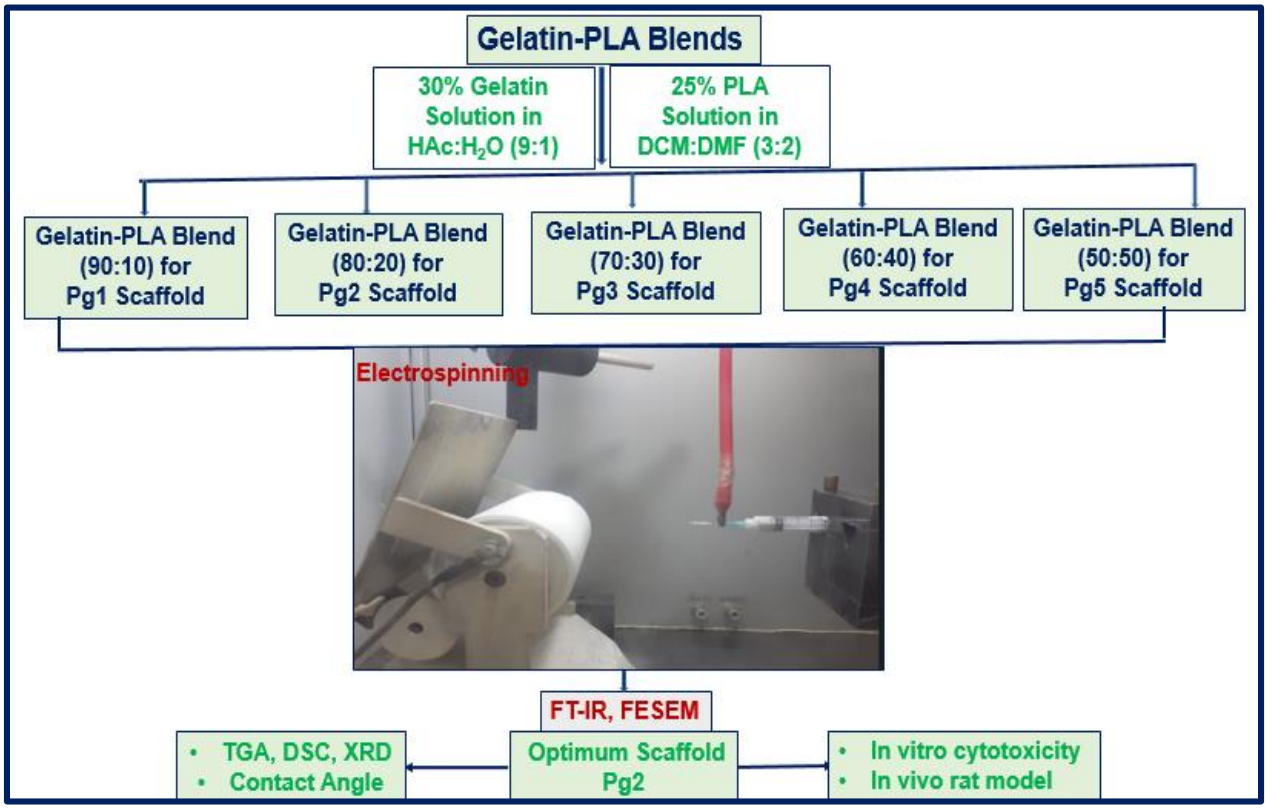

Figure 2.4 Process flow diagram of the preparation, and characterizations gelatin-PLA blend scaffolds (Pg1-Pg2)

2.4.1 Preparation of the Electrospinning Solutions

Different solutions of gelatin varying the ratio of HAc and water (20%, 50%, 70%, and 90% v/v) were prepared by stirring with a magnetic stirrer (rpm 500) for 3 hours at 40^{o}C. Different solutions of PLA varying the ratio of DCM and DMF (1:1, 2:1, and 3:2 v/v) were prepared by stirring with a magnetic stirrer (rpm 500) for 3 hours at 40 ^{o}C. Both gelatin and PLA solutions were tried to electrospun separately to attain the ideal conditions for producing nanofiber scaffolds of them individually. 25 g of PLA (w/v, in DCM and DMF as 3:2) and 30 g of gelatin (w/v, in 90% acetic acid in water) were observed to be good electrospinnable solutions from that fiber mats P, and G were obtained respectively without beads. Gelatin and PLA blend solutions were prepared by using the surfactant T80. Five blend solutions were prepared by mixing the optimum gelatin and PLA solutions at a ratio of 90:10, 80:20, 70:30, 60:40 and 50:50 (from these fiber mats Pg1, Pg2, Pg3, Pg4, and Pg5 were prepared respectively) (v/v) with the addition of 400 µl of T80 solution in distilled water which is 0.5% of the total volume of the blend solutions.

2.4.2 Preparation of the Electrospun Blend Scaffolds (P, G, Pg1-Pg5)

Super ES-1, an electrospinning unit originated from E-SPIN NENOTECH Pvt. Ltd., Indian Institute of Technology, Kanpur, was used for the electrospinning of the polymer solutions. Equipment operated with an input voltage 90-240 VAC+/- from a high voltage power supply (0-30 KV, 20 W, 0-400 μA), one-channel syringe pump of the two-channel syringe pump (flow rate, 0.1μl/sec - 3ml/min), a drum collector (D=100 mm, L=200 mm, 100 - 3500 rpm), a syringe of 5 ml (diameter- 12 mm) with needle (21G), and with other accessories such as aluminium foil paper to wrap the collector drum.

Electrospinning was conducted at room temperature by using a 5 ml syringe (disposable) with a needle (metal, 0.40 mm internal diameter). The pole (positive) of the high voltage source was connected to the tip of the needle of the syringe and the electrode (ground) was used to ground the drum collector. The syringe pump that was connected to the syringe controlled the flow rate. Operating parameters for electrospinning were used in this study as flow rate of 0.1 μl/sec, voltage within 20 kV-25 kV, and needle tip to drum collector distance of 10 cm. Rotation speed of the drum collector was 600 rpm. Electrospun scaffolds were collected on the drum collector covered with aluminum foil. For each scaffold, around 5 ml of polymer solution was used.

2.5 Characterization of Gelatin

Molecular weight of gelatin was measured by measuring the viscosity. The viscosity of gelatin solutions in deionized water was measured with varying concentrations (Table 2.2). Viscometer (Anton Paar Lovis falling ball) calibrated with millipore water was used for the viscosity measurement. A capillary (Lovis current capillary) was filled with the respective solutions (gelatin solutions) using 1 ml syringe, and a standard ball was placed inside the capillary. Viscosity of each solution was measured after reaching equilibrium (temperature) at zero shear rate. The viscosity (relative viscosity, inherent viscosity, specific viscosity, and reduced viscosity) were determined for each solution (Table 2.2). The intrinsic viscosity was obtained by extrapolating the line to infinite dilution (zero concentration) considering the plot of the reduced viscosity versus the concentration of the polymer solutions. Intrinsic viscosity (intersection point with the y-axis) was determined by using Huggins equation,

$$\eta_{sp}/c = [\eta] + k_H [\eta]^2 c \qquad (1)$$

where η_{sp} is the specific viscosity, c is the concentration (g/dl), and k_H is the Huggins constant.

The intrinsic viscosity of the gelatin solution by considering Huggins constant was thus obtained as 18.15 ml/g.

Table 2.2 Viscosity Measurement of gelatin in Deionized Water

Gelatin Concentrations (g/ml)	Relative Viscosity	Inherent Viscosity (ml/g)	Specific Viscosity	Reduced Viscosity* (ml/g)
0.010	1.21	19.76	0.22	21.85
0.020	1.41	17.22	0.41	20.55
0.030	1.73	18.29	0.73	24.37
0.040	2.12	18.76	1.12	27.94

*standard error within 0.02 to 0.05 ml/g

2.6 Measurement of Solution Properties

Elcometer 2300 rv-2 rotational viscometer was used for the determination of the viscosity of eletrospinning solutions. After the homogenization of the solutions, viscosity was measured at 25 ^{o}C temperature and it was measured three times for each solution (standard deviation ±2%).

Table 2.3 Solution properties of electrospinning solutions for scaffolds (P, G, and Pg1-Pg5)

Sample	Composition of Samples			*Viscosity	*Conductivity
	PLA solution %	Gelatin solution %	T80 (0.5%) solution µl	mPa-s	µS/cm
P	100	-	--	74	3.6
Pg1	10	90	400	218	690
Pg2	20	80	400	155	650
Pg3	30	70	400	136	559
Pg4	40	60	400	116	424
Pg5	50	50	400	86	289
G	-	100	400	300	772

*****Viscosity and conductivity values have a standard deviation ±2%

Conductivity of the solutions was measured by using Jenway™ 3540 Bench Combined Conductivity/pH Meter. Conductivity was measured for each homogenized solution at 25 ^{o}C and each solution was considered three times for this measurement (standard deviatio ±2%). Viscosity

and conductivity of the resultant electrospinning solutions with the composition of the solutions were presented in Table 2.3

2.7 Characterizations of Scaffolds (P, G, and Pg2)

2.7.1 Scanning Electron Microscopy (SEM) Analysis

Phenom pro scanning electron microscope and field emission scanning electron microscope FESEM (JSM-7610F) were used to analyze the surface morphology of electrospun scaffolds. All the samples were gold coated to achieve the micrographs. ImageJ-win64 software was used to draw the histogram of the scaffolds followed to determine the fiber diameters and pore size of the scaffolds with standard deviations.

2.7.2 FT-IR Spectroscopy Analysis

IR Prestige-21 spectrometer, Schimadzu, Japan, was used to obtain the FT-IR spectrum of scaffolds by making KBr pellet. 4000 to 400 cm^{-1} wave no. was used to receive the spectra with 8 cm^{-1} as spectral resolution and the no. of scans as 64.

2.7.3 Thermal Analysis

NETZSCH STA 449F5 (NETZSCH-Gerätebau GmbH, Germany) was used to conduct the thermogravimetric analysis to assess the thermal decomposition pattern of electrospun nanofibrous scaffolds. Around 5 mg of samples were heated from room temperature to 500 ^{o}C at a rate of temperature change of 10 $^{o}C\ min^{-1}$ in a nitrogen atmosphere. Derivative thermogravimetric (DTG) data was used to attain the weight loss rate. DTG graphs were also plotted using the temperature and the corresponding derivative of weight percentage. TGA and DTG data were plotted with temperature and weight percentage remaining by using Origin Pro 2018-64 bit software.

Derivative differential colorimetric (DDSC) data was obtained from the same machine to measure the heat flow rate. Around 5 mg of samples were first heated up to 300 ^{o}C at 30 $^{\circ}C\ min^{-1}$ to remove thermal history. This temperature was retained for 5 min and then cooled to room temperature at 10 $^{o}C\ min^{-1}$. Data for the test was obtained by secondly heating up to 300 ^{o}C at 10 $^{o}C\ min^{-1}$ as heating rate. Respective data was plotted by applying Origin Pro 2018-64 bit software.

2.7.4 XRD Analysis

X-ray diffraction studies of all the nanofibrous scaffolds were conducted using PW3040/60 X'pert PRO (PANalytical, The Netherlands). XRD studies was performed in the range of 5^{o} to 70^{o} as 2θ and at 15 °/min as scan speed.

2.7.5 Water Contact Angle Analysis

Nanofibrous scaffolds were analyzed for surface wettability based on deionized water by the water contact angle measurement using optical instrument (Sessile drop method, Format Version: 3.6, KYOWA interFAce Measurement and Analysis System FAMAS, KYOWA). Three measurements for each material were taken by slowly dropping 2 µl of deionized water on the surface of changed locations of the scaffolds. Water contact angle was measured by the angle in the middle of the drop outline and the surface baseline. Average of the data were considered for analysis.

2.7.6 Cytotoxicity Analysis

To assess the cytotoxicity of electrospun scaffolds, experiment was employed by using biological biosafety cabinet (Model: NU-400E, Nuaire, USA), CO_2 incubator (Nuaire, USA), microscope (trinocular with camera, Optika, Italy), and a hemocytometer. Cell cytotoxicity was observed on the Vero cell line, kidney epithelial cells extracted from an African green monkey which was preserved in DMEM (Dulbecco's Modified Eagles' medium) having penicillin–streptomycin (1:1 ratio) as 1%, gentamycin as 0.2%, and FBS (fetal bovine serum) as 10%. The cells of $6.0x\ 10^4$/400 µl were seeded onto 24-well plates and incubated at 37°C and 5% CO_2 for 24 hours. Following day, well was autoclaved and 100 µl sample was added to each well. Cytotoxicity was evaluated under an inverted light microscope (with Optikaproview software) at 40x magnification subsequently 48 hours incubation. Duplicate wells were considered for every sample.

2.7.7 Animal Wound Healing Experiment and Histopathology

The animal model experiments were permitted by the ethical committee of the Faculty of Bioscience, University of Dhaka. A total of eighteen (duplicate exposed rats for each scaffold including two controls) albino rats, male, weight 28–32 g, aged 7 weeks were purchased from the animal house of International Centre for Diarrhoeal Disease Research, Bangladesh. The rats were

raised and kept following the guidelines stated by the National Research Council's Guide for the Care and Use of Laboratory Animals (eight edition), National research council of the national academies, USA. The rats were sacrificed following the AVMA guidelines for the euthanasia of animals: 2020. The anaesthetization of rat was carried out following by IACUC (International Animal Care and use Committee) of the University of Pennsylvania showed guidelines. Ketamine HCl USP Injection IM/IV, was injected in the lower abdomen of rat to make them unconscious for about 15 minutes. The dorsal fur of the rat was shaved with an electric trimmer and the anticipated area of the wound to be created was outlined on the back of the rat on interscapular region i.e. 5 mm away from ears. Skin was prepared and sterilized, and excisions (bilateral, around equal in size, diameter as 1 cm, depth as 1 mm) were made on the skin of rat using a sterile punch. The excised wounds were covered with the fibrous scaffolds (approximately 1.5 cm / 1.5 cm). Each scaffold was applied in duplicate and two rats without any treatment were treated as control. The photographs of the wounds were taken with a camera (13 MP f/1.9 + 5 MP f/2.2 Ultra Wide Angle Camera) at 0, 3, 7, 10, and 14 day after post-surgery to assess the relative wound size reduction (%) which was calculated by using the following equation: Relative wound size reduction (%) = $(L_o - L_t / L_o) \times 100$, where L_o and L_t are the size of wound at 0 and the specific interval of time 't' respectively.

All rats were sacrificed at the day of 14, and the reformed skin tissues with adjacent injury borders were collected. The samples were secured in formalin (10%) with a buffer (neutral), dehydrated, and embedded in paraffin wax, and then block was prepared. Blocks were then cut with the help of microtome machine as 5-µm slides in successive sections. Sections were then deparaffinized with xylene. Staining of the slide tissues were made by haematoxylene (for nucleus) and counter staining with eosin (for cytoplasm). The stained slides were then dehydrated, cleared, mounted, and labelled. Images of stained slides were observed by inverted light microscope (trinocular with camera, Optikaproview software, Optika, Italy) at 10x magnification.

2.8 Preparation of Core-Sheath Gelatin-PLA Scaffolds (CSPG)

Overall preparation of electrospinning solutions, and subsequent scaffolds preparation are presented in Figure 2.6.

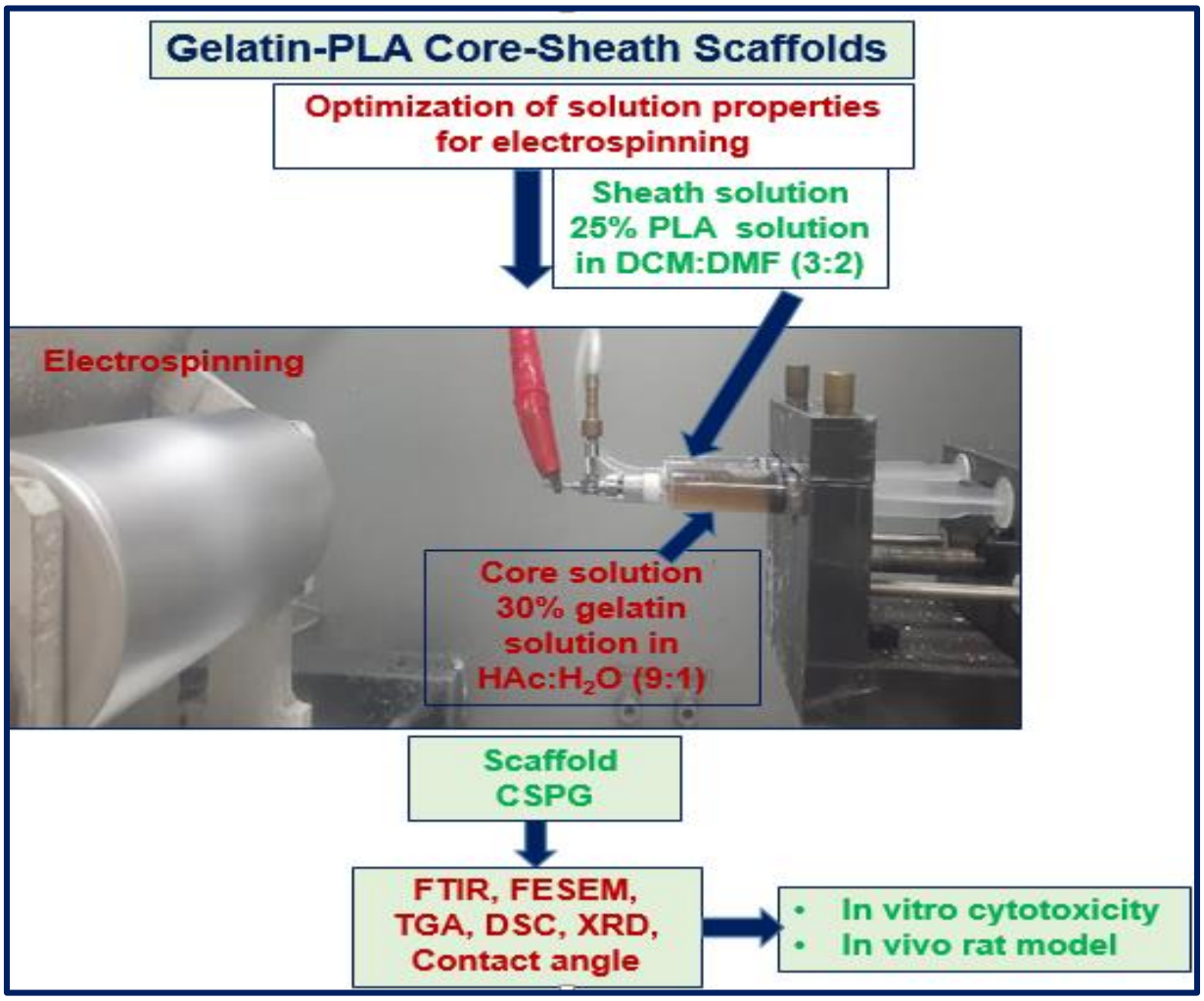

Figure 2.5 Process flow diagram of preparation and characterization of PLA-gelatin core-sheath scaffold (CSPG)

For the preparation of core-sheath scaffolds, single polymeric solutions were taken with the same concentrations as discussed in section 2.4.1, and the same solvent systems were considered.

Electrospinning was accompanied with the same operational parameters (discussed in section 2.4.2) by taking 5 ml of polymer solution. Core-sheath scaffold CSPG was obtained by taking gelatin solution as core, and PLA solution as sheath solution. Core, and sheath solutions were

individually delivered for a double positioned needle originated from E-SPIN NANOTECH, Pvt. Ltd. (Indian Institute of Technology, Kanpur).

2.9 Characterizations of Core-Sheath Gelatin-PLA Scaffold (CSPG)

Scaffold CSPG were characterized by considering FT-IR spectroscopy, field emission scanning electron microscopy, thermal analysis (STA- TGA, and DSC), XRD analysis, water contact angle measurement, in vitro cytotoxicity, and in vivo animal (rat) model test followed by histopathology in the same operational parameters as discussed in section 2.7.

2.10 Extraction of Acid Soluble Collagen (ASC) from Tilapia Fish Skin

Overview of the extraction process are displayed in Figure 2.6.

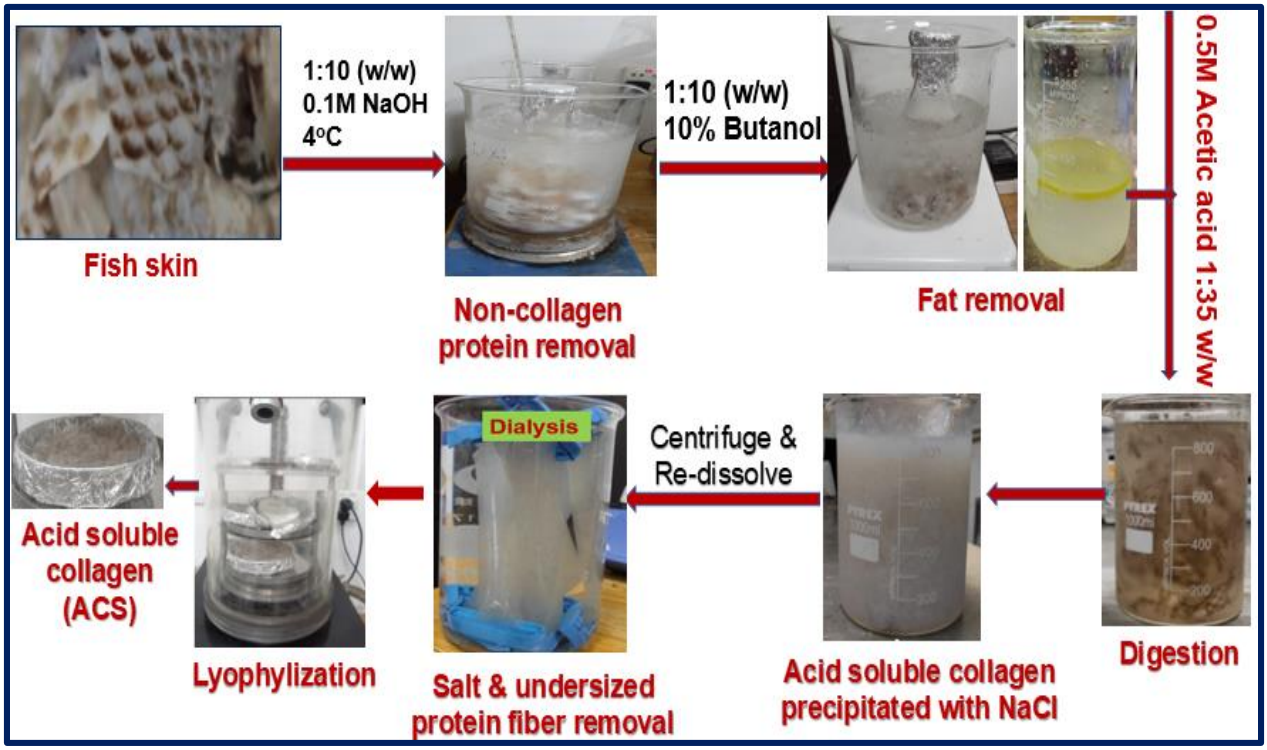

Figure 2.6 Process flow diagram for the extraction of acid soluble collagen (ASC) from Tilapia fish skin

Scales were manually removed from the skin, then the skin was separated from the fillet with subsequent removal of connective tissue, and fat. After washing the skin with distilled water, water

was removed from its surface with the help of kitchen towel. The entire process for the extraction of acid soluble collagen from the tilapia fish skin was carried out by maintaining the temperature as 4 ^{o}C. Skin was then sliced into small pieces, and 40 g of the skin was soaked in 0.1 M NaOH as 1:10 (w/v) ratio for 48 hours at 4^{o}C, and homogenized to take away non-collagenous substances and to exclude the influence of endogenous proteases on collagen. Subsequently it was then washed several times with distilled water until the pH of the wash water was reached to neutral value. Then the fat contents were extracted, and removed from the resultant skin by using butanol (10%) to the sample as the ratio 1:10 (w/v, solid to solvent) with subsequent homogenization for about 24 hours. After removing the fats, it was then washed several times with enough distilled water to remove the butanol from the resultant skin. Further the resulted skin was subjected for the solubilization, and extraction of acid soluble collagen by the gentle homogenization with 0.5 M acetic acid (1:50 as solid to solvent ratio) for about 96 hours. The viscous solution was then separated by using a sieve with subsequent squeezing the resultant skin. Precipitation of acid soluble collagen was done by considering the salting out process with the use of sodium chloride of final concentration as 2M. The precipitate was then separated by centrifugation at 10,000 g for 20 minutes. It was then re-dissolved in 0.5 M acetic acid as 1:5 (w/v) ratio, and dialyzed against 0.1 M acetic acid solution at 4^{o}C for 48 hours by using dialysis bag (membrane) of molecular weight cut-off as 12 kDa with successive change of the dialysis solution at each eight hours. After that the resultant solution was dialyzed several times with distilled water until the neutral pH was achieved in dialysis solution. Afterwards the resultant dialysate was lyophilized and thus obtained acid soluble collagen (ASC).

2.11 Preparation of Electrospinning Solutions and Scaffolds (B, ASCF, CSPC, and CSBC)

Several examinations were conducted to achieve the optimum concentration, suitable solvents, solvents ratio in case of binary solvents, and as well optimum parameters for electrospinning such as flow rate, needle tip to drum collector distance, rotation speed of drum, electric voltage etc. to achieve the continuous uniform fibrous scaffolds from the individual polymeric solution. Optimum electrospinning solutions for PLA-g-VAc was achieved by dissolving it as the same concentration like PLA with the same solvent system (25% (w/v) in binary solvent system such as DCM, and DMF as the ratio 3:2), and by subsequent homogenization of the solution at 40 ^{o}C for three hours

with the help of magnetic stirrer (with rpm 500). Ideal electrospinning solution for ASC was attained by dissolving ASC in 90 % acetic acid (AcOH) as 10% (w/v). For the preparation of core-sheath scaffolds, single polymeric solutions were taken with the same concentrations, and the same solvent systems were considered. Overall preparation of electrospinning solutions, and subsequent scaffolds preparation are presented in Figure 2.7.

Electrospinning was accompanied by applying the same operational parameters as discussed in section 2.4.2 for single polymers, and as discussed in section 2.8 for core-sheath scaffolds. For each scaffold, around 5 ml of polymer solution was used. Electrospun single polymeric scaffolds obtained from solutions of PLA-g-VAc, and ASC were denoted as B, and ASCF respectively. Core-sheath scaffold CSPC was obtained by taking ASC solution as core, and PLA solution as sheath solution. Core-sheath scaffold CSBC were prepared by using ASC solution as core, and PLA-g-VAc solution as sheath.

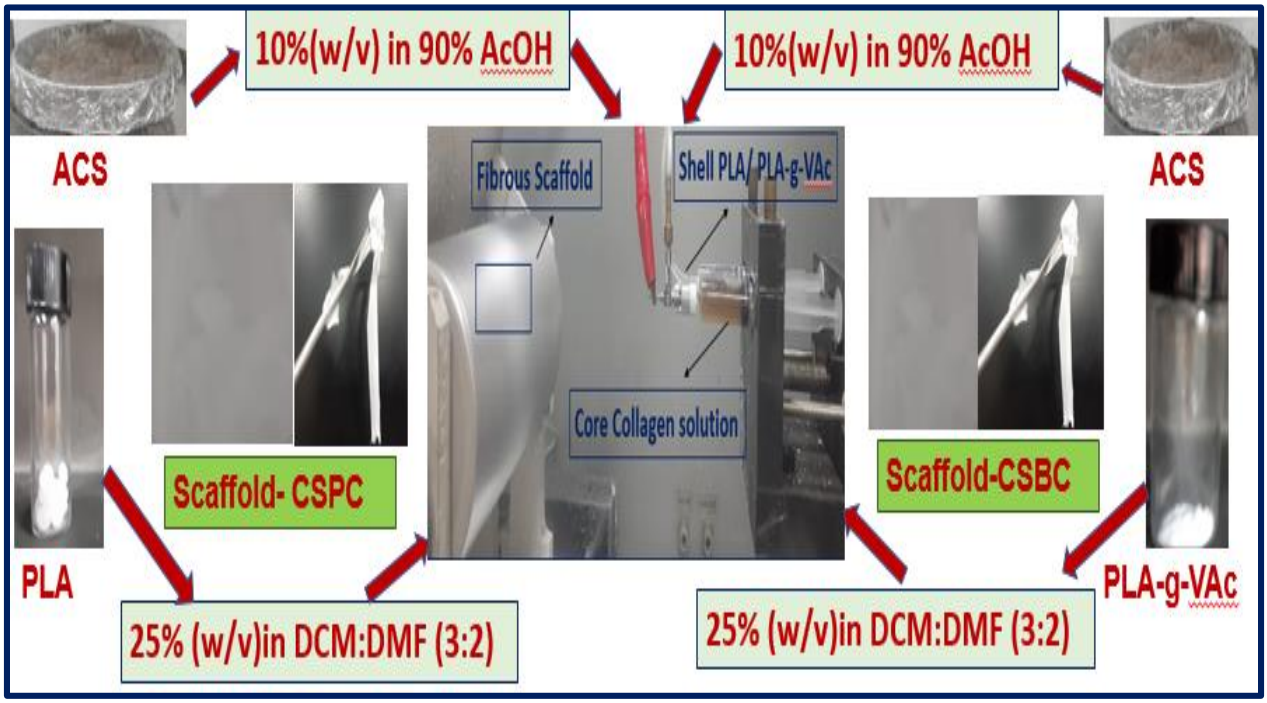

Figure 2.7 Process flow diagram for the preparation of core-sheath scaffolds (CSPC, and CSBC)

2.12 Characterizations of Acid Soluble Collagen (ASC)

2.12.1 Extraction Yield of ASC

Yield of extraction of ASC was measured based on the dry weight of starting raw materials (tilapia fish skin) by considering the subsequent equation:

Yield (%) = (Weight of lyophilized collagen in g /Weight of dry skin used for extraction in g) X 100

2.12.2 Amino Acids Composition of ASC

250 mg of dried ASC sample was solubilized with the hydrolysis solution that consists of 37% HCL (300 ml), deionized water (200 ml), and 0.5 g phenol for 500 ml solution. Sample was hydrolyzed at 120 ^{o}C for 24 hours. pH of the sample was then adjusted within 2.9-3.1 and followed to make up the stock of 250 ml. 900 µL of Na-acetate buffer (pH- 2.9 to 3.1) was added to the 100 µL of sample from stock after filtration (with 0.45µM syringe filter). 100 µL of the sample was then react with Ninhydrin reagent in a reaction chamber. Sample was analyzed on a Sykam AAA (S 433-D, Germany). Base line for the isolation of amino acids was considered with different buffers taking one acidic as pH, 1.9-3.1 and another basic as pH, 10.5-11.85. Residues of different amino acids were estimated as mg per gram of dried sample.

2.12.3 Sodium Dodecyl Sulphate-Polyacrylamide Gel Electrophoresis (SDS-PAGE) of ASC

ASC was considered for gel electrophoresis by SDS-PAGE as the method described [17], with separating and stacking gel as 7.5%, and 5% respectively. Sample (ASC) was dissolved in acetic acid solution (0.01 M) as the ratio 1:10 (w/v) maintaining temperature of 4 °C. Sample buffer that constitutes Tris–HCl buffer (0.5 M, pH 6.8), 30% glycerol (v/v), 10% β-mercaptoethanol (v/v), 5% sodium dodecyl sulphate (w/v), and 0.04% bromophenol blue was mixed with the resultant solubilized ASC at 1:1 ratio to makeup 2 ml. It was then heated in a boiling water bath for ten minutes and centrifuged to eliminate insoluble materials. Loading of sample on to polyacrylamide gel was carried out as 1:1 ratio and electrophoresis was done with the use of Bio-Rad electrophoresis with 120 V. Coomassie Brilliant Blue (G-250) in methanol as 15% (v/v), and acetic acid as 5% (v/v) were employed for staining the gel after electrophoresis. Destaining was done with methanol and acetic acid as 30% (v/v), 10% (v/v) respectively. Protein markers of high molecular weight were used for relative measurement of molecular weight of ASC.

2.12.4 Spectroscopic and Thermal characterization of ASC

ASC was further characterized by FT-IR, XRD, thermal analysis (STA-TGA and DSC) with the same operating conditions as discussed in section 2.7.

2.13 Characterizations of Electrospun Scaffolds (ASCF, B, CSPC, and CSBC)

All the scaffolds (ASCF, B, CSPC, and CSBC) were characterized by considering FT-IR spectroscopy, field emission scanning electron microscopy, thermal analysis (STA- TGA, and DSC), XRD analysis, water contact angle measurement, in vitro cytotoxicity, and in vivo animal (rat) model test followed by histopathology in the same operational parameters as discussed in section 2.7.

CHAPTER THREE

RESULTS AND DISCUSSIONS

Chapter Three
Results and Discussions

Results and discussions of the whole study were discussed in the four segments for well presentation as follows:

3.1 Analysis of Modified PLA
3.2 Analysis of Electrospun PLA-Gelatin Blend Scaffolds
3.3 Analysis of Electrospun Core-Sheath Gelatin-PLA Scaffolds (CSPG)
3.4 Analysis of Electrospun Core-Sheath ASC-PLA (CSPC), and ASC-PLA-g-VAc (CSBC) Scaffolds

3.1 Analysis of Modified PLA

Graphical Abstract

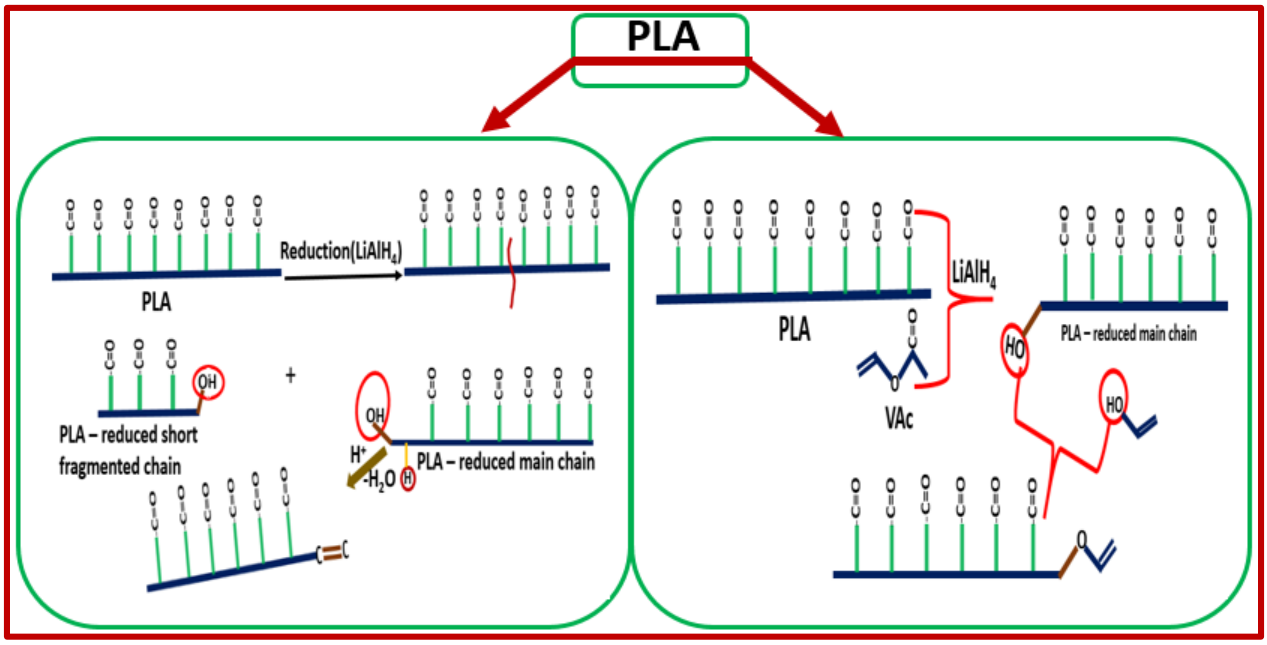

Abstract

Poly(lactic acid) (PLA) is a biodegradable and bioresorbable synthetic polymer which is already in use in many commercial biomedical devices such as sutures, implants, drug carriers, wound dressing, etc. Commercial PLA was modified in this study by grafting vinyl acetate (VAc) onto it using lithium tetrahydridoaluminate ($LiAlH_4$) in order to attach vinyl group to it for further chemical modifications of the PLA for different applications. Reduction based modification was applied aiming to form a number of hydroxyl groups in carbonyl groups in the polymer chain, which may enhance some hydrophilicity to the grafted polymer. Further attempt was taken to prepare vinyl acetate grafted PLA through free radical polymerization reaction using benzoyl peroxide as initiator. The chemical structure of the synthesized polymers was analyzed by FT-IR, ^{1}H-NMR, ^{13}C-NMR and hence the mechanism of the grafting process was proposed. Thermal analysis and X-ray diffraction studies of the products and the control PLA were conducted for further characterization.

3.1.1 Introduction

Nowadays renewable materials are more promising in the research and application of the polymeric resources considering environmental and sustainable perspectives. Poly(lactic acid) (PLA) is very attractive ecological thermoplastic that is now entirely resultant from renewable resources like cornstarch, wheat, rice, and sugar. PLA has been proved not only as a biocompatible and biodegradable material but also possess good mechanical and processable properties which widened its applications specifically in the fabrication of biomedical transplant materials, clinical suture, and controlled drug transport system along with other compatible thermoplastic goods [1, 2]. However, hydrophobicity and slow degradation properties made it incompatible in some sort of biomedical applications. Application range was also found restricted due to brittleness, slow crystallization, poor thermal stability, and poor barrier property of it. Several attempts have been established to improve such properties through incorporating numerous organic and inorganic materials by different methods. Adding bioactive molecules and hydrophilic groups on PLA may facilitate cell growth, division, and other functions [3].

Copolymerization of PLA through grafting showed remarkable modifications induced by enzymatic, chemical, photochemical, and radiation processes. Chemical grafting of PLA could proceed via ionic, and free radical processes in which initiator plays a key role to govern the pathway of the grafting. Poly(lactic acid) is an aliphatic polyester and was reported as very much sensitive to breakdown of its chain specifically in alkaline or acidic conditions. Most of the reported works were concentrated to the grafting on the PLA backbone via free radicals formation. A polymer chain or a small functional molecule was usually grafted on the poly(lactic acid) skeleton to improve its functionality [4]. Modification of PLA backbone was also reported through the blending with other polymers to increase the mechanical characteristics as well. Basic approaches for the compatibilization of the poly(lactic acid) based blends with several reactive compounds were reported by Zeng et al [5]. The PLA chain was functionalized by grafting of MA (Maleic anhydride) which was revealed as an active compatibilizer. Modification of the PLA chain with GMA (Glycidyl methacrylate), and AA (acrylic acid) were also stated in the compatibilization same as Poly(lactic acid)-g-Maleic acid. Several attempts with the derivatives of cellulose, natural rubber, and other polyesters to implant on PLA backbone were reported to improve the mechanical properties of PLA [4]. Reduced toughness and an enhancement of tensile modulus were observed in poly(lactic acid)-g- poly(acrylic acid) [6]. Inorganic compounds such as SiO_2, and TiO_2 are also

responsible for the improved thermal and mechanical characteristics of PLA-g-AA rather than PLA [7]. PLA grafted with halogens especially with bromine showed the toxicity towards E.coli but not to HeLa cells [4]. Continuous flow process was reported for anionic polymerization of 2-vinyl pyridine and styrene [8]. Polyester derivatives produced through anionic polymerization by using lithium diisopropylamide was reported to occur in changing degrees of chain session [9]. Modification of the surface of PLA film (propargylated PLA) without altering the basic PLA structure by anionic polymerization was noticed with the moderated chain fission, improved hydrophilicity, and antimicrobial activities against S. aureus, and E. coli [10]. Anionic copolymerization by using Lithium tetrahydridoaluminate ($LiAlH_4$) was reported in poly(alkyl methacrylate) systems where the ionic species were present mostly as ion pairs or their combinations reasonably than as free ions and involved in stereospecific copolymerization. Alongside it, macroinitiator with pendent groups fabricated by the reduction of poly(cyanophenylene arylene ether) to poly(aminomethylphenylene arylene ether) with $LiAlH_4$ were proved as solvable macroinitiator to produce graft copolymers. This metal hydride (Lewis-pairs) has been established as an effective reducing agent for laboratory products as well as bulk products in industrial applications since more than seventy years. In addition, it has been proved as stoichiometric reducing agent for carbonyl functional groups which proceeds smoothly without toxicity and as a plentiful, and biocompatible metal hydride [11].

Recently copolymers with vinyl groups are promising due to it's to add groups on polymers that enhances the opportunity of hydrophobic and hydrophilic balancing by grafting with hydrophobic macromolecules. The less solubility of vinyl based polymer such as poly(vinyl alcohol) in organic solvents restricted the graft copolymerization technique, on the contrary less solubility of copolymers in water limited its application in the many synthesis reaction to from copolymer solution due to restricted exchange of organic solvents against water. Several attempts for the improvement of macromolecular structures to regulate amphiphilic characteristics as well as length of the unit through grafting of poly(vinyl alcohol) with PLA have been reported which increased the prospects to alter the kinetics of drug release. Poly(vinyl acetate)-g-Poly(L-lactide) were synthesized from L-lactide and P(VA_c-co-VA) with $Sn(Oct)_2$ via ring-opening polymerization. The length of grafting as well as density of copolymer were reported to be controlled by considering the feed ratio and extent of hydrolysis during process. Poly(lactic acid)-g-poly(vinyl acetate) was produced by grafting of Poly(vinyl acetate) onto Poly(L-lactic acid) skeleton with

vinyl acetate in solution by free radical polymerization and that was applied for the blending of starch and PLA as a compatibilizer [12].

We proposed three simplified approaches for the amendment of hydrophobic PLA towards amphiphilic characteristics. First attempt was taken to amend PLA with $LiAlH_4$. Second attempt was taken to modify PLA by using vinyl acetate monomer with $LiAlH_4$. Further attempt was taken to graft vinyl acetate monomer on PLA backbone using benzoyl peroxide (BPO). This study resulted a remarkable change in the macromolecular structure of PLA towards a highly crosslinked copolymer. The copolymers structures were analyzed with the help of FTIR, ^{1}H-NMR, TGA, DTG, DSC and XRD analyses.

3.1.2 Viscosity Average Molecular Weight of PLA

The viscosity-average molecular weight ($\overline{Mv}$) of PLA was determined from the intrinsic viscosity [η], 35.15794 ml/g, in chloroform at 25 ºC by using the Mark-Houwink-Sakurada equation taking the constants K and α value as 2.21×10^{-3} and 0.77, respectively [13].

$$[\eta] = (2.21\times10^{-3})\times \overline{Mv}^{0.77} \quad (2)$$

The viscosity average molecular weight of PLA was obtained 286 kDa.

3.1.3 Solubility Test

Solubility behavior of the PLA and modified PLA (P-L, PV-L, and PLA-g-VAc) is tabulated in Table 3.1. PLA was sparingly soluble in diethyl ether, but soluble in chloroform, THF, and DCM.

Table 3.1 Solubility profile of PLA, P-L, PV-L, and PLA-g-VAc with dielectric constant

Solubility profile and dielectric constant of solvents					
Solvents (dielectric constant)	PLA	P-L	PV-L	PLA-g-VAc	VAc
Diethyl ether (4.267)	Sparingly soluble	Insoluble	Insoluble	Soluble	Soluble
Chloroform (4.81)	Soluble	Insoluble	Insoluble	Soluble	Soluble
THF (7.52)	Soluble	Insoluble	Insoluble	Soluble	Soluble
DCM (9.08)	Soluble	Insoluble	Insoluble	Soluble	Soluble
Acetone (21.01)	Insoluble	27%	31%	Soluble	Soluble
DMF (38.25)	Insoluble	39%	44%	Soluble	Soluble
DMSO (47)	Insoluble	56%	63%	Soluble	Soluble

PLA was observed as insoluble in acetone, DMF, and DMSO. Modified PLA (P-L, PV-L) were insoluble in diethyl ether, chloroform, and THF whereas P-L and PV-L both were sparingly soluble in DCM, acetone, DMF, and DMSO. PLA-g-VAc were shown as soluble in all the solvents mentioned here like VAc.

3.1.4 FTIR Analysis

The FTIR spectrum of PLA, P-L, VAc, PV-L, and PLA-g-VAc are presented in Figure 3.1, and Figure 3.2. In the Figure 3.1 (a), the characteristics peaks of PLA at 3296 cm^{-1}(area- 118), and 1746 cm^{-1} (area-194) are due to the presence of free –OH stretching and –C=O stretching [14]. For the P-L, significant IR peak positions were also observed at 1755 cm^{-1} (area- 212) and 1633 cm^{-1} (area- 767). A little shifting of carbonyl stretching frequency (from 1746 cm^{-1} to 1755 cm^{-1}) to a higher value with the increase of peak area for P-L was noticed [15]. During reduction of PLA, chain scission of PLA may form some fragmented parts and those oligomeric chains may form a condensation product with the main PLA chain and this is why the percentage of -C=O group show an increase. IR absorption peak at 1633 cm^{-1} indicated the presence of a –C=C group in P-L which can be attributed due to the acid catalyzed dehydration of alcohols produced from the reduction of PLA (during workout with hydrochloric acid). Hydrochloric acid catalyzed intermolecular dehydration (condensation) of alcohols was reported to be frequently accompanied by formation of –C=C double bond. A broad and intense band at 3445 cm^{-1} with an area of 3507 which is much higher than that corresponding to PLA is also present in the spectrum which may be due to the presence of alcoholic hydroxyl groups in the polymer molecule after the reduction of some of the carbonyl functional groups of the PLA chain along with slight depolymerization of PLA. Depolymerization of PLA at 50 °C may result in the formation of oligomers which is indicated by the prominent peak at 3500 cm^{-1} [16].

A major IR absorption peak at 2978 cm^{-1} was observed for VAc in the Figure 3.1 (b). Moreover, two peaks at 1761 cm^{-1} (area-194) and 1643 cm^{-1} (area-62) are for the presence of -C=O stretching and –C=C stretching in VAc, respectively. For VAc, the peak positioned at 1377 cm^{-1} can be assigned to –CH bending and three peaks at 1217 cm^{-1}, 1138 cm^{-1}, and 1024 cm^{-1} are observed for –C-O- stretching. The peaks observed at 957 cm^{-1} and 868 cm^{-1} can be explained as -C-H out of plane bending vibrations for substituted alkenes specially for vinyl group [17].

In Figure 3.1 (b), For the PV-L, peak positioned at 1761 cm^{-1} with an area of 202 is assigned to carbonyl stretching frequency. A little shifting of carbonyl stretching frequency to a higher value from the PLA but same as vinyl acetate with an increased peak area was noticed.

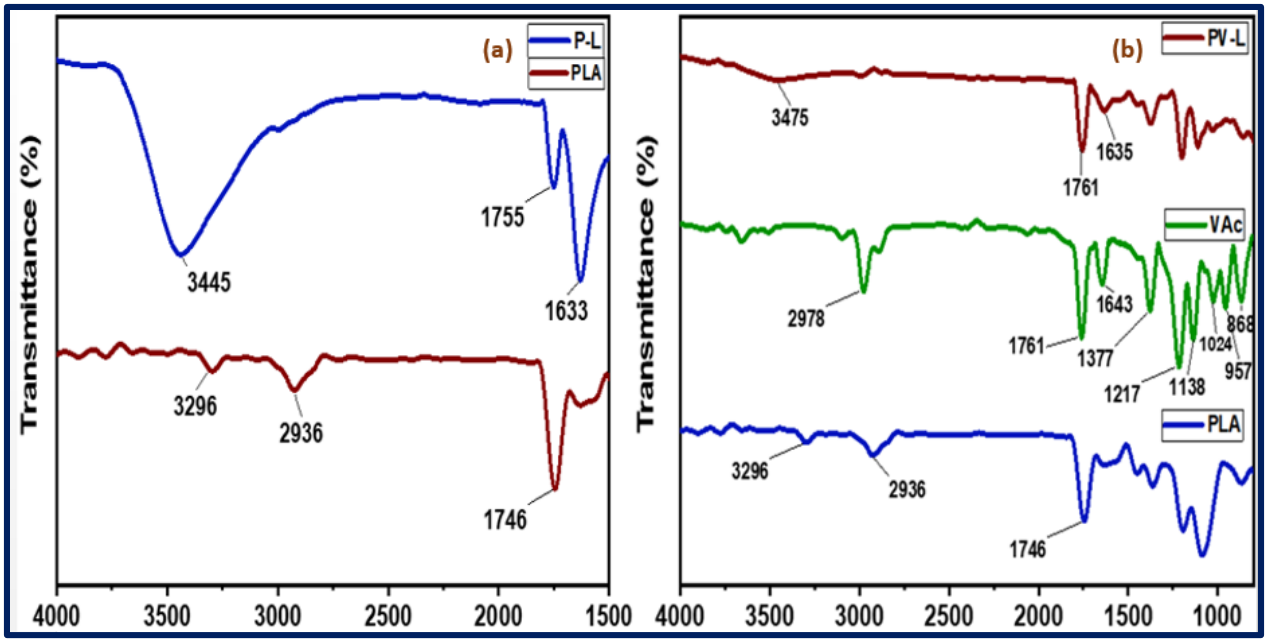

Figure 3.1 (a) FTIR spectrum of PLA and P-L, and (b) FTIR spectrum of PLA, VAc and PV-L

The percentage of -C=O group added to the PV-L due to condensation of the short-fragmented PLA parts to the main PLA chain is less than that for P-L. This is because, along with short fragmented reduced PLA chain, reduced VAc can be added followed by intermolecular dehydration (condensation) in case of PV-L synthesis. Hydrochloric acid catalyzed intermolecular dehydration of alcohols may yield ethers. In the spectrum of PV-L, stretching vibration frequency for –OH group was observed as a broad and intense band at 3475 cm^{-1} (area-3477) that may be resulted from the oligomerization, preferred grafting with reduction of few carbonyl groups. Comparing with the IR spectrum of PLA and vinyl acetate, a small but intense stretching absorption at 1635 cm^{-1} (peak area 792) in the spectrum of PV-L can be assigned to –C=C stretching vibration frequency which was also observed in vinyl acetate. This result indicated that –C=C bond of vinyl acetate was not involved in grafting of vinyl acetate onto the chain of PLA rather grafting may occur through reduced carbonyl group of vinyl acetate or PLA chain. The shifting of the peak due to carbonyl group of PV-L to a higher wavenumber compared to that of the PLA and even to that of the P-L is possibly because of the network formation and reduction of polymer chain length. The peak for -C=C in PV-L was noticed as shifted to a lower wavenumber than that of the VAc due to higher mass of PV-L than the mass of VAc. The peak area ratio of hydroxyl and carbonyl groups in the PLA was 1:6 and those for P-L and PV-L were 1: 0.06 and 1: 0.05.

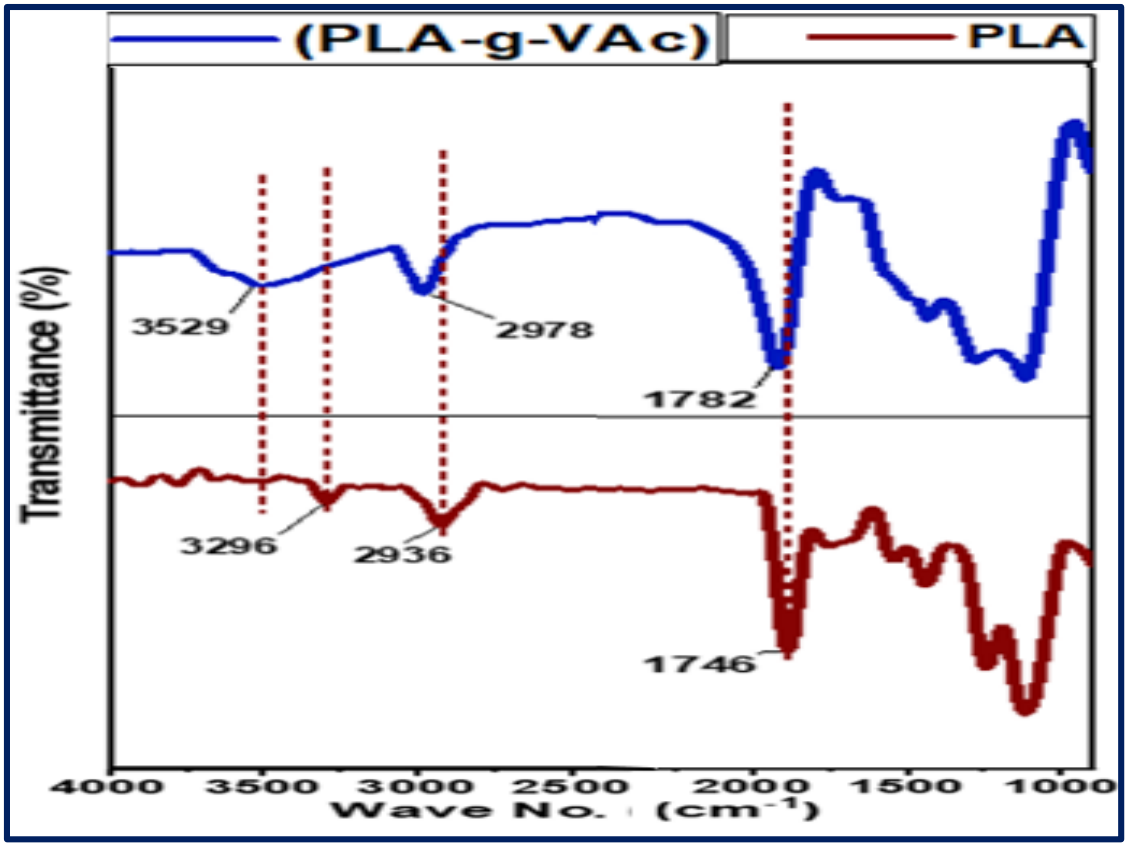

Figure 3.2 FTIR spectrum of PLA and PLA-g-VAc

This data proves that during modification a significant amount of chain scission has occurred and so the terminal hydroxyl group has increased. The peak area ratio of carbonyl group and alkenyl group are 1: 3.6 and 1: 3.9 for P-L and PV-L respectively. The result confirms the presence of more alkenyl groups in the PV-L polymer chain than that of P-L, and that is due to the attachment of vinyl group onto PV-L from the reaction with VAc.

Comparing of IR spectrum of PLA-g-VAc (Figure 3.2) with the IR spectrum of PLA (Figure 3.2 and vinyl acetate (Figure 3.1), it was revealed that –C=C stretching vibration frequency was observed in vinyl acetate but not observed in PLA-g-VAc like PLA. This result indicated that -C=C bond of vinyl acetate was involved in grafting of vinyl acetate onto the chain of PLA. The shifting of the peak of carbonyl group of PLA-g-VAc (1782 cm^{-1}) to a higher wavenumber compared to that of the PLA and even to that of the VAc is possibly because of the network formation and lessening of polymer chain length. –OH absorption in PLA-g-VAc spectrum was observed as broad, and also shifted to higher wave no. compared to PLA terminal –OH absorption. This data also indicated that during grafting a significant amount of chain scission has occurred and so the terminal hydroxyl group has increased.

3.1.5 ^{1}H-NMR Analysis

^{1}H-NMR data of PLA, P-L, VAc, and PV-L are presented in Table 3.2. The peak positions of the spectrums at different chemical shifts and their integrals are listed in the table. The resonance signal at (1.58-1.59) ppm in Figure 3.3 (A) is assigned to methyl protons (-CH_3) and the signal at (5.06–5.15) ppm is assigned to methine protons of PLA [18]. A weak peak at 7.28 ppm may be due to chloroform-d solvent and/or the end group OH (–COOH proton) [1, 13].

In the ^{1}H-NMR spectrum of P-L, Figure 3.3 (B), which is thought to be a reduced and degraded form of PLA, there were two types of methyl protons noticed. One methyl group as showed in the spectrum of the P-L, produced a doublet at (1.59-1.61) ppm. Another methyl group next to the newly formed C=C showed a small singlet at 2.14 ppm. The peaks for methine protons of P-L were observed almost in the same peak positions noted for PLA as the quartet at (5.16-5.21) ppm. A sharp and longer peak was observed at 7.28 ppm. This may be due to the solvent and also for the hydroxyl group formed during reduction of the carbonyl group on the P-L polymer chain. The integral (6.93) of the peak at (1.59-1.61) ppm due to methyl group was almost double of the integral (3.23) obtained for the same group of PLA at a similar position in chemical shift. The integrals due to the methine group of P-L is same as that of PLA. This suggests that the ratio of the amount of methyl group and that of methine group has increased almost two folds. This assumption completely supports the proposed structure of P-L showed in the mechanism (Figure 3.13).

It is proposed in the mechanism that PLA and VAc are firstly reduced by $LiALH_4$ and followed by grafting of VAc on PLA after condensation of the reduced PLA and the reduced VAc. In the ^{1}H-NMR spectrum of PV-L, Figure 3.3 (D), two types of methyl protons were noted. One methyl group as showed in PLA produced a doublet at (1.59-1.61) ppm. Another methyl group attached with methine carbon next to the oxygen, and newly formed –CH_2 showed a small singlet at 2.14 ppm. Peak positioned for methylene proton next to oxygen, and methine group at 2.7 ppm which may be available due to the attachment of reduced VAc group on the reduced PLA chain after condensation. The singlet at 5.19 ppm for methine protons of PV-L is observed almost in the same peak position as the quartet of PLA observed. A peak at 4.39 ppm is also noticed and that may be due to the double bonded methylene group of VAc attached to the PLA. A peak observed at 7.28 ppm is due to solvent and another peak at 7.30 ppm may be due to the double bonded methine group of VAc which was grafted on PLA chain. The last two peaks got overlapped in the spectrum. The integrals of the methyl group and the methine groups from PLA were obtained approximately

41 and 8 in the spectrum of PV-L, respectively. The integral of the double bonded methine group from VAc attached in the PV-L was obtained as 1 at 7.30 ppm.

Table 3.2 Chemical shifts in the ^{1}H-NMR Spectrum of PLA, P-L, VAc, and PV-L

Analyte	Peak Positions in ^{1}H-NMR (δ in ppm) & integrals					
	δ(CH_3)	δ(OCH_2CH)	δ(CH)	δ(CH=)	δ(=CH_2)	δ(CH_3C=C)
PLA	1.58-1.59, (d, 3H); 3.23		5.14-5.20 (q,1H); 1			
P-L	1.59-1.61 (d,3H); 6.93		5.16- 5.21 (q,1H); 1		4.39 (s); 1	2.14(s); 1
V_{Ac}	2.1(s, 3H); 3.65			7.28, 7.22- 7.16 (m, 1H), 1	4.81- 4.77 (1H, q), 4.48- 4.47(1H, q)	
PV-L	1.61 (d); 40.72	2.7(s); 0.09	5 .19 (s); 8.64	7.28, 7.30 (d); 1	4.39 (s); 0.08	2.14(s); 1

It can be suggested from the above data that one VAc is grafted in one PLA repeat unit. Then it can be calculated that one methine group from VAc and 7 methine groups from PLA are present in PV-L which showed chemical shift at 5.19 ppm. The ratio of methyl and methine groups in PV-L due to PLA was obtained 2:1 as it was noticed for the P-L. For the same types of proton, the NMR signals were reported to appear at 5.90 ppm and 5.40 ppm in the spectrum of MMA [19]. It was reported that the increase of no. of resonance may cause severe crowding and thus chemical shift degeneracy resulting in unresolvable ambiguities. Also, the peaks spacing if it is less than resolving capabilities, two lines could appear as singlet broad. Allylic couplings could give rise to peak broadening rather than discrete splitting [20]. That was also strongly supported that grafting occurred through the reduced carbonyl group of VAc by $LiAlH_4$ on to the PLA chain.

Comparative ^{1}H-NMR data of PLA, and PLA-g-VAc are presented in Figure 3.4. The peak positions of the spectrums at different chemical shifts are listed in the Table 3.3. In the ^{1}H-NMR spectrum of PLA-g-VAc, Figure 3.4, two types of methyl protons were noted. One methyl group as showed in PLA produced a doublet at (1.58-1.60) ppm.

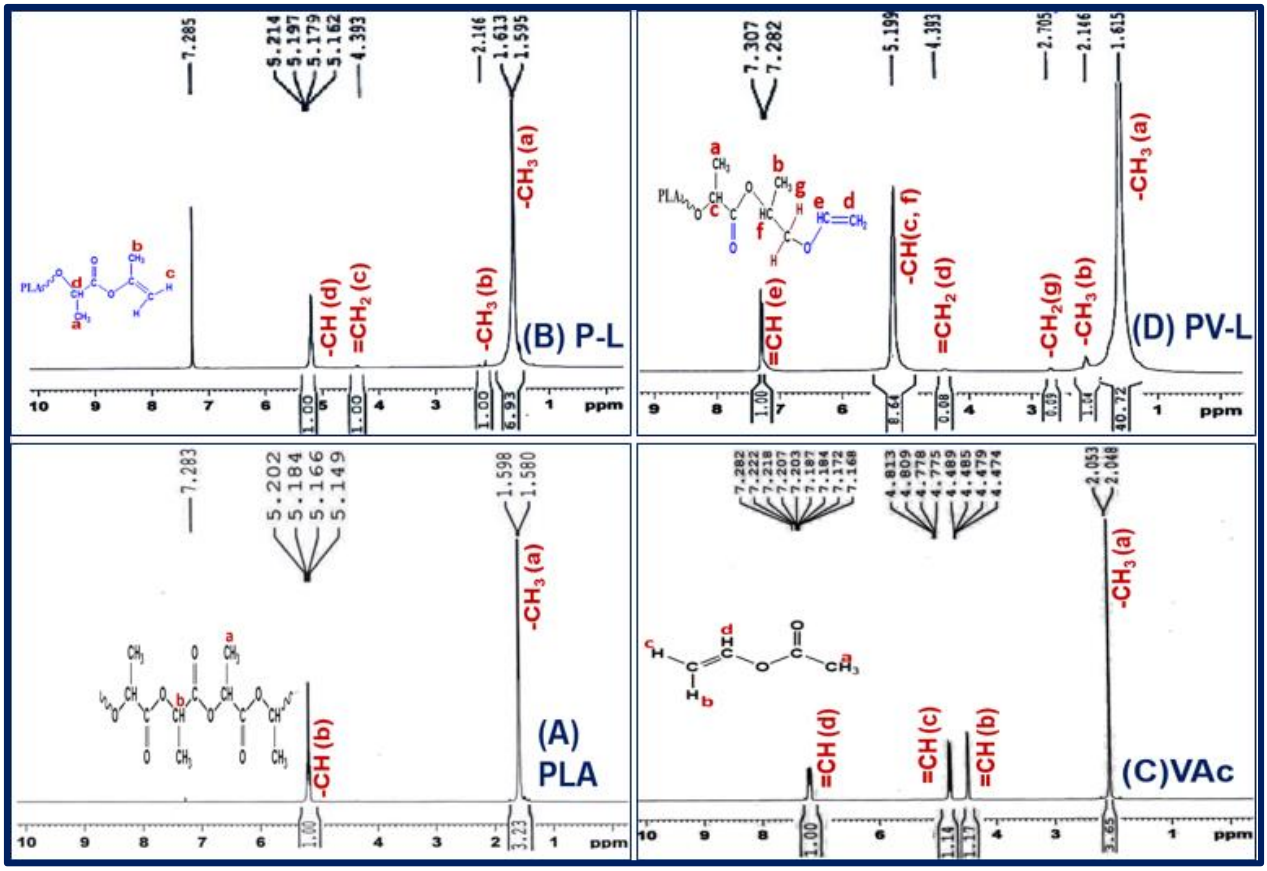

Figure. 3.3 [1]H-NMR spectrum of (A) PLA, (B) P-L, (C) VAc, and (D) PV-L.

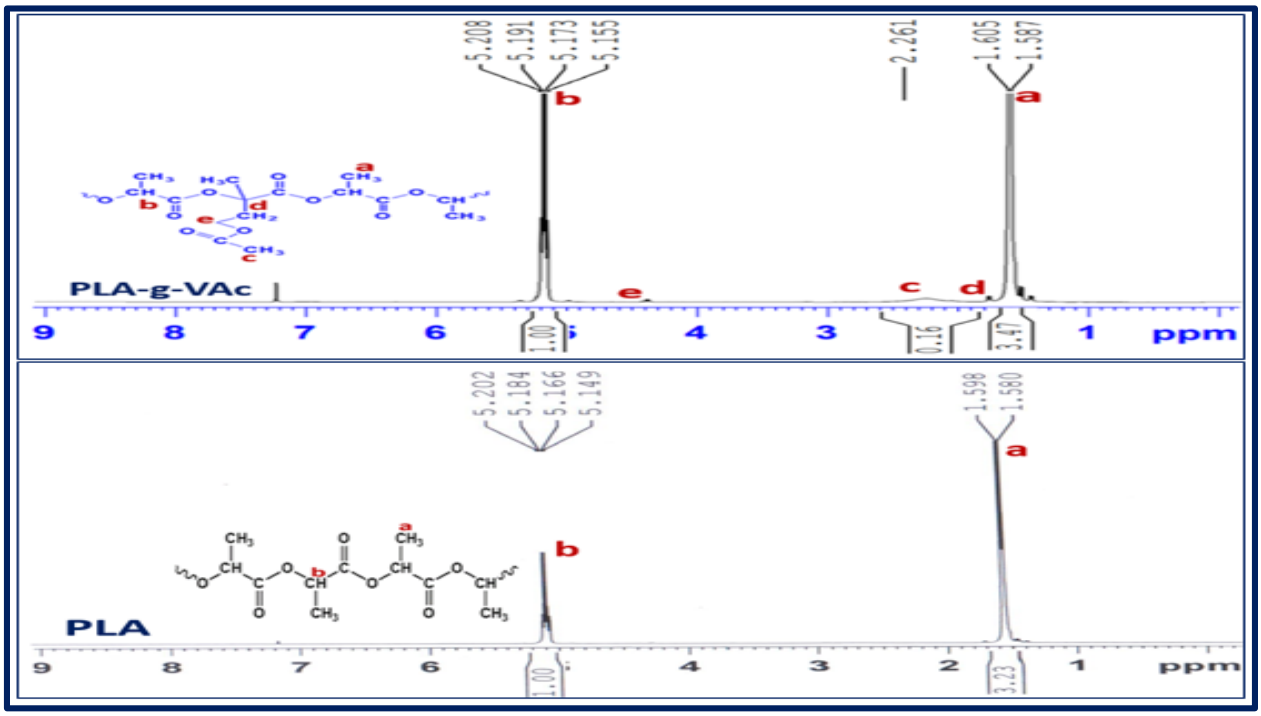

Figure 3.4 [1]H-NMR spectrum of PLA, and PLA-g-VAc

The another methyl group that showed a weak resonance signal at 2.26 ppm that can be assigned to the methyl group of vinyl acetate attributed in the spectrum of PLA-g-VAc due to the attachment of VAc group on the PLA chain after copolymerization (Figure 3.4).

Table 3.3 Chemical shifts in the ^{1}H-NMR Spectrum of PLA, and PLA-g-VAc

Analyte	Peak Positions in ^{1}H-NMR (δ in ppm) & integrals				
	δ(C-CH_3)	δ(CH)	δ(-OCO-CH_3)	δ(C-CH_2)	δ(-CH_2O)
PLA	1.58-1.59, (d, 3H); 3.23	5.14-5.20 (q,1H); 1	2.26 (s, 3H); 0.16	1.70	4.40
PLA-g-VAc	1.58-1.60 (d,3H); 6.93	5.15- 5.20 (q,1H); 1			2.14(s); 1

The peaks for methine protons of PLA-g-VAc were observed almost in the same peak positions noted for PLA as the quartet at (5.15-5.20) ppm. Resonance at 4.40 ppm, and at 1.7 ppm can be assigned to the two types of methylene protons present in the proposed structure of PLA-g-VAc. The weak peak at 4.40 ppm may be attributed in the spectrum of PLA-g-VAc for the methylene protons attached to the acetate group (-CH_2OCOCH_3) that was the new methylene group produced through grafting of vinyl acetate by free radical polymerization (addition polymerization) via the vinyl group (-CH=CH_2) which was in VAc as methine group (-CH). Another weak peak at 1.7 ppm in the PLA-g-VAc spectrum was for methylene group (-CH_2-PLA) which was attached to the PLA upon grafting that was the methylene group of vinyl group. This results also confirmed that grafting occurred involving the methine group of PLA and vinyl group of vinyl acetate. However, a peak observed around 7.23 ppm is due to solvent.

3.1.6 ^{13}C NMR Analysis

The ^{13}C-NMR of PLA showed peaks at chemical shift of 16.60 ppm for CH_3, at 68.98 ppm for CH, and at 169 ppm for C=O [21]. ^{13}C-NMR of P-L, and PV-L are displayed in Figure 3.5. The ^{13}C-NMR of P-L showed peaks at chemical shift of 16.60 ppm for CH_3, at 20 ppm for CH_3 next to C=C, at 68 ppm for CH, at 120 and 135 ppm for two carbons of the C=C, and at 169 ppm for C=O. The ^{13}C-NMR of PV-L showed chemical shifts of peaks at 22 ppm for CH_3, at 40.27-40.51 ppm for methyl group next to C=C, at 67 ppm for CH, at 97 ppm for vinylic CH_2, at 121 and 141 ppm for two carbons of the C=C, at 155 ppm for vinylic CH bond and at 169 ppm for C=O. Thus ^{13}C-NMR data also supported the structure proposed for P-L, and PV-L. ^{13}C-NMR of PLA-g-VAc are

presented in Figure 3.6. The ^{13}C-NMR of PLA-g-VAc showed chemical shifts for two types of methyl carbons of peaks at 16 ppm, and 21 ppm can be assigned to CH_3 carbon on PLA backbone, and CH_3 carbon on grafted part that came from vinyl acetate in the copolymer. Peaks at 63 ppm, and 37 ppm can be assigned to methylene carbons, first one is for $–CH_2$ next to oxygen of grafted part, and the other for $–CH_2$ attached to PLA. Resonance at 68 ppm for –CH of PLA skeleton, and at 169 ppm for C=O present in the grafted copolymer. Thus ^{13}C-NMR data supported the structure proposed for the grafted copolymer PLA-g-VAc. at 169 ppm for C=O present in the grafted copolymer. Thus ^{13}C-NMR data supported the structure proposed for the grafted copolymer PLA-g-VAc.

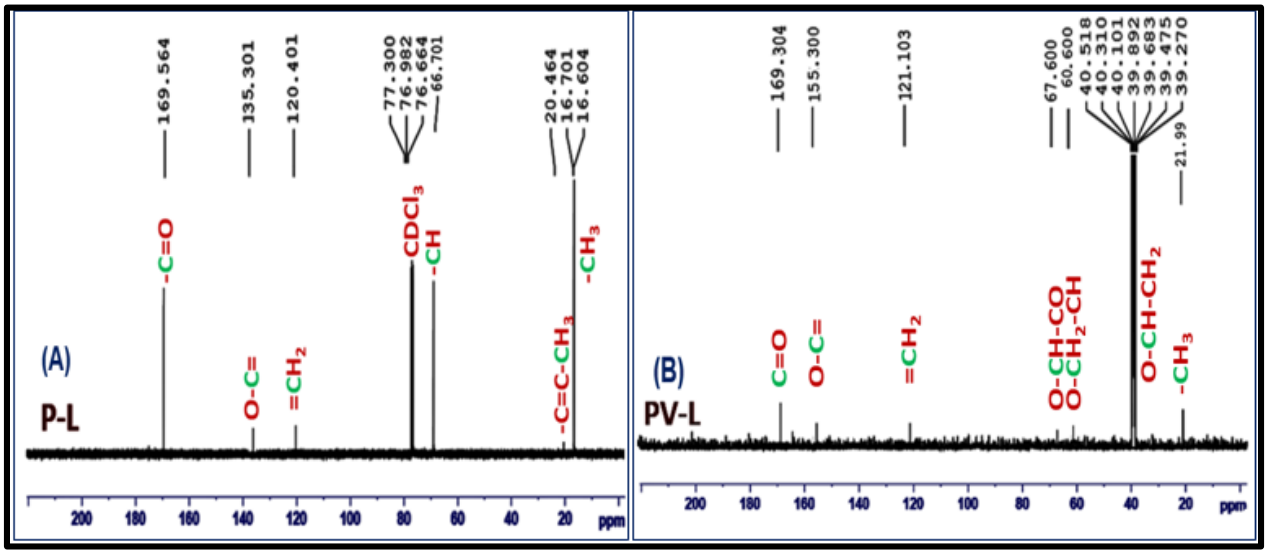

Figure 3.5 ^{13}C-NMR spectrum of (A) P-L, (B) PV-L.

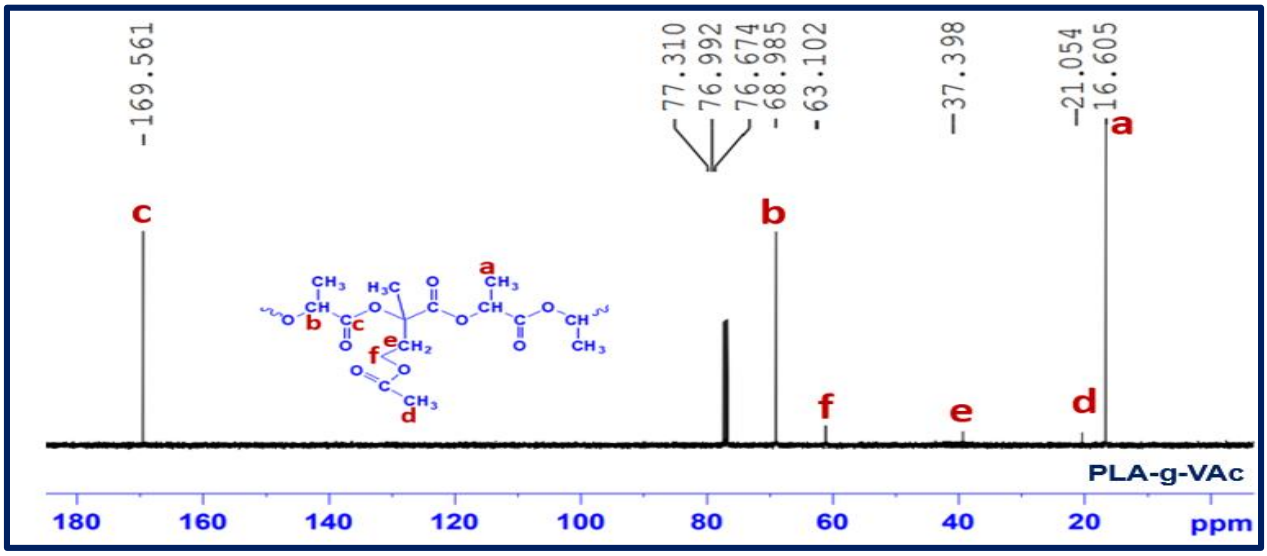

Figure 3.6 ^{13}C-NMR spectrum of PLA-g-VAc.

3.1.7 Thermogravimetric Analysis

The change of percentages of mass of PLA, P-L, and PV-L, and their derivative of mass as a function of onset temperature, end temperature and maximum temperature obtained from TGA and DTG analysis are presented in Table 3.4 (Figure 3.7).

Almost 100 percent mass loss was observed in a one stage mass loss with a single changeover of temperature which is associated to the process of decomposition of PLA. A trace (1.75%) amount of mass loss could be assigned to the removal of moisture. The temperature at which the most weight loss started, the temperature at which maximum weight loss occurred, and the temperature at which PLA was completely degraded were determined from the DTG analysis as 265 ^{o}C (T_{onset}), 342 ^{o}C (T_{max}), and 420 ^{o}C (T_{end}) respectively (Table 3.4). It was reported that the energy of activation of thermal decomposition of PLA is increased with the increasing of the molecular weight of it [22]. Thermogravimetric profile of the PLA is well in accord with its high molecular weight. Pristine PLA demonstrated a single degradation profile whereas P-L degraded at three steps at T_{max} as 41 ^{o}C, 260 ^{o}C, and 400 ^{o}C as observed in TG and DTG analysis. Through these degradation stages mass loss was occurred as 7.5%, 67.3%, and 25.1% in P-L which is different from the thermogravimetric profile of PLA. The 7.5% mass loss occurred below 100 ^{o}C can be assigned to the removal of moisture. This fact indicates that the structure of P-L was favorable to absorb more moisture compared to PLA. Decomposition of P-L that resulted with the maximum mass loss (around 67%) started at the temperature (135 ^{o}C) which is far below than that occurred in PLA (265 ^{o}C).

Table 3.4 Mass loss percentage and the respective temperatures of PLA, P-L, and PV-L (from TG & DTG Curves)

Analyte	Mass Loss (%)	T_{onset} (^{o}C)	T_{end} (^{o}C)	T_{Max} (^{o}C)
PLA	99.8	265	420	342
P-L	99.9	31, 135, 333	58, 333, 462	41, 260, 400
PV-L	99.2	155, 330	330, 484	275, 371
PLA-g-VAc	99.9	233	456	352

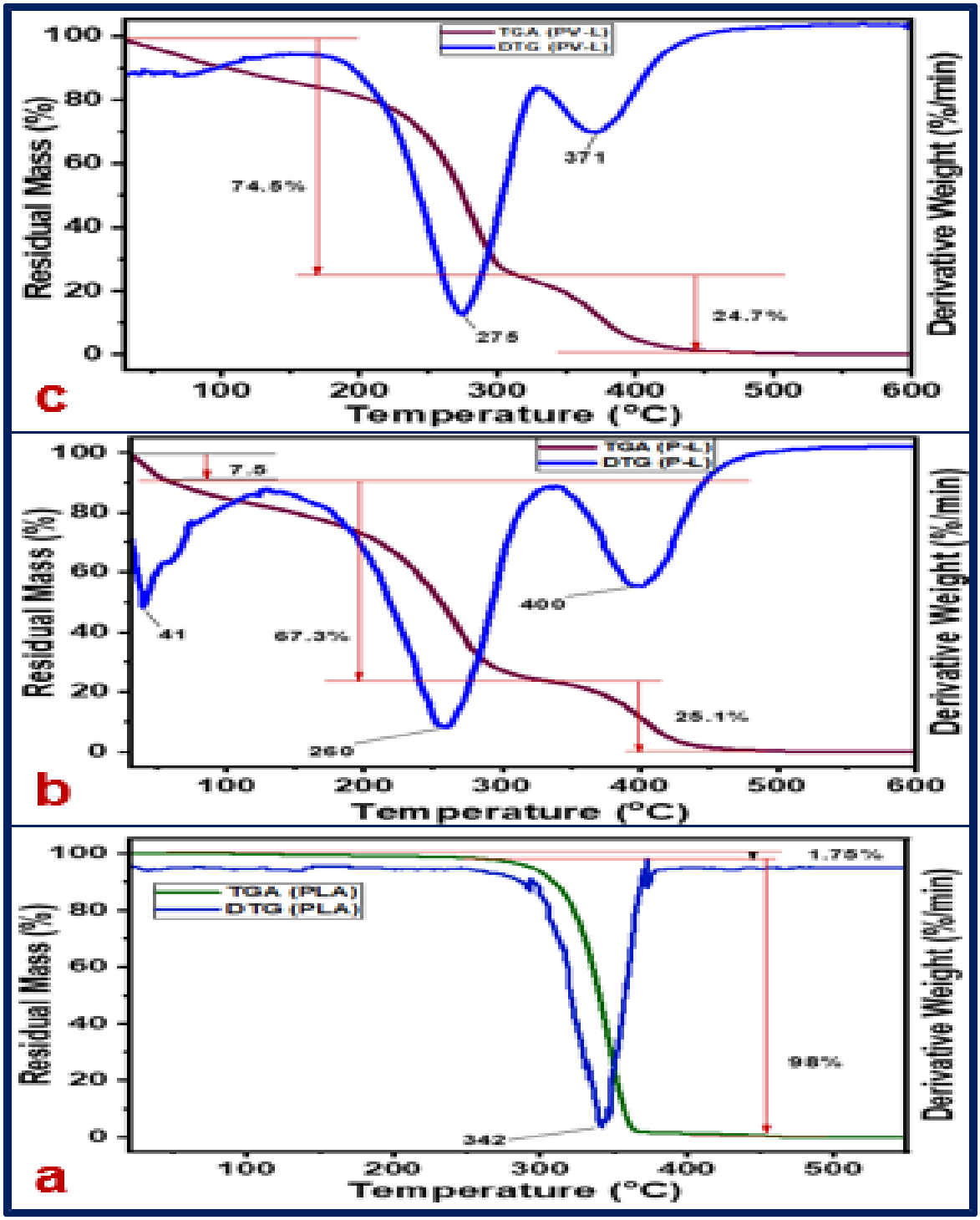

Figure 3.7 TGA, and DTG Thermogram of (a) PLA, (b) modified PLA (P-L), and (c) Vinyl acetate grafted PLA (PV-L).

The maximum decomposition temperature of the 2nd degradation step was 260 ^{o}C which is less by 82 ^{o}C than that of the PLA. Such a TG profile of P-L indicated that some sort of thermal destabilization occurred in P-L which may be caused through the interaction between $LiAlH_4$ and PLA during the process. Degradation of PLA was completed at 420 ^{o}C whereas the same in P-L (at 460 ^{o}C) followed by 40 ^{o}C more temperature with almost 100 % mass loss. It was reported that the degradation of thermoset polymer initiates its degradation with the degradation of the crosslinked network, that is then followed by random breakdown of the linear chain [1].

A single degradation pattern occurred in PLA while PV-L degraded at two steps at T_{max} as 275 ^{o}C, and 371 ^{o}C revealed from TG and DTG analysis. Mass loss occurred through these decompositions was as 74.5%, and 24.7% (Table 3.4). Almost same mass loss occurred in the thermogravimetric curves of PLA and PV-L indicates that PV-L absorbed a trace of moisture like PLA. Decomposition of PV-L that resulted with the maximum mass loss (74.5%) started at the temperature (155 ^{o}C) which is far below than that occurred in PLA (265 ^{o}C). The maximum decomposition temperature of that degradation step was 275 ^{o}C which is less by 67 ^{o}C than that of the PLA. Such a TG profile of PV-L indicates that PV-L is thermally less stable compared to PLA which may be resulted through the interaction between VAc and PLA by the catalysis of $LiAlH_4$ during the process. Degradation of the PV-L was ended at 484 ^{o}C with 99% mass loss which is 64 ^{o}C more temperature than the T_{end} temperature of PLA (420 ^{o}C). PLA modified with VAc and $LiAlH_4$ may be resulted with more crosslinking which reflected in the TG analysis by their two stages degradation. Figure 3.8 showed the comparative TGA, and DTG thermogram of PLA, and PLA-g-VAc. A single degradation pattern occurred in PLA-g-VAc like PLA. Almost 100 percent mass loss was observed in a one stage mass loss with a single change of temperature with initial trace (2.16 %) amount of mass loss which could be attributed due to the initial removal of moisture. The temperature at which the most weight loss started, the temperature at which maximum weight loss occurred, and the temperature at which the copolymer PLA-g-VAc was completely degraded were determined from the DTG analysis as 233 ^{o}C (T_{onset}), 352 ^{o}C (T_{max}), and 456 ^{o}C (T_{end}) respectively (Table 3.4). The maximum decomposition temperature of that degradation step was (352) ^{o}C which is more by 10 ^{o}C than that of the PLA. Such a TG profile of PLA-g-VAc indicates that though the degradation of that copolymer started at lower temperature (233 ^{o}C) than that of PLA (265 ^{o}C) but complete decomposition occurred at the higher temperature (456 ^{o}C, with almost 100 % mass loss) than that for PLA (420 ^{o}C). These results revealed that some sort of chemical

changes occurred during the grafting process to the formation of PLA-g-VAc rather than crosslinking.

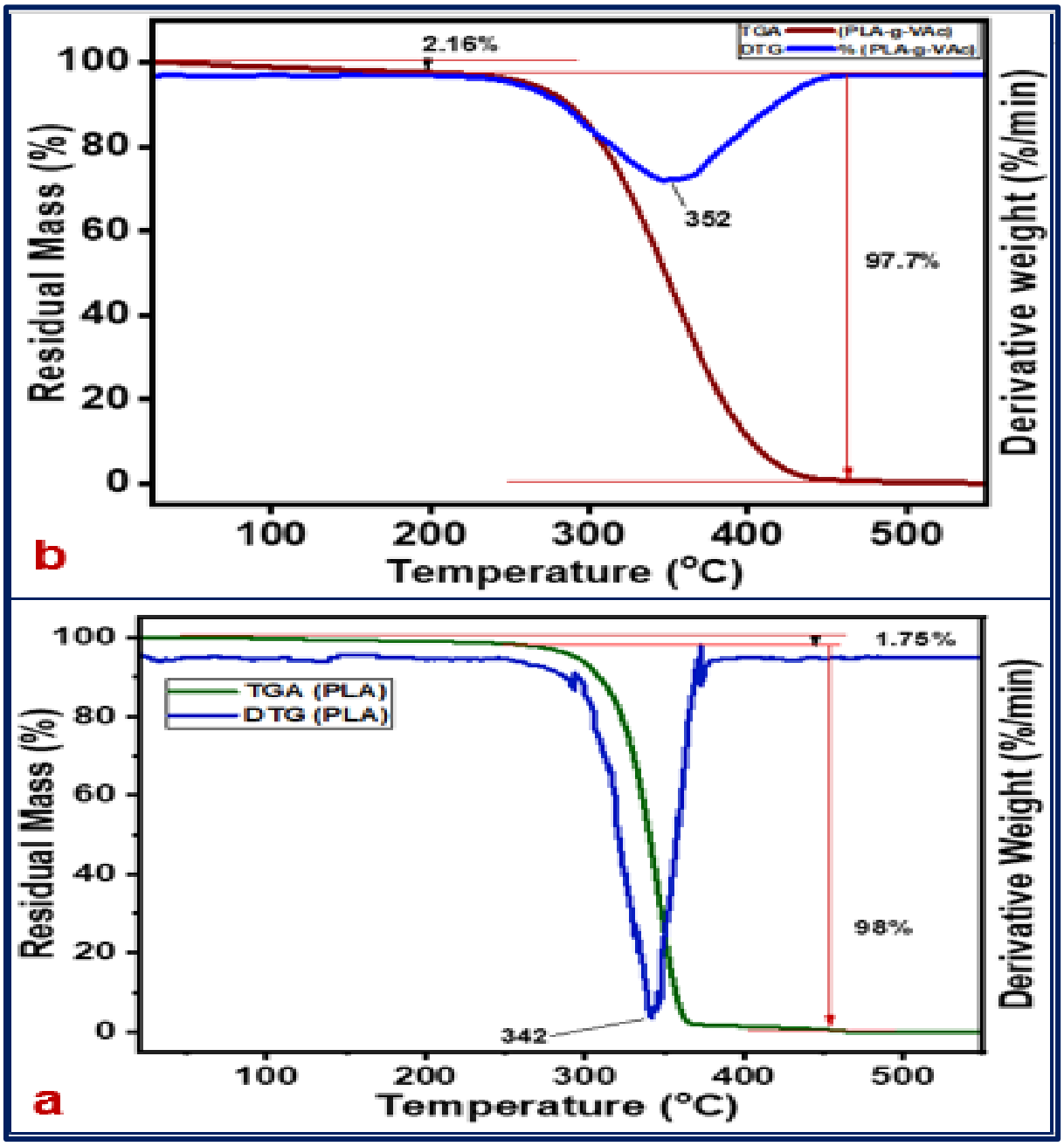

Figure 3.8 TGA, and DTG Thermogram of (a) PLA, and (b) PLA-g-VAc

3.1.8 DSC Analysis

Glass transition temperature (Tg), melting temperature (Tm), heat of melting (ΔH_m) and the change of specific heat capacity (ΔC_p) of PLA, P-L, and PV-L obtained from the second heating curve of DSC are presented in Table 3.5 (Figure 3.9). First heating and cooling were conducted to remove

if there any thermal history present in the materials. Thermal properties during cooling were not considered as no differences were revealed among the curves. A very weak endothermic peak and a strong endothermic peak observed for PLA at the temperatures 59 ^{o}C and 167 ^{o}C could be assigned for the Tg and the Tm respectively. Melting of PLA completed within a temperature difference by 19 ^{o}C (started at 153 ^{o}C and ended at 172 ^{o}C). PLA could be suggested as semi-crystalline as it has a true melting temperature corresponding to the transition from ordered phase to disordered phase and a small portion of amorphous region which relaxed over a temperature range. ΔH_m and ΔC_p of the polymer was estimated as 66 Jg^{-1} and 0.44 Jg^{-1o}C respectively which is agreed with the value reported in other publications [23].

Form the 2nd heating curves of the PLA and the P-L, it is observed that P-L showed the glass transition temperature at 65 ^{o}C which is higher than that of the PLA (59 ^{o}C). Melting of P-L started at a higher temperature (157 ^{o}C) than that of the PLA (153 ^{o}C) but completed at a temperature (168 ^{o}C) lower than that of the PLA (172 ^{o}C). T_m observed at 162 ^{o}C which is also lower than that of the PLA (167 ^{o}C). It is evident that melting occurred in P-L within a narrow range (11 ^{o}C) than that of the PLA (19 ^{o}C).

From Table 3.5, it can be noticed that PV-L showed the T_g at 86 ^{o}C which is higher than that of the PLA (59 ^{o}C). Melting of PV-L started at a higher temperature (156 ^{o}C) than that of the PLA (153^{o}C) but completed at a lower temperature (170 ^{o}C) than that of PLA (172 ^{o}C) as happened with P-L. T_m is also observed at 163 ^{o}C which is also lower than that of the PLA (167 ^{o}C). It is evident that melting occurred in PV-L within a narrow range (14^{o}C) than that of the PLA (19 ^{o}C).

The temperature of glass transition is related to the freedom of movement and ease of the branched portion to rotate along the linear backbone of a polymer. Modification of PLA by the $LiAlH_4$ might cause restriction to mobility somehow and thus more energy was required for relaxation which thus attributed as a higher glass transition temperature. It was reported that the higher T_g is an indication of the higher cross-linking in the polymer [23]. The decrease of melting temperature indicates that crystallites in P-L was less ordered than PLA. It could be explained by view of the faster formation of networks during the process which may affect the crystallization development. Highly crosslinked arrangements restricted the segmental mobility and thus formation of regular and ordered systems could also be hindered. Hence branching of chains may also lessen the melting temperature. Furthermore, modification could increase the entanglement of branched chains with PLA which may resulted as impurities and therefore melting temperature was decreased [24]. ΔH_m

of P-L was estimated as 77 Jg^{-1} which is higher than that of PLA (66 Jg^{-1}) whereas the change of specific heat capacity of melting (0.05 Jg^{-1} ^{o}C) is far lower than the change of specific heat capacity of melting of PLA (0.44 Jg^{-1} ^{o}C). The melting enthalpy of PV-L and the change of specific heat capacity were measured as 56 Jg^{-1} and 0.04 Jg^{-1} ^{o}C respectively. Those thermal properties of PV-L were also observed as lower than those of PLA. More chemical crosslinking could decrease enthalpy of melting and thus crystallinity [25]. The rate of formation of crosslinking may be faster than the rate of formation of crystallites.

Table 3.5 Thermal parameters of PLA, P-L, PV-L, and PLA-g-VAc from DSC thermogram

Analyte	Glass Transition Temperature T_g (^{o}C)	Melting Temperature T_m (^{o}C)	ΔH_m (Jg^{-1})	ΔC_p (Jg^{-1} ^{o}C)
PLA	59	167	66	0.44
P-L	65	162	77	0.05
PV-L	86	163	56	0.04
PLA-g-VAc	59	163	64	0.39

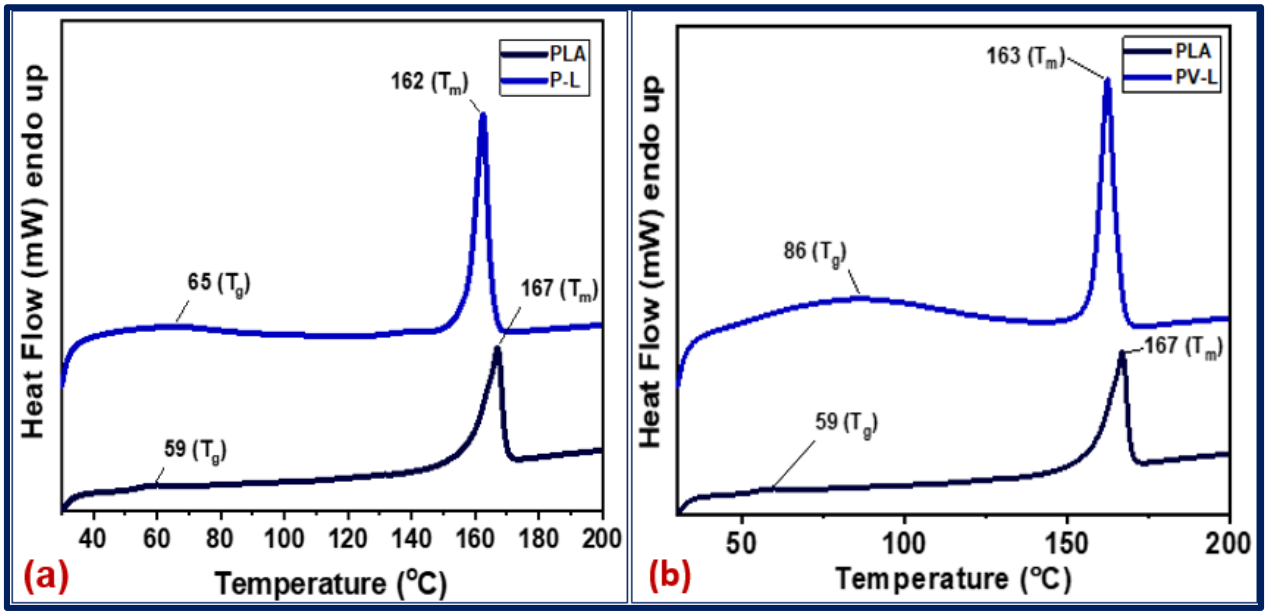

Figure 3.9 DSC Thermogram of (a) PLA and modified PLA (P-L) (b) PLA and Vinyl acetate grafted PLA (PV-L)

Lowering the melting temperature of P-L and PV-L could be agreed with the lowering of crystallinity which was supported by the XRD analysis.

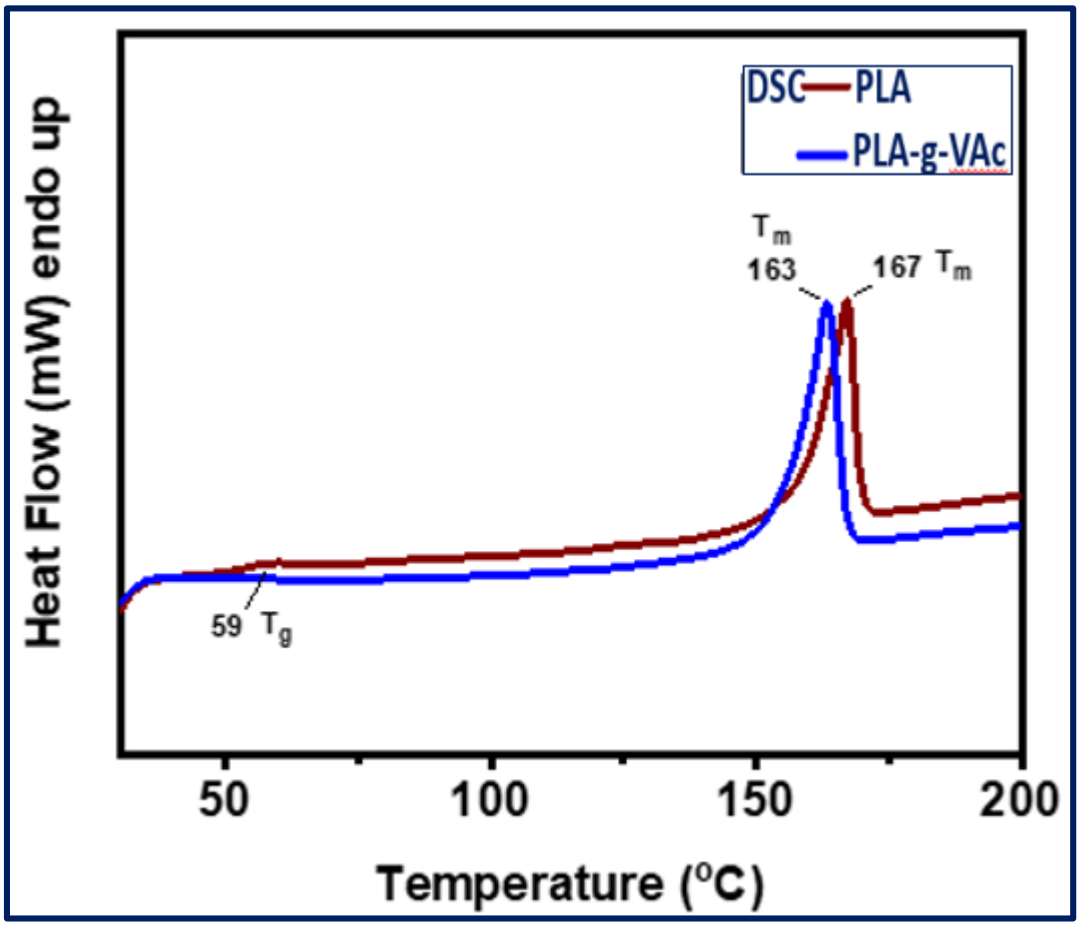

Figure 3.10 DSC Thermogram of PLA and grafted copolymer PLA-g-VAc

Form the 2nd heating curves of the PLA and the PLA-g-VAc (Figure 3.10), it is observed that PLA-g-VAc showed the glass transition temperature around 59 °C. Melting of PLA-g-VAc started at a higher temperature (156 °C) than that of the PLA (153 °C) but completed at a temperature (167 °C) lower than that of the PLA (172 °C). T_m observed at 163 °C which is also lower than that of the PLA (167 °C). It is evident that melting occurred in PLA-g-VAc within a narrow range (11 °C) than that of the PLA (19 °C). ΔH_m of PLA-g-VAc was estimated as 64 Jg^{-1} (Table 3.5) which is lower than that of PLA (66 Jg^{-1}), and the change of specific heat capacity of melting (0.39 Jg^{-1} °C) is also lower than the change of specific heat capacity of melting of PLA (0.44 Jg^{-1} °C). Slight decrease of melting temperature indicates that crystallites in PLA-g-VAc was not as ordered as

PLA. It could be due to the faster formation of networks during the process which may cause less ordered arrangement.

3.1.9 X-ray Diffraction Analysis

The value of 2θ, relative Intensity and FWHM left obtained from the X-ray diffractogram of PLA, P-L and PV-L were presented in Table 3.6 (Figure 3.11) along with the calculated value of d-spacing, percentage of crystallinity, crystallite size, hkl lattice planes and lattice parameters.

X-ray diffractogram of PLA revealed strong intense peaks at 2θ values as 16.7 °, and 19.1 ° supportive to the reflection from (210), and (211) lattice planes. Weak intense peaks that were observed at 2θ values as 12.8 °, 14.9 °, 22.3 °, 24.8 °, 27.3 °, and 29.3 °corresponding to the reflection from (111), (200), (221), (311), (321), and (400) crystallographic planes. Peaks observed in the XRD pattern with the 2θ values at 14.9 °, 16.7 °, 19.1 °, and 22.3 ° could be assigned to homopolymer crystal lattices where 12.8 °, 24.8 °, 27.3 °, and 29.3 °could be related to stereocomplex which is reported to be present as less percentage in PLA of high molecular weight [20]. The high intensity peak at 16.7° with interplanar spacing of 5.29 Å could be assigned as a distinctive peak for the orthorhombic form consists of twenty units in a cell of crystallite [18, 21]. However, the crystallite size of the PLA was estimated from XRD-profile as 27.02 nm. The crystallinity percentage was calculated by considering the area of the crystalline peaks and the area of all peaks region and that was observed as 96%. Such a high crystallinity percentage in PLA is reported in previous literature [22].

The X-ray diffractogram of P-L showed the peaks of 2θ values at 16.6 °, 19 °, 20.27 °, 22.29 °, 35.94 °, and 63.38 ° that could be the reflections from the 111, 200, 200, 210, 321, and 620 planes of crystals. The sharp peaks of 2θ values as 16.7 °, and 19.1 ° are characteristic of PLA homopolymer that were also present in the diffractogram of P-L but with a lower intensity and with a slightly lower value of 2θ as 16.6 °, and 19 °, respectively. The weak peaks at 12.8 °, 24.8 °, 27.3 °, and 29.3 ° in PLA which is related to the presence of less percentage of stereocomplex were not observed in the diffractogram of P-L rather two new weak intense peaks were observed at 2θ values as 35.94 °, and 63.38 °. Absence of peak at 24.8 ° could be resulted due to the segmental relaxation of polymer chains in solution throughout the process that may form more stable α crystal polymorph rather than α′ form [23]. A polymer with a large crystalline area is

reflected as a sharp and intense peak in the X-ray diffraction pattern whereas broad peak is responsible for amorphous region.

Table 3.6 XRD profile of PLA, P-L, PV-L, and PLA-g-VAc

Analyte	2θ (◦)	Relative Intensity (%)	FWHM Left [°2 θ]	d-spacing [Å]	Crystallinity (%)	Average Crystallite Size (nm)	hkl	Lattice Parameters (nm)
PLA	12.8	2.32	0.7872	6.91369	96	27.02	111	a-1.184 (200)
	14.9	6.28	0.4723	5.92231			200	b-0.224 (210)
	16.7	100	0.1574	5.29832			210	c- 0.234 (211)
	19.1	23.26	0.1574	4.64240			211	
	22.3	6.37	0.4723	3.97434			221	
	24.8	3.61	0.4723	3.58534			311	
	27.3	2.24	0.4723	3.25651			321	
	29.3	3.23	0.9446	3.04660			400	
P-L	16.60	100.0	0.2755	5.33865	95	19.64	111	a- 0.876 (200)
	19.00	25.34	0.3149	4.67729			200	b-0.966 (210)
	20.27	31.96	0.4723	4.38015			200	c-0.939 (111)
	22.29	13.02	0.3936	3.98932			210	
	35.94	14.70	0.7872	2.49857			321	
	63.38	13.66	0.6298	1.46756			620	
PV-L	16.58	100.00	0.2755	5.34597	91	17.01	111	a-0.935 (200)
	18.98	29.21	0.5510	4.67583			200	b-1.209 (210)
	20.36	29.84	0.3936	4.36111			210	c-0.773 (111)
	22.32	17.27	0.4723	3.98380			210	
	35.95	7.83	0.9446	2.49809			321	
	63.45	9.56	0.7872	1.46616			620	
PLA-g-VAc	12.5	2	0.9446	7.07073	89	14.93	111	a-1.21 (200)
	14.6	4	0.3149	6.08790			200	b- 1.13 (210)
	16.5	100	0.4330	5.36038			210	c- 0.98 (211)
	18.6	21	0.6298	4.69702			211	
	22.2	6	0.4723	4.00620			300	
	28.9	3	0.6298	3.09307			400	
	31.1	1	0.6298	2.86896			311	

Slight shifting of the main peaks along with the reduced intensity and the presence of new weak peaks could be explained as PLA was modified with a small reduction of crystallinity percentage which was calculated as 95% (less than PLA). Crystallite size of P-L (19.64 nm) was also lower than that of the PLA (27.02 nm) which indicated that the chemical modification of the solution of PLA in THF with $LiAlH_4$ decreased the crystallite size of PLA. Lattice parameters of the P-L were also revealed as different from that of PLA. During the synthesis of P-L, the movability of PLA chains was increased and the chains packing was somehow slightly decreased over and done with the crystallization. Crystallite size of P-L could not be developed as large as pristine PLA due to the fast nucleation rate in the process [7]. Moreover, changing of the hydrophilic or hydrophobic constituents could also be the basis of the change of crystallinity of the P-L [24].

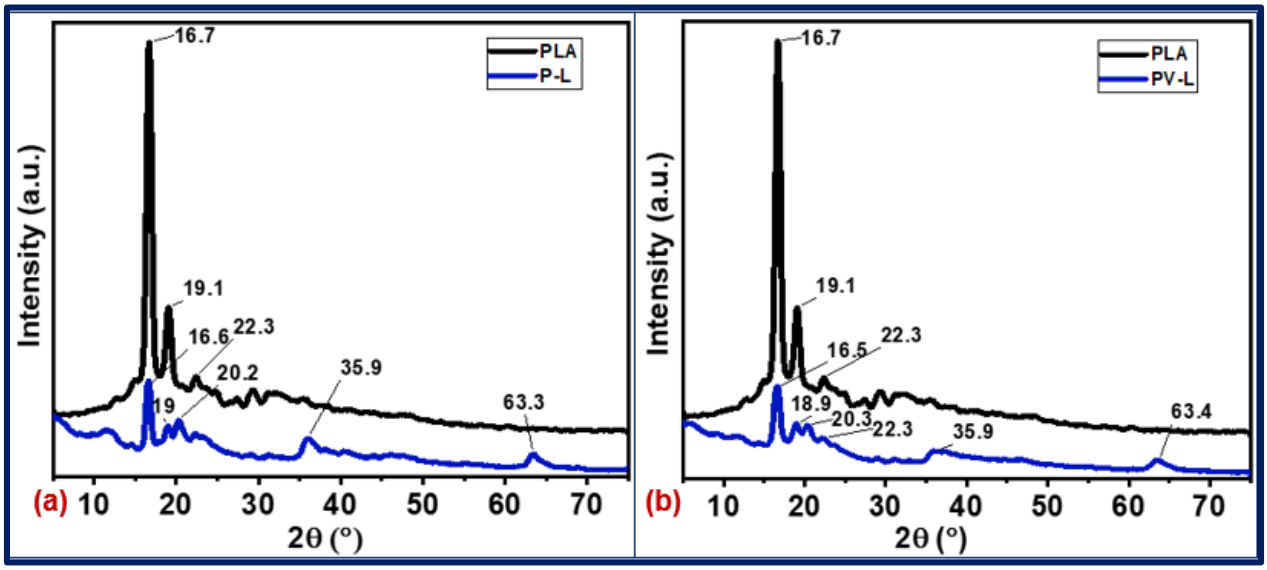

Figure 3.11 XRD patterns of (a) PLA and modified PLA (P-L), (b) PLA and Vinyl acetate grafted PLA (PV-L)

From the X-ray diffractogram of PV-L, the peaks of 2θ values obtained at 16.58 °, 18.98 °, 20.36 °, 22.32 °, 35.95 °, and 63.45 ° correspond to the planes of crystal lattices of 111, 200, 210, 210, 321, and 620. Almost similar X-ray diffraction pattern of PV-L was observed as that of P-L and the peaks agreeing with 2θ values of 16.7 °, and 19.1 ° for PLA were concordant to the less intense peaks at 2θ values of 16.58 ° and 18.98 ° of PV-L. Other weak peaks at 12.8 °, 24.8 °, 27.3 °, and 29.3 ° in PLA which resulted from the reflections of stereocomplex units were not also observed in the diffraction pattern of PV-L but as a replacement for this, two new peaks (weak intense) were revealed at 2θ values as 35.95 °, and 63.45 °. Such a small shifting of the main peaks beside with

the decreased intensity reflected in the lower crystallinity percentage estimated as 91% (less than both PLA and P-L). Crystallite size (17.01 nm) and lattice parameters of PV-L were found lesser than those of the PLA and P-L shown in Table 3.6. This could be resulted from the increased movement of oligomeric chains and furthermore lower packing throughout the process of grafting at that specified condition to the formation of copolymer crystal. This could also cause faster nucleation rate and as a result crystallite size would be lower in the copolymer. Furthermore, copolymer resulted from the compositional changes may as well is accountable for the change of crystallinity percentage, crystallite sizes, and also the lattice parameters [7, 24].

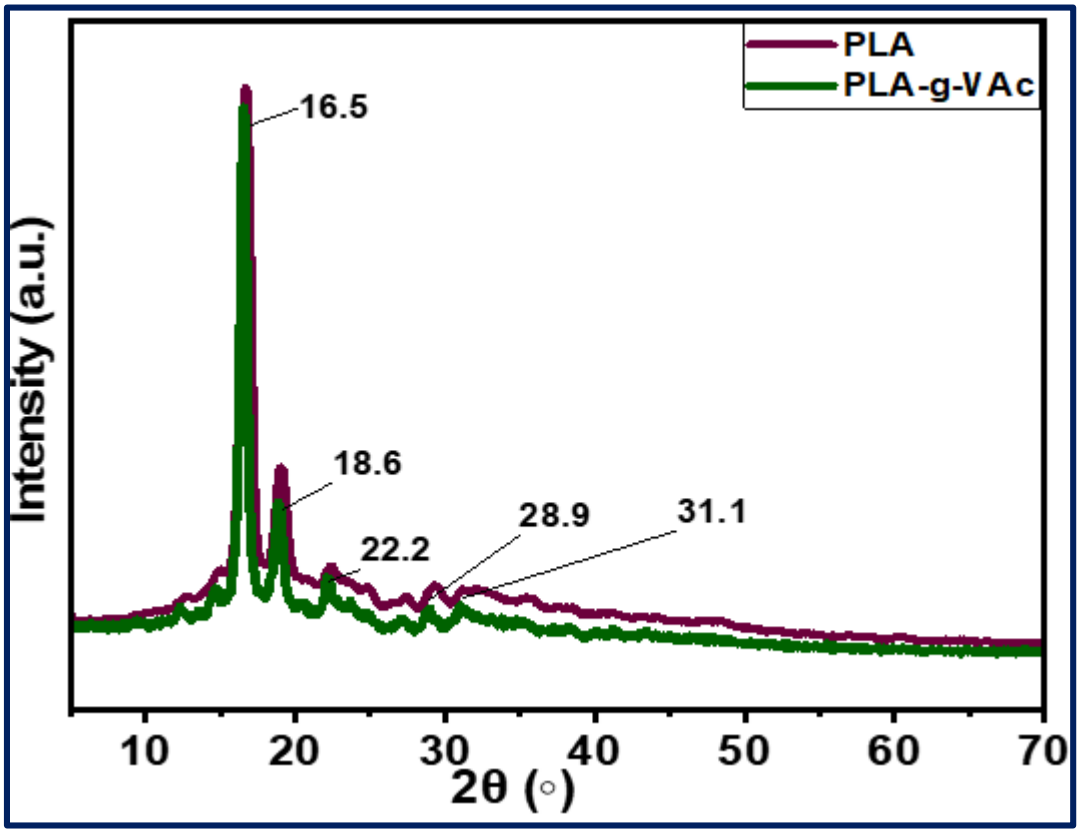

Figure 3.12 XRD patterns of PLA and grafted copolymer PLA-g-VAc

In X-ray diffractogram pattern of PLA-g-VAc (Figure 3.12), the peaks of 2θ values obtained at 12.5 º, 14.6 ° 16.5 °, 18.6 °, 22.2 °, 28.9 °, 31.1 °, correspond to the planes of crystal lattices of 111, 200, 210, 211, 300, 400, and 311. Almost similar X-ray diffraction pattern of PLA-g-VAc was observed as that of PLA and the peaks agreeing with 2θ values of 12.8 °, 14.3 °, 16.7 °, and 19.1 °, 22.3 ° for PLA were concordant to the less intense peaks at 2θ values of 12.5 °, 14.6 °, 16.5 °, 18.6 °, and 22.2 ° of PLA-g-VAc. Other weak peaks at 24.8 °, 27.3 °, and 29.3 ° in PLA which resulted from the reflections of stereocomplex units were not also observed in the diffraction

pattern of PLA-g-VAc but as a replacement for this, two new peaks (weak intense) were revealed at 2θ values as 28.9 °, and 31.1 °. Such a small shifting of the main peaks beside with the decreased intensity reflected in the lower crystallinity percentage estimated as 89% (less than PLA, 96%). Crystallite size of PLA-g-VAc (14.93 nm) was found lower than that of PLA and lattice parameters of PLA-g-VAc were found greater than those of the PLA shown in Table 3.6. Faster nucleation rate may result lower crystallite size in the copolymer. Copolymer resulted from the compositional changes may as well is responsible for the change of crystallinity percentage, crystallite sizes, and also the lattice parameters [26].

3.1.10 Proposed Structure with Synthetic Route

We proposed three simplified approaches for the amendment of hydrophobic PLA towards amphiphilic characteristics. First attempt was taken for reduction of carbonyl groups of PLA with $LiAlH_4$ that formed macroinitiators which thus propagated through reduction.

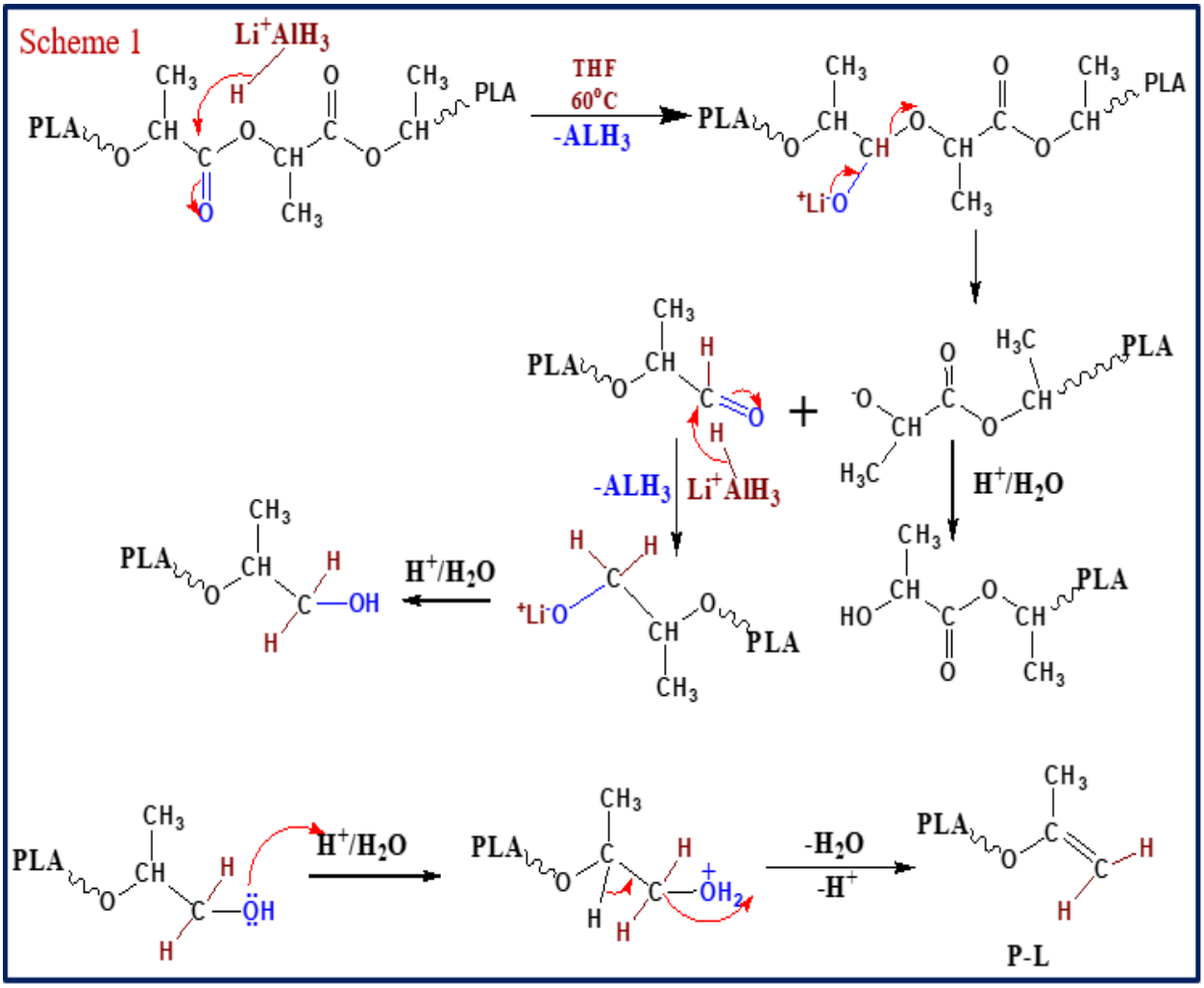

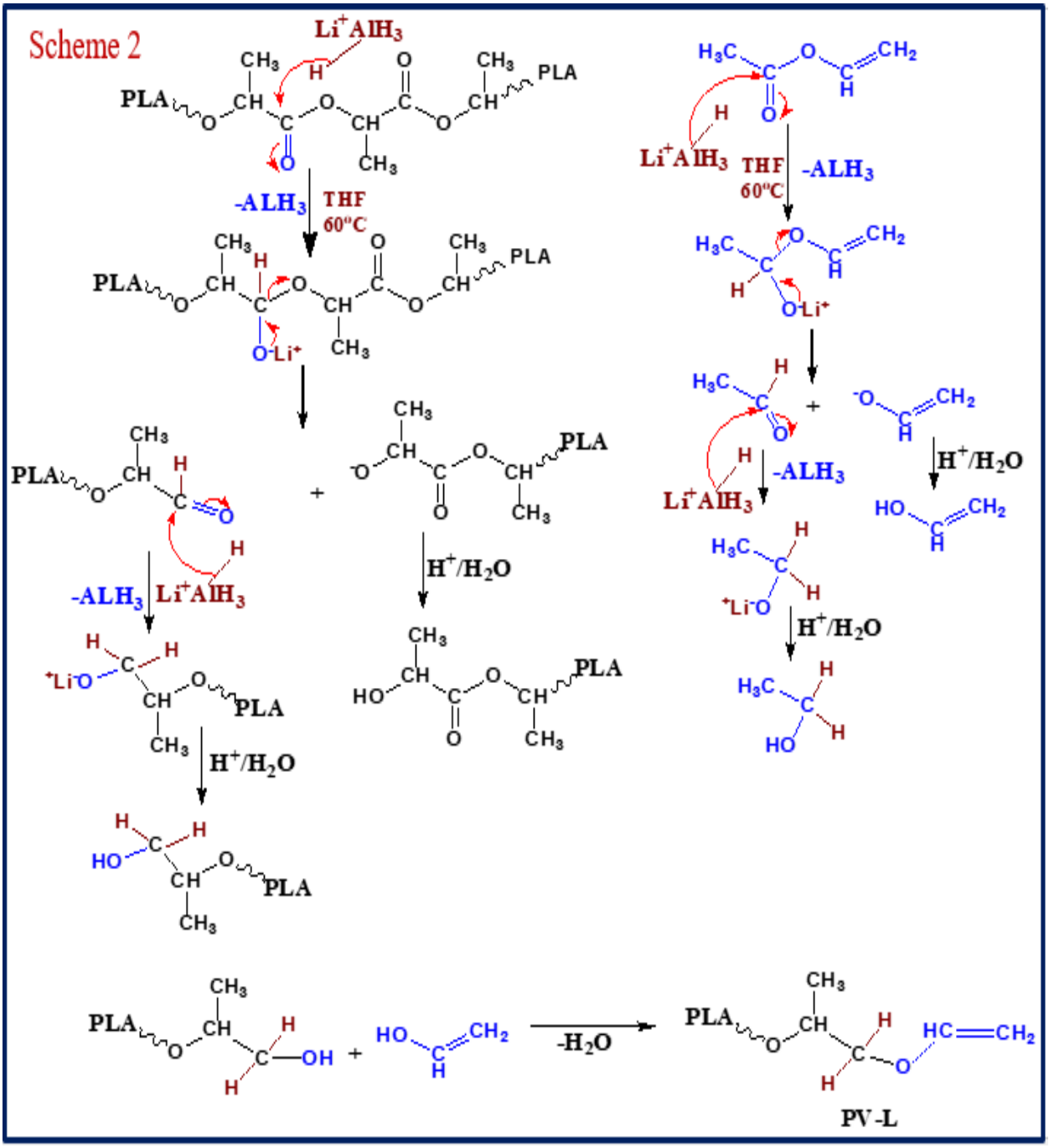

Figure 3.13 Reaction schemes: Scheme 1; proposed mechanism of reduction of PLA in THF solution with $LiAlH_4$, Scheme 2; proposed mechanism of modification of PLA using VAc and $LiAlH_4$.

Usually, one short chain (oligomeric) is fragmented from the main PLA chain. The process breaks up the ester bond and causes a chain scission with a hydroxyl group at the end of the two fragmented parts. The hydroxyl group of the fragmented PLA chain then takes up a proton and

removes as a water molecule, forming a carbon carbon double bond at the end (Scheme 1). The second endeavor was taken to modify PLA using vinyl acetate monomer with $LiAlH_4$. The hydroxyl group of fragmented short chain of PLA reacts with the hydroxyl group of the reduced form of vinyl acetate, a molecule of water is removed through a dehydration step, forming an ether linkage (Scheme 2).

Further attempt was taken to modify PLA by using vinyl acetate monomer with BPO as the initiator through free radicals polymerization. This study resulted the successful grafting of VAc on the macromolecular structure of PLA via addition copolymerization between the vinyl group of VAc and methine group of PLA (Scheme 3).

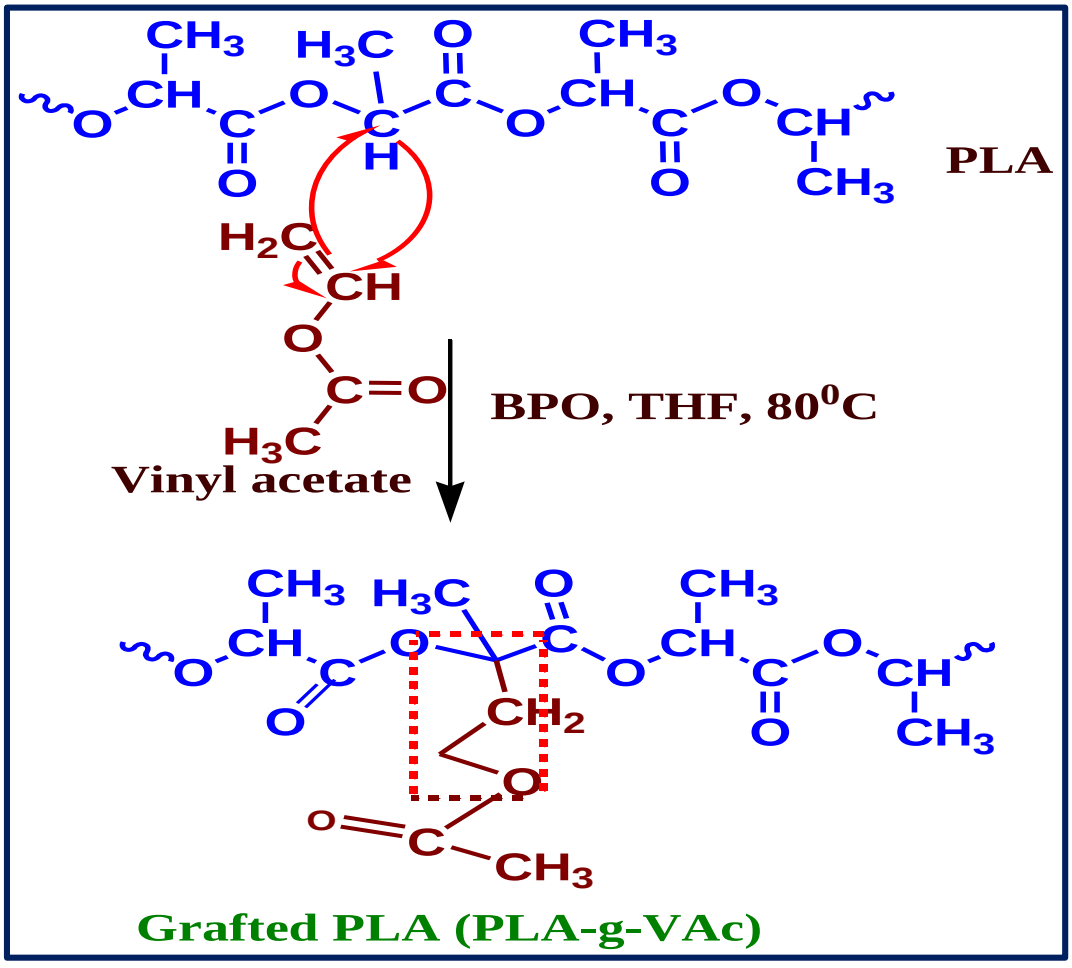

Figure 3.14 Reaction schemes: Scheme 3; proposed mechanism of graft copolymerization of PLA in THF solution with VAc and BPO

3.1.11 Conclusion

In this work, three very simple grafting approaches were demonstrated for the synthesis of PLA copolymers to make it amphiphilic. First attempt was accomplished positively through the formation of macroinitiators in solution of THF by using $LiAlH_4$. Second method was accustomed by using vinyl acetate as monomer with the $LiAlH_4$. Furthermore, another method was used by using vinyl acetate as monomer with the BPO as the initiator. Macromolecular structures resulted from all the methods were confirmed by FT-IR, ^{1}H-NMR, ^{13}C-NMR analysis which revealed the existence of the hydrophilic moiety on hydrophobic PLA in the copolymers which would be more suitable for various applications of them. Thermal and morphological properties of the functional copolymers were analyzed by TGA, DSC, and XRD and it is identified that increased thermal properties with less crystallinity and crystallite size were achieved. Amongst the three copolymers, PLA-g-VAc was considered for electrospinning to the preparation of electrospun scaffolds by taking into account the solubility, and the suitable solvents for electrospinning. However, further attempts for establishing the mechanical characteristics as well as their wide application ranges should be prime tasks.

References

[1] N. Esmaeili, A. Jahandideh, K. Muthukumarappan, D. Åkesson, and M. Skrifvars, "Synthesis and characterization of methacrylated star-shaped poly(lactic acid) employing core molecules with different hydroxyl groups," *J. Appl. Polym. Sci.*, vol. 134, no. 39, pp. 1–13, 2017, doi: 10.1002/app.45341.

[2] S. Deng, H. Bai, Z. Liu, Q. Zhang, and Q. Fu, "Toward Supertough and Heat-Resistant Stereocomplex-Type Polylactide/Elastomer Blends with Impressive Melt Stability via in Situ Formation of Graft Copolymer during One-Pot Reactive Melt Blending," *Macromolecules*, vol. 52, no. 4, pp. 1718–1730, 2019, doi: 10.1021/acs.macromol.8b02626.

[3] A. K. Aworinde, S. O. Adeosun, F. A. Oyawale, E. T. Akinlabi, and S. A. Akinlabi, "Comparative effects of organic and inorganic bio-fillers on the hydrophobicity of polylactic acid," *Results Eng.*, vol. 5, no. October 2019, p. 100098, 2020, doi: 10.1016/j.rineng.2020.100098.

[4] J. Coudane, H. Van Den Berghe, J. Mouton, X. Garric, and B. Nottelet, "Poly(Lactic Acid)-Based Graft Copolymers: Syntheses Strategies and Improvement of Properties for Biomedical and Environmentally Friendly Applications: A Review," *Molecules*, vol. 27, no. 13, 2022, doi: 10.3390/molecules27134135.

[5] J. B. Zeng, K. A. Li, and A. K. Du, "Compatibilization strategies in poly(lactic acid)-based blends," *RSC Adv.*, vol. 5, no. 41, pp. 32546–32565, 2015, doi: 10.1039/c5ra01655j.

[6] J. L. Orellana, M. Mauhar, and C. L. Kitchens, "Cellulose nanocrystals versus polyethylene glycol as toughening agents for poly(lactic acid)-poly(acrylic acid) graft copolymer," *J. Renew. Mater.*, vol. 4, no. 5, pp. 340–350, 2016, doi: 10.7569/JRM.2016.634126.

[7] J. T. Yeh, W. L. Chai, and C. S. Wu, "Study on the preparation and characterization of biodegradable polylactide/SiO2-TiO2 hybrids," *Polym. - Plast. Technol. Eng.*, vol. 47, no. 9, pp. 887–894, 2008, doi: 10.1080/03602550802189076.

[8] A. Natalello *et al.*, "Living Anionic Polymerization in Continuous Flow: Facilitated

Synthesis of High-Molecular Weight Poly(2-vinylpyridine) and Polystyrene," *Org. Process Res. Dev.*, vol. 18, no. 11, pp. 1408–1412, 2014, doi: 10.1021/op500149t.

[9] S. Ponsart, J. Coudane, and M. Vert, "A novel route to poly(ε-caprolactone)-based copolymers via anionic derivatization," *Biomacromolecules*, vol. 1, no. 2, pp. 275–281, 2000, doi: 10.1021/bm005521t.

[10] S. El Habnouni, V. Darcos, X. Garric, J. P. Lavigne, B. Nottelet, and J. Coudane, "Mild methodology for the versatile chemical modification of polylactide surfaces: Original combination of anionic and click chemistry for biomedical applications," *Adv. Funct. Mater.*, vol. 21, no. 17, pp. 3321–3330, 2011, doi: 10.1002/adfm.201100412.

[11] H. Elsen, C. Färber, G. Ballmann, and S. Harder, " LiAlH 4 : From Stoichiometric Reduction to Imine Hydrogenation Catalysis ," *Angew. Chemie*, vol. 130, no. 24, pp. 7274–7278, 2018, doi: 10.1002/ange.201803804.

[12] S. Buchatip and A. Petchsuk, "Preparation of Polylactic Acid Graft Polyvinyl Acetate Compatibilizers for 50 / 50 Starch / PLLA Blending," vol. 6, no. 5, pp. 474–476, 2012.

[13] K. Behera, Y. H. Chang, F. C. Chiu, and J. C. Yang, "Characterization of poly(lactic acid)s with reduced molecular weight fabricated through an autoclave process," *Polym. Test.*, vol. 60, pp. 132–139, 2017, doi: 10.1016/j.polymertesting.2017.03.015.

[14] E. Meaurio, N. López-Rodríguez, and J. R. Sarasua, "Infrared spectrum of poly(L-lactide): Application to crystallinity studies," *Macromolecules*, vol. 39, no. 26, pp. 9291–9301, 2006, doi: 10.1021/ma061890r.

[15] Y. N. Wang, Y. X. Weng, and L. Wang, "Characterization of interfacial compatibility of polylactic acid and bamboo flour (PLA/BF) in biocomposites," *Polym. Test.*, vol. 36, pp. 119–125, 2014, doi: 10.1016/j.polymertesting.2014.04.001.

[16] M. N. Siddiqui, L. Kolokotsiou, E. Vouvoudi, H. H. Redhwi, A. A. Al-Arfaj, and D. S. Achilias, "Depolymerization of PLA by Phase Transfer Catalysed Alkaline Hydrolysis in a Microwave Reactor," *J. Polym. Environ.*, vol. 28, no. 6, pp. 1664–1672, 2020, doi: 10.1007/s10924-020-01716-9.

[17] G. Meszlényi and G. Körtvélyessy, "Direct determination of vinyl acetate content of

ethylene-vinyl acetate copolymers in thick films by infrared spectroscopy," *Polym. Test.*, vol. 18, no. 7, pp. 551–557, 1999, doi: 10.1016/S0142-9418(98)00053-1.

[18] P. Singla, R. Mehta, D. Berek, and S. N. Upadhyay, "Microwave assisted synthesis of poly(lactic acid) and its characterization using size exclusion chromatography," *J. Macromol. Sci. Part A Pure Appl. Chem.*, vol. 49, no. 11, pp. 963–970, 2012, doi: 10.1080/10601325.2012.722858.

[19] D. Sugumaran, K. Juhanni, and A. Karim, "Removal of Copper (II) Ion Using Chitosan-Graft-Poly (Methyl Methacrylate) as Adsorbent," *eProceedings Chem.*, vol. 2, no. April 2018, pp. 1–11, 2017, doi: 10.13140/RG.2.2.33911.93601.

[20] V. J. A. Pavia D. L., Lampman G. M., kriz G. S., *Introduction to spectroscopy, 4th ed.; Cengage learning: Boston*.

[21] J. Contreras, J. Pestana, F. López-Carrasquero, and C. Torres, "Synthesis of ε-caprolactone-b-l-lactide block copolymers by mean sequential polymerization, using diphenylzinc as initiator," *Polym. Bull.*, vol. 71, no. 7, pp. 1661–1674, 2014, doi: 10.1007/s00289-014-1147-9.

[22] Y. L. MH Yang, "Measurement and Simulation of Thermal Stability of Poly(Lactic Acid) by Thermogravimetric Analysis," *J. Test. Eval.*, vol. 37, no. 4, 2009.

[23] S. lin Yang, Z. H. Wu, W. Yang, and M. B. Yang, "Thermal and mechanical properties of chemical crosslinked polylactide (PLA)," *Polym. Test.*, vol. 27, no. 8, pp. 957–963, 2008, doi: 10.1016/j.polymertesting.2008.08.009.

[24] H. Kaczmarek, M. Nowicki, I. Vuković-Kwiatkowska, and S. Nowakowska, "Crosslinked blends of poly(lactic acid) and polyacrylates: AFM, DSC and XRD studies," *J. Polym. Res.*, vol. 20, no. 3, 2013, doi: 10.1007/s10965-013-0091-y.

[25] L. Yang, Z. Yang, F. Zhang, L. Xie, Z. Luo, and Q. Zheng, "Star shaped long chain branched poly (lactic acid) prepared by melt transesterification with trimethylolpropane triacrylate and nano-ZnO," *Polymers (Basel).*, vol. 10, no. 7, pp. 1–19, 2018, doi: 10.3390/polym10070796.

[26] X. Dai, Y. Cao, X. Shi, and X. Wang, "Non-isothermal crystallization kinetics, thermal

degradation behavior and mechanical properties of poly(lactic acid)/MOF composites prepared by melt-blending methods," *RSC Adv.*, vol. 6, no. 75, pp. 71461–71471, 2016, doi: 10.1039/c6ra14190k.

3.2 Analysis of Electrospun PLA-Gelatin Blend Scaffolds

Graphical Abstract

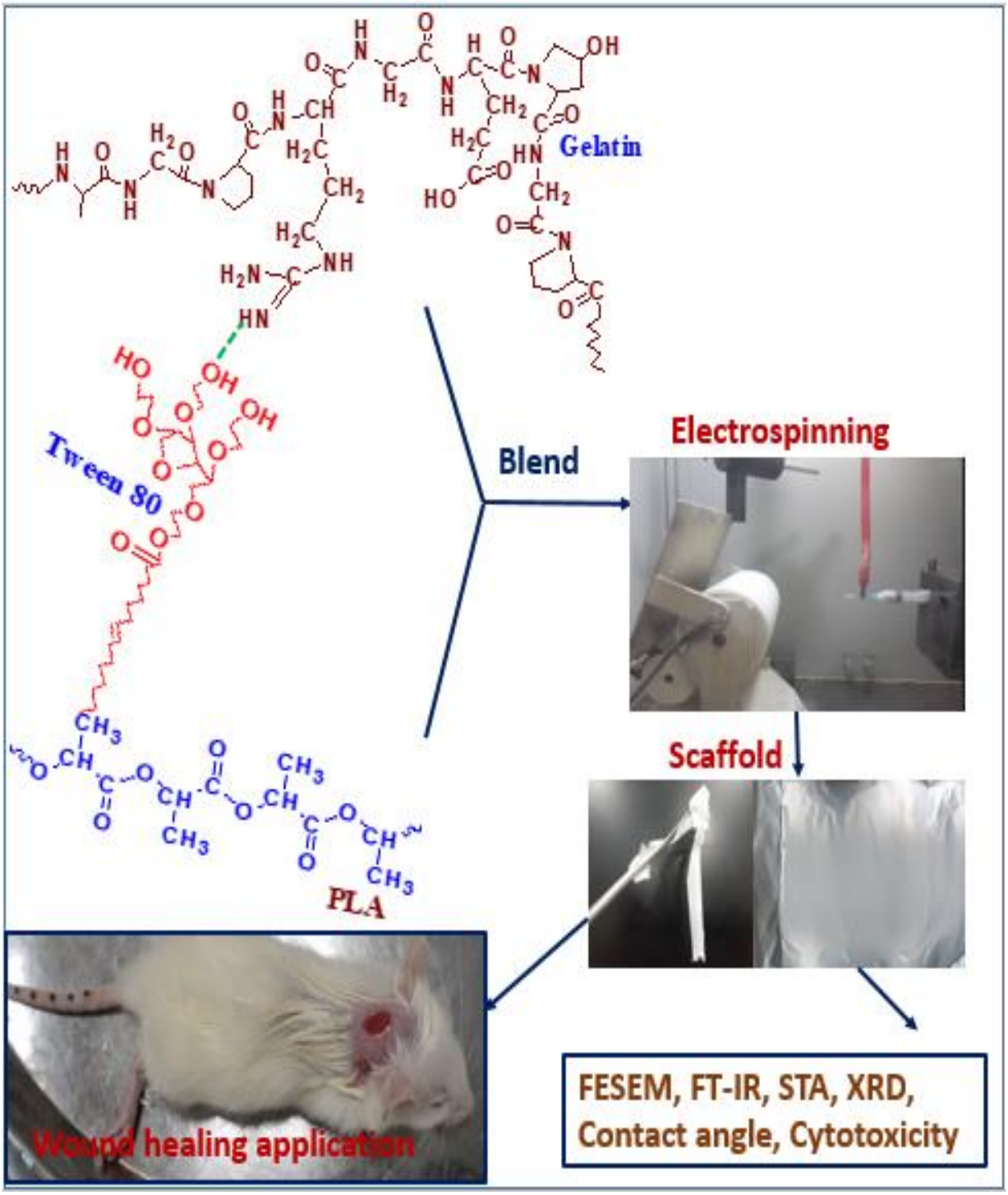

Abstract

Wound healing requires a substantial amount of moisture for faster recovery. Completely hydrophobic or hydrophilic biomaterials are not suitable to be applied for cell growth in wounded area. The study aimed to prepare nanofibrous scaffold from the blend of a solution of hydrophobic PLA and a solution of hydrophilic gelatin. The stability of the blend was achieved using a surfactant and an electrospun nanofibrous scaffold was made out of the solution. Optimum composition of gelatin and PLA to make a scaffold of uniform fiber diameter was achieved with the help of conductivity, viscosity and FESEM analysis. The optimum scaffold was characterized by TGA, DSC, and XRD analysis. Water contact angle of the optimum sample was observed 27 º. The blend scaffold was found nontoxic to cell and showed a 30% faster healing of wound in rat model test compared to healing rate of the PLA scaffold or the gelatin scaffold alone. Histological assay also supported the blend scaffold as an encouraging material for tissue regeneration.

3.2.1 Introduction

Skin is the main external structure of human body which provides basic protection to internal human organs from injury and helps in maintaining immunity from several biological functions. It may get damaged because of continuous exposure to various conditions of environment such as thermal, mechanical, chemical and prolonged pathophysiological environments etc. Skin wound may be life-threatening due to the excess loss of extracellular fluid if the size of the wound is more than 10% of the entire human skin size [1]. Wound curing is one of the utmost challenges in biomedical study as it is a multifaceted process to protect the injury against the outer hazards. The process must require suitable microenvironment to support the healing. Wound bandages are one necessary sort of medical device to accelerate the healing and to shield the open wound from the external risks which have been applied since the ancient periods. The materials used to treat injury exudate and guard wounds from microbial and external particles are recently modifying by making then functionalized to tailor their various properties [2]. Functional wound dressings such as hydrogels, hydrocolloids, and nanomaterials are now promising due to their multifunctional capacities such as hemostatic, antimicrobial, immune regulation, vascularization as well as traditional physical shield and exudate absorbing properties of traditional bandages [3].

Electrospinning has currently been extensively explored as a favorable technique to prepare nanofibrous nonwoven structures, which have increased attention in the arenas of tissue engineering and regenerative medicine such as drug carrier, wound healing etc. [4]. Electrospun nanofibrous scaffolds have numerous outstanding advantages as wound dressing materials. It possesses large specific surface area and thus provides more growth sites and cell adhesion. Such structures can well mimic the ECM (extra cellular matrix) of natural skin structure which obviously can produce microenvironment to promote healing of wound and thus regeneration of skin [5]. Nanofiber scaffolds obtained from electrospinning also possess small pore size and greater porosity which can block invasion of external pathogens effectively in addition provide high moisture and air penetrability. Through this technology, several bioactive and biocompatible materials can also be used to enhance the healing and regeneration process.

A wide variety of biomaterials both synthetic polymers such as polyvinyl alcohol, polylactic acid, polyethylene glycol, polycaprolactone etc. and natural polymers as for example collagen, gelatin, silk fibroin, alginate, chitosan, hyaluronic acid etc. have been using in biomedical purposes since last few decades. Bi-polymeric materials prepared from synthetic polymers in combination of

natural polymers possess the superior properties of respective materials and also have advantages to reduce any inherent limitations of single materials, thus have enough prospect for clinical use specially for tissue engineering [6].

Among the electrospun synthetic polymer materials, electrospun polylactic acid (PLA) is widely used in tissue engineering as approved materials by the Food and Drug Administration (US) due to its biocompatible, biodegradable, and good mechanical characteristics [6]. Hydrophobicity of this material is not supportive to rapid cell adhesion, cell migration, and also regeneration of cells. Gelatin which is the partial denatured form of collagen. Though electrospun gelatin can be a good substitute of native ECM, it cannot be used as an ideal substance for in-vivo application as it is highly hydrophilic, degradable, susceptible to microbial attack, and it has low mechanical properties. By considering the facts, PLA and gelatin bi-polymeric materials have developed to get the benefits of respective single polymers such as good mechanical properties with low in-vivo degradation rate [7]. Blending of polymers to obtain the electrospun bi-polymeric materials is a frequently used technology that could result materials with desirable properties. Electrospun membranes (tubular) from PLA-gelatin blend, and core shell PLA/gelatin were reported for blood vessel tissue engineering [7]. Polylactide/Silk-gelatin mats were exhibited applicable biomechanical characteristics, and provided a promising environs that supported the growth of cells [8]. PLA and gelatin in 1,1,1,3,3,3-hexafluoro-2-propanol was electrospun and reported that PLA-gelatin scaffolds accelerated the viability of cells as well as proliferation of cells [9]. Scaffolds fabricated from PLA-gelatin blend in Trifluoroacetic acid (TFA) incorporated with curcumin was reported in the use of controlled release of curcumin [10]. Scaffolds obtained from PLA, PCL, and gelatin with ascorbic acid was studied for regeneration of bone [11]. The fabrication of the fibrous scaffolds from continuous and uniform fiber with nano sized diameter) through electrospinning using nontoxic solvents is very demanding and challenging.

Additionally, the incorporation of a surfactant in the electrospinning solution to prepare homogeneous blend of hydrophobic PLA and hydrophilic gelatin could be another approach to improve the opportunity of constant fiber (nano) production. Tween 80, polyoxyethylene sorbitan monooleate (T80), is a nonionic surfactant. It is biodegradable, non-toxic, environment friendly and comparatively cost effective and is used in food industries and in pharmaceutical industries. The effect of T80 as the surfactant to prepare the constant nanofiber mat from the chitosan and

polyvinyl alcohol blend was reported and the study revealed that materials produced with T80 had higher mechanical strength and more wettability than the scaffolds prepared without T80 [12].

In the present study, different solutions of gelatin in acetic acid and different solutions of PLA in a mixture of dichloromethane and dimethylformamide were blended with T80 and subsequently electrospun to prepare nanofibrous scaffolds with continuous fiber from the blend of hydrophilic and hydrophobic polymers. Morphology of the electrospun bi-polymeric materials were investigated to observe the coherence of the blend. Thermal analysis, XRD analysis, and wettability of the scaffold was compared to the single polymeric scaffolds. Cytotoxicity of the bi-polymeric scaffolds were measured and the scaffolds were applied in an in-vivo rat (animal) model to investigate the healing progress by them.

3.2.2 Viscosity Average Molecular Weight of Gelatin

$\overline{M_v}$ of gelatin was determined from the intrinsic viscosity [η], 18.15 ml/g in deionized water at 30 ^oC by considering the equation, $[\eta] = 0.1621 \text{ X } (M/M_o)^{0.8554}$ where Mark-Houwink parameters, K value and α value are 0.1621 and 0.8554 respectively. M_o is the molecular weight of the repeating unit which was calculated from percent of amino acid content as 110 g/mol [7], [9].

The viscosity average molecular weight of gelatin was calculated as 27 kDa.

3.2.3 Solution Properties of Electrospinning Solutions

Electro spinnability of any solution depends largely on viscosity and conductivity of a solution. Viscosity and conductivity of electrospinning solutions (for P, G, and Pg1 to Pg2) are presented in Table 3.7. Viscosity and conductivity of solution for P was observed as 74 cP and 3.6 µS/cm respectively whereas viscosity and conductivity of solution for G was noticed as 300 cP and 772 µS/cm respectively. It was reported that gelatin solution of relatively low concentration (20% to 30%) in high acetic acid content favored the interaction of gelatin with acetic acid and hence induced the optimum viscosity and conductivity for the electrospinning to prepare fiber mat. Electrospun gelatin fiber mat fabrication was also reported as favorable within viscosity range 200 cP to 1500 cP [13]. Solution viscosity and conductivity of blend solution for Pg1 were observed as 218 cP and 690 µS/cm which were less than that of solution for G but more than that of the solution for P. As the percentage of the PLA solution content in the blend solution was increased a noticeable decrease of the resultant viscosity and conductivity was observed in solutions for Pg2 to Pg5 (Figure 3.15). The decrease of viscosity in the blend solution is probably due the effect of addition of T80 surfactant. T80 molecules interact with the hydrophobic PLA and hydrophilic

gelatin polymer chains with their hydrophobic tail and hydrophilic head and thus facilitate the polymer solutions to disperse well with the decrease in viscosity. Similar trend of change in viscosity was reported in the addition of T80 to the solution of polyvinyl alcohol and chitosan [12].

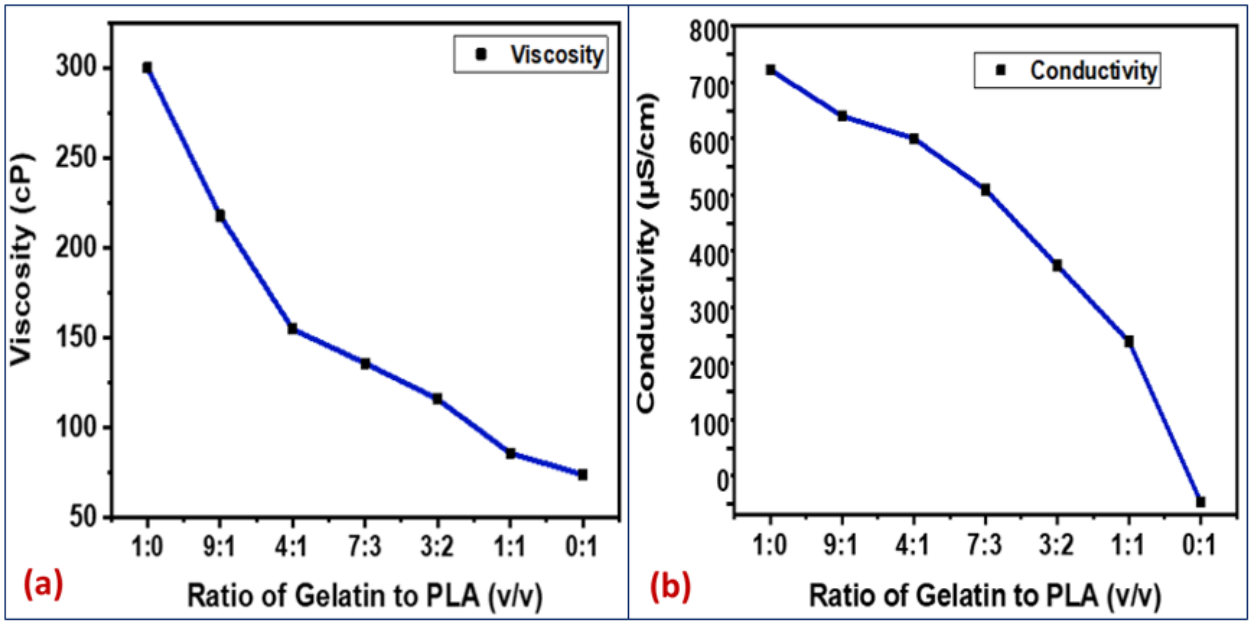

Figure. 3.15. (a) Viscosity and (b) conductivity of different compositions of the gelatin/PLA blend solutions

3.2.4 Morphology of Electrospun Scaffolds

Morphology of the surface of electrospun mats are shown in Figure 3.16 and mean fiber diameters and mean pore areas with standard deviations are presented in Table 3.7. SEM micrographs of P and G showed uniform and continuous fiber with the mean fiber diameter (729±265) nm and (441±169) nm respectively. Mean pores area of the P and G mats were observed as (4±6) μm^2 and (4±7) μm^2 correspondingly. In the same way Pg1 and Pg2 fiber mats also showed the well uniform, continuous fibers with the average fiber diameters (525±197) nm and (139±51) nm respectively. Pg1 and Pg2 scaffolds were exposed with the mean pore areas as (3±8) μm^2 and (0.2±0.3) μm^2 respectively. In Pg3, there were no fibers noticed whereas micrographs of Pg4 and Pg5 showed beaded fibers with a mean fiber diameters of (598±243) nm and (295±129) nm respectively. This is due to the fact that the respective blend solutions did not reach the required entanglements between polymer chains as well viscosity and conductivity to be electrospun. Mean pore areas of the Pg4 and Pg5 were observed as (3±8) μm^2 and (0.6±2) μm^2 respectively. SEM image of P showed relatively larger fiber diameter because of the resistance of high viscous solution compared

to electrical stretching [14]. The observed fiber diameter of gelatin is agreed with the previously reported value (257 nm to 646 nm) which resulted from increased concentration or viscosity. Increase of viscoelastic forces that attributed from the enhancement of chain entanglements was reported to be responsible for decreasing of stretching of polymeric jet and thus lead to the formation of thicker fibers [15]. It was also reported that fiber mats produced by the electrospinning of PLA-gelatin blend (obtained from the addition of gelatin to PLA) resulted in decreased fiber diameter with the increased gelatin content [16]. Average fiber diameter of Pg2 was observed as lower than the average fiber diameter of Pg1 though Pg2 contained lower gelatin content than Pg1. These observations may be attributed to the variations in viscosity and conductivity influenced by the gelatin content as well as PLA content and with the use of surfactant. It was noticed that among the PLA-gelatin scaffolds, Pg2 showed more homogeneity with the lowest mean fiber diameter and the lowest mean pore areas. Pg-2 was considered as the optimum scaffolds obtained from the bi-polymer blends and thus was taken into account for further characterizations and application.

Table 3.7 Average Fibers diameter and pores diameter of electrospun scaffolds with viscosity and conductivity of solutions

Sample	*Viscosity mPa-s	*Conductivity µS/cm	Mean Fiber Diameter ± SD nm	Mean Pores Area ± SD μm^2
P	74	3.6	729±265	4±6
Pg1	218	690	525±197	3±8
Pg2	155	650	139±51	0.2±0.3
Pg3	136	559	No fibers	No fibers
Pg4	116	424	598±243 (fibers with beads)	3±8
Pg5	86	289	295±129 (fibers with beads)	0.6±2
G	300	772	441±169	4±7

*****Viscosity and conductivity values have a standard deviation ±2%

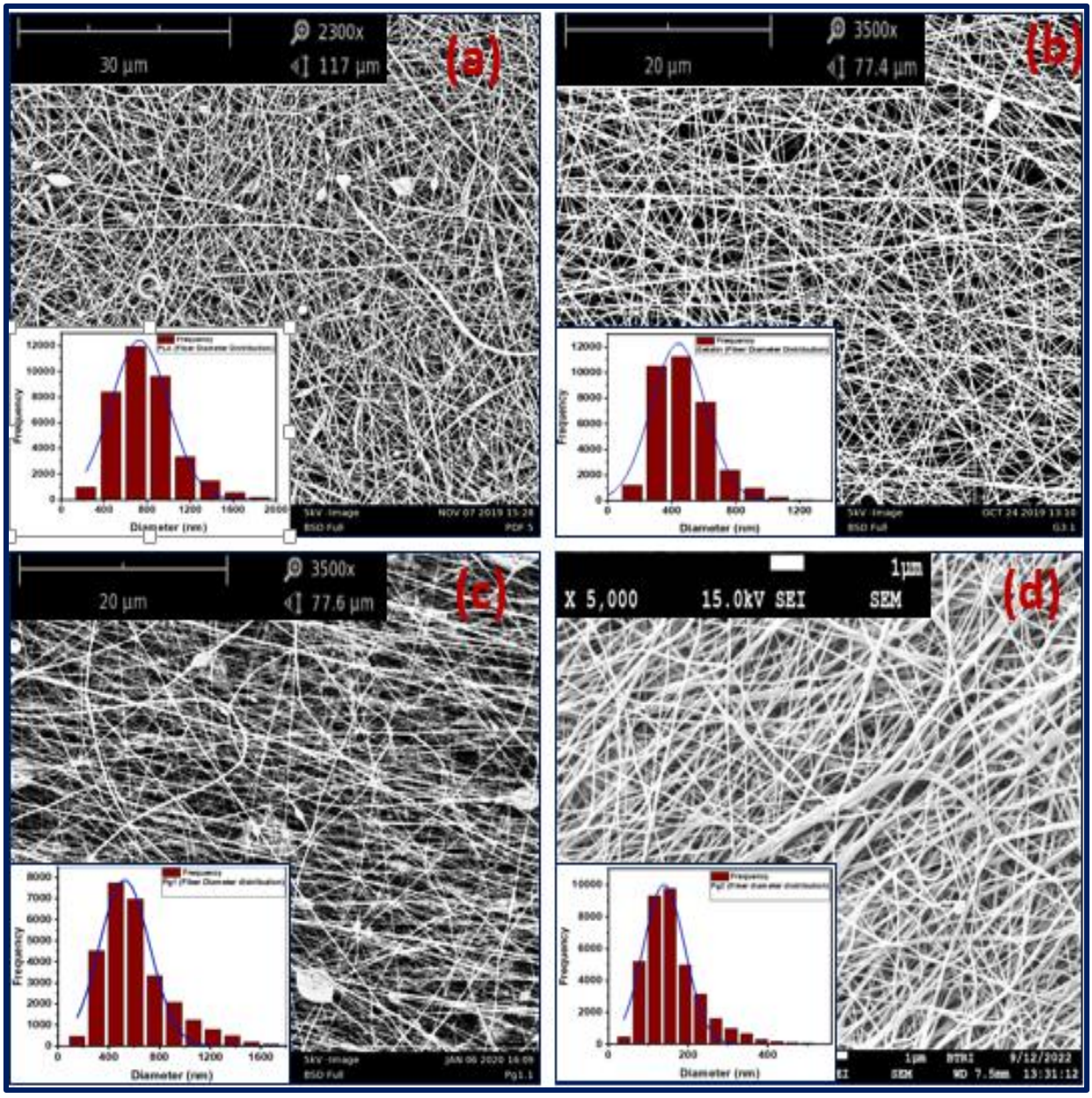
30 µm
2300x
117 µm
(a)
Frequency
Diameter (nm)
20 µm
3500x
77.4 µm
(b)
Frequency
Diameter (nm)
20 µm
3500x
77.6 µm
(c)
Frequency
Diameter (nm)
X 5,000
15.0kV SEI
SEM
1µm
(d)
Frequency
Diameter (nm)

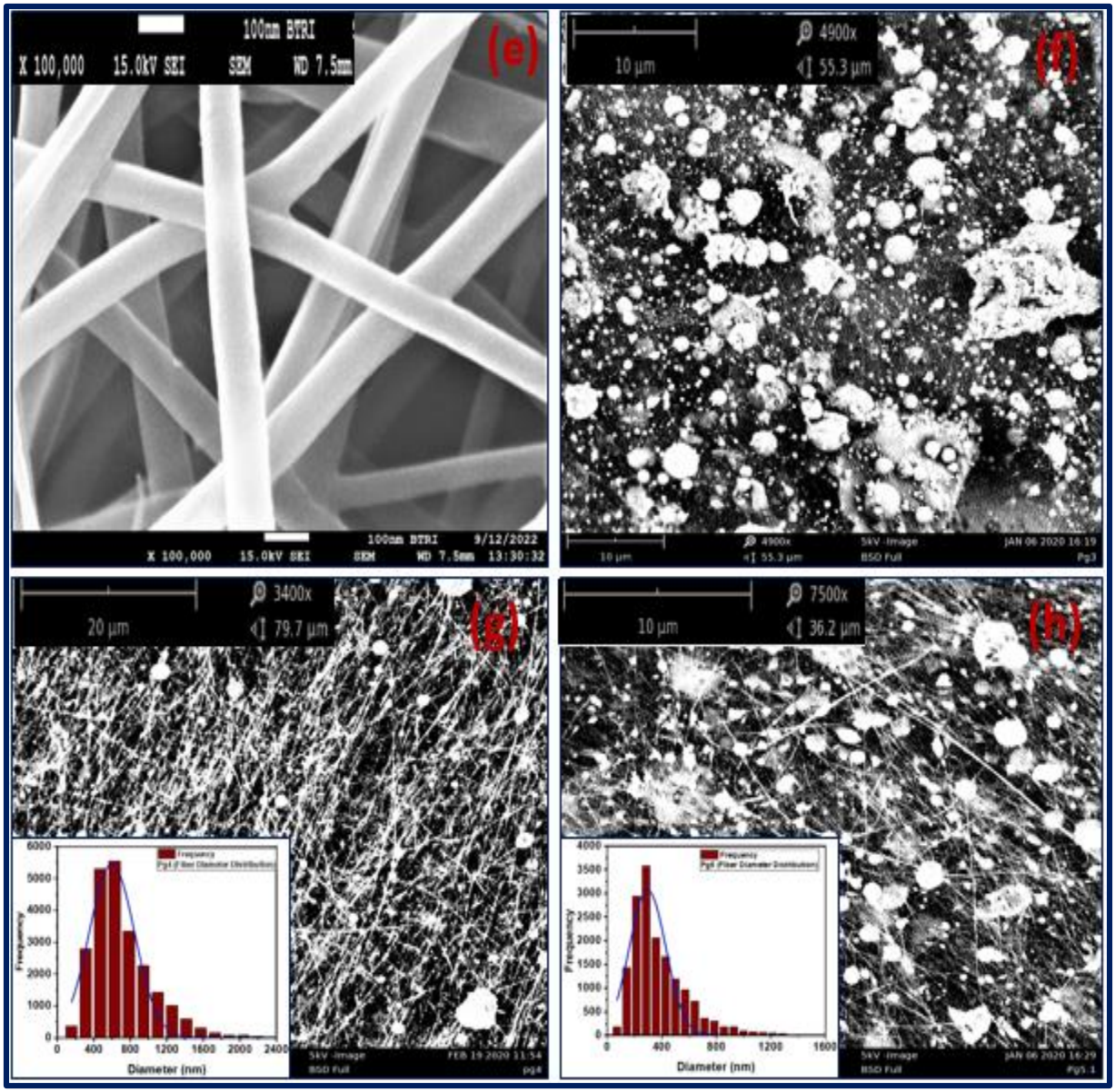

Figure. 3.16 SEM micrographs of the scaffolds and histogram of fibers diameters: (a) P (b) G, (c) Pg1 (d) Pg2 (e) Pg2 (higher magnification, 100,000x) (f) Pg3, g)Pg4, and (h) Pg5

3.2.5 IR Analysis

Figure 3.17 shown the IR spectrum of P, G, and Pg1 to Pg5. Peaks at 3290 cm^{-1}, 2930 cm^{-1}, and 1746 cm^{-1} can be assigned to the terminal –OH stretching, -CH- stretching, and –C=O stretching in P. Two weak peaks at 1447 cm^{-1} and 1362 cm^{-1} in P were attributed due to the –CH bending mode of vibrations of –CH- and $–CH_3$ group. IR absorption bands in P for –C-O stretching modes were appeared at 1199 cm^{-1} and at 1090 cm^{-1} [17].

IR spectrum of G shown a broad peak at 3285 cm^{-1} for the H-bonded -OH and -N-H stretching modes whereas band at 1638 cm^{-1} (amide I) was observed for -C=O stretching vibration that coupled with -C-N stretching vibration. Band at 1533 cm^{-1} (amide II) can be assigned to the combination of –C-N (out-of-phase) stretching vibration with the in plane bending mode of N-H vibration. Another characteristic band which was attributed at 1239 cm^{-1} (amide III) was for the C-N stretching mode and N-H bending mode together with the wagging mode of -CH_2 of adjacent amino acid residues [13]. FT-IR spectrum of Pg1 to Pg5 revealed the characteristic vibration bands of both polymer fibers (Figure 3.17). A broad band in the spectrum of Pg1-Pg5 at 3285 cm^{-1} (amide A), a peak at 1638 cm^{-1} (amide I), and at 1533 cm^{-1} (amide II), are characteristic peaks for G. Peak positioned at 1746 cm^{-1}, 1191 cm^{-1}, and 1086 cm^{-1} are the characteristic peaks for P were also observed in the spectrum of all blended scaffolds except Pg1. It could be due to the less (10%) percentage of PLA in Pg1. The intensity of these peaks was noticed as increased with the increase of PLA percentages in the blended electrospun scaffolds. However, characteristic peaks for T80 (-OH stretching, -C=O stretching, -CH stretching, -CO stretching) which was added only 8% (v/v) for the preparation of blended scaffolds may be overlapped with characteristic peaks of PLA or gelatin [18]. The IR spectrum of the electrospun blended scaffolds is also a good indication of physical interactions between the polymers with the help of T80.

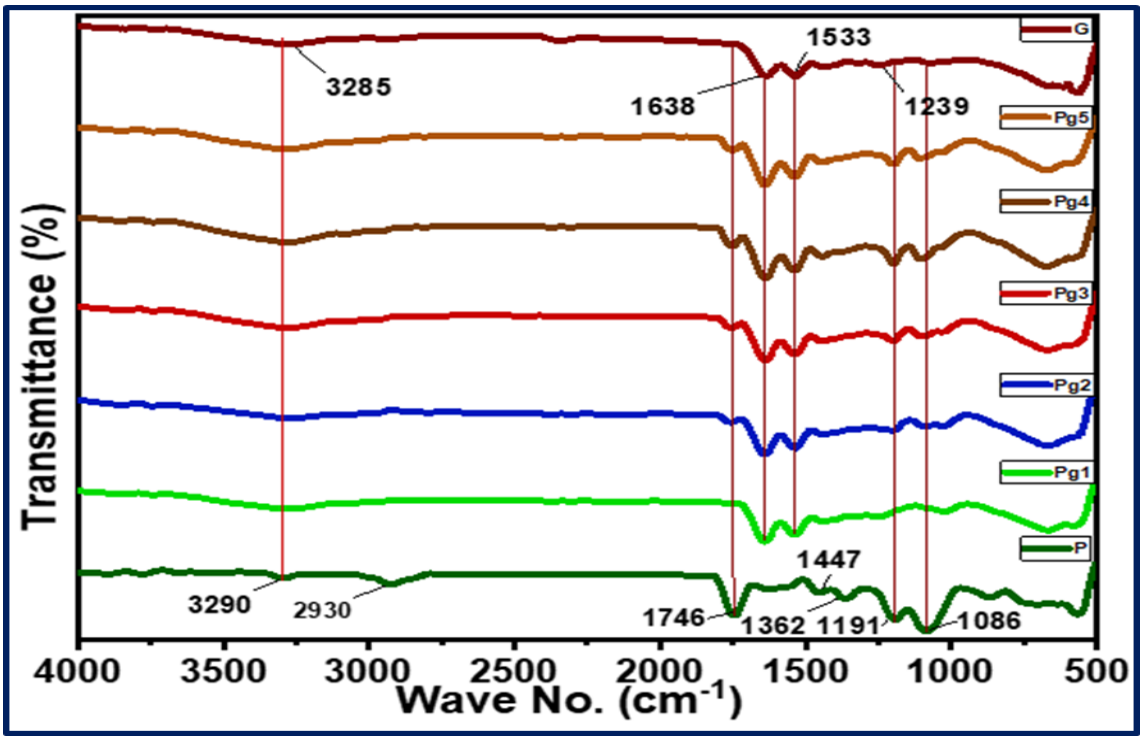

Figure 3.17 FT-IR spectrum of nanofibrous scaffolds of P, G, and Pg1-Pg5

3.2.6 Thermal Analysis

TG and DTG thermogram of electrospun scaffolds are shown in Figure 3.18. Single stage thermal changes occurred in P whereas two stages thermal changes were observed in G and Pg2. Maximum mass loss in P was started at 266 ^{o}C, maximum decomposition occurred at 348 ^{o}C, and that was ended at 377 ^{o}C with the mass loss of 97.6%. G showed a noticeable mass loss at temperature of 85 ^{o}C and finally decomposed at 327 ^{o}C with 23% of the residue left. Initial mass loss of Pg2 was 6.5% at 81 ^{o}C and maximum decomposition occurred at 320 ^{o}C with 34% of the residue left. This is because of the presence of comparatively more thermally resistant PLA remain at 320 ^{o}C. Pg2 was observed thermally less stable than that of G.

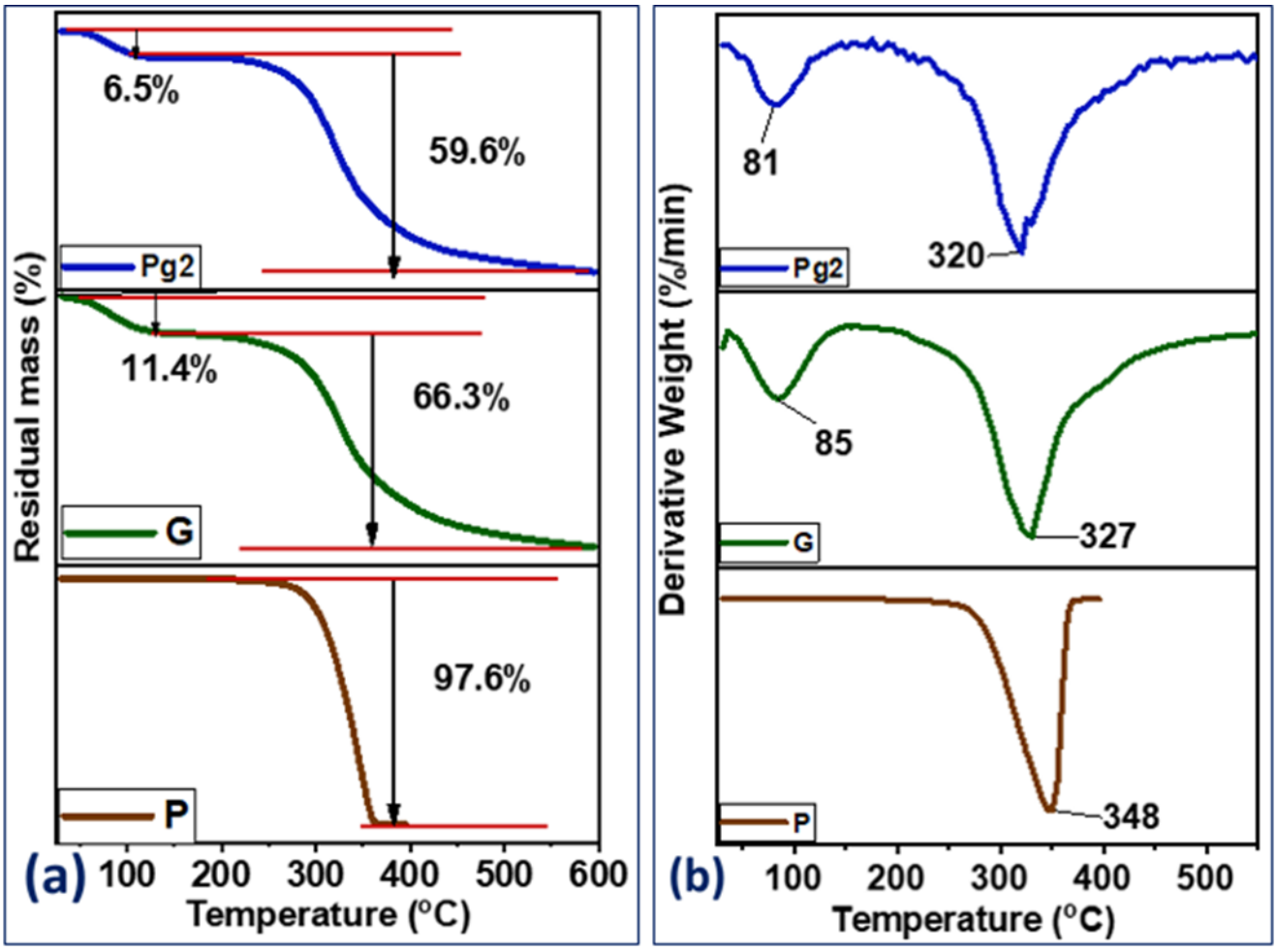

Figure 3.18 (a) TG and (b) DTG curves of nanofibrous scaffolds P, G, and Pg2

DSC and DDSC thermograms of the fibrous mats are showed in Figure 3.19. The peak at 54 ^{o}C, and a sharp peak at 155 ^{o}C in P can be assigned as T_g and melting temperature respectively. It was

reported in the previous work that electrospun PLA fiber showed a T_g, and T_m at 58.5 °C, and 152.3 ^oC respectively [19]. An endothermic peak at 48 ^oC in the DSC curve of G could be attributed for the denaturation of G in association with the destruction of helical structure. Another peak which was observed at 70°C is the melting temperature of G, and the peak at 218 ^oC is for the decomposition of gelatin reported in the earlier research work [10]. DSC curve of Pg2 showed an endothermic peak observed at 60 °C. Sometimes crystallization is not facilitated due to the rapid vaporization of the solvent and consequent solidification of stretched polymers during electrospinning[19] . DDSC of Pg2 showed a less intense peak at 160°C like P (temperature of melting at 155°C), and a small peak at 215°C like G temperature of decomposition (at 218 °C). T_g for a bi-polymer blend could be attributed between the T_g of the two polymers [20].

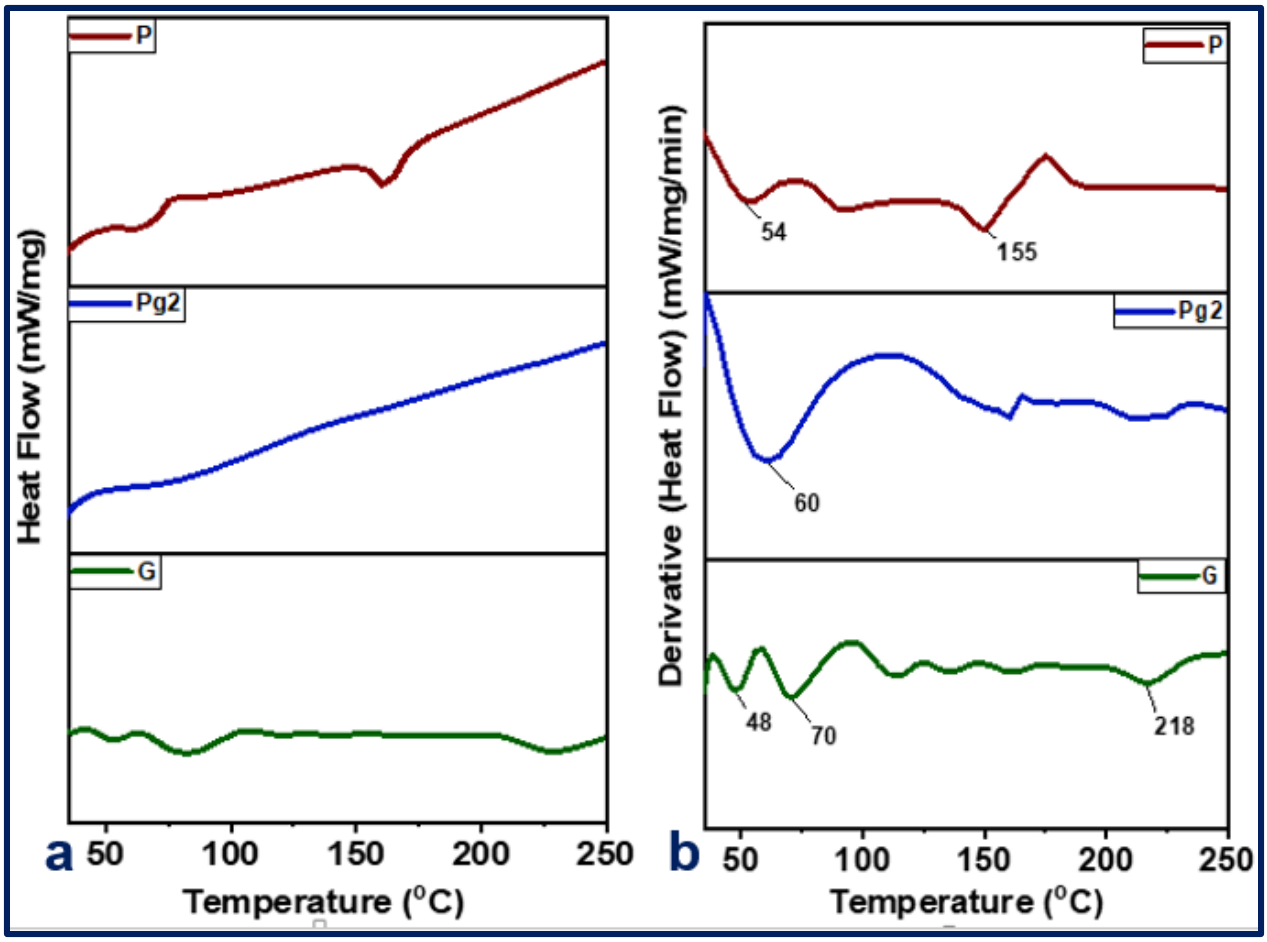

Figure 3.19 (a) DSC, and (b) DDSC curves of scaffolds P, G, and Pg2

This is also a good indication of the uniform blending of the bi-polymers (Pg2) during electrospinning.

3.2.7 XRD Analysis

The XRD profile of P, G, and Pg2 are presented in Figure 3.20, and Table 3.8. It was reported that PLA pellet has the characteristic peaks at 16.5 º, and 19.1 º in its XRD pattern which is the indication of its semicrystalline structure [7]. Electrospun scaffolds P and Pg2 showed the similar semicrystalline molecular pattern with the characteristic peaks in the XRD curves at 16.9 º and 19.3 º as 2θ value whereas XRD profile observed for G shows the amorphous nature of it. XRD peak at 16.9 º occurred in P with d spacing value of 1.31 Å, FWHM (Full width half maximum) value as 12.3. The d spacing and FWHM found in Pg2 were 5.27 Å and 0.62 respectively. As compared with the P, crystallite size in Pg2 is greater than that of P because the lower FWHM value indicates the higher crystallite size [21]. Crystallinity percentage for Pg2 was calculated as 64.64% and the same for P was observed as 48.35%.

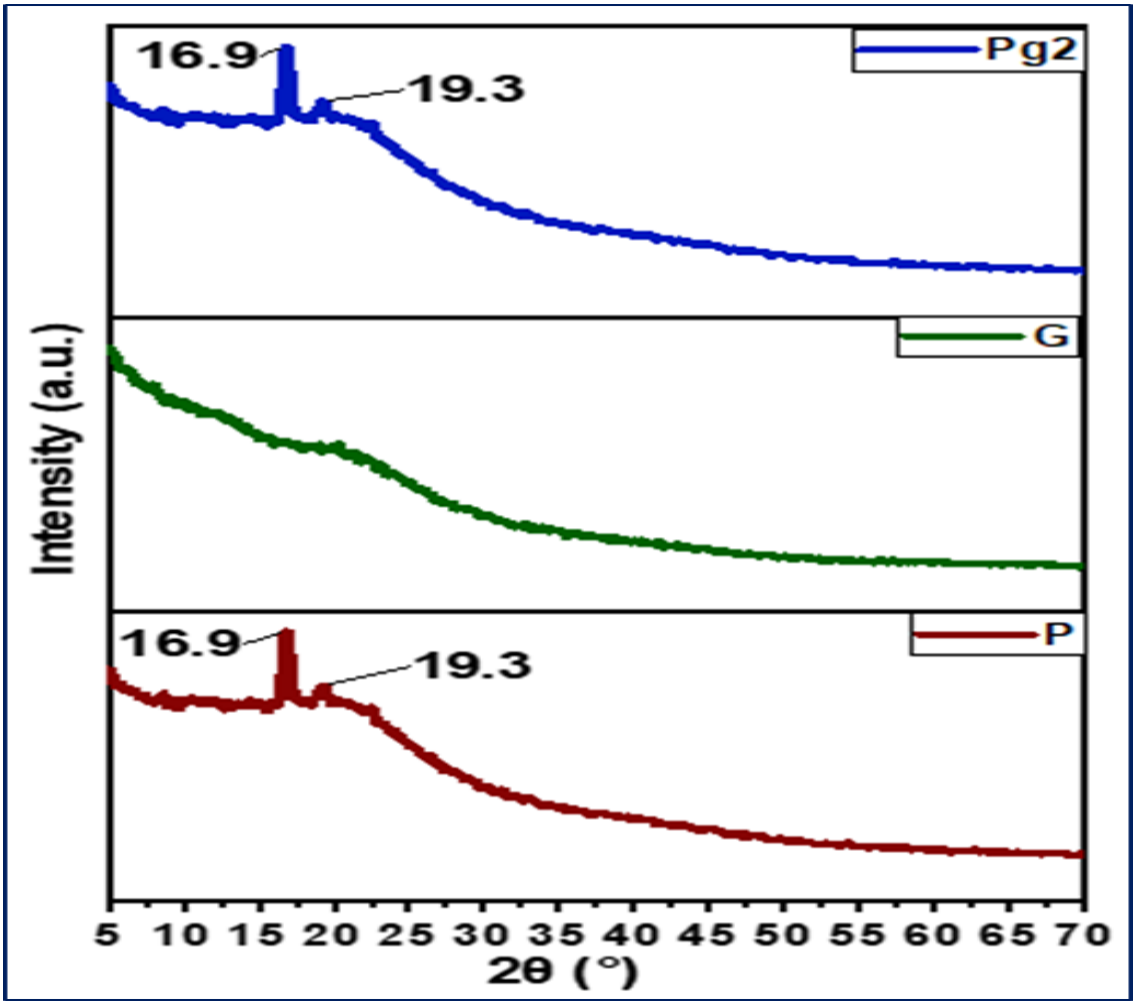

Figure 3.20 X-ray diffractogram of scaffolds P, G, and Pg2

Table 3.8 XRD parameters of scaffolds P, G, and Pg2

XRD Parameters	P		G	Pg2	
2θ °	16.9	19.3	-	16.9	19.3
d (Å)	1.31	-	-		-
FWHM, °	12.3	-	-	0.62	-
Crystallinity (%)	48.35		-	64.64	

3.2.8 Contact Angle Measurement of Scaffolds

Bar diagram and the images of water contact angle of electrospun scaffolds are presented in Figure 3.21. Average water contact angle of P was observed as (96.3 ± 2.9) °, that is within hydrophobic region [6]. Scaffold G rapidly dispersed in water when the water droplet was dropped on the G.

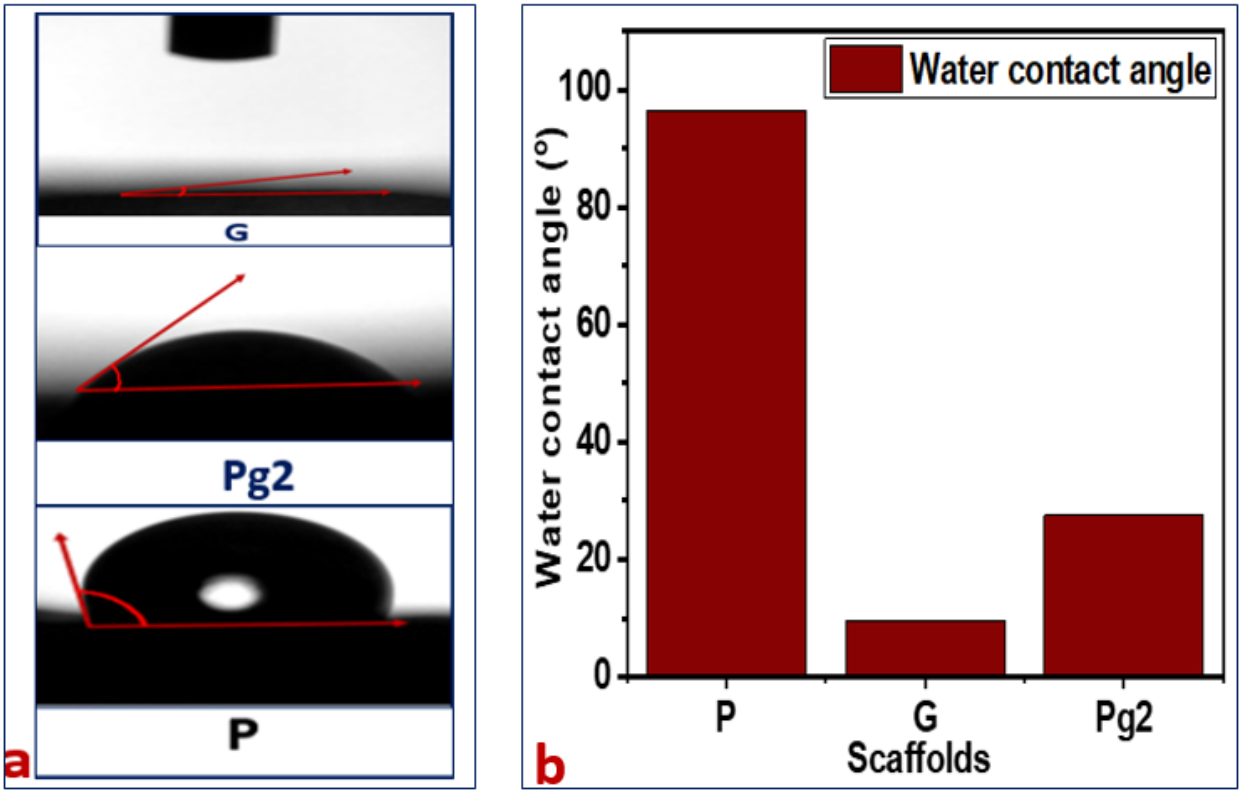

Figure 3.21. (a) Water contact angle of scaffolds of P, G, and Pg2 (b) Bar diagram of water contact angle of scaffolds

G was easily soluble in water as quickly as water was dropped on to it and average water contact angle was revealed (9.5±6.4)°. Blended scaffold Pg2 showed average water contact angle as

(27.5±1.4) ^{o} which is also in hydrophilic region. Optimum adhesion for cell requires moderate wettable materials [22]. Pg2 may contribute to cell adhesion as well as proliferation and differentiation of cell, and thus may create preferable environment for wound healing.

3.2.9 In Vitro Cytotoxicity Assay

Optical micrographs of cytotoxicity analysis are displayed in Figure 3.22, and the results are presented in Table 3.9, which revealed that all the scaffolds have more than 95% cell viability whereas control has 100% cell viability. This suggests that scaffolds are not cytotoxic.

Table 3.9 Cytotoxicity remarks of control, and scaffolds (P, G, and Pg2)

Sample ID	Survival of Vero cells	Remarks
Control	100%	No cytotoxicity
P	>95%	No cytotoxicity
G	>95%	No cytotoxicity
Pg2	>95%	No cytotoxicity

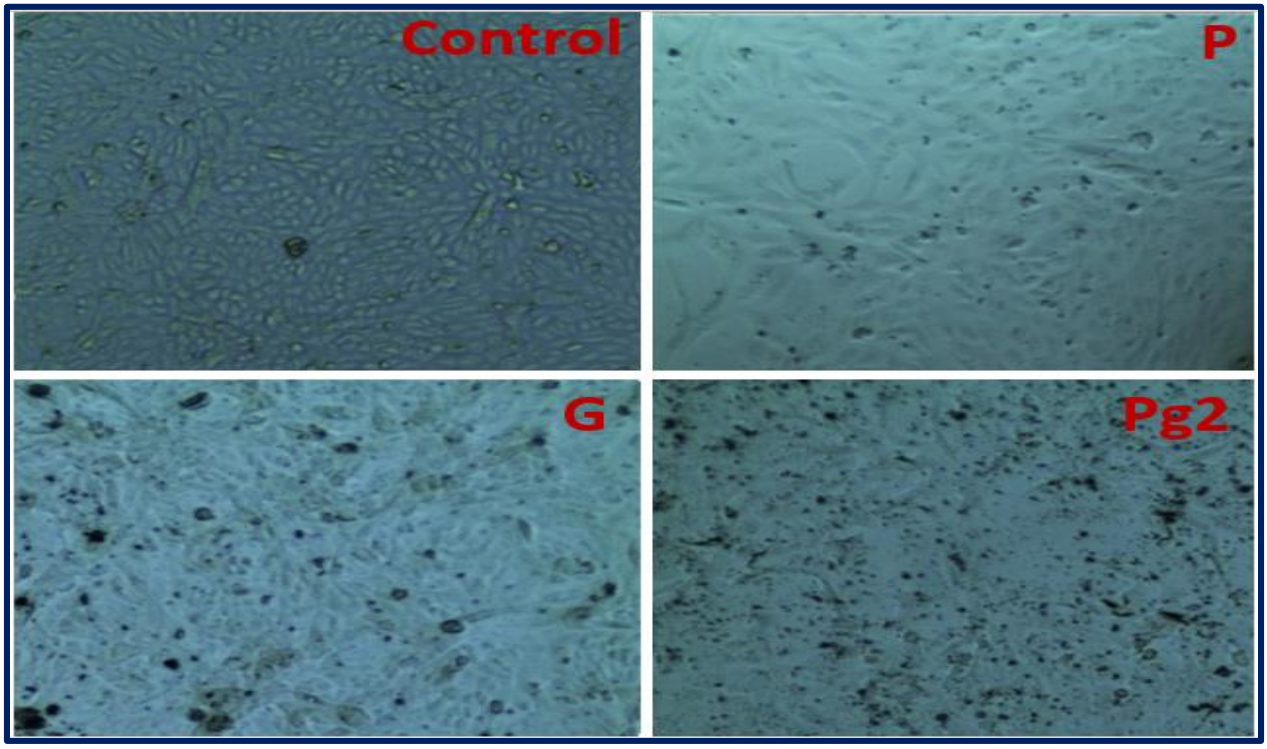

Figure 3.22 Optical microscopic images of Vero cell line with control, P, G, and Pg2 medium after 48 h of incubation

3.2.10 In Vivo Animal (Rat) Model Assay

The overall observations of wound beds created surgically with scaffolds or without treatment (control) are presented in Figure 3.23. At the day of wound created, no noticeable changes observed in the exterior of wound for all cases. All wound size was becoming reduced with the time and almost closed at the day of 14. However, the wound bed treated with Pg2 nanofibrous scaffold showed the higher relative wound reduction size (%) with time than that of the others.

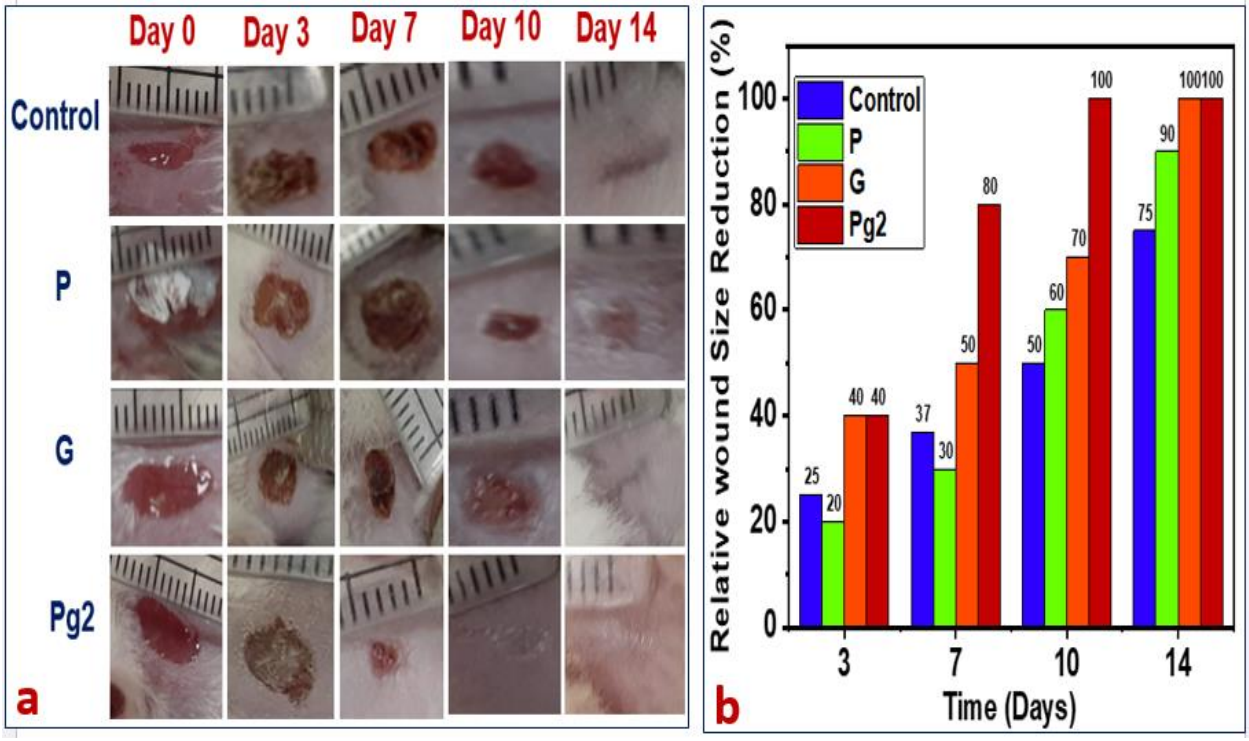

Figure 3.23. (a) Images of wound healing (b) Bar diagram of relative wound size reduction with time

At the day of 3, Pg2 and G showed 40% relative wound reduction whereas P, and control showed the same as 20%, 25% respectively. At the day 7, wound bed treated with Pg2 observed as 80% healing but the wound bed treated with G, P, and control showed relatively slower healing rate as 50%, 30%, and 37% respectively. Granulating tissues are formed after about 4 days of wound. A decrease in the inflammatory stage of the wound is progressively observed for the duration of the growing of migration phase which continues about two weeks and it was greater for Pg2 treated group rather than the other group [2]. Whole closing of wound was observed (100% closure) after 10 days of wound healing for Pg2. In addition, developing new skin observed plane while 70%, 60%, and 50% wound closure were observed during the period for G, and P treated groups as well the

control group respectively. At day 14, G treated group showed 100% healing with the hair coverage but P treated, and control group were healed 90%, and 75% correspondingly. Wound of control rat and rat treated with scaffold P showed comparatively slow wound restorative process. Thus the decrease in the size of wound area of the rat treated with Pg2 scaffold was noticeable than the same treated with other scaffolds applied. Pg2 could speed up the rate of wound closing possibly due to the combination of the healing properties such as cell-matrix interactions, biocompatibility, and other physicochemical properties of the constituents (PLA, gelatin) used in the preparation of Pg2 [23].

3.2.11 Histological Assay

Healing status of wound was assessed by observing the histology of the externally healed rat skin of treated and control groups at day 14 of post wound creation. Wound repairing was examined by considering the coverage of wound by epithelium, penetration of inflammatory cells, regeneration of collagen and its array, tissue granulation, and skin appendages regeneration [24]. Such processes are basic progress of wound towards healing until the completion of wound repairing [25].

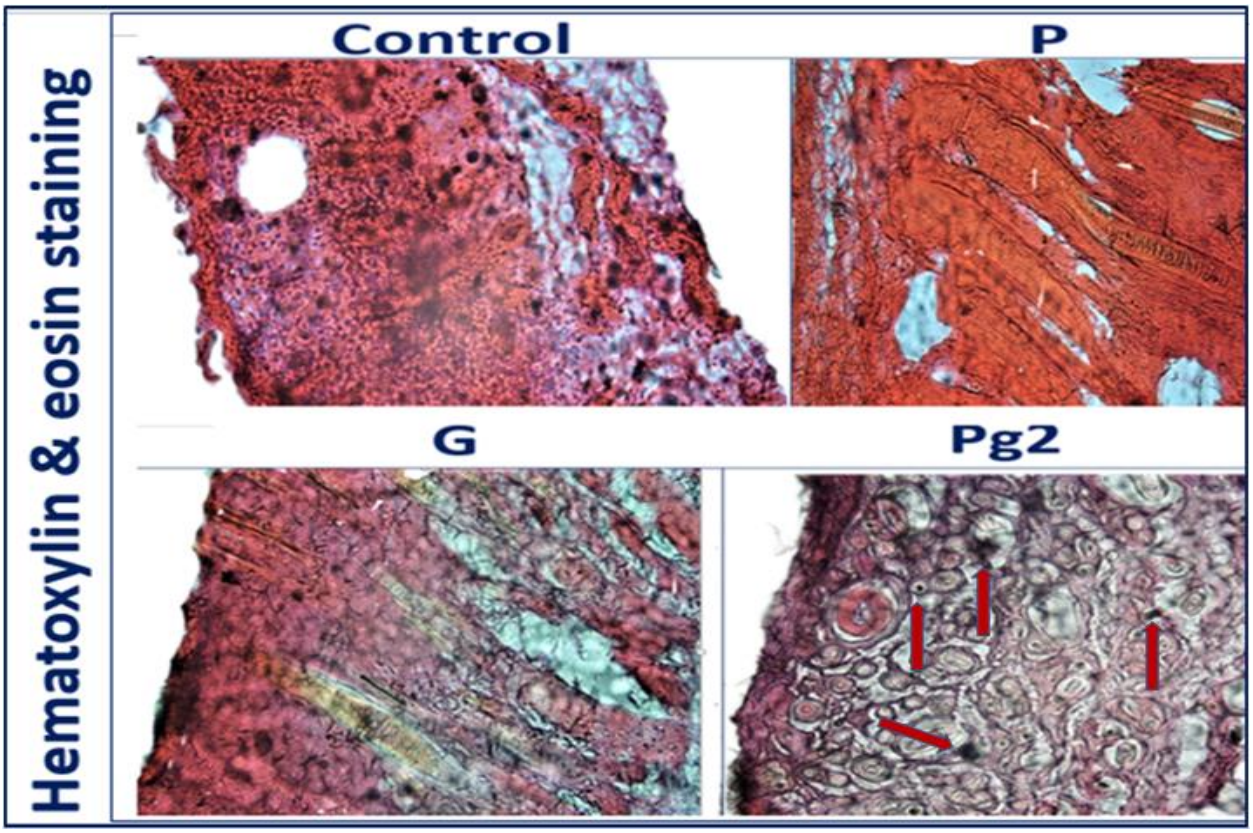

Figure 3.24 Photomicrographs of the histological responses to the nanofibrous scaffolds (control, P, G, and Pg2) after being applied in rat skin for 14 days

In Figure 3.24, it is evident that dermal structure is complete in Pg2 treated (shown in Figure 3.24 with arrow) skin tissue. Hair follicles, and collagen pattern were also seen in Pg2 treated skin tissue. In control, structured coverage with epithelium was not observed and there was some disorder at the epithelium. Collagen production and the presence of hair follicle were also absent in control. P, and G treated tissue showed partial re-epithelization. G treated tissue though showed some structural arrangement, and some skin appendages but in P treated tissue, there was structured pattern without any skin appendages such as hair follicles. These observations were also in line with the healing percentages observed from the images of wound healing of treated and untreated groups. Thus Pg2 (bi-polymeric nanofibrous scaffold) treated tissue revealed a better wound healing which started earlier than the P treated, and control groups and this progress of healing was continued all over the healing process. This trend was not observed in G treated group though earlier healing was also stared in the G treated group.

3.2.12 Conclusion

Gelatin and polylactic acid (PLA) blends of different compositions were prepared with T80 as surfactant. Among them Pg2 scaffold has a more uniform and smaller average fiber diameter of 139±51 nm with almost no bead in the scaffolds. Conductivity and viscosity measurement of the Pg2 were obtained 650 μS/cm and 155 cP which were higher than that of PLA alone and thus addition of PLA in gelatin increases the spinnability of PLA. Further work could be considered to observe the effect of temperature in the spinnability of the blended solution as viscosity depends on temperature. IR, thermal and X-ray analysis showed that the blend scaffold actually maintains properties that is a combination of the properties of PLA and gelatin without any adverse change. Water contact angle of Pg2 exposed that the hydrophilicity of the blend scaffold was neither too hydrophobic nor too hydrophilic. The nano size and the hydrophilic quality of the Pg2 scaffold may facilitate adherence and growth of cell within it in a controlled manner. Thus Pg2 may adhere to cell in a controlled manner unlike scaffold obtained from pristine gelatin which may work for rapid cell adhesion and also unlike scaffold obtained from PLA which was hydrophobic in nature. The rat model data has justified the above conclusion giving a faster healing of the wounded area of the rat compared to that obtained by using P or G alone.

References

[1] T. Li, M. Sun, and S. Wu, "State-of-the-Art Review of Electrospun Gelatin-Based Nanofiber Dressings for Wound Healing Applications," *Nanomaterials*, vol. 12, no. 5, p. 784, 2022, doi: 10.3390/nano12050784.

[2] P. Zahedi, I. Rezaeian, S. O. Ranaei-Siadat, S. H. Jafari, and P. Supaphol, "A review on wound dressings with an emphasis on electrospun nanofibrous polymeric bandages," *Polym. Adv. Technol.*, vol. 21, no. 2, pp. 77–95, 2010, doi: 10.1002/pat.1625.

[3] W. Liu *et al.*, "Bioactive antiinflammatory antibacterial hemostatic citrate-based dressing with macrophage polarization regulation for accelerating wound healing and hair follicle neogenesis," *Bioact. Mater.*, vol. 6, no. 3, pp. 721–728, 2021, doi: 10.1016/j.bioactmat.2020.09.008.

[4] A. Memic, T. Abdullah, H. S. Mohammed, K. Joshi Navare, T. Colombani, and S. A. Bencherif, "Latest Progress in Electrospun Nanofibers for Wound Healing Applications," *ACS Appl. Bio Mater.*, vol. 2, no. 3, pp. 952–969, Mar. 2019, doi: 10.1021/acsabm.8b00637.

[5] N. Mamidi *et al.*, "Recent Advances in Designing Fibrous Biomaterials for the Domain of Biomedical, Clinical, and Environmental Applications," *ACS Biomater. Sci. Eng.*, vol. 8, no. 9, pp. 3690–3716, Sep. 2022, doi: 10.1021/acsbiomaterials.2c00786.

[6] H. Chen *et al.*, "Instant in-situ Tissue Repair by Biodegradable PLA/Gelatin Nanofibrous Membrane Using a 3D Printed Handheld Electrospinning Device," *Front. Bioeng. Biotechnol.*, vol. 9, no. July, pp. 1–12, 2021, doi: 10.3389/fbioe.2021.684105.

[7] A. A. Leyva-Verduzco *et al.*, "Electrospun tubes based on PLA, gelatin and genipin in different arrangements for blood vessel tissue engineering," *Polym. Bull.*, vol. 77, no. 11, pp. 5985–6003, 2020, doi: 10.1007/s00289-019-03057-7.

[8] S. Wang, Y. Zhang, H. Wang, G. Yin, and Z. Dong, "Fabrication and properties of the electrospun polylactide/silk fibroin-gelatin composite tubular scaffold," *Biomacromolecules*, vol. 10, no. 8, pp. 2240–2244, 2009, doi: 10.1021/bm900416b.

[9] H. W. Kim, H. S. Yu, and H. H. Lee, "Nanofibrous matrices of poly(lactic acid) and gelatin polymeric blends for the improvement of cellular responses," *J. Biomed. Mater. Res. - Part A*, vol. 87, no. 1, pp. 25–32, 2008, doi: 10.1002/jbm.a.31677.

[10] N. Mamidi, I. L. Romo, E. V. Barrera, and A. Elías-Zúñiga, "High throughput fabrication of curcumin embedded gelatin-polylactic acid forcespun fiber-aligned scaffolds for the

controlled release of curcumin," *MRS Commun.*, vol. 8, no. 4, pp. 1395–1403, 2018, doi: 10.1557/mrc.2018.193.

[11] S. F. Hashemi, M. Mehrabi, A. Ehterami, A. M. Gharravi, F. S. Bitaraf, and M. Salehi, "In-vitro and in-vivo studies of PLA / PCL / gelatin composite scaffold containing ascorbic acid for bone regeneration," *J. Drug Deliv. Sci. Technol.*, vol. 61, no. August, p. 102077, 2021, doi: 10.1016/j.jddst.2020.102077.

[12] C. Boonpratum, P. Naemchanthara, P. Limsuwan, and K. Naemchanthara, "Effects of chitosan and Tween 80 addition on the properties of nanofiber mat through the electrospinning," *E-Polymers*, vol. 22, no. 1, pp. 234–248, 2022, doi: 10.1515/epoly-2022-0029.

[13] M. Erencia *et al.*, "Electrospinning of gelatin fibers using solutions with low acetic acid concentration: Effect of solvent composition on both diameter of electrospun fibers and cytotoxicity," *J. Appl. Polym. Sci.*, vol. 132, no. 25, pp. 1–11, 2015, doi: 10.1002/app.42115.

[14] T. Abudula, U. Saeed, A. Memic, K. Gauthaman, M. A. Hussain, and H. Al-Turaif, "Electrospun cellulose Nano fibril reinforced PLA/PBS composite scaffold for vascular tissue engineering," *J. Polym. Res.*, vol. 26, no. 5, 2019, doi: 10.1007/s10965-019-1772-y.

[15] B. Journal, E. Niehues, and M. G. N. Quadri, "Spinnability, morphology and mechanical properties of gelatins with different bloom index," vol. 34, no. 01, pp. 253–261, 2017.

[16] E. Hoveizi, M. Nabiuni, K. Parivar, S. Rajabi-Zeleti, and S. Tavakol, "Functionalisation and surface modification of electrospun polylactic acid scaffold for tissue engineering," *Cell Biol. Int.*, vol. 38, no. 1, pp. 41–49, 2014, doi: 10.1002/cbin.10178.

[17] E. Meaurio, N. López-Rodríguez, and J. R. Sarasua, "Infrared spectrum of poly(L-lactide): Application to crystallinity studies," *Macromolecules*, vol. 39, no. 26, pp. 9291–9301, 2006, doi: 10.1021/ma061890r.

[18] K. Pramod, C. V. Suneesh, S. Shanavas, S. H. Ansari, and J. Ali, "Unveiling the compatibility of eugenol with formulation excipients by systematic drug-excipient compatibility studies," *J. Anal. Sci. Technol.*, vol. 6, no. 1, 2015, doi: 10.1186/s40543-015-0073-2.

[19] H. Batista *et al.*, "Electrospun composite fibers of PLA/PLGA blends and mesoporous silica nanoparticles for the controlled release of gentamicin sulfate," *Int. J. Polym. Mater. Polym. Biomater.*, vol. 71, no. 9, pp. 635–646, 2022, doi: 10.1080/00914037.2021.1876053.

[20] I. M. Kalogeras, “Glass-Transition Phenomena in Polymer Blends,” *Encycl. Polym. Blends*, vol. 3, pp. 1–134, 2016, doi: 10.1002/9783527653966.ch1.

[21] J. J. Senkevich and S. B. Desu, “Morphology of poly(chloro-p-xylylene) CVD thin films,” *Polymer (Guildf).*, vol. 40, no. 21, pp. 5751–5759, 1999, doi: 10.1016/S0032-3861(98)00793-9.

[22] P. B. van Wachem *et al.*, “Adhesion of cultured human endothelial cells onto methacrylate polymers with varying surface wettability and charge,” *Biomaterials*, vol. 8, no. 5, pp. 323–328, 1987, doi: 10.1016/0142-9612(87)90001-9.

[23] F. Xu, H. Wang, J. Zhang, L. Jiang, W. Zhang, and Y. Hu, “A facile design of EGF conjugated PLA/gelatin electrospun nanofibers for nursing care of in vivo wound healing applications,” *J. Ind. Text.*, vol. 51, no. 1, pp. 420S-440S, 2022, doi: 10.1177/1528083720976348.

[24] H. J. Choi *et al.*, “AgNP and rhEGF-incorporating synergistic polyurethane foam as a dressing material for scar-free healing of diabetic wounds,” *RSC Adv.*, vol. 7, no. 23, pp. 13714–13725, 2017, doi: 10.1039/c6ra27322j.

[25] H. Liu *et al.*, “A functional chitosan-based hydrogel as a wound dressing and drug delivery system in the treatment of wound healing,” *RSC Adv.*, vol. 8, no. 14, pp. 7533–7549, 2018, doi: 10.1039/c7ra13510f.

3.3 Analysis of Electrospun Core-Sheath Gelatin-PLA Scaffolds (CSPG)

Graphical Abstract

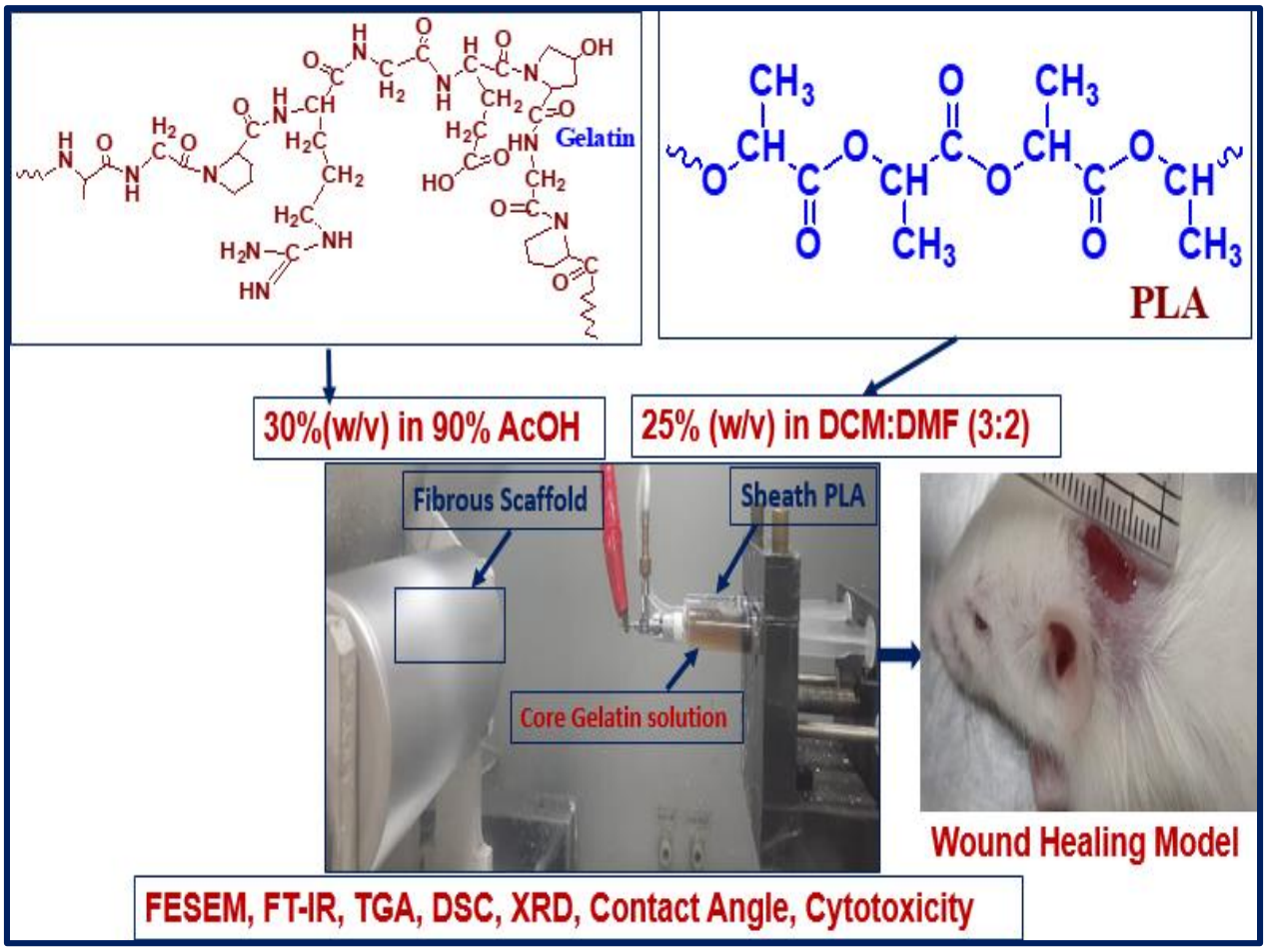

Abstract

Electrospun scaffolds possess nano, and biomimic structure which has exhibited with a sustainable and encouraging biomaterials particularly in biomedical appliances. Gelatin and poly (lactic acid) (PLA) both have cellular compatibility and biodegradability and are extensively used in the number of biomedical applications. Core-sheath bi-polymeric scaffold has been substantiated as a promising material centered on the requirement of scaffolds of component materials in which one polymer is covered (core) with another polymer. This work intended to prepare core-sheath scaffold by using gelatin as core material and PLA as sheath material to get the utmost properties of the polymers. PLA and gelatin fibrous scaffolds (named as P and G respectively) were made by applying 25% PLA (w/v) solution in dichloromethane (DCM) and dimethylformamide (DMF) at the ratio 3:2 (v/v) and 30% gelatin solution in 90% acetic acid in water (v/v). Core-sheath fibrous mats (CSPG) were prepared by taking gelatin as core material PLA as sheath material. Morphology of the scaffolds were determined by the FESEM that resulted that CSPG exhibited with the decreased average fiber diameter than that of the single polymer mats. Further characterizations of the fibrous mats through FTIR, TGA, DSC, and XRD revealed that CSPG retains intermediate compositional, thermal, and structural characteristics compared to P, and G. Core-sheath scaffold, CSPG maintained amphiphilic characteristics unlike hydrophobic or hydrophilic properties like P or G which established from water contact angle measurements. In vitro cytotoxicity assay confirmed the biocompatible nature of the scaffolds. In vivo rat model applications followed by the histological assay showed the improved cellular interactions towards wound curing steps in case of core-sheath bi-polymeric materials in comparison with single polymeric scaffold.

3.3.1 Introduction

From the past few decades, biomedical applications especially tissue engineering has been aimed to sustain, improve and regenerate numerous functions of tissues. Such an aim could be attained by making scaffolds that can mimic ECM (extracellular matrix) [1]. Scaffolds could provide necessary structural design for specific cellular functions such as cell propagation, differentiation, and movement of cell as well as play other supporting roles based on other physicochemical properties along with mechanical properties [2]. The prime scaffold standard for the purpose of tissue regeneration has biocompatibility. Along with scaffolds should be biodegradable, should possesses good mechanical properties, and outstandingly interlinked porosity with specific pore size. Fabrication of scaffolds with nanofibrous structure employed several technology such as self-assembly, electrospinning, and phase separation. Amongst them electrospinning is the utmost widely used practice for its simplicity, economical and capability to practice with wide-ranging of polymers [3]. Recently, several amendments have been employed to the fundamental electrospinning procedure with the aim to improve the excellence and functionality of the subsequent nanofibrous structures. One of the most promising amendment or core-shell bi-polymeric nanofibrous scaffolds through the coaxial electrospinning which has expanded considerations in a choice of application is the preparation of core-sheath process which is also named as two-fluid electrospinning process. This process usually employed two polymer solutions that should be provided individually over a coaxial tube or capillary and thus stretched by electrospinning process to produce nanofiber mats as core-sheath arrangement (one polymer as core material, and other as sheath material) [4]. Synthetic polymers such as several polyesters, polyamides, polysulfones, polyurethanes, and polycarbonates have been proven with good mechanical properties but their uses in tissue regeneration functions are discouraged due to their poor cell attraction for the lacking of recognition of cellular sites. On the contrary, polymers those can be obtained from natural sources as for example chitosan, gelatin, silk fibroin, elastin and collagen can be mixed with synthetic polymers as blend solutions to prepare scaffolds for the enhancement of the desired properties of synthetic polymers for the cellular functions [1]. Continuous advancements of technology for the preparation of scaffolds is demanding as infection can be caused from implantation, assured cytokines are as well necessary to be transported to the wounded site to make sure the cell sustainability and propagation. As the scaffold must own the capability to hold bioactive components as for example those require for growth, several proteins, drugs, and

enzymes to hold their cellular activity, and regulate their discharge in a sustainable mode, single polymeric scaffolds face restraint [5]. Biomolecules incorporated into single fibers are typically distributed homogeneously inside the fiber matrix or located in regions near to fiber surface because of phase separation within the fiber. Such environments are problematic for controllable and tunable release, and the bioactivity of biomolecules also could be endangered. Core–sheath fibrous scaffolds have been encouraged due to its ability for controlled, and adjustable release in cellular interactions. Core-shell nanofibrous mat prepared from PCL (polycaprolactone) as the sheath material, and gelatin as the core material was reported as the suitable structure for drug transportation and tissue regeneration [6]. Using of collagen as sheath, and PCL exhibited with the structure which has been proven as the preferred material for the proliferation of fibroblast cell and subsequent migration through it [7]. Poly(vinyl pyrrolidone) (PVP) as the core and PLA as sheath material were used for the core-sheath scaffolds which was reported to have the all potentials for drug transfer applications [8] . A core-sheath tubular scaffold prepared from polylactide fibers as the outer material and silk fibroin with gelatin fibers as inner material which has shown applicable biomechanical characteristics, and offered a promising environs for the growth of cells [9]. Keratin with gelatin as the natural polymer were employed in the coaxial electrospinning with polylactide as the synthetic polymer. Resulted scaffold showed increased properties to cell adhesion, propagation, and migration as well cell sustainability [10]. Core-shell nanofibrous bandages with PCL/ gelatin loaded with minocycline hydrochloride used as a shell and gelatin embeded with extracts of G. sylvestre as the core lead to improved mechanical properties when compared to pristine mats [11]. Gelatin is a high biocompatible, and biodegradable polymer materials which is a derivative of collagen, which could mimic ECM, and has nearly similar structures and properties for cellular functions like collagen [12]. Amongst the synthetic biodegradable polymer material, PLA have become the talented materials. However, PLA has hydrophobic characteristics, and is established as poor bioactive component which has less cellular interactions [13] . However, PLA is mostly hydrophobic, and gelatin is hydrophilic, this study aimed to prepare the core-sheath electrospun scaffolds by taking gelatin as core material, and PLA as sheath material to get the most of these synthetic and natural polymers specially to regulate the release of such bioactive components in wound dressing applications.

3.3.2 Morphology of Electrospun Scaffolds

Figure 3.25 displayed the FESEM micrographs of the electrospun scaffolds, histogram of the scaffolds as well the distribution of fibers in the scaffolds. Average fiber diameter, and mean pore area with the composition of electrospinning solution are presented in Table 3.10. All the scaffolds showed uniform and smooth surfaces containing constant aligned fibers. Fiber diameter depends on the composition of the solution with the operational parameters used for electrospinning and also with the differences in technology. Scaffold P presented random distribution of fiber with the average fiber diameter as (729±265) nm with the mean pore area as (4±6) μm^2.

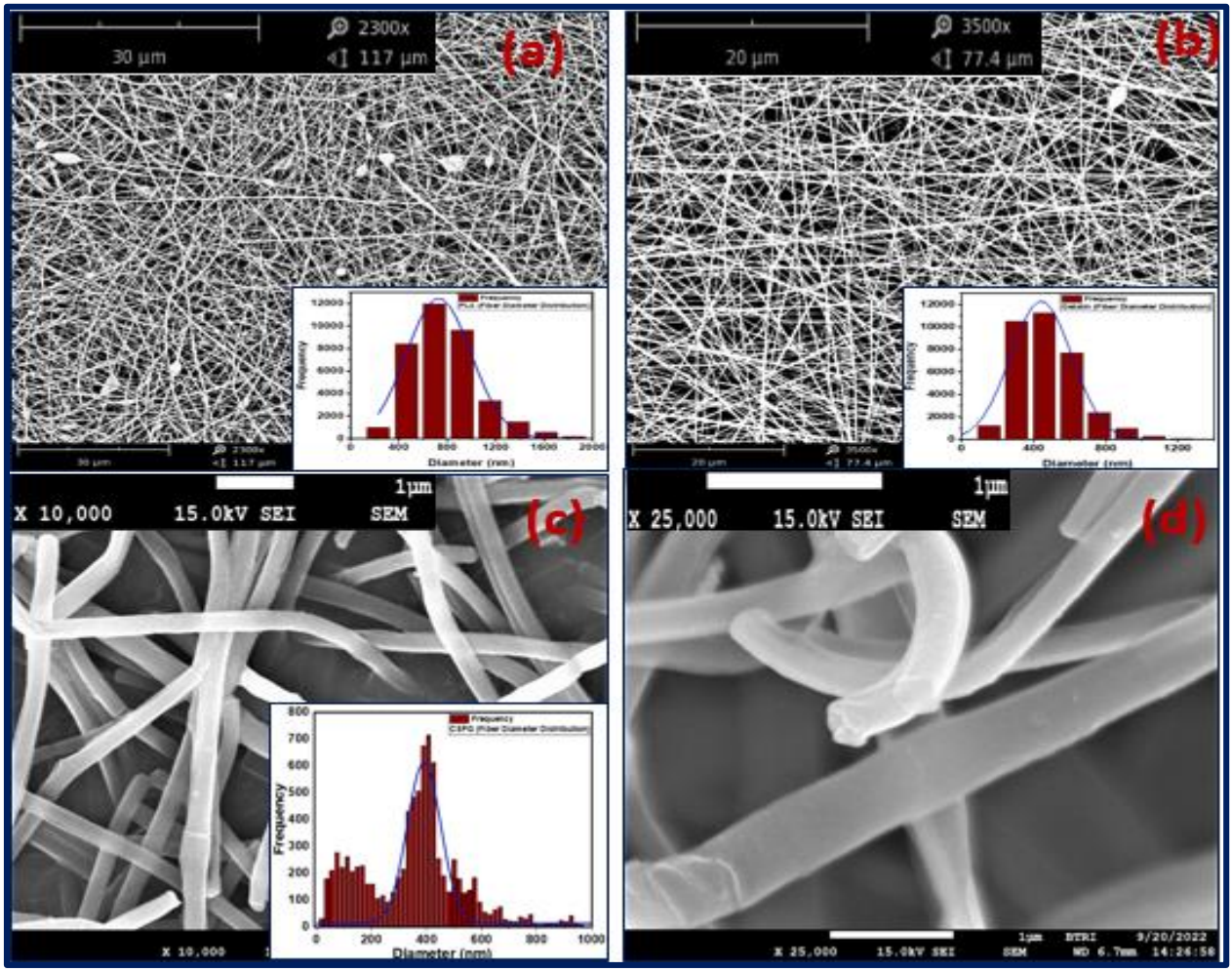

Figure 3.25 SEM micrographs of the scaffolds and histogram of fibers diameters: (a) P (b) G, (c) CSPG, (d) CSPG (higher magnification, 25,000x)

Table 3.10 Average Fibers diameter and pores diameter of electrospun scaffolds (P, G, and CSPG) with composition of electrospinning solutions

Sample	Composition of Samples (w/v)		Mean Fiber Diameter	Mean Pores Area
	PLA solution	Gelatin solution	± SD nm	± SD μm^2
P	25%	-	729±265	4±6
G	-	30%	441±169	4±7
CSPG	25%	30%	390±61	0.9±2

G was prepared from gelatin that showed the mean fiber diameter as (441±169) nm with the mean pore area as (4±7) μm^2. Mean pore area of P, and G were found as almost same, but mean fiber diameter G was observed as lower than that of P. Since the both the single polymeric scaffolds were prepared with the same operating conditions these morphological variations may be attributed from the variations in their concentrations, choice of solvents, and other solution parameters as well the molecular level. Core-sheath fibrous scaffold CSPG showed the lowest fiber diameter (390±61) amongst them with the pore area as (0.9±2) μm^2. These results revealed that mean fiber diameter of CSPG scaffold was around 47% decreased than that of P scaffold, and around 12% reduced than that of G scaffold. PLA-gelatin core-shell fibers where PLA was taken as core material, and gelatin was taken as the shell material were reported to have average fiber diameter as 347 ± 88 nm in the earlier research work [14].

3.3.3. FT-IR Analysis of Electrospun Scaffolds

IR spectrum of P, and G discussed in the section (3.2.5). Peaks in the spectrum of G at 3285 cm^{-1}, 1638 cm^{-1}, 1533 cm^{-1}, and 1239 cm^{-1} were attributed for the -OH and -N-H stretching, -C=O stretching coupled with -C-N stretching, –C-N (out-of-phase) stretching coupled with in plane bending mode of N-H vibration together with the wagging mode of $-CH_2$ vibrations respectively. Peaks at 3290 cm^{-1}, 2930 cm^{-1}, and 1746 cm^{-1} were assigned to the terminal –OH stretching, -CH- stretching, and –C=O stretching in P. In Figure 3.26, comparative FTIR spectrum of P, G, and CSPG are shown. CSPG showed a broad peak within 3500 cm^{-1} to 3000 cm^{-1} which was broader than that of the G , revealed the presence of more H-bonded –NH in CSPG. Peaks positioned within 1600 cm^{-1} to 1000 cm^{-1} in CSPG spectrum were showed similar pattern as both spectrum of G, and P with little shifting of absorption frequency as well as integration. Carbonyl absorption peak at 1746 cm^{-1} in the spectrum of P was not observed in the spectrum of CSPG. This can be

happened due to the nonbonding to π antibonding interactions amongst carbonyl groups of neighboring polymer chains where a nucleophile gives nonbonding lone-pair electrons to the empty π antibonding orbital of a nearby carbonyl group [15]. However spectrum of CSPG showed the presence of constituent single polymers.

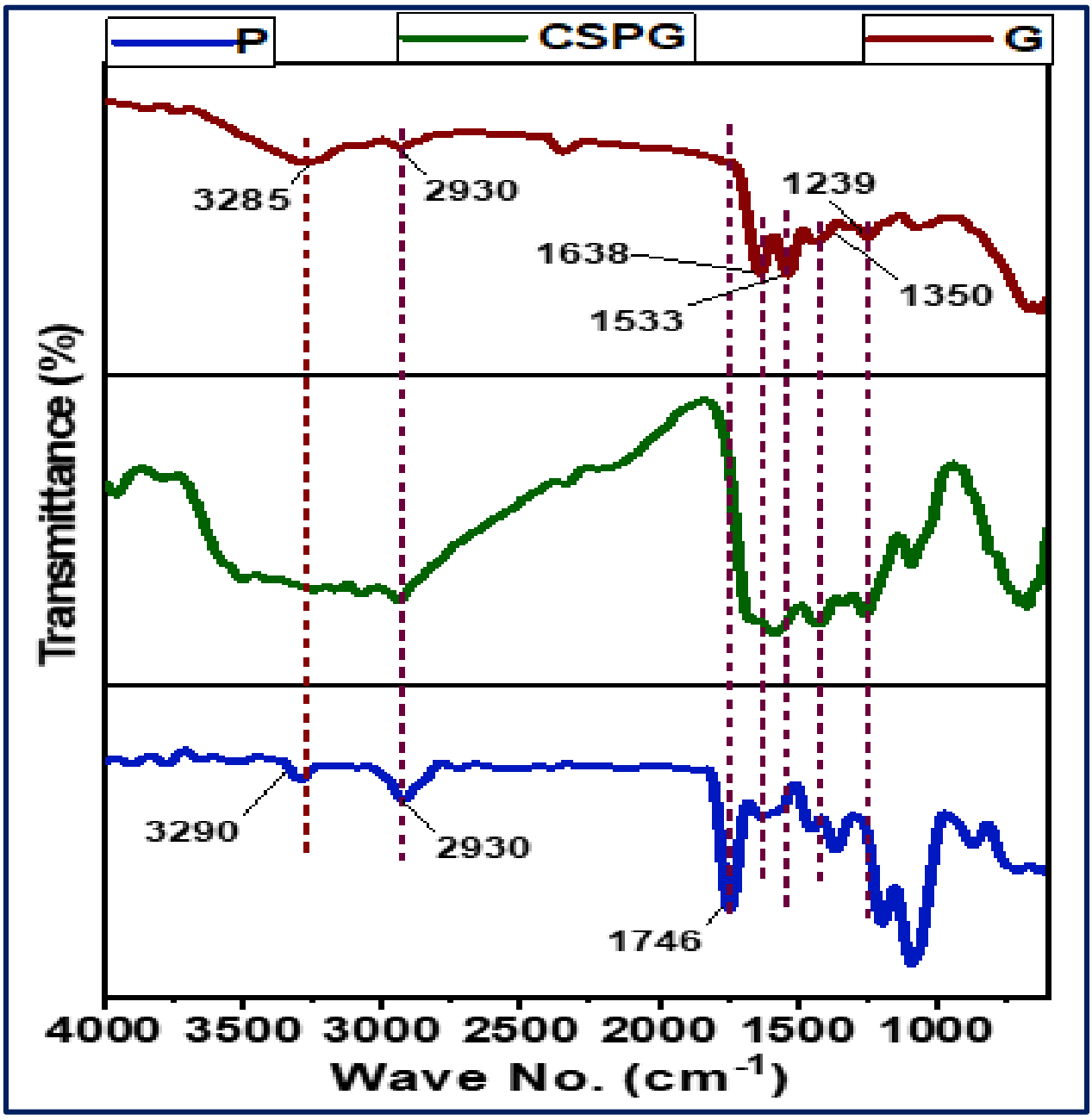

Figure 3.26 FT-IR spectrum of P, G, and CSPG

3.3.4 Thermal Analysis of Electrospun Scaffolds

TG and DTG thermogram of electrospun scaffolds P, G, and CSPG are displayed in Figure 3.27 One phase thermal change observed in P whereas two phase thermal changes were observed in G, and CSPG. Thermal decomposition pattern of P, and G was discussed in section 3.2.3.5. Almost similar thermal decomposition pattern was occurred for G, and CSPG. Preliminary mass loss of CSPG was observed as 6.9% at a T_{max} (Temperature of maximum mass loss) of 86 ^{o}C and

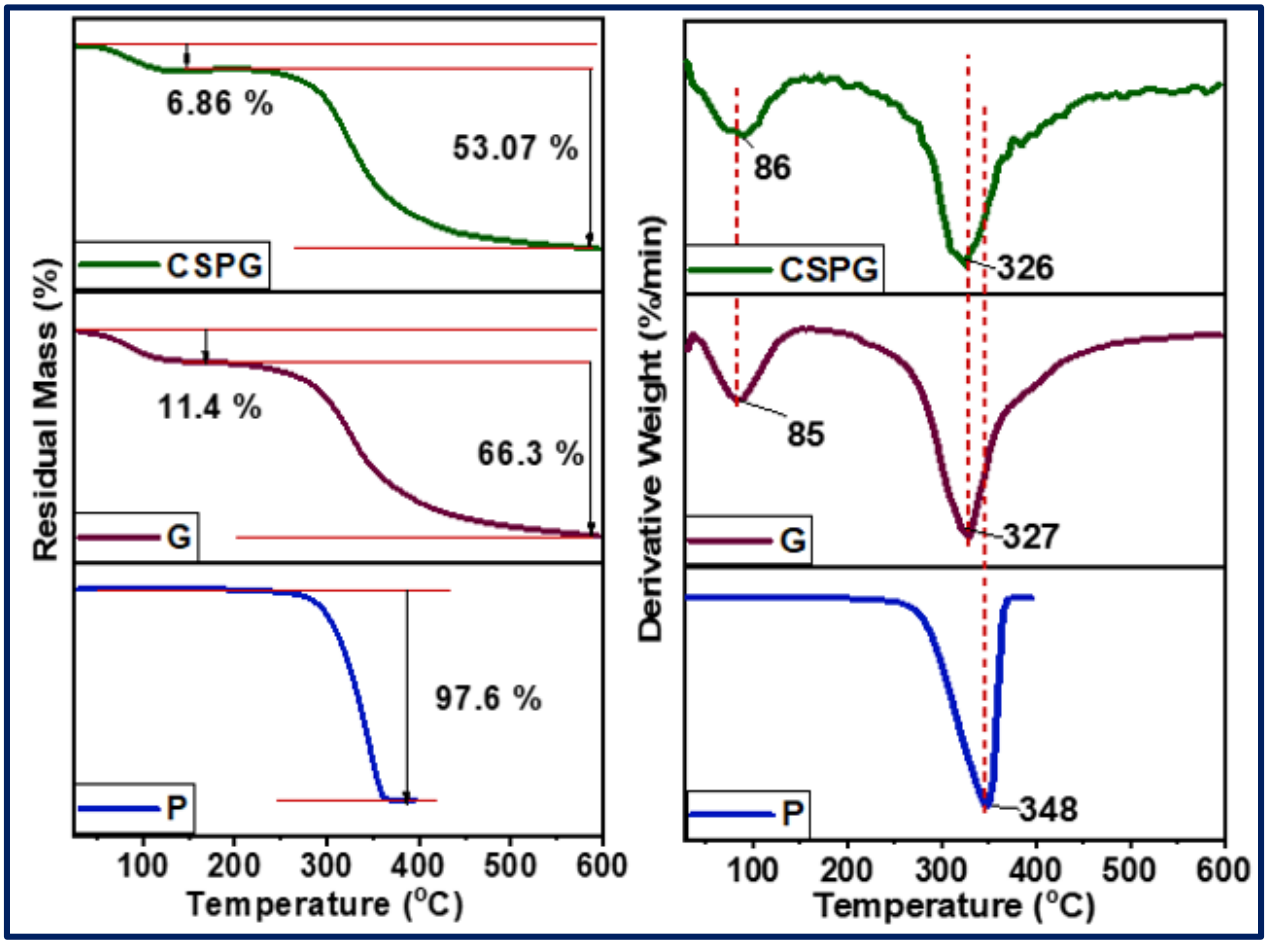

Figure 3.27 TGA and DTGA thermogram of electrospun scaffolds (P, G, and CSPG)

maximum degradation occurred at 326 ^{o}C whereas G showed maximum decomposition at 327 ^{o}C. Initial mass loss of G occurred about 11.4 % at T_{max} as 85^{o}C but final decomposition of G occurred with the remaining mass as about 22 %. CSPG was decomposed finally with the remaining residue as around 40 %. Some sort of chemical changes may be happened in the preparation of CSPG that reflected in its thermal properties. Figure 3.28 showed the comparative DSC, and DDSC thermogram of P, G, and CSPG. The peak at 54 ^{o}C, and a sharp peak at 155 ^{o}C in P is T_g and temperature of melting respectively. A peak at 48 ^{o}C in the DSC curve of G is for the denaturation

of G with the loss of helical structure. Peak which was observed at 70°C is the temperature of melting, and the peak at 218 °C is for the decomposition of gelatin. DSC curve of CSPG showed no distinctive features but the DDSC curve for the same showed a broad endothermic peak at 58 °C which was greater than the T_g of P but higher than the denaturation temperature of G, and lower than the melting temperature of G. There was no peak observed in the DDSC of CSPG around the melting temperature of P rather than a less intense peak at 220 °C. These results also support that some sort of chemical changes occurred during electrospinning of core and sheath solutions which was evident from the TGA, and DTGA analysis as well as FTIR analysis of CSPG.

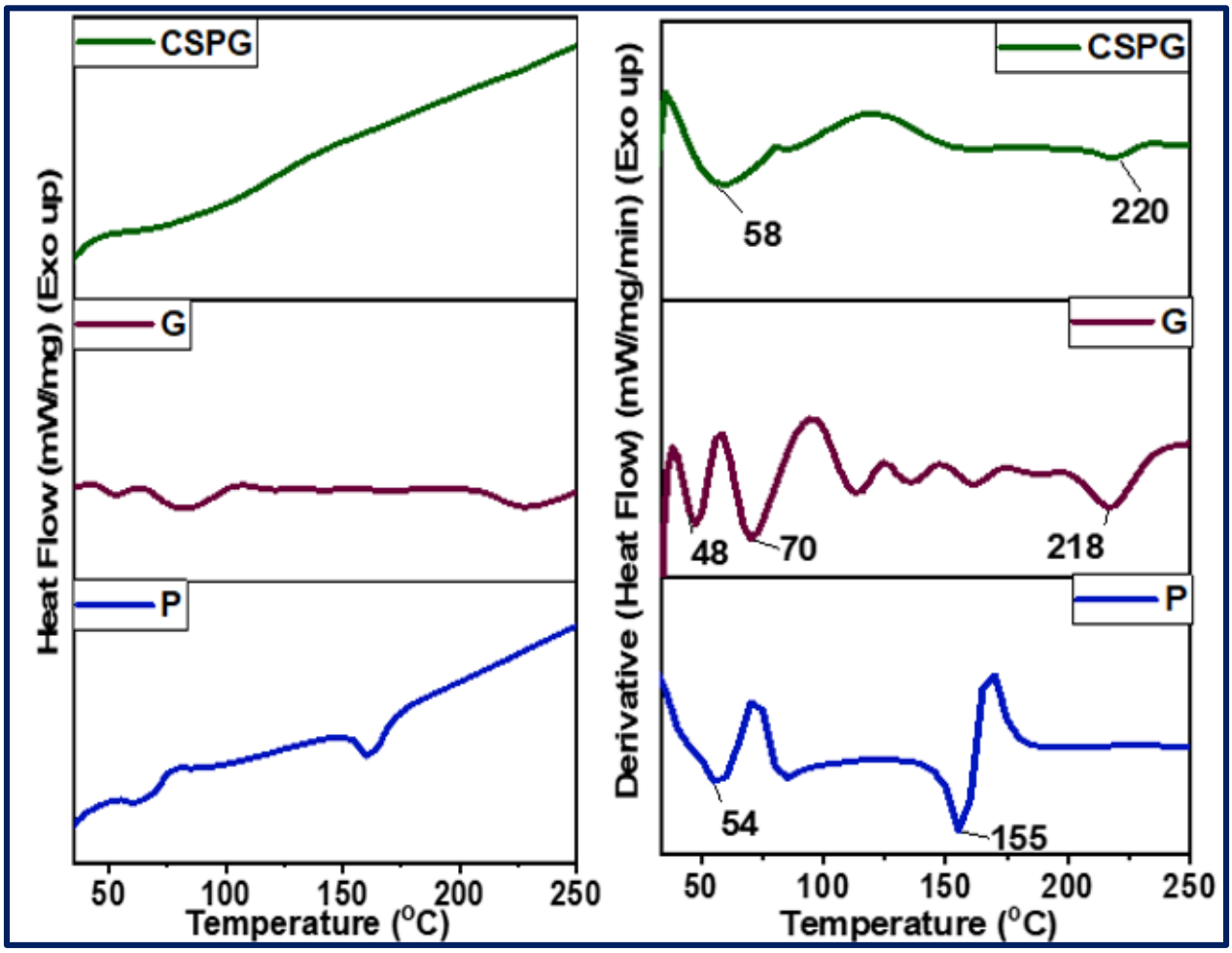

Figure 3.28 DSC, and DDSC curves of scaffolds P, G, and CSPG

3.3.5 XRD Analysis

The XRD pattern of P, G, and CSPG are shown in Figure 3.29. As discussed in the previous section (3.2.7) that electrospun scaffold P possesses semicrystalline molecular pattern with the

characteristic peaks in the XRD graph at 16.9 º and 19.3 º as 2θ value like PLA. XRD profile of G

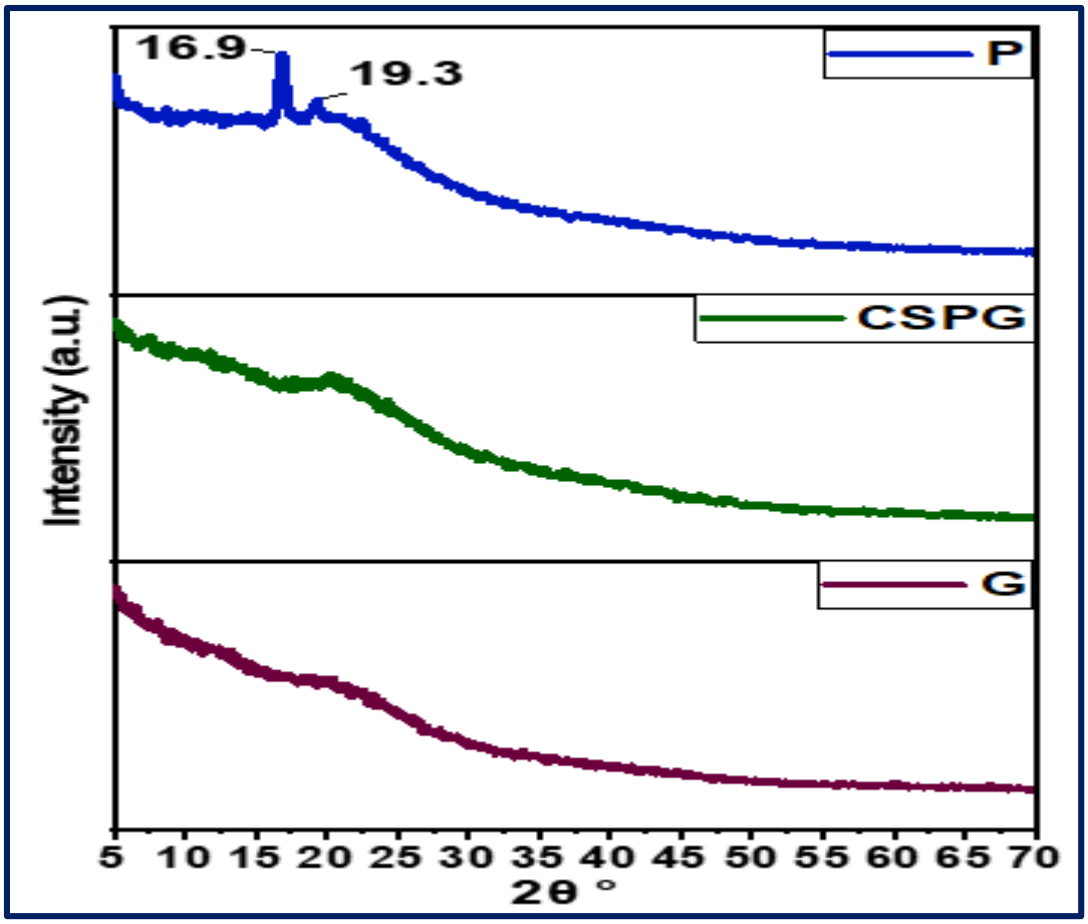

Figure 3.29 X-ray diffractogram of scaffolds P, G, and CSPG

indicates the amorphous nature of it. XRD graph of CSPG revealed the similar profile like G that indicated that CSPG was also amorphous in nature. This results indicated that for the duration of electrospinning crystallization was not preferred due to the fast vaporization of the solvent and successive solidification of stretched polymer solutions caused poor ordered structural organization in CSPG.

3.3.6 Water Contact Angle of Electrospun Scaffolds

Water contact angle image of electrospun scaffolds, and representative bar diagram are shown in Figure 3.30. Average contact angle of P, and G (discussed in section 3.2.8) were observed as (96.3 ± 2.9) º, and (9.5±6.4) º that were within hydrophobic region, and hydrophilic region respectively [16]. Core-sheath scaffolds CSPG showed contact angle in the hydrophilic region as (65 ± 7) ° which was lower than that of the P, but higher than that of G. It was reported in earlier research work that water contact angle within 60 ° to 80 ° was preferable environs for the cell growth. Thus

CSPG may contribute positively to cell adhesion as well as proliferation and differentiation of cell, and thus can be considered for wound healing applications.

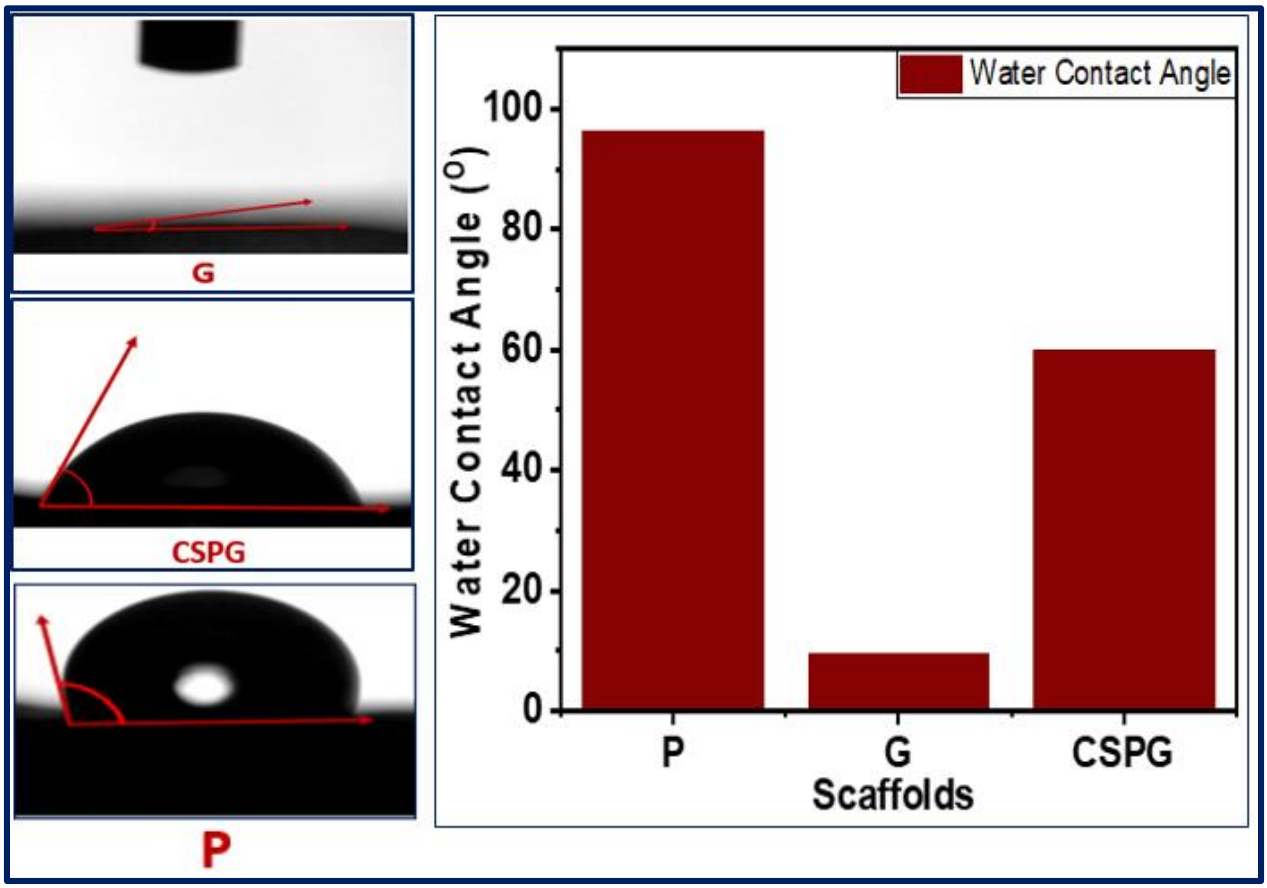

Figure 3.30 Water contact angle, and bar diagram of water contact angle of scaffolds (P, G, and CSPG)

3.3.7 In Vitro Cytotoxicity Assay

Optical micrographs of in vitro cytotoxicity analysis are shown in Figure 3.31, and results are tabulated in Table 3.11, which indicated that all the scaffolds have more than 95% cell sustainability whereas control has 100% cell sustainability. This suggests that scaffolds are not cytotoxic, and are biocompatible.

Table 3.11 Cytotoxicity remarks of control, and scaffolds (P, G, and CSPG)

Sample ID	Survival of Vero cells	Remarks
Control	100%	No cytotoxicity
P	>95%	No cytotoxicity
G	>95%	No cytotoxicity
CSPG	>95%	No cytotoxicity

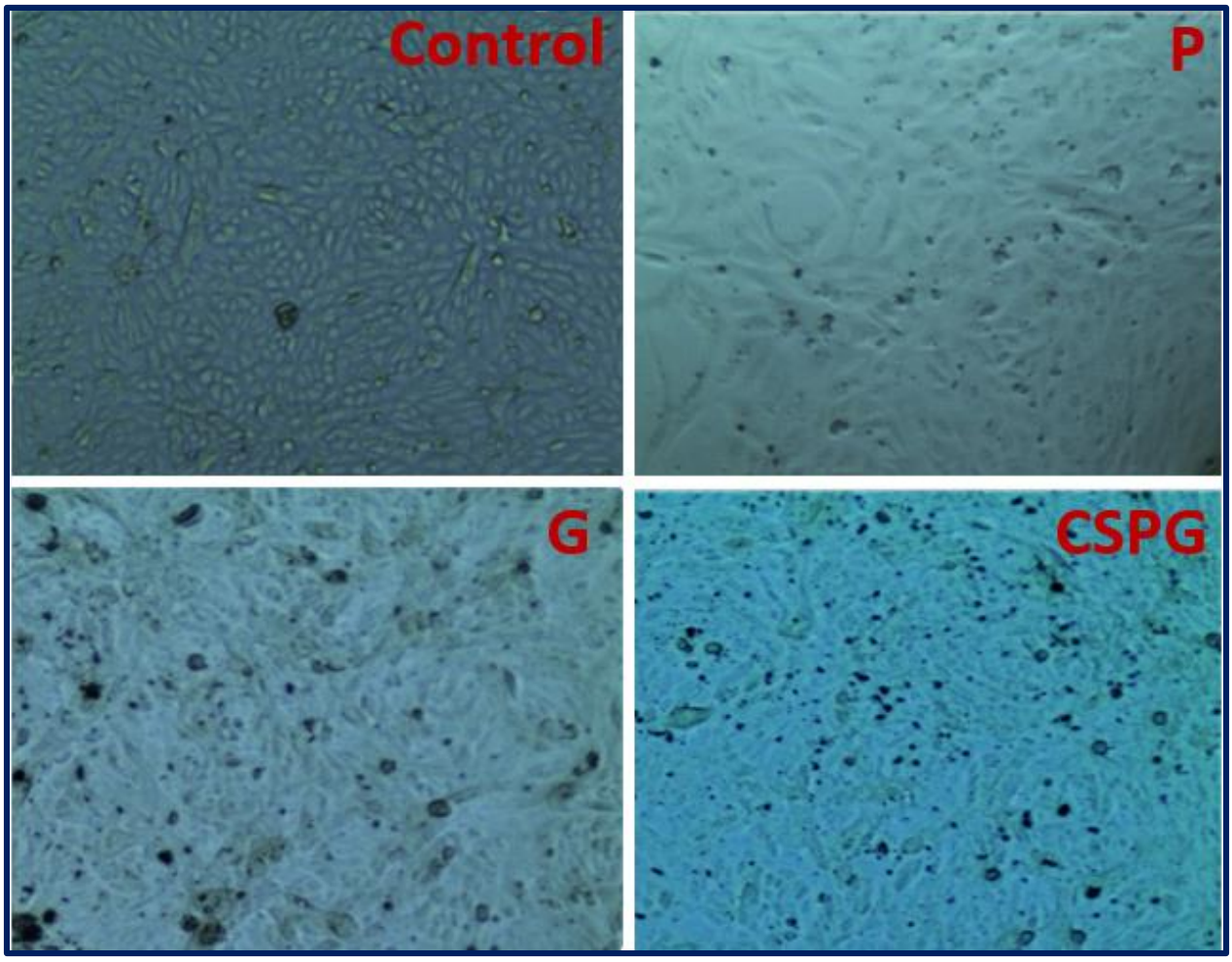

Figure 3.31 Optical microscopic images of Vero cell line with control, P, G, and CSPG medium after 48 h of incubation

3.3.8 In Vivo Animal (Rat) Model Assay

The general observations of wound beds produced surgically with scaffolds or without treatment (control) are displayed in Figure 3.32. First day of wound created, no noticeable changes observed in the exterior of wound for all cases. The scaffolds G, and CSPG readily dispersed into the wound

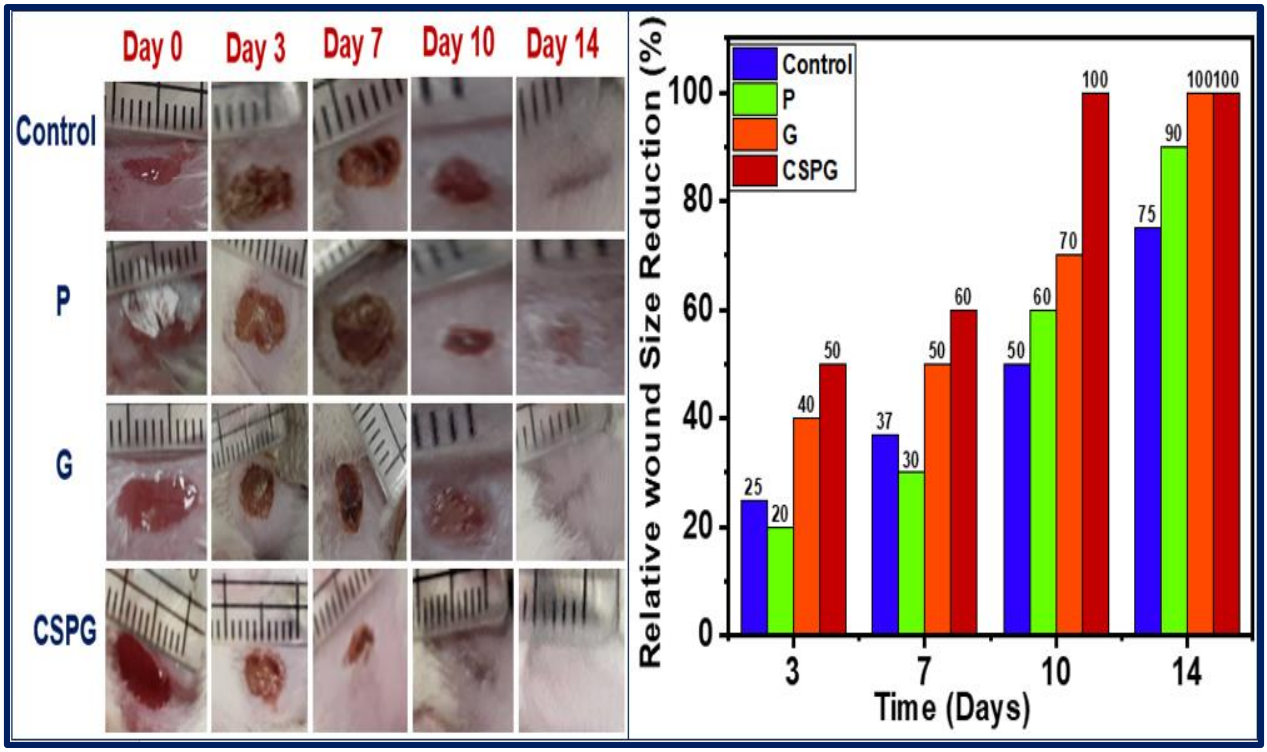

Figure 3.32 Images of wound healing (for control, P, G, and CSPG), and bar diagram of relative wound size reduction with time

bed when they were placed in the respective wound beds. This was as due to the hydrophilic nature of the scaffolds. All wound size was pretty reduced with the time and almost closed at the day of 14. The wound beds which were treated with CSPG scaffolds revealed the higher relative wound reduction size (%) with time than that of the others. At the day of 3, CSPG and G showed 50%, and 40 % relative wound reduction respectively whereas P, and control treated wound reduced as 20%, 25% respectively. Initial wound reduction with P was lower due to the hydrophobic nature of P, there may less interaction of P with the wound bed. At the day 7, wound bed with CSPG observed as 60% healing but the wound bed with G, P, and control showed relative healing rate as lower, and it was observed as 50%, 30%, and 37% respectively. A decrease of inflammatory stage of the wound to the growing of migration phase may be faster for CSPG treated wound than the other wound. Entire closing of wound with new skin, and without noticeable hair was found (100%

closure) after 10 days of wound curing for CSPG. Still G, P, and control showed 70%, 60%, and 50% wound closure respectively. That day, healing rate for P was found as greater than that of control. At day 14, CSPG, and G treated group showed 100% healing with the hair coverage but P treated, and control group were healed 90%, and 75% respectively. Control, and P showed reasonably slow wound curative process. Thus the reduction of wound area with CSPG scaffold was more visible than the wound size reduction with other scaffolds applied. CSPG could increase the rate of wound closing probably due to the combination of the properties of material as well its increased cell-matrix interactions, and biocompatibility.

3.3.9 Histological Assay

Healing status of wound was evaluated by noting the histology of the externally healed rat skin of scaffolds treated and control groups at day 14 after wound creation. Wound repairing was examined by considering the coverage of wound by epithelium, permeation of inflammatory cells,

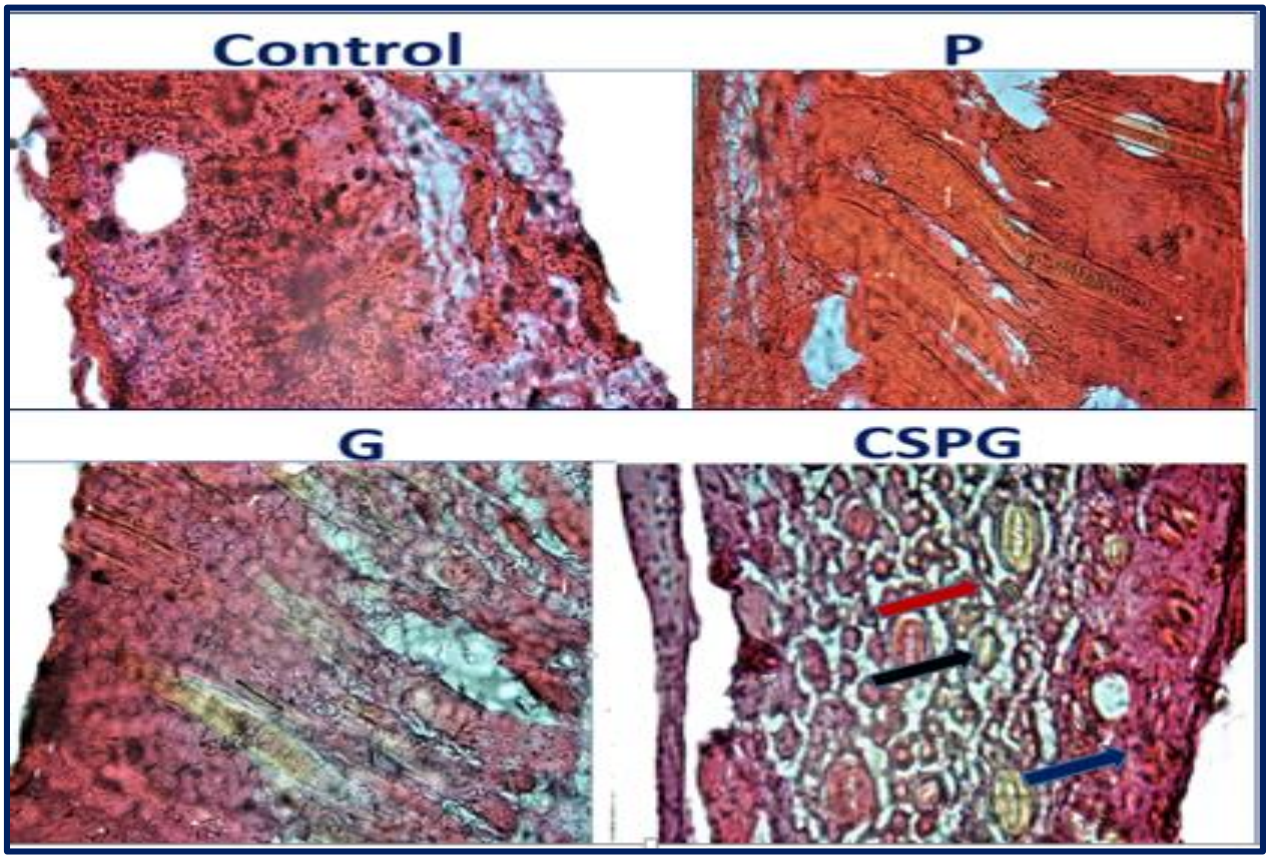

Figure 3.33 Photomicrographs of the histological responses to the nanofibrous scaffolds (control, P, G, and CSPG) after being applied in rat skin for 14 days

reformation of collagen and its array, tissue granulation, and skin appendages regeneration. Such processes are fundamental improvement of wound towards curing until the wound repairing. In Figure 3.33, it is evident that dermal structure is complete in CSPG treated skin tissue. Hair follicles, and collagen pattern were also seen in CSPG treated skin tissue ((shown in Figure 3.33 with arrow). In control, structured coverage with epithelium was not completed and there was some disorder at the epithelium. Visibility of collagen arrangement, and hair follicle were not in the micrograph for control. P, and G treated tissue showed incomplete re-epithelization. G treated tissue though exhibited with some structural arrangement, and skin appendages but micrographs of P treated tissue noticed without skin appendages such as hair follicles. These results were supported the healing percentages observed from the optical micrographs of wound healing groups. Thus CSPG (core-sheath bi-polymeric nanofibrous scaffold) treated tissue revealed a superior wound healing which in progress earlier than the P treated, and control groups and this improvement of healing was sustained all over the healing process. This trend was not noticed in G treated group though faster initial healing was also observed in the G treated group.

3.3.10 Conclusion

Gelatin, polylactic acid (PLA), and core-sheath gelatin-PLA scaffolds were achieved through the optimization of the solution properties of the constituents as well operational conditions. Amongst all core-sheath gelatin-PLA scaffold, CSPG showed the uniform morphology with no beads, and with the average fiber diameter as 390±61 nm which was lower than that of the constituent single polymeric scaffolds. Scaffolds were characterized by IR, thermal and X-ray analysis that revealed the existence of intermediate properties of its constituent materials without any adverse difference. Average water contact angle of CSPG revealed that the CSPG was neither too hydrophobic nor too hydrophilic. The relatively nano structure and the wettability of the CSPG may facilitate adherence and growth of cell within it in a controlled mode. CSPG may adhere to cell in a controlled mode than the probable cell adhesion that may observe in case of gelatin, and PLA scaffold as gelatin scaffold may function for rapid cell adhesion, and PLA scaffold was hydrophobic in nature. The rat model results for CSPG were justified the above inference giving a faster healing of the injured bed of the rat compared to that obtained by using P or G alone.

References

[1] L. E. Sperling, K. P. Reis, P. Pranke, and J. H. Wendorff, "Advantages and challenges offered by biofunctional core-shell fiber systems for tissue engineering and drug delivery," *Drug Discov. Today*, vol. 21, no. 8, pp. 1243–1256, 2016, doi: 10.1016/j.drudis.2016.04.024.

[2] J. Xue, T. Wu, Y. Dai, and Y. Xia, "Electrospinning and electrospun nanofibers: Methods, materials, and applications," *Chem. Rev.*, vol. 119, no. 8, pp. 5298–5415, 2019, doi: 10.1021/acs.chemrev.8b00593.

[3] B. Feng *et al.*, "Bioresorbable electrospun gelatin/polycaprolactone nanofibrous membrane as a barrier to prevent cardiac postoperative adhesion," *Acta Biomater.*, vol. 83, no. October, pp. 211–220, 2019, doi: 10.1016/j.actbio.2018.10.022.

[4] M. F. Elahi and W. Lu, "Core-shell Fibers for Biomedical Applications-A Review," *J. Bioeng. Biomed. Sci.*, vol. 03, no. 01, 2013, doi: 10.4172/2155-9538.1000121.

[5] M. F. Abdullah, T. Nuge, A. Andriyana, B. C. Ang, and F. Muhamad, "Core-Shell fibers: Design, roles, and controllable release strategies in tissue engineering and drug delivery," *Polymers (Basel).*, vol. 11, no. 12, pp. 1–49, 2019, doi: 10.3390/polym11122008.

[6] Y. Zhang, Z. M. Huang, X. Xu, C. T. Lim, and S. Ramakrishna, "Preparation of core-shell structured PCL-r-gelatin bi-component nanofibers by coaxial electrospinning," *Chem. Mater.*, vol. 16, no. 18, pp. 3406–3409, 2004, doi: 10.1021/cm049580f.

[7] Y. Z. Zhang, J. Venugopal, Z. M. Huang, C. T. Lim, and S. Ramakrishna, "Characterization of the surface biocompatibility of the electrospun PCL-Collagen nanofibers using fibroblasts," *Biomacromolecules*, vol. 6, no. 5, pp. 2583–2589, 2005, doi: 10.1021/bm050314k.

[8] Q. Zhang *et al.*, "Electrospun polymeric micro/nanofibrous scaffolds for long-term drug release and their biomedical applications," *Drug Discov. Today*, vol. 22, no. 9, pp. 1351–1366, 2017, doi: 10.1016/j.drudis.2017.05.007.

[9] S. Wang, Y. Zhang, H. Wang, G. Yin, and Z. Dong, "Fabrication and properties of the

electrospun polylactide/silk fibroin-gelatin composite tubular scaffold," *Biomacromolecules*, vol. 10, no. 8, pp. 2240–2244, 2009, doi: 10.1021/bm900416b.

[10] M. E. SantosMiranda *et al.*, "I . The role of N-carboxymethylation of chitosan in the thermal stability and dynamic," *Polym Int*, vol. 55, no. March, pp. 961–969, 2006, doi: 10.1002/pi.

[11] R. Ramalingam *et al.*, "Core-Shell Structured Antimicrobial Nanofiber Dressings Containing Herbal Extract and Antibiotics Combination for the Prevention of Biofilms and Promotion of Cutaneous Wound Healing," *ACS Appl. Mater. Interfaces*, 2021, doi: 10.1021/acsami.0c20642.

[12] S. Haider *et al.*, "Highly aligned narrow diameter chitosan electrospun nanofibers," *J. Polym. Res.*, vol. 20, no. 4, 2013, doi: 10.1007/s10965-013-0105-9.

[13] B. M. Baker and R. L. Mauck, "The effect of nanofiber alignment on the maturation of engineered meniscus constructs," *Biomaterials*, vol. 28, no. 11, pp. 1967–1977, 2007, doi: 10.1016/j.biomaterials.2007.01.004.

[14] S. Rashedi, S. Afshar, A. Rostami, M. Ghazalian, and H. Nazockdast, "Co-electrospun poly(lactic acid)/gelatin nanofibrous scaffold prepared by a new solvent system: morphological, mechanical and in vitro degradability properties," *Int. J. Polym. Mater. Polym. Biomater.*, vol. 70, no. 8, pp. 545–553, 2021, doi: 10.1080/00914037.2020.1740987.

[15] R. W. Newberry and R. T. Raines, "The n→π∗ Interaction," *Acc. Chem. Res.*, vol. 50, no. 8, pp. 1838–1846, 2017, doi: 10.1021/acs.accounts.7b00121.

[16] H. Chen *et al.*, "Instant in-situ Tissue Repair by Biodegradable PLA/Gelatin Nanofibrous Membrane Using a 3D Printed Handheld Electrospinning Device," *Front. Bioeng. Biotechnol.*, vol. 9, no. July, pp. 1–12, 2021, doi: 10.3389/fbioe.2021.684105.

3.4 Analysis of Electrospun Core-Sheath ASC-PLA (CSPC), and ASC-PLA-g-VAc(CSBC) Scaffolds

Graphical Abstract

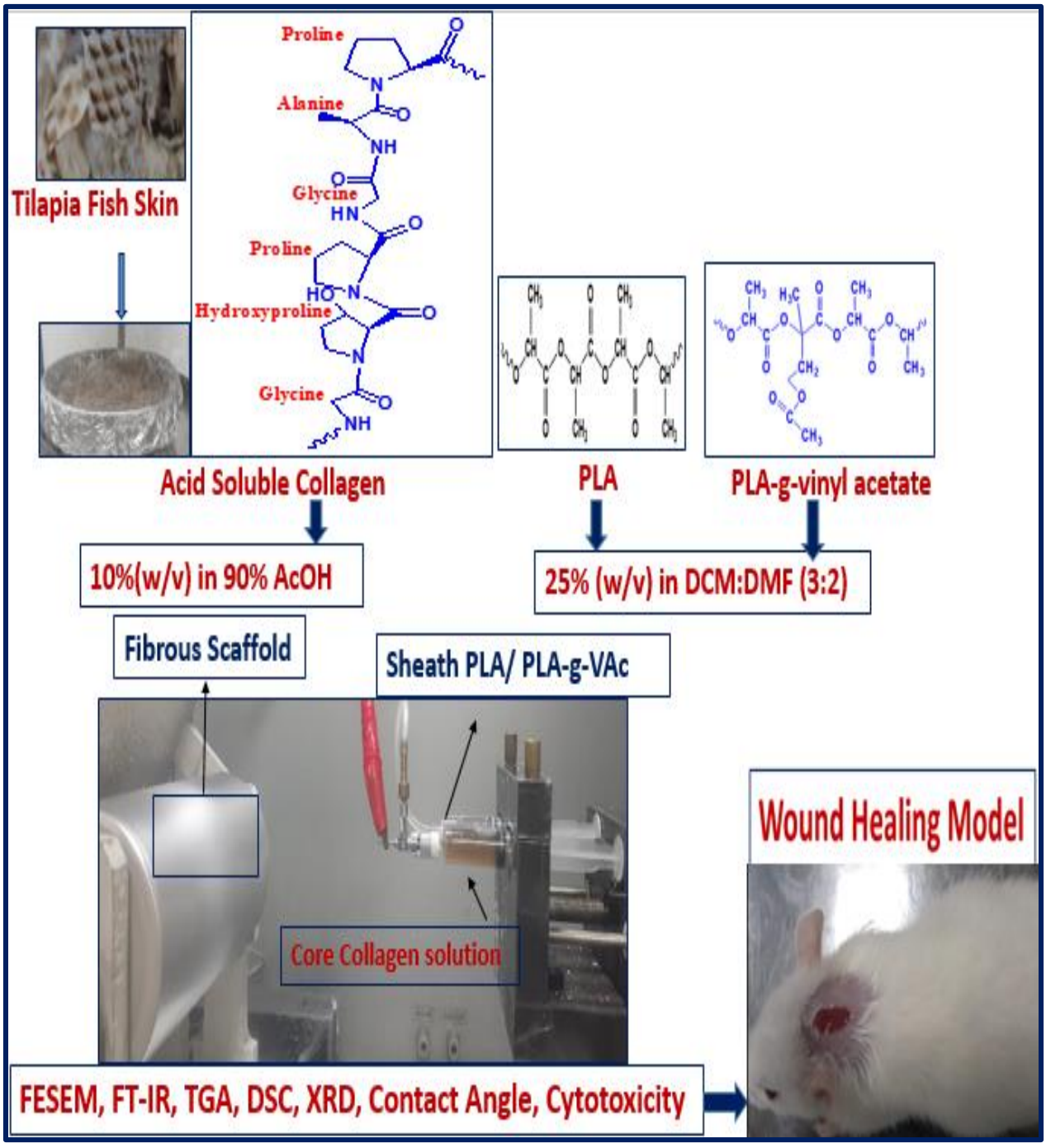

Abstract

Electrospun nanofibrous scaffolds possess biomimic structure and have promising applications in tissue regeneration especially in wound healing purposes. Collagen and poly(lactic acid) (PLA) both are biocompatible and biodegradable polymers and are widely used in the several biomedical applications. Core-sheath bi-polymeric scaffold has been proved as an encouraged material based on the requirement of scaffolds of two materials in which one polymer is bounded over the matrix of another polymer. This study aimed to prepare core-sheath scaffolds by using collagen as core material and PLA as sheath material to get the most of the polymers. Acid soluble collagen (ASC) was extracted from waste Tilapia fish skin. Amino acids profile of ASC revealed its triple helix structure whereas SDS-PAGE confirmed the existence of α1 (130 kDa), α2 (120 kDa) cross linked with β (280 kDa) chain. Viscosity average molecular weight of PLA was determined as 286 kDa. PLA-g-vinyl acetate was prepared through free radical polymerization by using the benzoyl peroxide as the initiator. PLA, and PLA-g-vinyl acetate (PLA-g-VAc) were subjected to characterize by FT-IR, ^{1}H NMR, ^{13}C NMR, TGA, DSC, and XRD. Spectrum analysis indicated PLA-g-VAc was produced through the grafting between the double bond of vinyl acetate and the methine group of PLA. PLA and ASC fibrous scaffolds (named as P and ASCF respectively) were prepared by using the 25% PLA (w/v) solution in dichloromethane (DCM) and dimethylformamide (DMF) at the ratio 3:2 (v/v) and 10% collagen solution in 90% acetic acid in water (v/v). Core-sheath fibrous mats (CSPC, and CSBC) were prepared by taking collagen as core material with PLA, and PLA-g-vinyl acetate as sheath materials. Morphology of the scaffolds were determined by the FESEM. All the materials were characterized further by FT-IR, TGA, DSC, and XRD. Cytotoxicity of the materials were measured as well prior to in vivo application and cytotoxicity was not observed on Vero cell line. Water contact angle measurement of the fibrous scaffolds revealed that bi-polymeric scaffolds were more wettable than the single polymeric scaffolds. Scaffolds were applied to the surgically produced wounding of skin in a rat model followed by histological assay to observe their improved properties towards wound healing process. Relative wound size reduction as well healing was observed as more by the use of core-sheath scaffolds than the use of single polymeric scaffolds.

3.4.1 Introduction

Tissue engineering is a part regenerative medicine that aims to mend or substitute injured, ailing, or lost tissues with proper bioconstructs in vitro or in vivo transplantation. Fabrication of biomaterials from the last few decades has been proved as promising to sustain, improve, or restore such a functionality. ECM (extra cellular matrix) functions as connective tissue which can give the physical support in cell arrangement as well the space for extracellular molecules for proper signaling mechanism [1]. Thus scaffolds that mimic the extra cellular matrix are key in tissue engineering as well as cellular compatibility with the competency for regeneration of tissue. Electrospinning is an extensively used technology for the preparation of such scaffolds that yields fibrous scaffolds with fiber diameters within nanometers to micrometers by applying high electrical voltage. Electrospun scaffolds has been proved to have the structural similarity to the ECM of skin [2]. It possesses high surface to volume ratio, hence high porosity, promotes cell adhesion as well as cell migration to progress tissue regeneration. Such structures also have been reported to have the good oxygen permeability, preventive functions towards dehydration of wound beds, and hold effective barrier counter to microbes [3]. A usual electrospinning technology can be amended considering the necessary morphologies and structures of fibers. As for example, the spinneret can be developed for coaxial electrospinning and also for the near field electrospinning to achieve continuous nanofibers of several structures such as core-shell, hollow, nanowire-in microtube and three-dimensional fiber scaffold [2]. Since several characteristics such as mechanical strength, hydrophilicity, surface conditions, along with bioactive constituents, and compatibility are main considerations in applying electrospun scaffolds for tissue engineering, the core-sheath fibers obtained from coaxial electrospinning with controlled discharge were found to exhibit superior performance on tissue engineering [4]. It has been recognized that core-sheath fibrous scaffolds promote wound curing from hemostasis to form epithelial tissue. A number of growth factors are associated with the process, and thus promotes the differentiation, and migration of cells such as endothelial cells, fibroblasts, etc. in tissues of skin.

Poly(lactic acid) (PLA) is one of the synthetic polymer that can be obtained from renewable sources, and widely used in the biomedical field. Polylactic acid like other polyesters degrades through non-enzymatic hydrolysis, and the byproducts of PLA are excluded over usual cell metabolism. Biocompatibility, and biodegradability of PLA mark it as a distinctive material for implantable appliances. Food and Drug Administration (FDA) has raised up more concern in the

usage of PLA in the arena of tissue engineering. Electrospun nanofibrous PLA scaffolds has been widely applicable for tissue regeneration as well as drug delivery materials. As hydrophobicity of PLA limits some of its applications, hydrophilic materials can be integrated into PLA through several ways for flexible applications. Core-sheath electrospun PLA based scaffolds where one compatible material (drug) as the core and outer PLA layer as sheath regulates release kinetics and shields the drug from the adjacent environs. In the arena of regeneration, PLA based nanofibrous scaffolds can be privileged as drug transport vehicles with providing a hydrophobic obstacle against the loss of water and the environments. Electrospun polylactic acid also has been employed to entrap and transport drugs that encourage wound curing, usually molecules having anti-inflammatory and antioxidant properties, and to assist nucleic acid (non-viral) transport [5].

Collagen is a naturally abundant protein which as the key element of ECM regulates cell functions. It is a biodegradable, biocompatible, and biorosorbable hydrophilic polymer. Electrospun collagen scaffolds give microenvironment that is especially required for tissue regeneration. Pristine collagen was usually mixed with synthetic polymers for electrospinning as its poor mechanical properties. For core-sheath electrospun fibrous scaffolds, collagen can be used for core or sheath layer. Because of its superior biological activity, collagen is generally used for core-sheath fibrous scaffold as the core with a synthetic polymer as the sheath to increase the mechanical properties [6]. Core-shell nanofibers mats with a core of polylactic acid and a shell of collagen was investigated for repairing of surgical tears, reported that core-shell scaffolds have prospective in accelerating reparation of avascular tears (meniscus) [7]. PLA-gelatin core-shell nanofiber mats were prepared to observe in vitro degradation studies [8]. Coaxial PLA-collagen fibrous mat was examined for gentamicin discharge properties, and the result showed that drug-loaded scaffolds can be used for drug transport with robust and time controlled antibacterial characteristics [9]. Biodegradable collagen-PLLA core–shell nanofibrous mats with berberine chloride was reported as a suitable material for controllable longstanding discharge of the hydrophilic drug [10]. Physical and biological properties of core-shell PLA-kefiran scaffolds were examined, and it was revealed that these hybrid scaffolds had desired characteristics to use in skin tissue engineering [11]. Electrospun nanofibrous collagen-PLCL scaffolds designed for vascular tissue engineering which resulted promising mechanical and biological characteristics [12]. Coaxial electrospun fiber mats of polylactic acid (core), and polyvinylpyrrolidone (shell) with cefazolin, and polyethylene oxide investigated for evaluation of the efficiency of the mats in wound healing. This scaffold showed promising antimicrobial characteristics, and controlled release of cefazolin [13]. Polylactic acid-chitosan fiber mats with cod liver oil revealed as a suitable material in diabetic wound curing [14]. PLA-collagen with levofloxacin incorporated nanofibrous scaffolds exhibited a great deal of

hydrophobicity, which resulted better encapsulation of the drug [15]. The core-shell PLA-chitosan nanofiber mats with curcumin drug incorporated in core (PLA) showed successive release of curcumin drug with initial fast release trailed by a constant release, and suggested to be used in the biomedical arenas such as drug transport, and wound bandages [16].

This study was taken to prepare core-sheath fibrous scaffolds from acid soluble collagen (natural hydrophilic polymer) as core material, and polylactic acid or PLA-g-VAc (synthetic hydrophobic polymer) as sheath material to observe their properties as wound dressings. Acid soluble collagen was extracted from tilapia fish skin. Morphology of the electrospun core-sheath bi-polymeric materials were investigated in comparison with the single polymeric materials. FT-IR spectroscopic analysis, thermal analysis, XRD analysis, and wettability of the scaffolds were compared to the single polymeric scaffolds. In vitro cytotoxicity was measured followed by in-vivo rat model assay to investigate the healing efficacy of them.

3.4.2 Extraction Yield of ASC

Acid soluble collagen was successfully extracted from the tilapia fish skin with the percentage of yield as 23.1% (based on lyophilized dry weight). The yield percentage of the acid soluble collagen obtained from tilapia fish skin was reported in the earlier literature as 27.2% [18]. The same was reported as 19.8% obtain from the skin of tilapia. Yield percent of extracted collagen from several aquatic species was suggested to be within 19-20% [19]. The variation in the yields of the ASCs indicated that the yield of collagen may be related with cross-linking of interchains at the telopeptide region of the collagen that could make collagen comparatively less soluble in acidic environs [18].

3.4.3 Amino Acids Profile of ASC

Individual amino acid residues observed (Figure 3.34) in acid soluble collagen are tabulated in Table 3.12 as weight percentage. Glycine is the most generous amino acid that was found in ASC as 27.85%. Beside it, acid soluble collagen was rich in glutamic acid (10.80 %), and alanine (10.37%). ASC was also found as distinctive in its proline, and hydroxyproline content (12.87%). Isoleucine and tyrosin were present as lower content, 0.47 %, and 0.59 % respectively. High glycine content comprises about one-third of the entire residue of amino acids in ASC. Glycine was reported to present mostly as third residue of α chain of collagen which includes all through the inner region. It revealed that the $(Gly\text{-}X\text{-}Y)_n$ was secured repeatedly in the polypeptide chain of acid soluble collagen where X and Y are generally proline, and hydroxyproline respectively.

Table 3.12 Amino acid profile of ASC (weight %) of ASC

Amino acids	Weight %
Aspartic acid	7.19
Threonine	2.40
Serine	3.26
Glutamic acid	10.80
Glycine	27.85
Alanine	10.37
Cysteine	3.36
Valine	1.12
Methionine	1.77
Isoleucine	0.47
Leucine	2.45
Tyrosine	0.59
Phenylalanine	2.05
Histidine	1.57
Lysine	3.11
Arginine	8.74
Proline & Hydroxyproline	12.82

All types of the collagen were identified by dominions with recurrences of such tri-peptides in the formation of the triple helical structure of collagen apart from the N-terminus first fourteen amino acid residues and the C-terminus first ten amino acid residues of collagen molecules [19]. This indication for the triple helix structure of ASC is also in line with the type I collagen extracted from tilapia fish skin, reported in literature [20]. Proline and hydroxyproline residues (imino acids) are important for the triple helix structure as they form H-bonds between the three polypeptide strands which is also associated with the thermal stability of the molecule. Pyrrolodine rings of the imino acids enforce the constraints on the conformation of the chain and thus support the triple helical structure. Especially hydroxyproline preserve such a structure by the formation of H-bond through the – OH group [18]. However, imino acids percentage in collagen is associated with species and their living habitation [20]. Tryptophan residues were not identified in ASC but cysteine residues were present in ASC as 3.36 %, similar findings were reported in previous

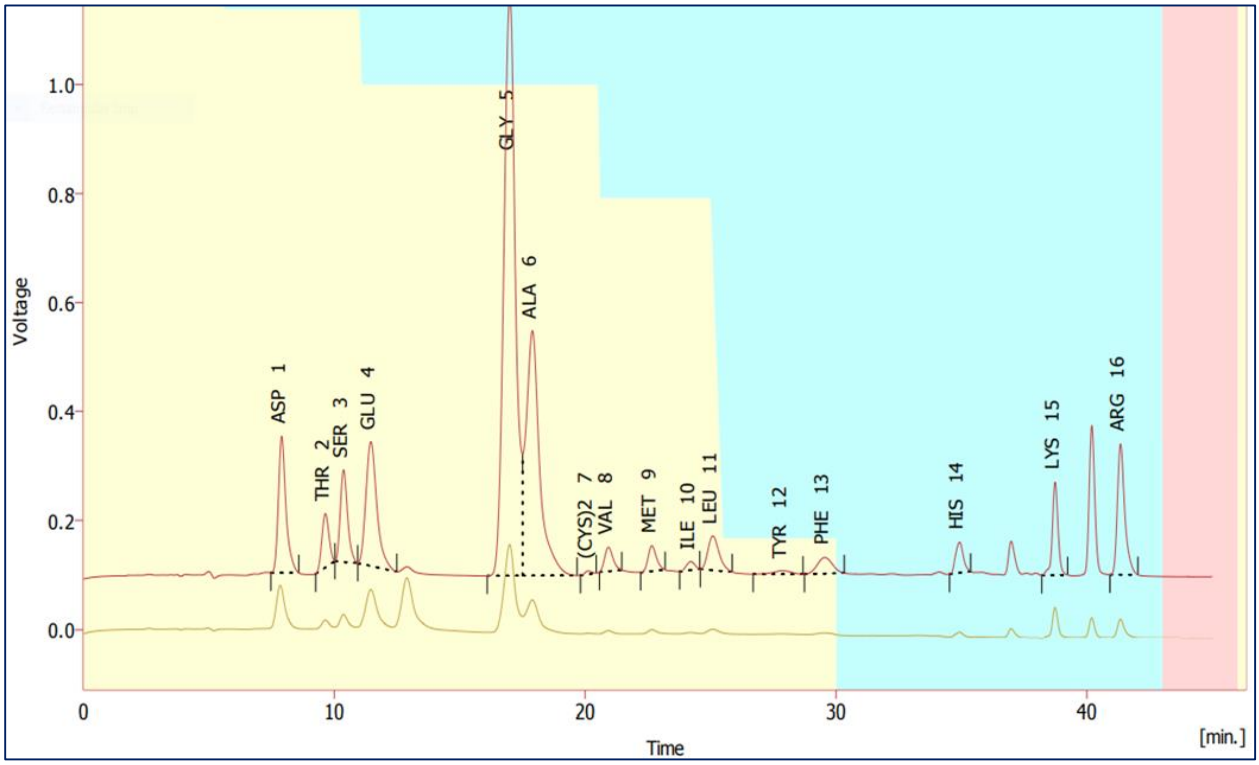

Figure 3.34 Amino acid profile of ASC

literature [21] though cysteine was not reported to present in collagen extracted from the same [19].

3.4.4 SDS-PAGE Pattern of ASC

SDS-PAGE profile of ASC is shown in Figure 3.35 that consisted of two α chains (α_1 and α_2) along with a β chain as the main components. Moreover, high molecular weight cross linked components molecular weights of α_1, α_2, β, and γ components were appeared approximately at 130 kDa, 120 kDa, 280 kDa, 300 kDa respectively. The intensity of band for α_1 chain was found around two times higher than that of the α_2 chain. This result proposed that the extracted ASC from tilapia fish skin was typical as type I collagen, a heterotrimer holding two same α_1 chains and one α_2 chain. Previous literature reported ASCs obtained from fish skin as type I collagen as well as the skin of tilapia [18]. More intense β band is an indication that extraction of ASC preserved mostly α_1, and α_2 chains cross linkage with high molecular weight β component. Beside it, there was no impurity band observed in the electrophoretic pattern.

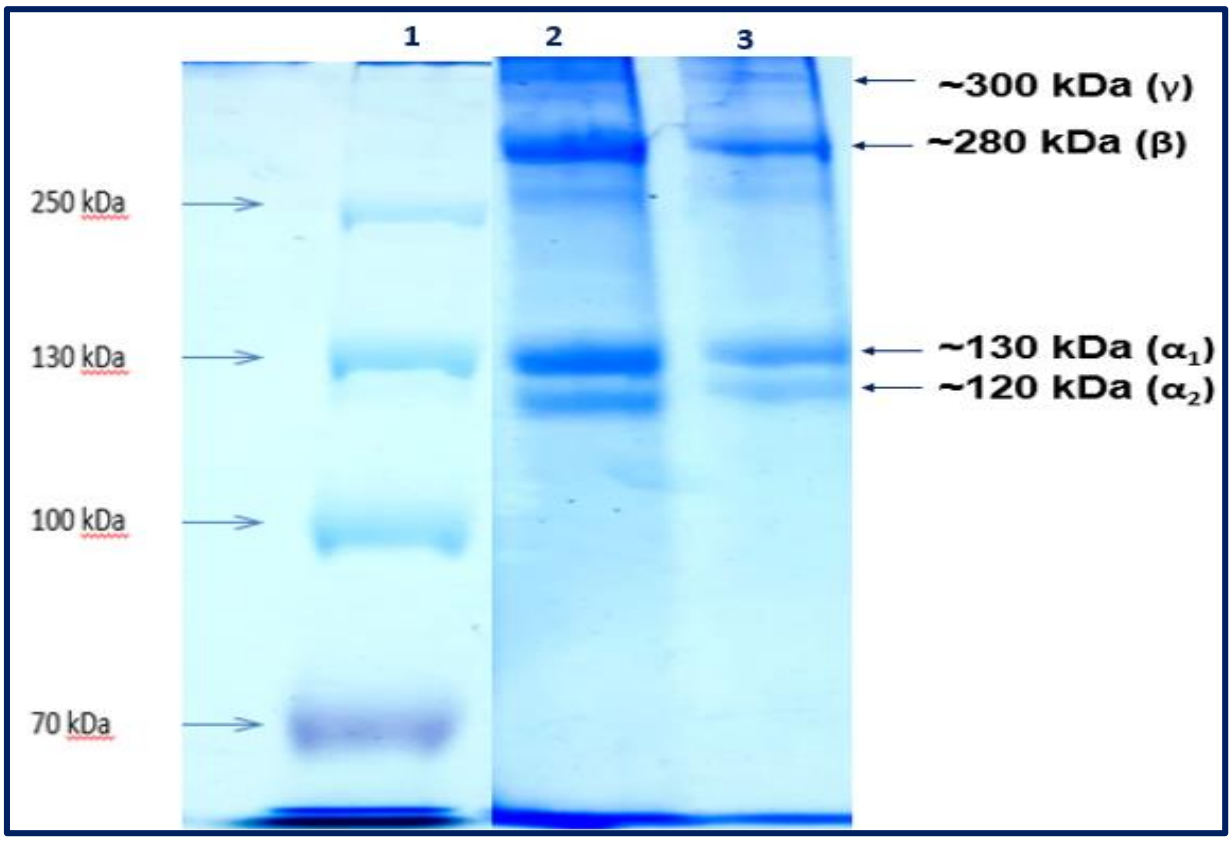

Figure 3.35 SDS-PAGE pattern of ASC, line 1: standard protein marker, line 2 & 3: ASC such as β (dimer, more intense band) and γ (trimer, less intense band) were also observed in ASC

3.4.5 FT-IR Analysis of ASC

Characteristic peaks observed in the FT-IR spectrum of ASC are presented in Figure 3.36, Table 3.13. Amide A peak of ASC was found at 3305 cm^{-1} that reported to occur usually at 3400–3440 cm^{-1} [18]. Shifting to a lower wave no. region may be due to the H-bonding –NH which is the indication of the greater structural stability of ASC as hydrogen bond is directly related to the structure of collagen protein. Amide B band of ASC positioned at 2930 cm^{-1} with another peak at 3091 cm^{-1}, these peaks were attributed for $–CH_2$ asymmetric and symmetric stretching [22]. Amide I peak was found at 1641 cm^{-1} which is responsible for carbonyl stretching absorption. That peak was reported to locate generally at 1600–1700 cm^{-1} and it would be observed at the lower wave no. due to decrease of molecular order. The region of amide I peak also suggested that the molecule preserved the triple helix structure which was associated between –NH group and –C=O of the fourth residue [23]. The absorption occurred at 1541 and 1240 cm^{-1} in the spectrum of ASC can be assigned as amides II, and III respectively for -NH bending vibrations coupled with -CN stretching vibration, and –NH deformation coupled with -CN stretching vibration.

Table 3.13 Main Peak Positions in the FT-IR Spectrum of ASC

	Peak Assignments	Peak Positions (cm^{-1})
Amide A	-NH stretch coupled with hydrogen bonding	3305
Amide B	$-CH_2$ asymmetrical stretch	3091, 2930
Amide I	C=O stretch/hydrogen bond coupled with C-N stretch	1641
Amide II	-NH bending vibration coupled with CN stretch	1541
Amide III	-NH deformation coupled with CN stretch	1240
-	$-CH_2$ bend	1450
-	COO symmetrical stretch	1392
	C-O ester	1080

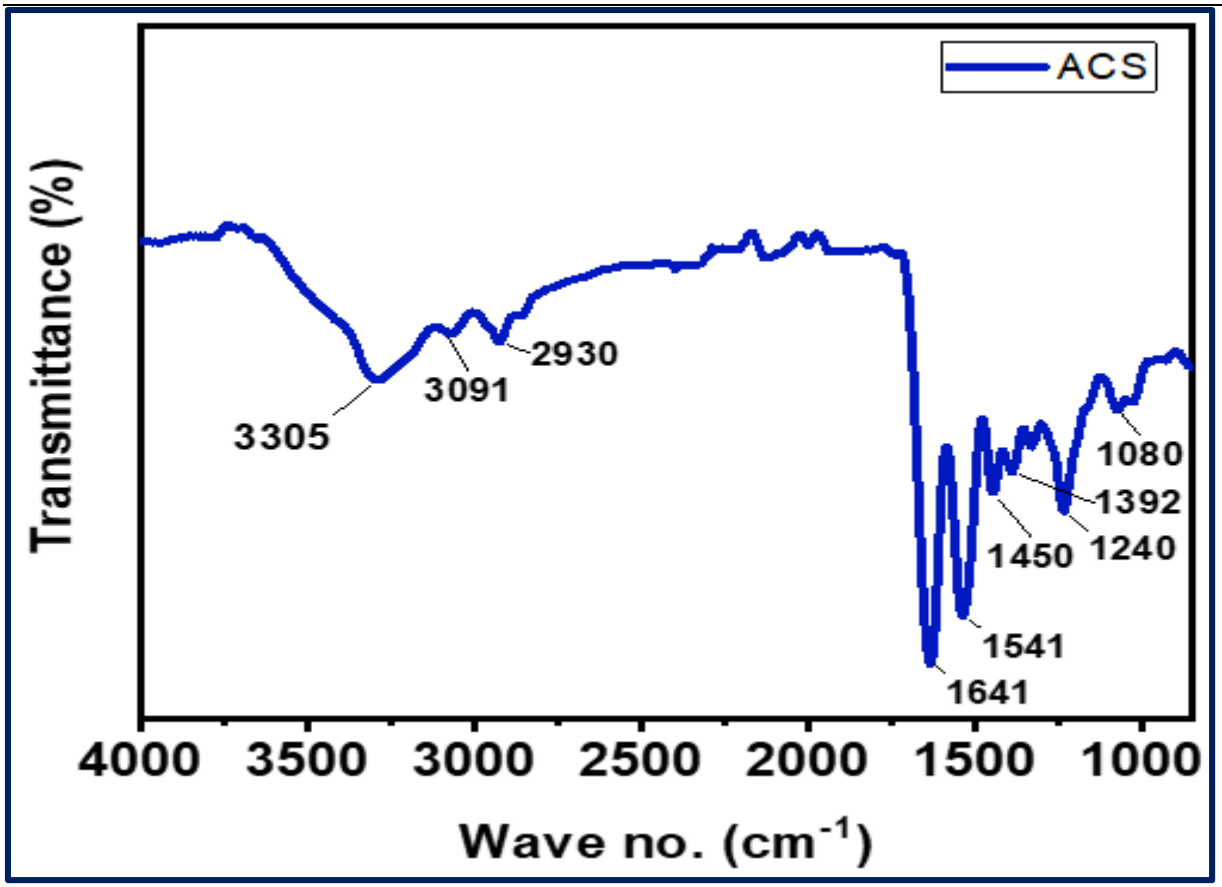

Figure 3.36 FT-IR spectrum of ASC

Amide III peak was also reported to relate the triple helical structure of collagen. It was proposed that peak integration ratio between amide III peak and the peak at 1450 cm^{-1} ($-CH_2$ bend) if one or greater than one, triple helical structure of the molecule retained. The peak integration ratio

between amide III peak and the peak at 1450 cm^{-1} was observed in the spectrum as greater than one, thus indicated that the ASC was extracted with the retention of triple helix.

3.4.6 XRD Analysis of ASC

X-ray diffraction pattern of the ASC showed two diffraction peaks (Table 3.14, Figure 3.37). One peak of 2θ ° value at 7.67 ° which was observed as a sharp peak with the d-spacing as 11.5 Å. Another wide peak observed at 21.12 ° (2θ °) with d-spacing value as 4.2 Å. The 1st diffraction peak reflected from the distance amongst the molecular chains of ASC which also indicated the triple helical structure of ASC [18]. The 2nd diffraction peak was resulted due to the scattering from structural layers of ASC, and that reflects the space between ASC skeletons. These results were in line with the observed value in the previous literature, and agreed with the diameter of ASC molecule that retained triple helical configuration and a single helix (left-handed).

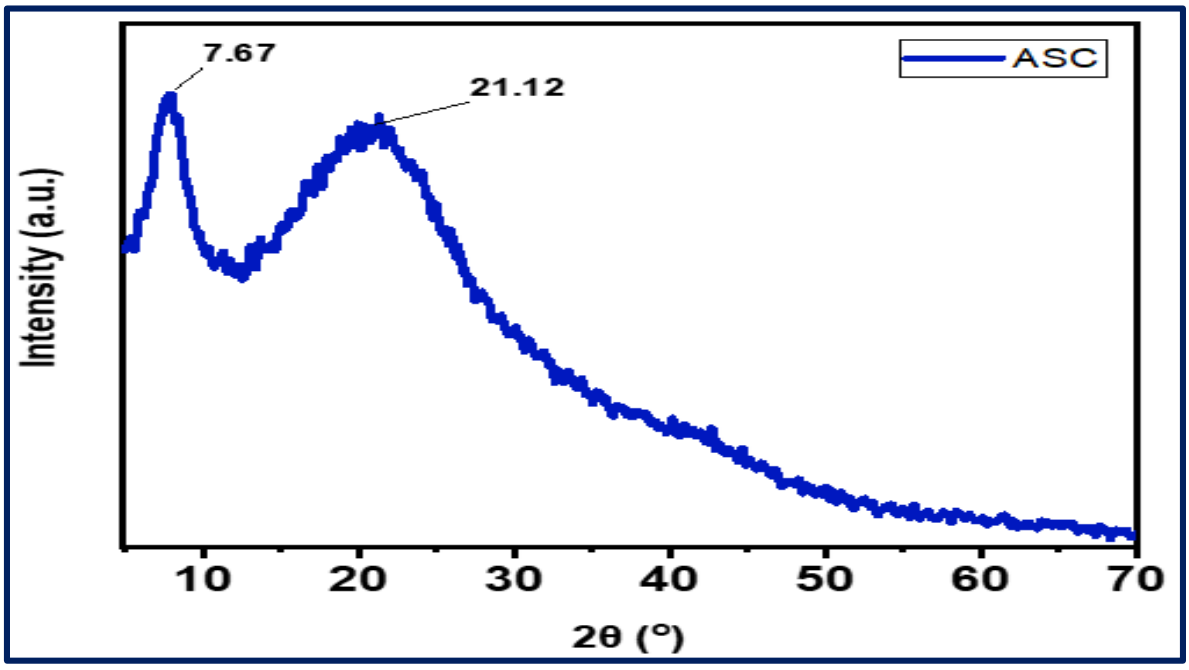

Figure 3.37 X-ray diffractogram of ASC

Table 3. 14 XRD Parameters of ASC

XRD Parameters	ASC	
2θ °	7.67	21.12
d (Å)	11.5	4.2
FWHM	2.98	8.5
Crystallinity (%)	15.16%	

Thus ASC extracted with its native conformational and denatured form. The crystallinity of ASC were estimated as 15.16% which is also agreed with the reported value [21].

3.4.7 Thermal Analysis of ASC

TG and DTG thermogram of ASC are shown in Figure 3.38 (a). Two stages thermal changes occurred in ASC. ASC showed a noticeable mass loss around 12.6% at temperature of 89 ^{o}C and finally decomposed with the 64% mass loss at 320 ^{o}C. Residual mass left as 23.46%, this is due to the inorganic residue present in ASC.

Figure 3.38 (b) showed the DSC, and DDSC profile of ASC. Denaturation temperature (T_d), and melting temperature (T_m) of ASC was revealed as 32 ^{o}C, and 65 ^{o}C respectively. T_d of pepsin soluble collagen obtained from tilapia fish scale, and fish skin were reported as 32.09 ^{o}C, and 28.20 ^{o}C respectively whereas the acid soluble collagen obtained from fish skin of the same species was denatured at 26.80 ^{o}C [24].

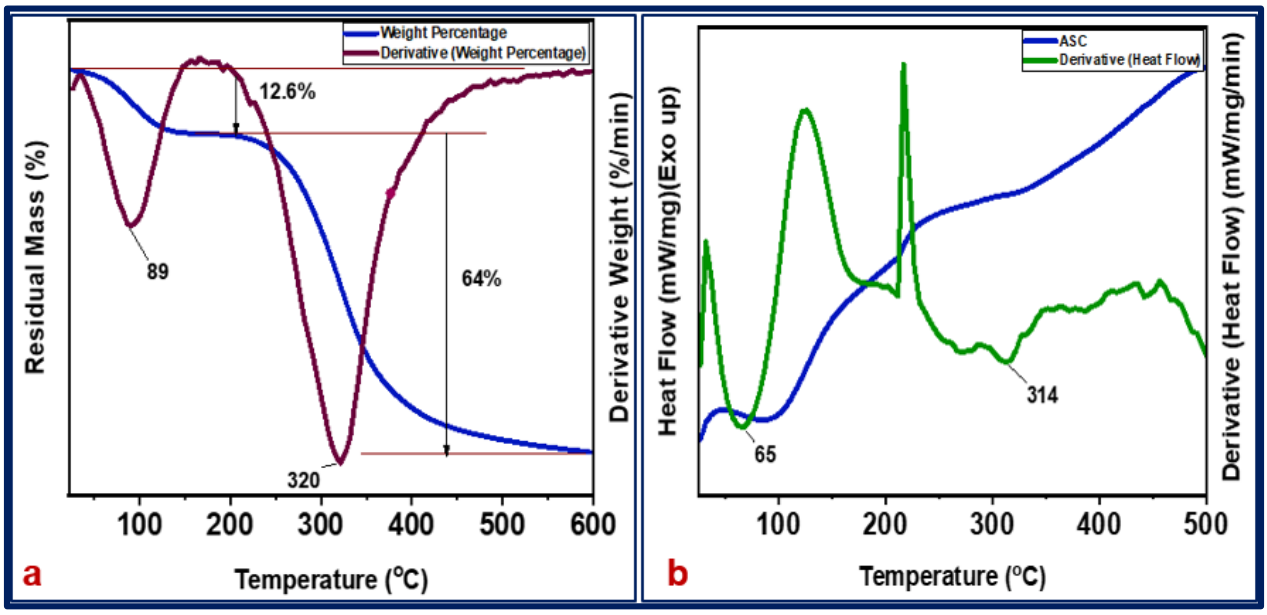

Figure 3.38 (a) TGA, and DTG thermogram of ASC, (b) DSC, and DDSC thermogram

T_d which is the reflection of thermal stability of ASC was associated with amino acid composition, molecular weight, environment of habituation, and body temperature of the species. Furthermore, the denaturation temperature of collagen was observed as associated directly with the imino acid content in collagen as imino acids are responsible for inter and intra-molecular cross-linkage. This result was agreed with the imino acid content obtained from amino acids analysis, and molecular weight obtained from SDS-PAGE [25].

3.4.8 Morphology of Electrospun Scaffolds

Figure 3.39 showed the FESEM micrographs of the electrospun scaffolds, histogram of the scaffolds as well the distribution of fibers in the scaffolds. Average fiber diameter, and mean pore area with the composition of electrospinning solution are included in Table 3.15. All the scaffolds observed as uniform with smooth surfaces consisting continuous aligned fibers. Diameter of the fiber depends on the composition of the electrospinning solution with the conditions used for electrospinning and with the variations of technology. Scaffold P presented random distribution of fiber with the average fiber diameter as (729±265) nm with the mean pore area as (4±6) μm^2 whereas scaffold B obtained from the vinyl acetate grafted PLA copolymer (PLA-g-VAc) showed fine structure with the lowest average fiber diameter as (87±19) nm with the mean pore area as

Table 3.15 Average Fibers diameter and pores diameter of electrospun scaffolds with composition of electrospinning solutions

Sample	Composition of Samples			Mean Fiber Diameter ± SD nm	Mean Pores Area ± SD μm^2
	PLA solution	ASC solution	PLA-g-VAc Solution		
P	25%	-		729±265	4±6
B	-	-	25%	87±19	0.03±0.04
ASCF	-	10%	-	160±73	0.3±0.6
CSPC	25%	10%	-	118±6	0.1±0.1
CSBC	-	10%	25%	107±19	0.08±0.1

(0.03±0.04) μm^2. All the scaffolds were prepared with the same operating conditions. Concentrations of P, and PLA-g-VAc in the electrospinning solutions were also same. Thus these morphological change may be attributed from the variations in the molecular level. ASCF which scaffold obtained from ASC showed the average fiber diameter as (160±73) nm with the mean pore area as (0.3±0.6) μm^2. Average fiber diameter as well mean pore area of ASCF was in between than that of P, and B in case of single polymeric scaffolds. Intermediate sized fibers were identified for the core-sheath electrospun scaffolds. CSPC showed average fiber diameter as (118±6) nm, and mean pore area as (0.1±0.1) μm^2. These results indicated that average fiber

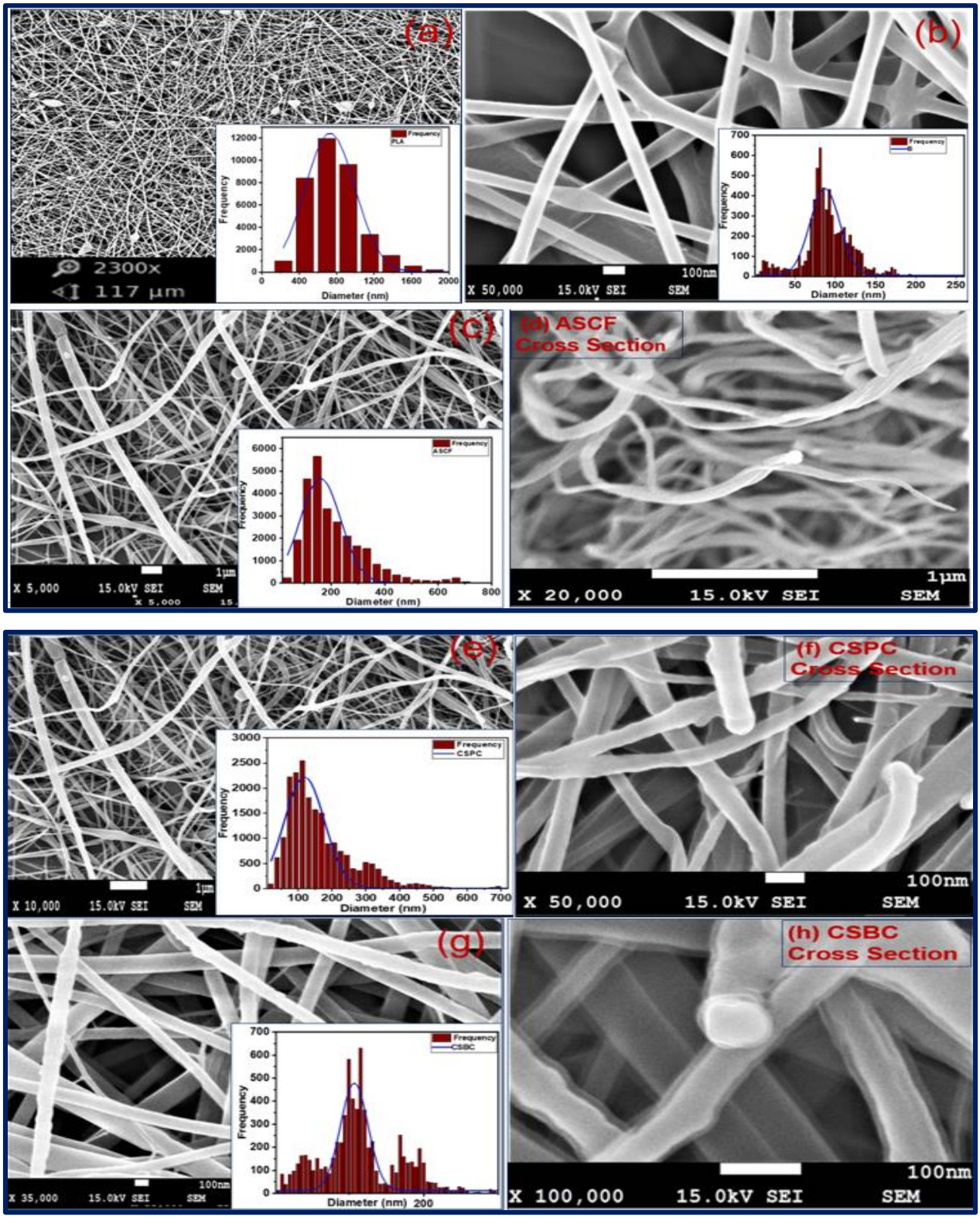

Figure 3.39 SEM micrographs of the scaffolds and histogram of fibers diameters: (a) P (b) B, (c) ASCF, (d) cross section ASCF, (e) CSPC ,(f) cross section CSPC, g) CSBC, and (h) cross section CSBC

diameter of CSPC scaffold was about 26% reduced than that of ASCF scaffold, and around 84% reduced than that of P scaffold. Total mean fiber diameter reduction percentage (110%) was close to the average fiber diameter of the CSPC (118 nm). In case of core-sheath scaffold CSBC, average fiber diameter was found as (107±19) nm, and mean pore area as (0.08±0.1) μm^2. Reduction of average fiber diameter of CSBC from that of ASCF was observed around 33% whereas increase of the same occurred from that of B around 23%. It was reported in the earlier literature that the average fiber diameter in the core-shell scaffolds were comparatively bigger than that of the single polymeric scaffold due to the increased amount of solids from the shell solution in the scaffolds [8]. That trend was only observed in case of CSBC and B. This study revealed the presence of intermediate fiber diameter in core-sheath scaffolds compared to the constituent single polymer scaffolds. In the previous literature, that trend was also observed specifically in PLA based collagen coaxial fibers [9].

3.4.9 FT-IR Analysis of Electrospun Scaffolds

Figure 3.40 (a), displayed the FT-IR spectrum of P, ASCF, and CSPC. Beside it, Figure 3.40 (b) showed the same of B, ASCF, and CSBC. Main characteristics bands at 3290 cm^{-1}, 2930 cm^{-1}, and 1746 cm^{-1} can be assigned to the terminal –OH stretching, -CH- asymmetrical stretching, and –C=O stretching in P (Table 3.16). Similar IR absorption bands were observed for electrospun PLA fiber in earlier literature [16]. IR spectrum of ASCF showed a peak at 3578 cm^{-1} for -N-H stretching modes whereas band at 1678 cm^{-1} (amide I) was observed for -C=O stretching vibration that coupled with -C-N stretching vibration. Band at 1523 cm^{-1} (amide II) can be assigned to the combination of –C-N (out-of-phase) stretching vibration with the in plane bending mode of N-H vibration. Another characteristic band which was attributed at 1249 cm^{-1} (amide III) was for the C-N stretching mode and N-H bending mode together with the wagging mode of $-CH_2$ of adjacent amino acid residues [26] . Peak integration ratio between the amide III, and the peak at 1407 cm^{-1} was not distinctive in ASCF spectrum as ASC spectrum. This findings indicated that during electrospinning, triple helical structure of ASC was distorted which was also reported in earlier literature [27]. Spectrum of CSPC showed similar pattern as ASCF but carbonyl absorption band at the region like P was absent. Similar findings were also observed in the spectrum co-electrospun PLA/gelatin scaffolds [8]. This can be explained by considering the $n \rightarrow \pi^*$ interaction between carbonyl groups of adjacent polymer chains where a nucleophile provides nonbonding lone-pair electron to the vacant π^* orbital of an adjacent carbonyl group [28]. Spectrum of B showed almost

similar IR absorption bands like P except carbonyl stretching band which was shifted to the higher wave no. as well as its intensity increased and observed in B spectrum at 1755 cm^{-1}. This scaffold obtained from the vinyl acetate grafted PLA copolymer. Increased carbonyl absorption with the peak shifting supported that grafting retained the carbonyl group of PLA and vinyl acetate as well remained in the electrospun scaffold.

Table 3.16 Main Peak Positions in the FT-IR Spectrum of Scaffolds

Scaffolds	Peak Positions (cm^{-1}) and Peak Assignments
P	3290 (-OH stretching), 2930 (-CH asymmetric stretch), 1746 (-C=O stretch)
B	1755 (-C=O stretch)
ASCF	3578 (-NH stretch), 3036 ($-CH_2$ asymmetric stretch), 1678 (-C=O stretch), 1523 (-NH bend coupled with –CN stretch), 1249 (-NH deformation coupled with –CN stretch), 1407 ($-CH_2$ bend)
CSPC	Similar pattern as ASCF, No peak for –C=O of PLA
CSBC	Similar pattern as ASCF, an weak peak at 1755 (–C=O stretch)

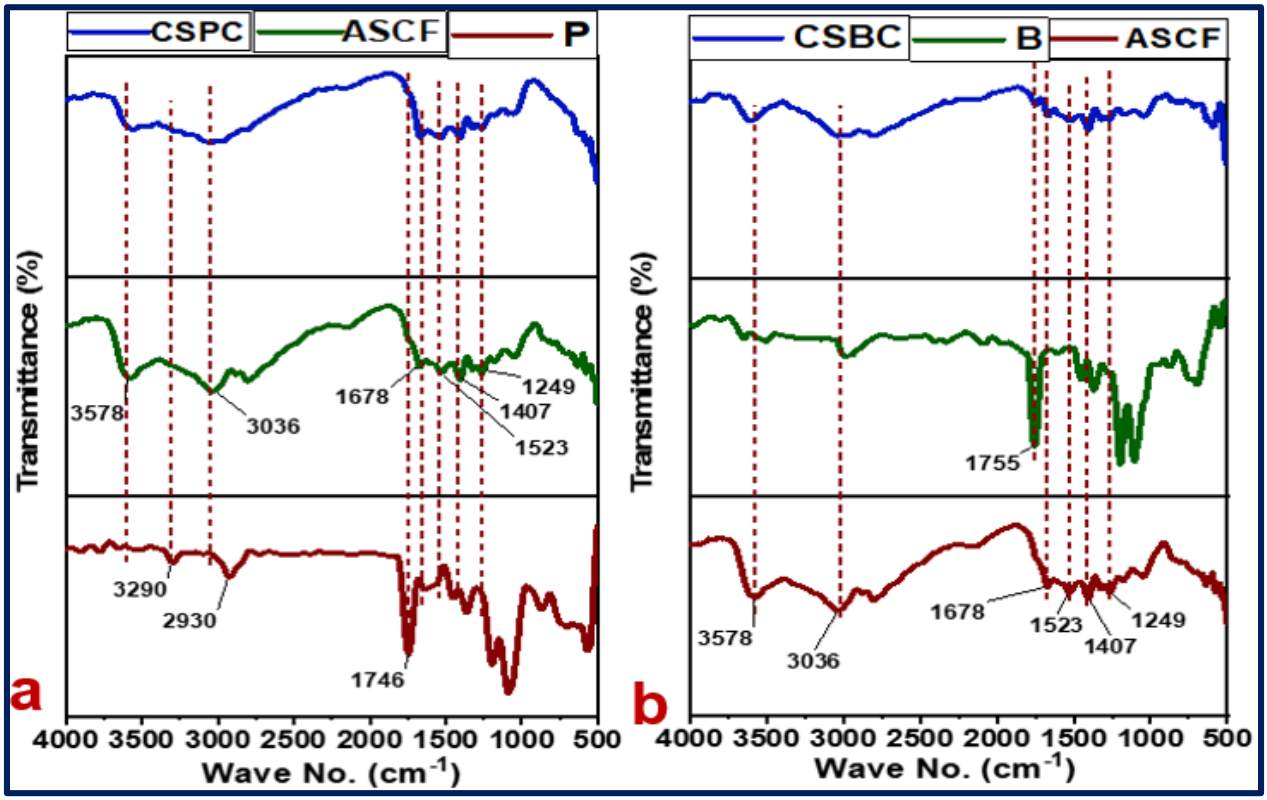

Figure 3.40 FT-IR spectrum: (a) P, ASCF, and CSPC (b) B, ASCF, and CSBC

Spectrum of CSBC showed similar pattern as ASCF unlike the CSPC as a weak carbonyl absorption peak observed in CSBC at 1755 cm^{-1}. This findings can be explained by considering that the weak peak may be attributed due to the carbonyl group that came from vinyl acetate or due to the grafting steric hindrance restricted some of carbonyl groups of copolymer to interact with the carbonyl group of adjacent polymer chains.

3.4.10 Thermal Analysis of Electrospun Scaffolds

TG and DTG thermogram of electrospun scaffolds are shown in Figure 3.41, and Figure 3.42. Single stage thermal changes occurred in P whereas two stages thermal changes were observed in ASCF, CSPC, and CSBC. Maximum mass loss in P was started at 266 ^{o}C, maximum decomposition occurred at 348 ^{o}C, and that was ended at 377 ^{o}C with the mass loss of 97.6%. ASCF showed a noticeable mass loss around 6.8% at temperature of 81 ^{o}C that started at 27 ^{o}C temperature.

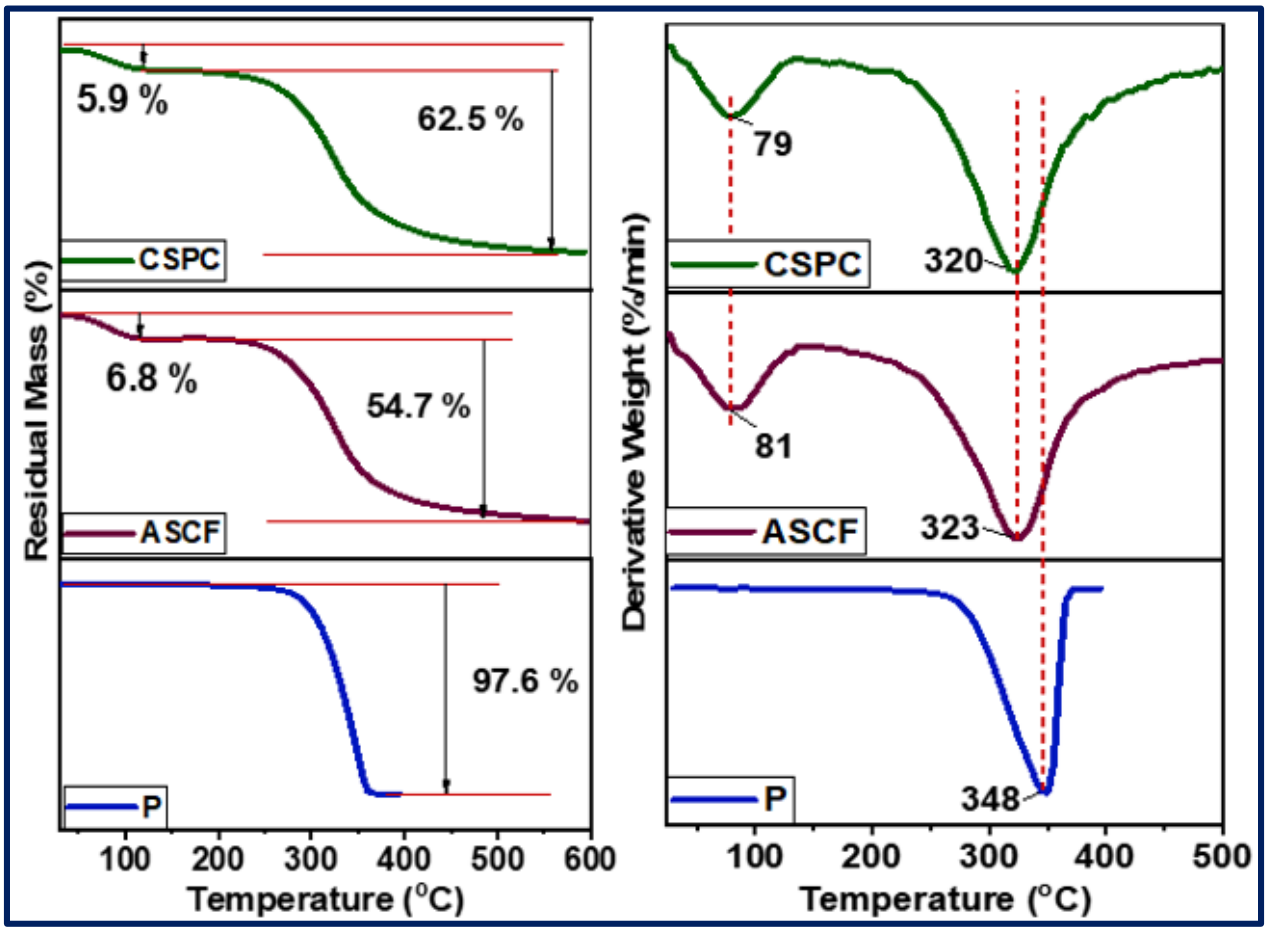

Figure 3.41 TGA and DTGA thermogram of electrospun scaffolds (P, ASCF, and CSPC)

Maximum decomposition of ASCF occurred at 323 ^{o}C with the 38.5% residue. Initial mass loss of CSPC was 5.9% at a T_{max} (Temperature of maximum mass loss) as 79 ^{o}C with an onset temperature same as ASCF and maximum degradation occurred at 320 ^{o}C with 31.6% residue. This similar pattern degradation indicated the presence of ASC in CSPC as well PLA as remaining residue percentage at the maximum degradation temperature was observed as lower in case of CSPC than that of in case of ASCF. B (Figure 4.11) showed single degradation profile like P, degradation started at 240 ^{o}C. Maximum degradation occurred at 337 ^{o}C with the 99.2 % mass loss in B. CSBC showed two stages thermal decomposition pattern like ASCF, and CSPC.

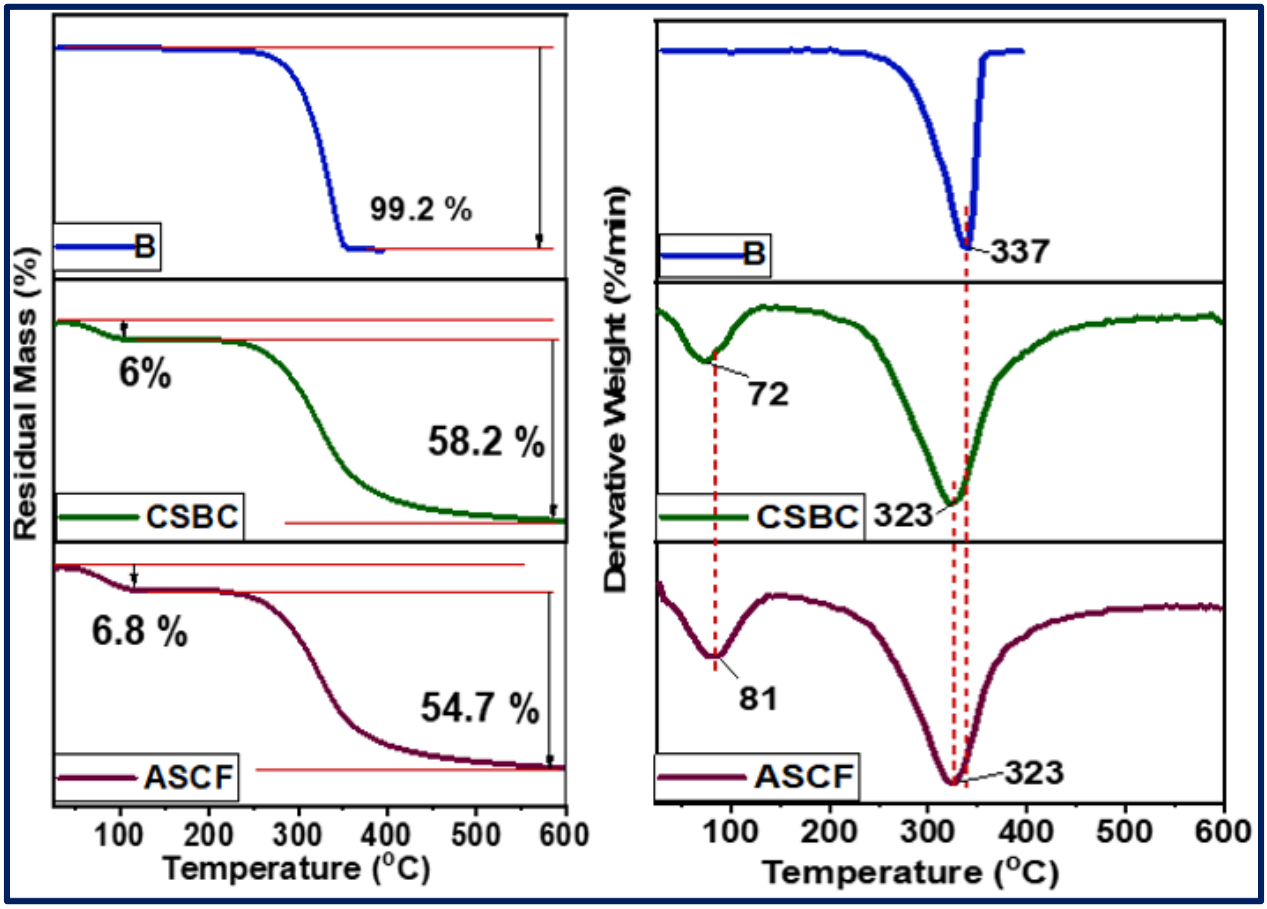

Figure 3.42 TGA and DTGA thermogram of electrospun scaffolds (B, ASCF, and CSBC)

Similar initial thermal degradation of CSBC like ASCF which was around 6% mass loss at 72 ^{o}C (less than the initial mass loss in ASCF, about 6.8 %) revealed the presence of ASC in CSBC. Maximum decomposition of CSBC occurred at the same temperature region as ASCF but end temperature of final degradation was higher in CSBC (446 ^{o}C) than that of B (358 ^{o}C) but less than that of ASCF (465 ^{oC}) revealed the presence of PLA-g-VAc copolymer in CSBC as well. Residual

mass after thermal degradation of CSBC was 35.8% whereas the same for ASCF was observed as 38.5%, this result also supported the presence of PLA-g-VAc copolymer in CSBC.

Figure 3.43, and 3.44 showed the DSC, and DDSC thermogram of electrospun scaffolds. In Figure 4.12, peak at 54 ^{o}C, and a sharp peak at 155 ^{o}C in P can be assigned as T_g and melting temperature respectively. An endothermic peak at 61 ^{o}C in the DDSC curve of ASCF could be attributed for the denaturation of ASCF in association with the destruction of helical structure. It was reported that denaturation of collagen fibers occurred at a temperature of 67 ^{o}C [29] . The weak endothermic peak at 212 ^{o}C is for the ending phase change revealed from the decomposition of ASCF. DDSC curve of CSPC showed similar pattern as ASCF, an endothermic peak was observed at 60 °C which was slightly less than the denaturation and helical structure distortion temperature of ASCF. As well CSPC showed an endothermic peak at 208 ^{o}C which was also lower than the end endothermic peak appeared for ASCF. Thus the bi-polymeric scaffold CSPC showed intermediate thermal properties than that of the single polymers. It was reported that the coaxial PLA (shell)-collagen (core) electrospun fibers resulted less thermal stability than its constituent fibers [9]. DDSC thermogram of B showed an endothermic peak at 60 ^{o}C that can be assigned to the T_g of the copolymer scaffold, and another peak which was appeared at 160 ^{o}C could be the T_m of B.

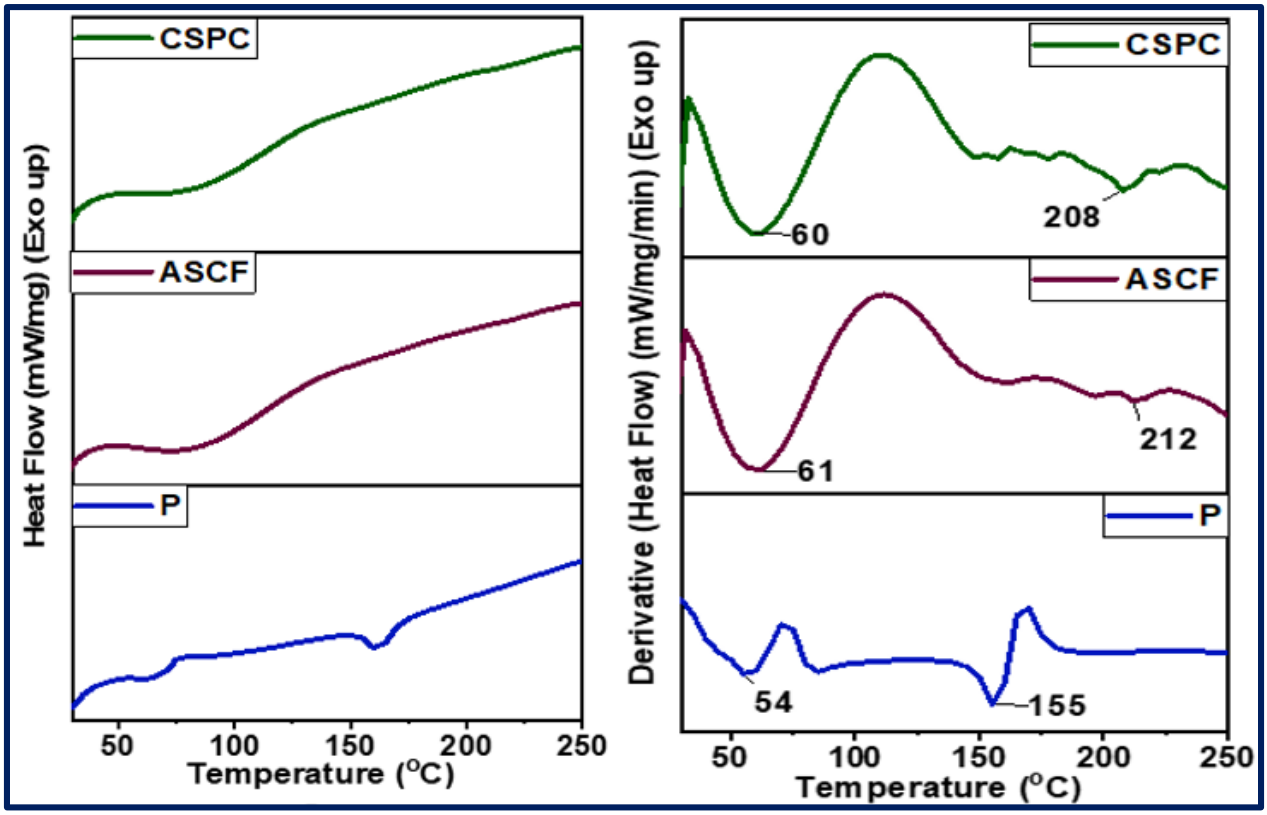

Figure 3.43 DSC and DDSC thermogram of electrospun scaffolds (P, ASCF, and CSPC)

CSBC showed similar DSC, and DDSC pattern like ASCF but endothermic peaks were at different temperatures. First peak observed at 56 ^{o}C which was lower than that of its constituent single polymeric scaffolds. Decomposition temperature of CSBC was appeared at 215 ^{o}C which was higher than the T_m of B, and degradation temperature of ASCF. Though CSBC was thermally less stable initially than the constituent scaffolds but decomposition at higher temperature suggested that CSBC possessed more thermal stability at higher temperature.

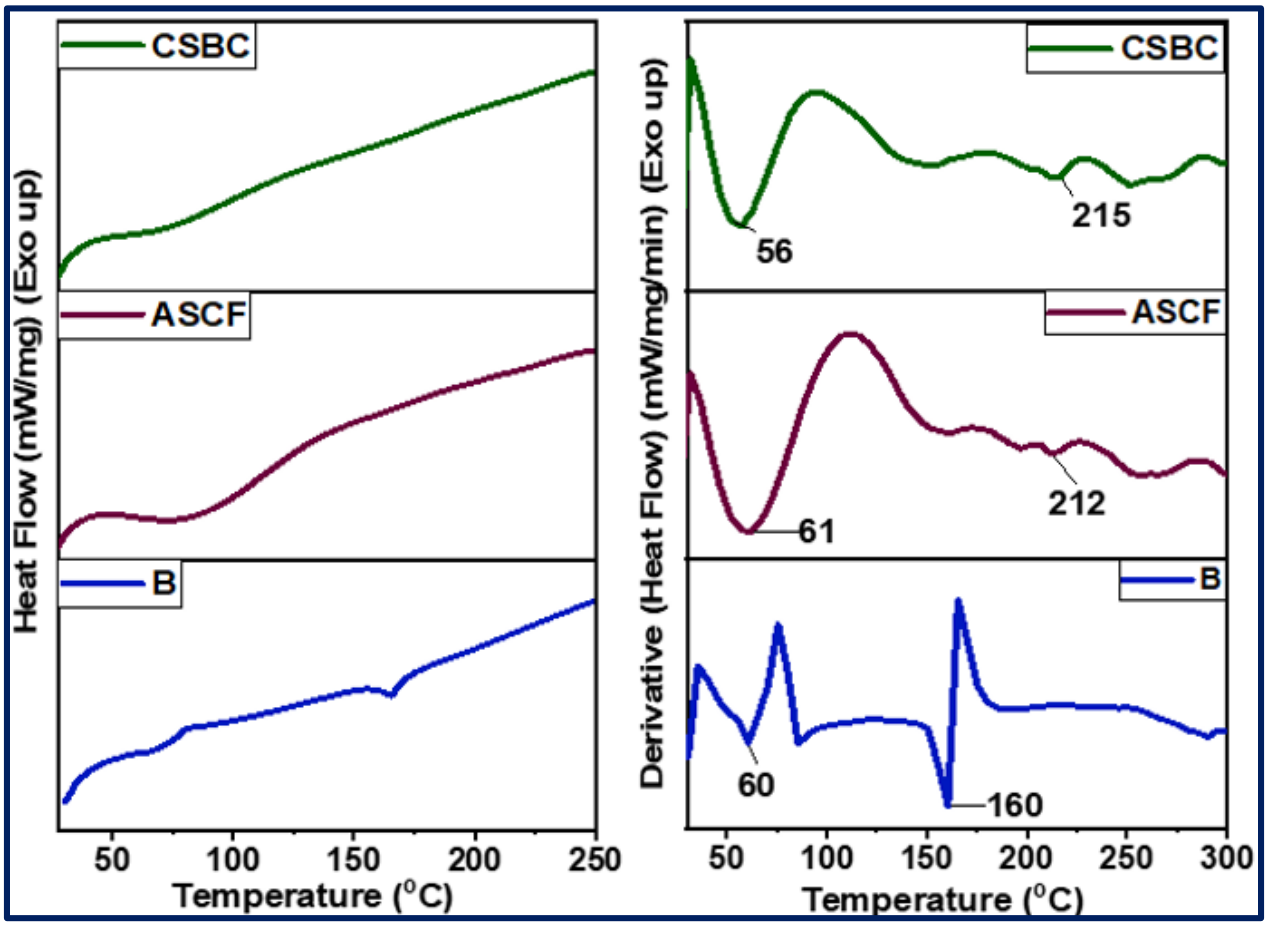

Figure 3.44 DSC and DDSC thermogram of electrospun scaffolds (B, ASCF, and CSBC)

3.4.11 XRD Analysis of Electrospun Scaffolds

The diffractograms of the electrospun scaffolds are shown in Figure 3.45 and corresponding XRD parameters are included in Table 3.17. P exhibited two peaks at 2θ values as 16.9 ^{o} (d-spacing 1.31, FWHM 12.3 ^{o}) and 19.1 ^{o}. First peak is sharp and the other peak was observed with less intensity. It was reported that Polylactic acid showed two peaks at 16.5 ^{o}, and 19.1 ^{o} in its XRD profile indicative of its semicrystalline structure [30]. Previous studies also reported that electrospun PLA

showed a broad peak at 16.1 º [11]. XRD profile of B showed a wide peak at 16.9 º (d-spacing 5.2, FWHM 0.54). As compared with the P, crystallite size in B is greater than that of P because the lower FWHM value indicated the higher crystallite size [31]. Crystallinity percentage of P and B were calculated as 48.35%, and 23.14% respectively. Diffractogram of ASCF showed only a wide peak at a 2θ value as 21.8 º indicated that during electrospinning triple helical order of collagen was distorted. This XRD profile of ASCF agreed with the previous literature which reported that electrospun collagen fiber showed a broad peak within 15 º-30 º as 2θ [32]. It was also suggested that electrospun collagen fiber showed a weak peak at around 8.8 º and a broad peak at 22.8 º [33].

Table 3.17 XRD parameters of scaffolds P, ASCF, B, CSPC, and CSBC

XRD Parameters	P		ASCF	B	CSPC	CSBC
2θ °	16.9	19.3	21.8	16.9	-	-
d (Å)	1.31	-	0.39	5.2	-	-
FWHM, º	12.3	-	-	0.54	-	-
Crystallinity (%)	48.35		-	23.14	-	-

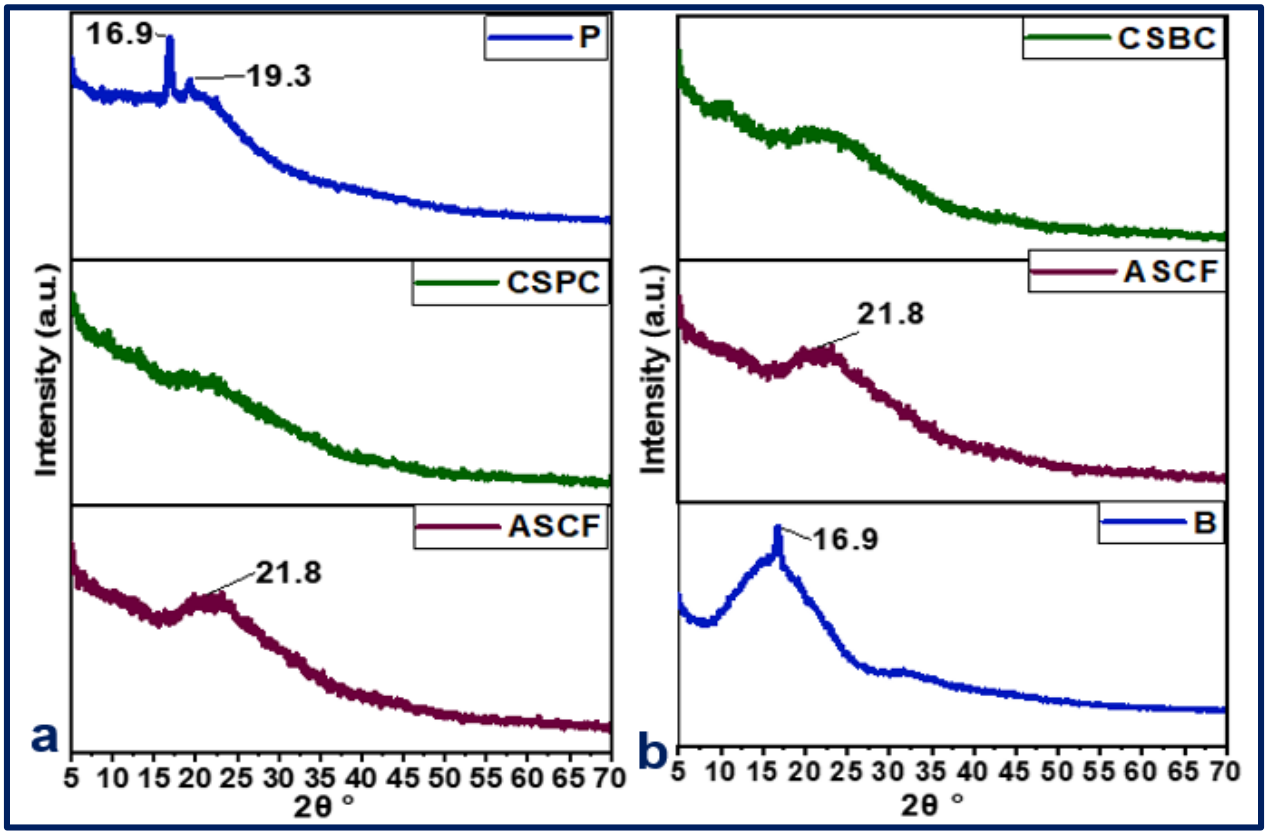

Figure 3.45 XRD diffractogram of electrospun scaffolds (P, B, ASCF, CSPC, and CSBC)

However electrospun collagen revealed mostly as amorphous nature. CSPC, and CSBC showed the similar diffraction pattern and exhibited amorphous nature. This can be explained that during electrospinning crystallization was not favored due to the fast evaporation of the solvent followed by the solidified form of stretched polymer solutions resulted less ordered structure in CSPC, and CSBC.

3.4.12 Water Contact Angle of Electrospun Scaffolds

Images of water contact angle of electrospun scaffolds with the bar diagram of water contact angle of all scaffolds are displayed in Figure 3.46.

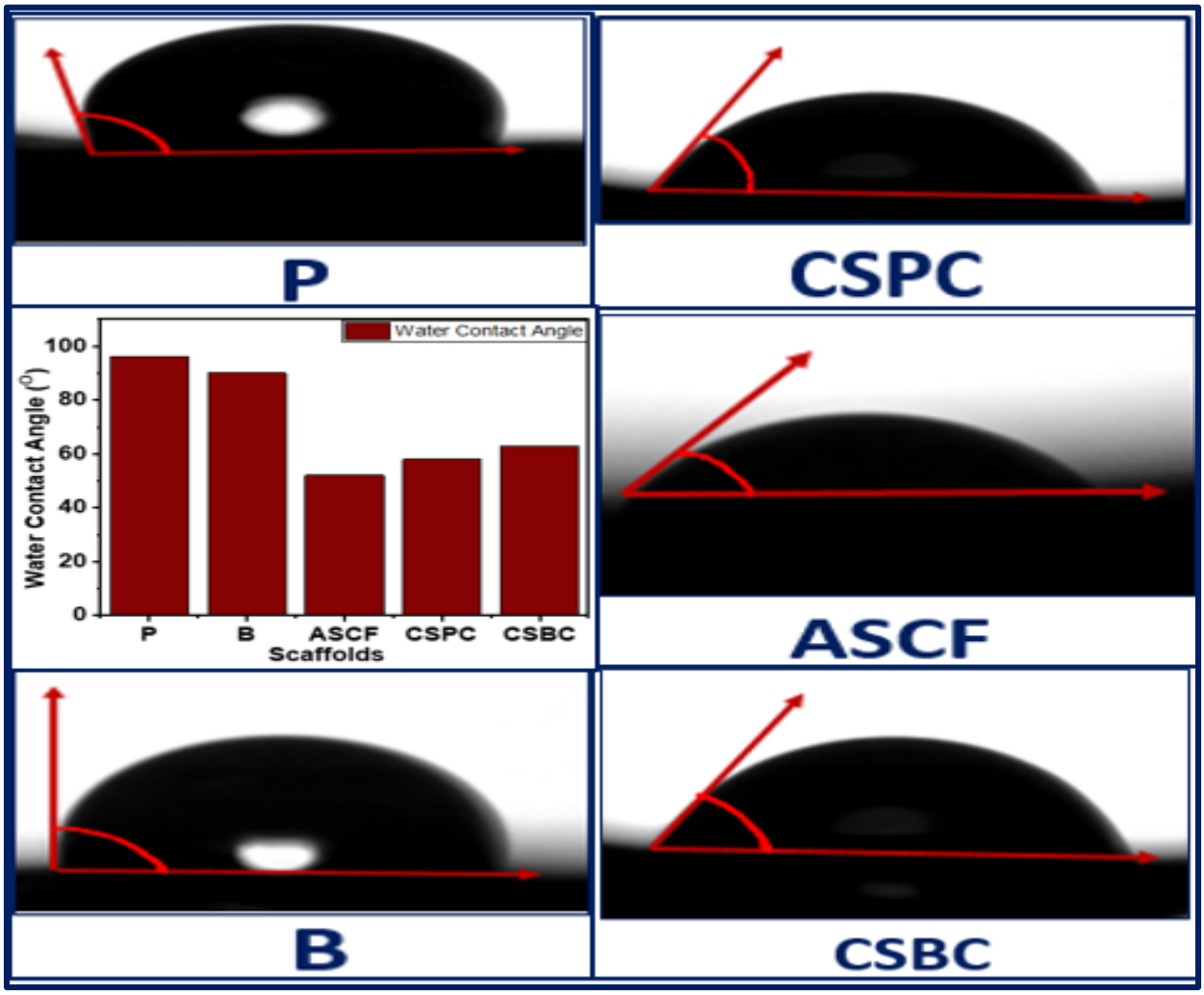

Figure 3.46 Water contact angle of electrospun scaffolds, and bar diagram of water contact angle of scaffolds (P, B, ASCF, CSPC, and CSBC)

Average water contact angle of P was observed as (96.3 ± 2.9) °, which is within hydrophobic region [34]. Scaffold B showed (90 ± 15) ° as average water contact angle. Scaffold B was more

wettable than scaffold P. Scaffold ASCF comparatively took less time to disperse in water when the water droplet was dropped on to the ASCF. Thus ASCF was observed relatively more soluble in water as it dispersed in water faster than the other scaffolds. Average water contact angle of ASCF was revealed as (52±6) ^{o}. When a droplet of water was dropped on the surface of ASCF, the greater contact region led to a greater extent of interaction among the surface of ASCF and water droplet, resulted in more surface dispersion of the water droplet and thus the lesser contact angle or greater wettability observed. Contact angle of aligned uncrosslinked, and crosslinked scaffold obtained from type I collagen was reported as 26 ^{o,} and 41 ^{o} respectively [35]. Core-sheath scaffolds CSPC, and CSBC showed water contact angle in the hydrophilic region as (58 ± 9) °, and (63 ± 9) °. Core-sheath scaffolds exhibited with the lower water contact angles than that of the P, and B, but higher contact angle than that of ASCF. Previous study revealed that the polymer surface with water contact angle within 60 ° to 80 ° provide favorable environs for the cell growth [36]. Thus CSPC, and CSBC may contribute to cell adhesion as well as proliferation and differentiation of cell, and thus may create preferable environment for wound healing.

3.4.13 In Vitro Cytotoxicity Assay

Optical micrographs of cytotoxicity analysis are displayed in Figure 3.47, and results are presented in Table 3.18, which revealed that all the scaffolds have more than 95% cell viability whereas control has 100% cell viability. This suggests that scaffolds are not cytotoxic, and are biocompatible.

Table 3.18 Cytotoxicity remarks of control, and scaffolds

Sample ID	Survival of Vero cells	Remarks
Control	100%	No cytotoxicity
P	>95%	No cytotoxicity
B	>95%	No cytotoxicity
ASCF	>95%	No cytotoxicity
CSPC	>95%	No cytotoxicity
CSBC	>95%	No cytotoxicity

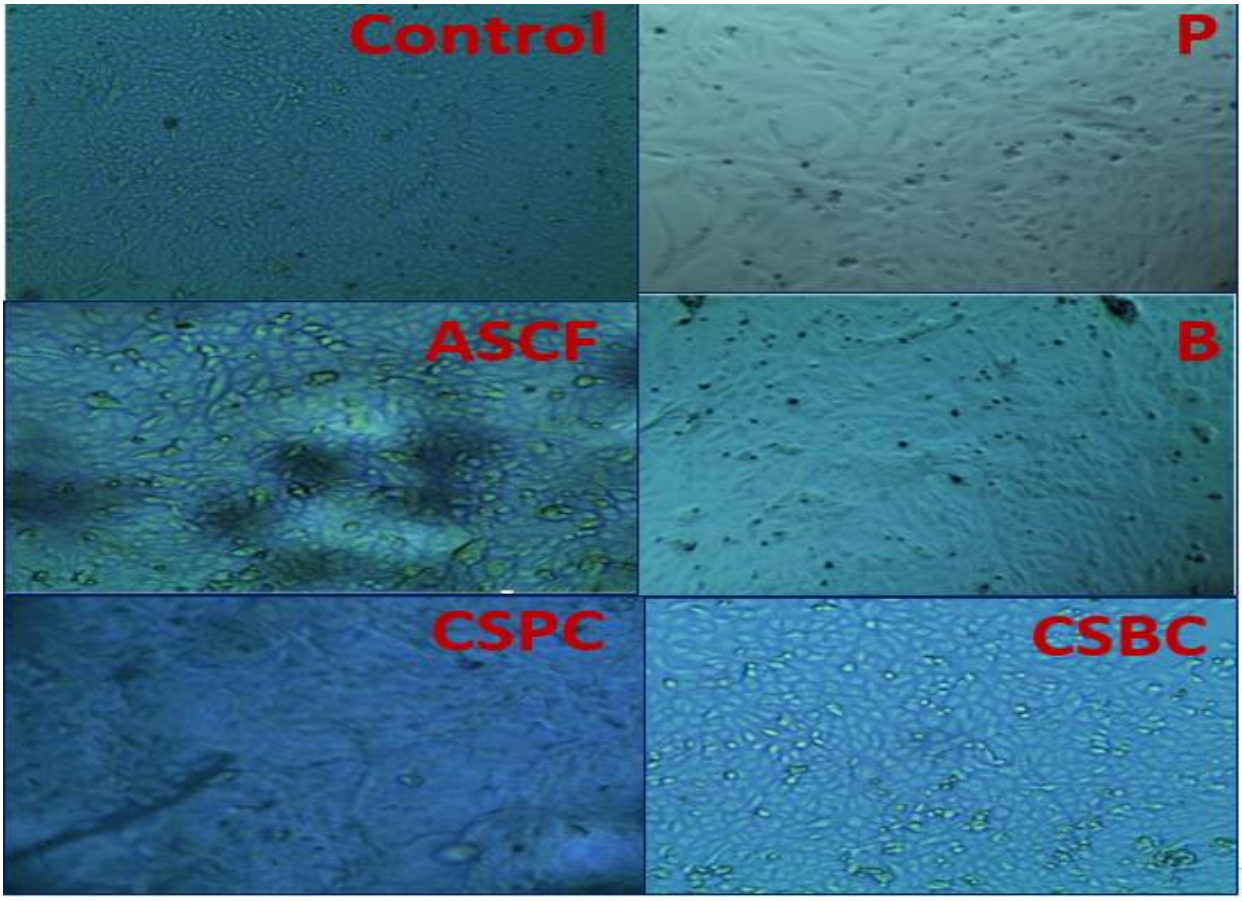

Figure 3.47 Optical microscopic images of Vero cell line with control, P, B, ASCF, CSPC and CSBC medium after 48 h of incubation (P, B, ASCF, CSPC, and CSBC)

3.4.14 In Vivo Animal (Rat) Model Assay

The external observations of wound beds produced surgically with scaffolds or without any treatment (control) are presented in Figure 3.48. At the day of wound made, no visible changes observed apparently for all wound beds. All wounds were becoming reduced with the period and more or less closed at the day of fourteen. However, the wound bed treated with CSPC scaffold showed the highest percentage of relative wound reduction with time than that of the others (Figure 3.49). At of the day of three, CSPC treated wound showed highest reduction around 60% of initial wound created whereas CSBC treated wound bed showed about 33% relative reduction of wound. P treated wound bed exhibited lowest healing about 20% but B, and ASCF treated wound beds revealed healing about 30%. P as it was hydrophobic exhibited less cell adhesion, thus resulted less wound healing initially. At seventh day, similar healing pattern like 3rd day was observed with the relative healing percentage as 70%, 44%, 50%, 50%, 30%, and 37% for CSPC, CSBC, ASCF, B, P, and control wound bed. At the day of ten, CSPC showed 100% relative reduction of

wound that was followed by the other scaffolds treated wound such as for CSBC (89%), ASCF (70%), B (60%), P (60%), and that was for control observed as 50%. These results are in line with the water contact angle of the respective scaffolds. At day fourteen, 100% closing of wound was also occurred in case of CSBC, ASCF, as well as CSPC with the hair coverage whereas 90% healing observed for B, and P treated wound beds. Control showed 75% healing at the day of fourteen as well. Wound of control rat and rat treated with scaffold P showed comparatively slow wound restorative process. Thus the decrease in the size of wound area of the rat treated with CSPC scaffold was noticeable initially although CSBC, and ASCF also showed higher healing rate later on than the wound with other scaffolds or control wound bed.

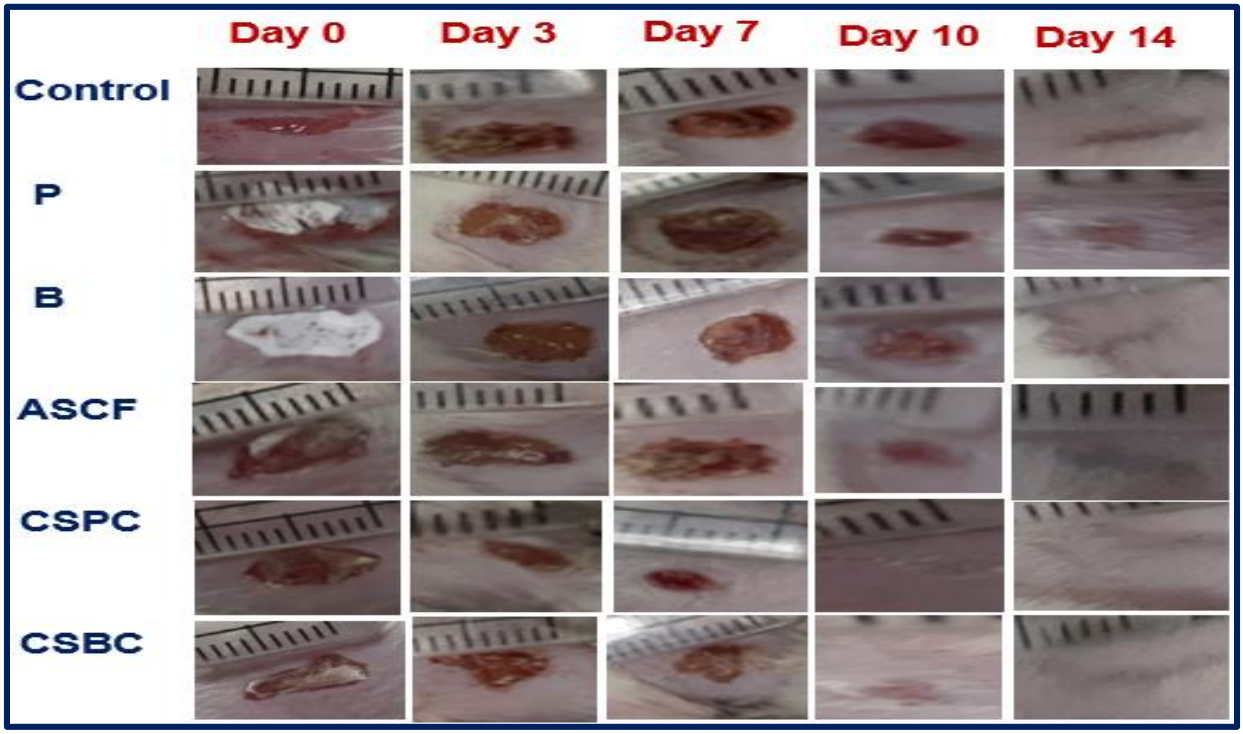

Figure 3.48 Images of wound healing (P, B, ASCF, CSPC, and CSBC)

CSPC, CSBC, and as well ASCF could speed up the rate of wound closing possibly due to the combination of the healing properties such as cell-matrix interactions, biocompatibility, and other physicochemical properties of the constituents (PLA, ASC) used in the preparation of the respective scaffolds. PLA, and collagen both are biocompatible and biodegradable. All the scaffolds more or less maintained the ideal morphology of the fiber (porosity, high surface area to volume ratio) that could mimic the ECM at the wound area, and accelerated healing process through exudates absorption, exchanges of gas and fluid, and as well bacterial protection especially for the possible antibacterial properties of PLA [14].

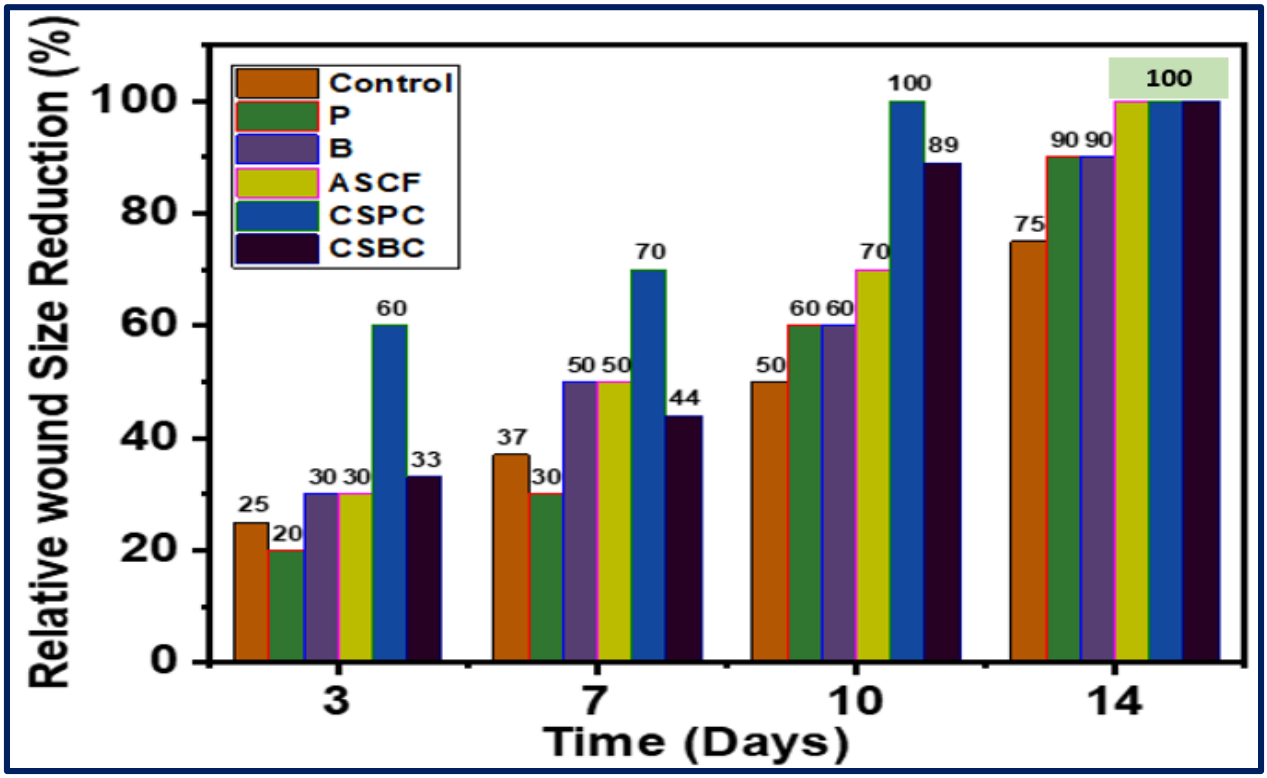

Figure 3.49 Bar diagram of relative wound size reduction with time (P, B, ASCF, CSPC, and CSBC)

Core-sheath scaffolds possessed the good combination of properties of constituents specifically PLA is hydrophobic, and ASC is hydrophilic. Thus there was a possible controlled absorption of exudates of wound which maintained a moist microenvironment, and caused the acceleration of healing by shortening the phases required for healing. Scaffolds may exhibited high cellular interactions, promoted regeneration of tissues, all of that facilitated healing of wound, and regeneration of tissues.

3.4.15 Histological Assay

Healing of wound is usually observed by considering the factors such as vascular restoration, collagen content of skin, and reconstruction of epithelial [13]. Cell inflammation and wound fibroblasts were also considered through hematoxylin and eosin staining of the wound samples at day fourteen after surgical wound. Thus the status of recovery from wound was studied by taking into account the coverage of wound by epithelium, penetration of inflammatory cells, regeneration of collagen and its array, tissue granulation, and skin appendages regeneration. These are the basic improvement of wound on the way to healing until the completion of wound mending. The histological studies of wound tissue on day fourteen are displayed in Figure 3.50. ASCF, CSPC,

and CSBC treated tissues showed complete dermal structure with epithelium whereas P, and B treated tissues showed disorder in epithelium. Hair follicles (indicated with blue arrow), collagen array (indicated with red arrow), and new blood vessels (indicated with black arrow) were observed in CSPC, and CSBC treated skin tissues. New blood vessels formation is an essential process in wound curing [30]. Dermal coverage with epithelium was not complete in control tissue but new blood vessels were observed. Collagen arrangement was not noticeable in control, P, and B treated tissues. Though ASCF treated tissue showed complete re-epithelization but less collagen, and hair follicles were observed in that tissue. In P, and B treated tissues, skin appendages such as hair follicles were not observed. These results supported the healing percentages that observed in the images of wound healing of treated groups, and control.

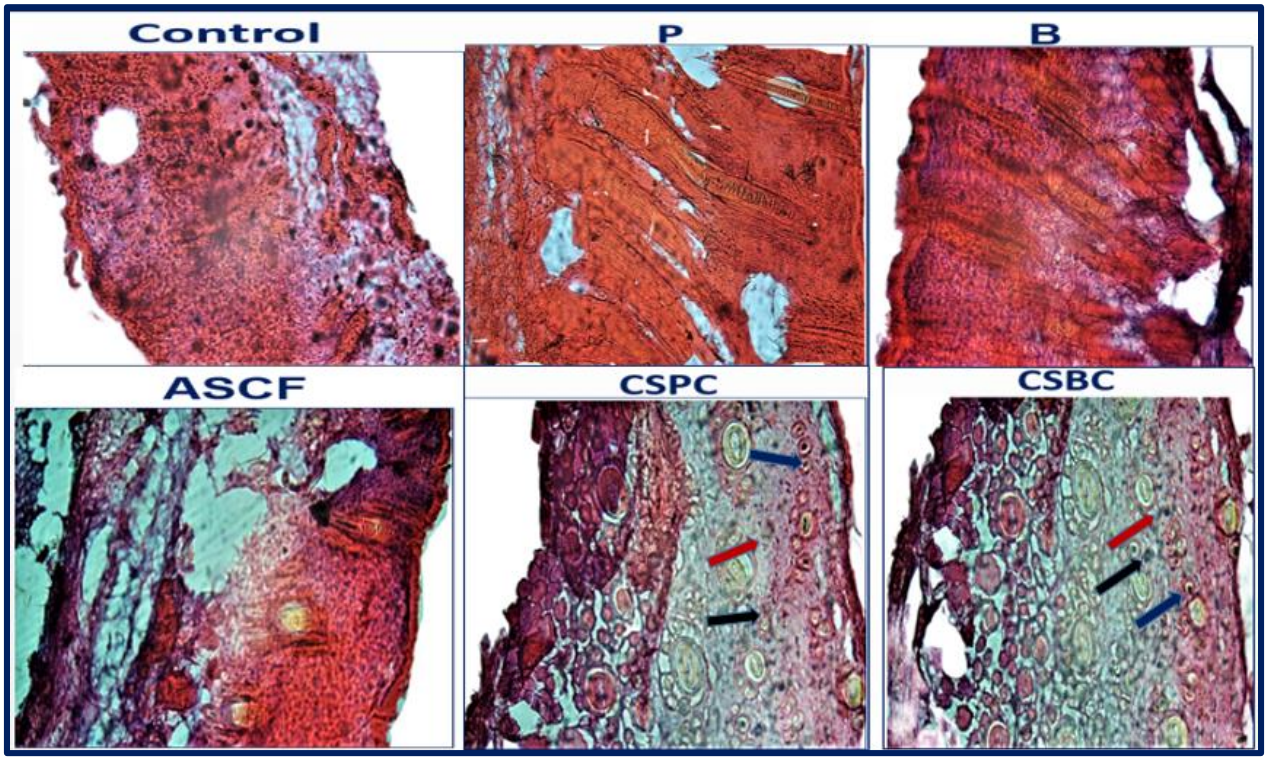

Figure 3.50 Photomicrographs of the histological responses to the nanofibrous scaffolds (control, P, B, ASCF, CSPC, and CSBC) after being applied in rat skin for 14 days

Thus core-sheath bi-polymeric scaffolds treated tissues revealed a better wound curing which started earlier than the tissues of single polymeric scaffolds treated tissues as well as control tissue. Such progress of healing was continued all over the healing process. This trend was not observed in ASCF treated group though 100% healing was also observed in the ASCF treated group at the day of fourteen.

3.3.16 Conclusion

Acid soluble collagen was extracted from tilapia fish skin composed of α1 (130 kDa), and α2 (120 kDa) cross linked with β (280 kDa) chain. Glycine content was revealed as one third of the total amino acids residue in ASC, and (Glycine-Pro-Pro-OH)n was secured as repeated unit in ASC. XRD profile indicated the triple helical structure in ASC was conserved during extraction. DSC thermogram indicated the Td of ASC as 32 ^{o}C. Appropriate concentrations, solvent systems for the preparation of spinnable solutions in addition with other required operational parameters were investigated to find the optimum conditions for the preparation of electrospun scaffolds. Core-sheath electrospun scaffolds (CSPC, and CSBC) were prepared by using ASC as core material, and PLA or PLA-g-VAc as the sheath material. Single polymeric electrospun scaffolds P, B, and ASCF were also considered for the comparison with the bi-polymeric core-sheath scaffolds. Average fiber diameter of core-sheath fibrous scaffolds was observed as (118 ± 6) nm for CSPC, and (107 ± 19) nm for CSBC which were lower than that of the single polymeric scaffolds except B. Core-sheath fibrous scaffolds were more wettable than the single polymeric scaffolds (except ASCF). The uniform nano fibrous structure of the core-sheath scaffolds and the relative hydrophilicity may well facilitate adherence and growth of cell within it in a controlled manner. Thus core-sheath scaffolds may adhere to cell in a controlled manner unlike scaffold ASCF which may work for rapid cell adhesion and also unlike scaffold P, or B which was hydrophobic in nature. All the electrospun fibrous scaffolds were observed as biocompatible. Rat model investigations validated that core-sheath fibrous scaffolds had shown all the potential to accelerate skin wound healing rapidly and effectively.

References

[1] I. N. Amirrah, Y. Lokanathan, I. Zulkiflee, M. F. M. R. Wee, A. Motta, and M. B. Fauzi, "A Comprehensive Review on Collagen Type I Development of Biomaterials for Tissue Engineering: From Biosynthesis to Bioscaffold," 2022.

[2] M. Liu, X. Duan, Y. Li, and Y. Long, "Materials Science and Engineering C," vol. 76, pp. 1413–1423, 2017, doi: 10.1016/j.msec.2017.03.034.

[3] K. C. Tang *et al.*, "Human adipose-derived stem cell secreted extracellular matrix incorporated into electrospun poly(lactic-co-glycolic acid) nanofibrous dressing for enhancing wound healing," *Polymers (Basel).*, vol. 11, no. 10, pp. 1–13, 2019, doi: 10.3390/polym11101609.

[4] Y. Lu *et al.*, "Coaxial electrospun fibers: applications in drug delivery and tissue engineering," *Wiley Interdiscip. Rev. Nanomedicine Nanobiotechnology*, vol. 8, no. 5, pp. 654–677, 2016, doi: 10.1002/wnan.1391.

[5] M. Santoro, S. R. Shah, J. L. Walker, and A. G. Mikos, "Poly(lactic acid) nanofibrous scaffolds for tissue engineering," *Adv. Drug Deliv. Rev.*, vol. 107, pp. 206–212, 2016, doi: 10.1016/j.addr.2016.04.019.

[6] J. X. Law, L. L. Liau, A. Saim, Y. Yang, and R. Idrus, "Electrospun Collagen Nanofibers and Their Applications in Skin Tissue Engineering," *Tissue Eng. Regen. Med.*, vol. 14, no. 6, pp. 699–718, 2017, doi: 10.1007/s13770-017-0075-9.

[7] J. Baek, M. K. Lotz, and D. D. D'lima, "Core-Shell Nanofibrous Scaffolds for Repair of Meniscus Tears," *Tissue Eng. - Part A*, vol. 25, no. 23–24, pp. 1577–1590, 2019, doi: 10.1089/ten.tea.2018.0319.

[8] S. Rashedi, S. Afshar, A. Rostami, M. Ghazalian, and H. Nazockdast, "Co-electrospun poly(lactic acid)/gelatin nanofibrous scaffold prepared by a new solvent system: morphological, mechanical and in vitro degradability properties," *Int. J. Polym. Mater. Polym. Biomater.*, vol. 70, no. 8, pp. 545–553, 2021, doi: 10.1080/00914037.2020.1740987.

[9] S. Torres-Giner, A. Martinez-Abad, J. V. Gimeno-Alcañiz, M. J. Ocio, and J. M. Lagaron,

"Controlled delivery of gentamicin antibiotic from bioactive electrospun polylactide-based ultrathin fibers," *Adv. Eng. Mater.*, vol. 14, no. 4, pp. 112–122, 2012, doi: 10.1002/adem.201180006.

[10] W. Y. Huang, T. Hibino, S. I. Suye, and S. Fujita, "Electrospun collagen core/poly-l-lactic acid shell nanofibers for prolonged release of hydrophilic drug," *RSC Adv.*, vol. 11, no. 10, pp. 5703–5711, 2021, doi: 10.1039/d0ra08353d.

[11] F. Lopresti *et al.*, "Core-shell PLA/Kef hybrid scaffolds for skin tissue engineering applications prepared by direct kefiran coating on PLA electrospun fibers optimized via air-plasma treatment," *Mater. Sci. Eng. C*, vol. 127, no. June, p. 112248, 2021, doi: 10.1016/j.msec.2021.112248.

[12] W. Fu *et al.*, "Electrospun gelatin/PCL and collagen/PLCL scaffolds for vascular tissue engineering," pp. 2335–2344, 2014.

[13] M. Hajikhani, Z. Emam-Djomeh, and G. Askari, "Fabrication and characterization of mucoadhesive bioplastic patch via coaxial polylactic acid (PLA) based electrospun nanofibers with antimicrobial and wound healing application," *Int. J. Biol. Macromol.*, vol. 172, pp. 143–153, 2021, doi: 10.1016/j.ijbiomac.2021.01.051.

[14] P. Khazaeli, M. Alaei, M. Khaksarihadad, and M. Ranjbar, "Preparation of PLA/chitosan nanoscaffolds containing cod liver oil and experimental diabetic wound healing in male rats study," *J. Nanobiotechnology*, vol. 18, no. 1, pp. 1–9, 2020, doi: 10.1186/s12951-020-00737-9.

[15] I. J. H. Barrientos *et al.*, "Electrospun Collagen-Based Nanofibres: A Sustainable Material for Improved Antibiotic Utilisation in Tissue Engineering Applications," *Int. J. Pharm.*, 2017, doi: 10.1016/j.ijpharm.2017.08.071.

[16] S. Afshar, S. Rashedi, H. Nazockdast, and M. Ghazalian, "Preparation and characterization of electrospun poly(lactic acid)-chitosan core-shell nanofibers with a new solvent system," *Int. J. Biol. Macromol.*, vol. 138, pp. 1130–1137, 2019, doi: 10.1016/j.ijbiomac.2019.07.053.

[17] A. A. El-Rashidy, A. Gad, A. E. H. G. Abu-Hussein, S. I. Habib, N. A. Badr, and A. A.

Hashem, “Chemical and biological evaluation of Egyptian Nile Tilapia (Oreochromis niloticas) fish scale collagen,” *Int. J. Biol. Macromol.*, vol. 79, pp. 618–626, 2015, doi: 10.1016/j.ijbiomac.2015.05.019.

[18] J. Chen, L. Li, R. Yi, N. Xu, R. Gao, and B. Hong, “Extraction and characterization of acid-soluble collagen from scales and skin of tilapia (Oreochromis niloticus),” *Lwt*, vol. 66, pp. 453–459, 2016, doi: 10.1016/j.lwt.2015.10.070.

[19] J. Li *et al.*, “Extraction and characterization of type I collagen from skin of tilapia (Oreochromis niloticus) and its potential application in biomedical scaffold material for tissue engineering,” *Process Biochem.*, vol. 74, pp. 156–163, 2018, doi: 10.1016/j.procbio.2018.07.009.

[20] S. kui Zeng, C. hua Zhang, H. Lin, P. Yang, P. zhi Hong, and Z. Jiang, “Isolation and characterisation of acid-solubilised collagen from the skin of Nile tilapia (Oreochromis niloticus),” *Food Chem.*, vol. 116, no. 4, pp. 879–883, 2009, doi: 10.1016/j.foodchem.2009.03.038.

[21] L. Sun, H. Hou, B. Li, and Y. Zhang, “Characterization of acid- and pepsin-soluble collagen extracted from the skin of Nile tilapia (Oreochromis niloticus),” *Int. J. Biol. Macromol.*, vol. 99, pp. 8–14, 2017, doi: 10.1016/j.ijbiomac.2017.02.057.

[22] A. Veeruraj, M. Arumugam, T. Ajithkumar, and T. Balasubramanian, “Isolation and characterization of collagen from the outer skin of squid (Doryteuthis singhalensis),” *Food Hydrocoll.*, vol. 43, pp. 708e716-716, 2015, doi: 10.1016/j.foodhyd.2014.07.025.

[23] R. Ahmed, A. T. Getachew, Y. J. Cho, and B. S. Chun, “Application of bacterial collagenolytic proteases for the extraction of type I collagen from the skin of bigeye tuna (Thunnus obesus),” *Lwt*, vol. 89, pp. 44–51, 2018, doi: 10.1016/j.lwt.2017.10.024.

[24] J. Zhang *et al.*, “Structural characterization, in-vivo acute systemic toxicity assessment and in-vitro intestinal absorption properties of tilapia (Oreochromis niloticus) skin acid and pepsin solublilized type I collagen,” *Process Biochem.*, vol. 51, no. 12, pp. 2017–2025, 2016, doi: 10.1016/j.procbio.2016.08.009.

[25] Z. Song *et al.*, “Characterization and comparison of collagen extracted from the skin of

the Nile tilapia by fermentation and chemical pretreatment," *Food Chem.*, vol. 340, no. May 2020, p. 128139, 2021, doi: 10.1016/j.foodchem.2020.128139.

[26] P. Chandika *et al.*, "Electrospun porous bilayer nano-fibrous fish collagen/PCL bio-composite scaffolds with covalently cross-linked chitooligosaccharides for full-thickness wound-healing applications," *Mater. Sci. Eng. C*, vol. 121, no. December 2020, p. 111871, 2021, doi: 10.1016/j.msec.2021.111871.

[27] K. H. Sizeland *et al.*, "Nanostructure of electrospun collagen: Do electrospun collagen fibers form native structures?," *Materialia*, vol. 3, no. July, pp. 90–96, 2018, doi: 10.1016/j.mtla.2018.10.001.

[28] R. W. Newberry and R. T. Raines, "The n→π∗ Interaction," *Acc. Chem. Res.*, vol. 50, no. 8, pp. 1838–1846, 2017, doi: 10.1021/acs.accounts.7b00121.

[29] S. Torres-Giner, J. V. Gimeno-Alcañiz, M. J. Ocio, and J. M. Lagaron, "Comparative performance of electrospun collagen nanofibers cross-linked by means of different methods," *ACS Appl. Mater. Interfaces*, vol. 1, no. 1, pp. 218–223, 2009, doi: 10.1021/am800063x.

[30] F. Xu, H. Wang, J. Zhang, L. Jiang, W. Zhang, and Y. Hu, "A facile design of EGF conjugated PLA/gelatin electrospun nanofibers for nursing care of in vivo wound healing applications," *J. Ind. Text.*, vol. 51, no. 1, pp. 420S-440S, 2022, doi: 10.1177/1528083720976348.

[31] J. J. Senkevich and S. B. Desu, "Morphology of poly(chloro-p-xylylene) CVD thin films," *Polymer (Guildf).*, vol. 40, no. 21, pp. 5751–5759, 1999, doi: 10.1016/S0032-3861(98)00793-9.

[32] Y. Zhou, H. Yao, J. Wang, D. Wang, Q. Liu, and Z. Li, "Greener synthesis of electrospun collagen/ hydroxyapatite composite fibers with an excellent microstructure for bone tissue engineering," *Int. J. Nanomedicine*, vol. 10, pp. 3203–3215, 2015, doi: 10.2147/IJN.S79241.

[33] J. Wu, S. Wang, Z. Zheng, and J. Li, "Fabrication of Biologically Inspired Electrospun Collagen/Silk fibroin/bioactive glass composited nanofibrous scaffold to accelerate the

treatment efficiency of bone repair," *Regen. Ther.*, vol. 21, pp. 122–138, 2022, doi: 10.1016/j.reth.2022.05.006.

[34] H. Chen *et al.*, "Instant in-situ Tissue Repair by Biodegradable PLA/Gelatin Nanofibrous Membrane Using a 3D Printed Handheld Electrospinning Device," *Front. Bioeng. Biotechnol.*, vol. 9, no. July, pp. 1–12, 2021, doi: 10.3389/fbioe.2021.684105.

[35] S. Zhong *et al.*, "An aligned nanofibrous collagen scaffold by electrospinning and its effects on in vitro fibroblast culture," 2006, doi: 10.1002/jbm.a.

[36] Y. Tamada and Y. Ikada, "Fibroblast growth on polymer surfaces and biosynthesis of collagen," *J. Biomed. Mater. Res.*, vol. 28, no. 7, pp. 783–789, 1994, doi: 10.1002/jbm.820280705.

CHAPTER FOUR

EXECUTIVE SUMMARY

Chapter Four

Executive Summary

This study aimed to prepare electrospun bi-polymeric nanofibrous scaffolds to observe their efficacy in skin wound healing. Completely hydrophobic or hydrophilic biomaterials are not suitable to be applied for cell growth in a wounded area. Hydrophobic PLA was attempted to modify using vinyl acetate and $LiAlH_4$. Another attempt was taken to modify PLA using vinyl acetate and benzoyl peroxide. Macromolecular structures of the resultant materials were confirmed by FT-IR, ^{1}H-NMR, ^{13}C-NMR analysis. Thermal and morphological properties were also analyzed by TGA, DSC, and XRD. Additionally, Gelatin and PLA blend solutions of different compositions were prepared using T80 as surfactant. Solution properties such as viscosity, and conductivity of the blended solutions were measured, and electrospun scaffolds were prepared from the blended solutions. A uniform fibrous scaffold of average fiber diameter 139±51 nm resulted from the blended solution having conductivity and viscosity of 650 μS/cm and 155 cP respectively. This attempt revealed that the addition of PLA solution to the gelatin solution increased the spinnability of PLA. IR, thermal and X-ray analysis showed that the blended scaffold maintained the combination of the properties of PLA and gelatin. Acid soluble collagen was extracted from Tilapia fish skin which constitutes a α1 (130 kDa) chain, a α2 (120 kDa) chain cross linked with a β (280 kDa) chain. Electrospun bi-polymeric core-sheath scaffolds were prepared by using ASC or gelatin as the core polymer, and PLA or PLA-g-VAc as the sheath polymer. FESEM micrographs revealed the uniform nanofibrous structures of the scaffolds with the average fiber diameter lower than the single polymeric scaffolds. The water contact angle of bi-polymeric scaffolds is revealed as more wettable than the PLA scaffolds. All the electrospun fibrous scaffolds were observed as biocompatible. The uniform nano-fibrous structure of the bi-polymeric scaffolds and the relative hydrophilicity facilitated adherence and growth of cells within them in a controlled manner, that was validated by rat model investigations which revealed that bi-polymeric scaffolds maintained all the potential to accelerate skin wound healing rapidly and effectively.

CHAPTER Five

PUBLICATION

Chapter Five

Publication

5.1 Book Chapter (Published)

Nasima Akter Mukta, Md. Didarul Islama, Rasheda Begum Dina, Wahida Haque, and Papia Haque, (2021), Radiation processed polysaccharides in food production, preservation and packaging applications, Radiation- Processed Polysaccharides, Emerging Roles in Agriculture; 107-148, Academic Press.

5.2 Paper Presented in Conference

Nasima Akter Mukta, Samina Ahmed, A M Sarwaruddin Chowdhury, Papia Haque, Fabrication and properties of electrospun core-shell nanofibrous scaffolds from poly(lactic acid) and collagen for wound healing application, International Conclave on Materials, Energy & Climate (ICMEC- 2022), 19-20 December 2022, Department of Applied Chemistry And Chemical Engineering, Paper ID- A6060.

5.3 Paper under Revision for Publication

1. Manuscript titled "Reduction based one step synthesis of vinyl acetate-g-poly(lactic acid) copolymer" submitted to the journal Chemistry Select. The manuscript number of submission is slct.202303505.

Author (s)

N. A. Mukta[a,d], S. Ahmed[b], S.M. Tareq[c], A. M. S. Chowdhury[d], S. B. A. Monsur[d], and P. Haque[d]

2. Manuscript titled "Poly(lactic acid) blended gelatin based nanofibrous mats for soft tissue regeneration" submitted to the journal of Journal of Medical Engineering & Technology. The manuscript ID of submission is 237044526

Author (s)

Nasima Akter Mukta[1,3], Samina Ahmed[2], A M Sarwaruddin Chowdhury[3], M. Nuruzzaman Khan[3], Md. Sahadat Hossain[2], Gawsia W. Chowdhury[4], Papia Haque[3]

3. Manuscript titled “Effect of core-sheath bi-polymeric scaffolds fabricated from acid-soluble collagen and poly(lactic Acid) derivatives on wound healing” submitted to the Journal of Applied Polymer Science. The manuscript number of submission is app.20232253.

Author (s)

Nasima Akter Mukta, [1, 3] Samina Ahmed, [2] A M Sarwaruddin Chowdhury, [3] Shafi M Tareq, [4] Abu Ashfaqur Sajib, [5] M. S. Bashar, [2] Papia Haque, [3]